Engineering the Properties of Indium Sulfide for Thin Film Solar Cells by Doping

Thesis submitted to
Cochin University of Science and Technology

By
Meril Mathew

In partial fulfillment of the requirements
for the award of the degree of

DOCTOR OF PHILOSOPHY

Department of Physics
Cochin University of Science and Technology
Cochin – 682 022, Kerala, India

January 2009

Engineering the Properties of Indium Sulfide for Thin Film Solar Cells by Doping

Ph.D thesis in the field of Thin Film Photovoltaics

Author:

Meril Mathew
Thin Film Photovoltaic Division,
Department of Physics
Cochin University of Science and Technology
Kochi - 682 022, Kerala, India
E-mail: meril.mathew@gmail.com

Guide:

Dr. C. Sudha kartha
Department of Physics
Cochin University of Science and Technology
Kochi - 682 022, Kerala, India
E-mail: csk@cusat.ac.in

Cochin University of Science and Technology
Kochi - 682 022, Kerala, India
January 2009

Dedicated

To Appachan & Mummy

Dr. C. Sudha Kartha
Department of Physics
Cochin University of Science and Technology
Cochin – 682 022

23rd January2009

Certificate

Certified that the work presented in this thesis entitled "*Engineering the Properties of Indium Sulfide for Thin Film Solar Cells by Doping*" is based on the authentic record of research done by Ms. Meril Mathew under my guidance in the Department of Physics, Cochin University of Science and Technology, Kochi - 682 022, India and has not been included in any other thesis submitted for the award of any degree.

Dr. C. Sudha Kartha
(Supervising Guide)

Phone : +91 484 2577404 extn 31 Fax: 91 484 2577595 email: csk@cusat.ac.in

Declaration

I hereby declare that the work presented in the thesis entitled "*Engineering the Properties of Indium Sulfide for Thin Film Solar Cells by Doping*" is based on the original research work done by me under the guidance of Dr. C Sudha Kartha, Department of Physics, Cochin University of Science and Technology, Kochi - 682022, India and has never been included in any other thesis submitted for the award of any degree.

Meril Mathew

Kochi – 682022
23 January 2009

Acknowledgement

The paramount purpose of writing this is to express my heartfelt gratitude to all those who were instrumental in helping me to realize this doctoral thesis.

Foremost, I would like to express my deepest respect and most sincere gratitude to my guide, Dr. C. Sudha Kartha for her guidance and encouragement throughout my work. Her constructive criticism, expert remarks and personal guidance have been the heart and soul of this work from conception to completion. I am greatly indebted for her concern and understanding which helped me endure all obstacles.

I am very grateful to Dr. K. P. Vijayakumar for the inspiration and guidance he provided. In spite of all responsibilities and duties, he found time for in-depth discussions which provided invaluable guidance to ensure steady progress of my research program. I greatly acknowledge his valuable insights and suggestions. His vision and dedication in developing a low cost solar cell had a remarkable influence on me. I am extremely thankful for the support and encouragement received from him.

I am thankful to Dr. Godfrey, Professor& Head of the Department of Physics for all the facilities extended to me in the department. I would like to express my sincere appreciation to all the teachers of the faculty of Physics for their help and guidance.

I am grateful to Y Kashiwaba and Abe, Department of Electrical and Electronic Engineering, Iwate University, Japan for XPS measurements and the support they have extended for my Ph. D work.

I am thankful to all the office and library staff of the Department of Physics and the technical staff at USIC for their help and cooperation.

I specially appreciate expertise and experience of my seniors Dr. Teny Theresa John, Dr. Shyamala, Dr. Ramkumar, Dr. Saravanan, Dr. Paulraj, Dr.Ratheesh Kumar, Wilson and Dr. Sreekumar. Their support came quite handy during the initial stages of my research work.

I am indebted and thankful to Beena, Jayakrishnan, Sreekumar, Deepa, Tina, Vimal, Anitha, Pramitha, Sajeesh, Angel, Manju, Rajesh Menon and Anu Philip for being my surrogate family during the days at CUSAT. The discussions sparkled with novel ideas and iced with pretty jokes provided the perfect learning environment would be cherished in my memory. Words are inadequate to thank them for the sincere and untiring help they have provided.

I warmly thank all my colleagues Dhanya, Kishore, Rajesh C S, Rajesh Mon, Nimmi, Subramanyan, Jafar, Poornima and Sree Roop for all the help they had extended to me. I owe to all my friends who are many more to name, for their support and encouragement.

I record my deep and utmost gratitude to my parents, brother, sisters and in-laws for their selfless support and encouragement during the entire period of my work. Anything I inscribe here will be inadequate to express my feelings for them.

The profound support and guidance I received from my husband, Dr. Joe has to be mentioned with great gratitude and love.

Let me conclude this by praising God for all the blessings He showered upon me.

Meril Mathew

Contents

Preface

Photovoltaic conversion of solar energy appears to be one of the most promising ways of meeting the increasing energy demands of the future when conventional energy sources are being depleted. Growing interest in photovoltaic conversion is a consequence of the concern to identify future sources of energy that will be inexpensive as well as ecofriendly.

Semiconductors have emerged as frontrunner among the class of materials that can convert sunlight directly into electrical energy. Currently, a wide range of semiconductors are explored for their potential use in photovoltaic applications. General criteria determining the choice of a particular semiconductor are efficiency, cost, availability and toxicity of the raw material along with environmental conditions (eg. terrestrial or space applications and duration of sunshine). Each material requires a particular solar cell device structure for optimum performance, and the choice is primarily determined by the available processing techniques and the photovoltaic properties that can be achieved under these conditions.

Lowering the cost of solar cell production is among the most important intentions in photovoltaic research. To achieve this, thin film technology need to be developed with thin film materials having good photovoltaic properties and appropriate band gap that can be deposited uniformly over large areas. Furthermore, the constituents of these compounds should be non-toxic. Nowadays lot of research is going on for the replacement of the CdS buffer layer. Among the various materials with wide bandgap investigated (Zn(OS), Zn(OH,S), ZnO, ZnS, , ZnSe, In_2S_3, $In(OH)_3$, $In(OH,S)_3$ [29,30]) the best performance was achieved using the CdS buffer material. This is contrary to the performance gain expected for wider band gap materials due to lower light absorption. This underline the fact that alternate buffer layers are not yet optimized to capture its full potential.

Indium sulfide (In_2S_3) is a rare case of ordered crystalline material with large number of vacancies and has proved its potential as a Cd- free buffer layer. Owing to tetragonal sites formed by the incompletely coordinated sulfur atoms, indium sulfide can serve as a host for a number of metal ions. Doping In_2S_3 produces materials with exceptional optical, electrical, and magnetic properties that can be adjusted by the concentration of the guest ion.

In the present work, structural, optical and electrical properties of indium sulfide are tuned by specific and controlled doping. Silver, tin, copper and chlorine were used as the doping elements. In_2S_3 thin films for the present study were prepared using a simple and low cost "Chemical Spray Pyrolysis (CSP)" technique. This technique is adaptable for large-area deposition of thin films in any required shape and facilitates easiness of doping and/or variation of atomic ratio. It involves spraying a solution, usually aqueous, containing soluble salts of the constituents of the desired compound onto a heated substrate. Doping process was optimized for different doping concentrations. On optimizing doping conditions, we tuned the structural, optical and electrical properties of indium sulfide thin films making them perform as an ideal buffer layer. This thesis is divided into seven chapters. A brief description of each chapter is given below.

CHAPTER 1 is a general introduction to buffer layer in thin film photovoltaics. It briefs about the importance of thin films in solar cells and the role of buffer layer. Further it continues with discussion on present hurdles of thin film photovoltaics, toxicity of cadmium and Cd-free buffer layers. The chapter concludes by discussing the factors limiting the efficiency of solar cell and thoughts to overcome it.

CHAPTER 2 presents an exhaustive review on indium sulfide, the material under study. This chapter provides a thorough insight on the studies done so far in this material

CHAPTER 3 presents the anomalous behavior of silver doped indium sulfide thin films. It was observed that silver got diffused into In_2S_3 films at room temperature itself without any post deposition treatments. These samples were characterized using different techniques. Depth profile using X-ray Photoelectron Spectroscopy clearly showed diffusion of silver into In_2S_3 layer without any annealing. X-ray analysis revealed significant enhancement in crystallinity and grain size up to an optimum percentage of doping concentration. This optimum value showed dependence on thickness and atomic ratio of indium and sulfur in the film. Sample having optimum doping was found to be more photosensitive and low resistive when compared with pristine sample. Impact of post annealing on the optimum doping was also studied; results proved that optimum value of silver decreased on enhancing the diffusivity by thermal assistance and excess silver retraced to the surface of the films on annealing. Thus silver diffused indium sulfide surpassed pristine sample for crystallinity and photosensitivity.

CHAPTER 4 deals with the studies on tin doped indium sulfide thin films. The motive behind this was to reduce resistivity of the films. Effect of both in-situ and ex-situ doping were analyzed. Ex-situ doping was done through thermal diffusion which was realized by annealing Sn/In_2S_3 bilayer films. In-situ doping was done by introducing Sn into the Spray solution using $SnCl_4.5H_2O$. Interestingly, it was noted that by ex-situ doping, the conductivity of the sample enhanced by five orders without affecting any of the physical properties, such as crystallinity or band gap. Analysis also showed that higher doping percentage resulted in samples with lower crystallinity and negative photosensitivity. However, in-situ doping resulted in amorphous films. Conductivity of the samples increased for with low doping concentrations and at higher doping concentration conductivity decreased. Oxygen incorporation was also found to be very high with in-situ doped samples and resulted in widening of the optical bandgap. These films were highly photosensitive even when it exhibited very wide bandgap. These observations proved that tin incorporation modified the band

gap and electrical properties of the In_2S_3: Sn films favorably over wider ranges making it highly suitable for different optoelectronic applications.

CHAPTER 5 describes copper doping in indium sulfide thin films. Doping was achieved through thermal diffusion by annealing bi layer films having structure Cu/In_2S_3. XRD analysis revealed formation of $CuInS_2$ in addition to tetragonal β-In_2S_3 phase at high doping concentration. Optical absorption edge of these films showed a shift towards longer wavelength due to the presence of $CuInS_2$. Electrical measurements indicated a considerable reduction in the sheet resistance of the sample. Hot probe measurements showed that Cu diffused samples resulted in p-type conductivity. Photoactive junction could be fabricated by controlling the diffusion of copper by adjusting the thickness of Cu and In_2S_3 layers at optimized temperature.

Role of chlorine in indium sulfide films, prepared by chemical spray pyrolysis method employing indium chloride precursor solution is discussed in **CHAPTER 6**. The role of incorporated Cl in the films prepared using chemical methods was not revealed. Hence, in order to find the part played by chlorine atoms, it was purposefully doped. Chlorine was omitted in the pristine films by replacing the precursor solution of indium chloride by indium nitrate. Films prepared from indium nitrate precursor solutions were amorphous. Chlorine was found to be instrumental in imparting crystallinity to films. Controlled doping of chlorine resulted in micro/nano structures. Chlorine also initiated defect level absorption. Photosensitivity of chloride based samples could be increased by introducing chlorine. Persistent photoconductivity was also observed for doped films. This study proved the implicit role played by chlorine in giving highly crystalline films with specific optical and electrical properties.

CHAPTER 7 is a summary of the entire work. The important points are highlighted. The chapter ends with future scope of the present work.

Journal publications

1. Anomalous behavior of silver doped indium sulfide thin films, **Meril Mathew**, R. Jayakrishnan, P. M. Ratheesh Kumar, C. Sudha Kartha, K. P. Vijayakumar, T. Abe, Y. Kashiwaba, J. Appl. Phys. 100, 033504 (2006)
2. In_2S_3:Ag, An ideal buffer layer for thin film solar cells, **Meril Mathew**, C. Sudha Kartha, K. P. Vijayakumar, J Mater Sci: Mater Electron 1085, 49591-7 (2008)
3. $CuInS_2/In_2S_3$ thin film solar cell using spray pyrolysis technique having 9.5% efficiency, Teny Theresa John, **Meril Mathew**, C. Sudha Kartha, K. P. Vijayakumar, T. Abe, Y. Kashiwaba, Sol. Energy. Mat. Sol. Cells 89(1), 27-36 (2005).

Conference publications - International

4. Effect of doping on spray pyrolysed Indium Sulfide thin films, **Meril Mathew**, Teny Theresa John, C. Sudha Kartha and K. P. Vijayakumar., Proc. International conference on Optoelectronic Materials and Thin films for Advanced Technology-2005, Pages 445-451
5. Bandgap engineering in In_2S_3 thin films by tin mixing, **Meril Mathew**, C. Sudha Kartha, K. P. Vijayakumar and Parameswar Hari, Mater. Res. Soc. Symp. Proc. Volume 1012, Warrendale, PA, 2007, 1012-Y12-14
6. Thermal diffusion of copper: A different approach for the preparation of $CuInS_2$ / In_2S_3 p-n junction, **Meril Mathew** , C Sudha Kartha and K P Vijayakumar, Proc. International Conference on optical, optoelectronic, Photonic Materials and applications 2007.

7. In_2S_3:Ag, An ideal buffer layer for thin film solar cells, **Meril Mathew** , C Sudha Kartha and K P Vijayakumar, Proc. International Conference on optical, optoelectronic, Photonic Materials and applications 2007.
8. Silver Diffused In_2S_3 With and Without Thermal Assistance; An ideal Buffer layer for Thin film solar Cells, **Meril Mathew**, C. Sudha Kartha and K. P. Vijayakumar, Proc. 22nd European Photovoltaic Solar Energy Conference, 2007,Pages 2104-2108.
9. Tuning the Properties of Indium Sulfide to realize an Ideal Buffer layer for Thin film Solar Cells, **Meril Math**ew, Angel Susan Cherian, C. Sudha Kartha and K. P. Vijayakumar, Proc. International conference on solar cells-2008, Page 149.

Conference publications - National

10. Device quality indium sulfide thin films by silver doping, **Meril Mathew**, C. Sudha Kartha and K. P. Vijayakumar, Proc. National conference on Advances in Energy Research Technology-2006, Pages 217-222.
11. Enhanced conductivity in In_2S_3 thin films by Sn Doping, **Meril Mathew**, C. Sudha Kartha and K. P. Vijayakumar, Proc. Materials for Energy Generation, Conservation and Storage, MRSI-2007, Page 106.
12. Variation on the properties of spray pyrolysed In_2S_3 films due to sodium doping, Angel Susan Cherian, **Meril Mathew**, C. Sudha Kartha, Tina Sebastian, K. P. Vijayakumar, Proc. Materials for Energy Generation, Conservation and Storage, MRSI-2007, Page 102.
13. Highly Photosensitive Wide Bandgap Thin Film for Photovoltaic Application, **Meril Mathew**, C. Sudha Kartha and K. P. Vijayakumar,

National Conference on Current Trends in Materials Science, CTMS-2007, Page 167.

14. Role of Chlorine on opto-electronic properties of β-In_2S_3 thin films, Angel Susan Cherian, **Meril Mathew**, C Sudha Kartha, K P Vijayakumar, Proc. New Horizons in Theoretical and Experimental Physics-2007.
15. Deposition of Copper Indium Sulfide with widely varying optoelectronic properties by chemical spray pyrolysis, Tina Sebastian, T. T. John, **Meril Mathew**, Vijayakumar. K. P, C. Sudha Kartha, Proc. of 17th AGM of MRSI, Lucknow University-2006, Page 128.

Chapter 1

Buffer Layer for Thin Film Heterojunction Solar Cells

1.1 Introduction

The conversion of sunlight directly into electricity using the electronic properties of suitable materials appears to be an elegant energy conversion process and an ideal alternative to conventional energy sources. Being a laboratory curiosity for more than a hundred years, the solar cell technology has seen enormous development during the last four decades, initially for providing electrical power for spacecrafts and more recently for terrestrial applications. The driving force for this technological development is the realization that the traditional fossil energy resources such as coal, oil and gas are not only rapidly depleting, but also contribute to unpredictable and possibly irreversible climate changes in the near future through the high emission levels of greenhouse gases (e.g. CO2, CO, SO_2 and P_2O_5) and acidification. Moreover our energy infrastructure should be distributed and close to the source. The photovoltaic source of energy, i.e. solar irradiation, has the advantage of being widely distributed over the world. The solar irradiation impinging on the earth's surface is not a limiting factor and supersedes our needs by far.

Photovoltaic industry was leapfrogging the barriers in the last three decades from merely concepts to a full-fledged industry. Recent major investments and on hand manufacturing facilities are mainly for silicon based technologies, with over a 93% market share, due mainly to its maturity and huge government subsidies in countries such as Germany, the world's greatest user of solar energy. The incumbent now faces a fresh challenge by the new wave of thin-film technologies developed in last decade. Traditional silicon cell manufacturers are now constrained by the shortage, high prices, weight and fragility of silicon. Thin film solar cells (TFSC), using inorganic or organic compounds as active layers, represent the most promising technology for beating the cost of conventional silicon solar systems - both up front

cost (including transport and installation) and cost per watt. These technologies potentially provide variety of choices in device designing and fabrication. A choice of substrates (flexible or rigid, metal or insulator) can be made for deposition of different layers (contact, buffer, absorber, reflector, etc.) using diverse techniques (PVD, CVD, ECD, plasma-based, hybrid, etc.). Such versatility allows tailoring and engineering of the layers to improve device performance. The enormous potential of thin film solar cell (TFSC) technology to contribute to the overall photovoltaic (PV) portfolio has been the impetus for the present research.

1.1.1. Why Thin Film Materials?

To appreciate this query, we need to be acquainted about thin films. A thin film is a material created by the random nucleation and growth processes of individually condensing / reacting atomic / ionic / molecular species on a substrate. The structural, chemical, metallurgical and physical properties of such materials are strongly dependent on a number of deposition parameters and thickness. Thin-films encompass a considerable thickness range, varying from few nanometers to tens of micrometers and thus are best defined in terms of 'birth processes' rather than thickness. The atomistic random nucleation and growth processes bestow new exotic properties to thin-film materials [1]. These properties can be controlled and reproduced by precisely modulating a range of deposition parameters [2]

The following features of thin-film process were of interest in solar cell preparation technologies.

1. A variety of physical, chemical, electrochemical, plasma based and hybrid techniques are available for depositing thin-films of the same material.
2. Microstructure of the films of most materials can be varied from one extreme of amorphous/ nanocrystalline to highly oriented and/or epitaxial growth, depending on the technique, deposition parameters and substrate.
3. A wide choice of shapes, sizes, areas and substrates are available.

4. Because of relaxed solubility conditions and relaxed phase diagram, doping and alloying with even incompatible materials [in many cases] can be obtained.
5. Surface and grain boundaries can be passivated with suitable materials.
6. Different types of electronic junctions, single and tandem junctions, are feasible.
7. Graded bandgap, composition and lattice constants can be obtained to meet the requirements for a designer solar cell.
8. In case of multicomponent materials, composition, and hence bandgap and other optoelectronic properties, can be graded in desired manner.
9. Surfaces and interfaces can be modified to provide an interlayer diffusion barrier and surface electric field.
10. Surfaces can be modified to achieve desired optical reflectance/transmission characteristics, haze and optical trapping effects.
11. Integration of unit processes for manufacturing solar cells and integration of individual solar cells can be easily accomplished.
12. In many cases the energy requirement for the film deposition processes is much smaller than that required in silicon based process. Hence the 'energy pay back period' becomes shorter.
13. Besides conservation of energy and materials, thin-film processes are in general eco-friendly [For example, the Chemical Bath Deposition process accepted for depositing CdS window layer] and qualify as 'Green' processes.

Since all good things come for a price, the ability to tailor numerous properties of thin-films required for an efficient solar cell demands a good understanding of the material so produced with the help of a range of monitoring and analytic facilities.. Also the high sensitivity of film properties to deposition parameters can produce a multitude of undesired results. Thus it becomes evident that though thin

film photovoltaic devices are attractive, the materials and the deposition techniques need due care and understanding.

1.1.2. Thin-film solar cell devices

In principle, a solar cell is a junction device obtained by placing two electronically dissimilar materials together with a thin electronic barrier in between to separate the charges. However, efficient devices must ensure high conversion efficiency of solar photons and high collection efficiency of excited charge carriers. A variety of junctions such as Schottky barrier, homojunction and heterojunction have been studied. Junctions can be abrupt, graded, buried, heteroface, etc involving materials of different conductivity/ type of conductivity [3].

Thin film solar cells consist of layers of different materials in thin film form. In general, the solar cell consists of substrate to hold on the thin film layers, transparent conducting oxide (TCO) to draw the current to the outer circuit, buffer layer (*p* or *n* type) to create the junction with the absorber layer with minimum absorption losses and to drive the generated carries to the electrode, absorber layer (*i* or *p* type) for generating carriers on absorbing light with minimal transmission or reflection losses and metal contact layer as the bottom electrode. Each material has different physical and chemical properties and affects the overall performance of the device. A critical understanding of behavior of these individual components is essential for designing device. Also important are the interfaces between different layers, since each layer has different crystal structure, microstructure, lattice constant, electron affinity/work function, thermal expansion coefficient, diffusion coefficient, chemical affinity, mobility, mechanical adhesion etc, the interfaces can cause stress, defect and interface states, surface recombination centers, interdiffusion and chemical changes with attendant electro-optical changes.

In heterojunction solar cells absorber and the buffer layers are made of two different materials and this introduces a fair possibility of using materials having different band gaps. Buffer layer with a wider band gap could enhance the amount of light reaching the junction which is the main bottle neck in homojunction solar cells. Yet another advantage of heterojunction solar cells (p-n junction between different semiconductors) compared to homojunctions is that recombination in the wide band gap semiconductor is quite low. On the other hand, the risk from interface recombination is higher for heterojunction due to defects and imperfections at the junction. Buffer layer, in combination with other window layers can minimize the interface recombination losses and help to attain large band-bending.

1.2. The role of the Buffer layer in Thin Film Heterojunction Solar Cells

The primary function of a buffer layer in a heterojunction is to form a junction with the absorber layer while admitting a maximum amount of light to the junction region and absorber layer [4].In addition, this layer should have minimal absorption losses and should be capable of driving out the photogenerated carries with minimum recombination losses and transporting the photo generated carriers to the outer circuit with minimal electrical resistance. For high optical throughput with minimal resistive loss the bandgap of the window layer should be as high as possible and the layer should be as thin as possible to maintain low series resistance. It is also important that any potential ‘spike’ in the conduction band at the heterojunction be minimized for optimal minority carrier transport. Lattice mismatch (and consequent effects) at the junction is important for consideration for epitaxial or highly oriented layers. In the case of microcrystalline layers, mismatch varies spatially and thus the complicated effect, if any, averages out. The requirements are listed below.

(i) Large energy band gap for high optical transmission in the visible region: Novel p-type material like CuI with a band gap of 2.9 eV may even outperform traditional CdS material (E_g = 2.4 eV) from this point of view.

(ii) Optimal band discontinuities: Ideal solar cell junction will separate electrons and holes, letting through only one carrier type. This may be achieved if the energy band discontinuity, between the wide band gap buffer layer and the absorber material, is distributed in such a way that there is no band offset for the minority carriers. However, there should be a large barrier for majority carrier. The second condition is fulfilled if the first is fulfilled, provided the difference between the band gaps is significant. If there is a band offset for the minority carriers in the buffer layer, then it may lead to the formation of 'spike' or a 'cliff', depending on sign of the offset. If the band offset produces a cliff, probability of the interface cross-recombination is increased, and flat band condition is achieved at bias smaller than E_g/q of the absorber [5]. One consequence is that output voltage of the cell is limited in this case, because of the lack of barrier height. Band alignment with a moderate spike is rather optimal, although the presence of a spike means the band offset for the minority carrier decreases and the interface becomes less selective. In a more general case even a moderate spike may be dangerous as far as efficiency is concerned. Band discontinuities are usually studied using photoemission spectroscopy. Recent measurement using X-ray photoemission spectroscopy of the valence band discontinuity at $CuInS_2$/CuI interface resulted in virtually no band offset [6], making this material combination attractive for solar cell applications.

(iii) Lattice mismatch (and consequent effects) at the junction is important for consideration for epitaxial or highly oriented layers. In the case of microcrystalline layers, mismatch varies spatially and thus the complicated effect, if any, is averaged out.

(iv) Doping density in the buffer layer has to sufficiently exceed than the absorber in order to confine the space charge region at absorber, where its

electric field helps to separate charge carriers [7]. Moreover larger doping density in the buffer layer is necessary to suppress the minority carrier generation in order to reduce the bucking current density and to hold the Fermi level away from the middle of the band gap at the interface in order to suppress the interface recombination. However, strongly doped buffer layer material or buffer material with a doping limitation can induce the tunneling-enhanced interface recombination current [8] if there is a corresponding doping limitation in the absorber or in the presence of a spike band alignment.

(v) Interestingly the oldest and only well studied buffer layer material is CdS. Work on cells using CdS started in 1954, almost at the same time work on silicon started. But people are now trying to avoid cadmium containing materials.

1.2.1. Critical role of the buffer layer

Efficiency gain of the thin film solar cells greatly depends upon the quality and thickness of the buffer layer. The standard CIS solar cell needs optimized thickness of buffer layer between the absorber layer and the transparent front contact layer to improve efficiency. It drives out the photo generated carriers with minimal losses while coupling light to the junction with minimum absorption losses, yielding a highly efficient solar cell. Thin film heterojunction solar cells provide more light towards the junction as it has wide band gap buffer layer in contrast with optimal low bandgap absorber layer. This provides the most reliable way of increasing the efficiency of the cell. The beneficial effects of the buffer layer ranges from modifying the absorber surface chemistry to protecting the sensitive interface during the subsequent window deposition [9]. Favorable properties of the interface are suggested to be related to the match between lattice parameters.

The current understanding is that candidates for buffer material should hold wider bandgap for limited light absorption. The process for deposition should have a capability to passivate the surface states of the absorber layer and should provide an alignment of the conduction band with the absorber to yield better efficiency. Binary sulfides, oxides and oxy-sulfides are frequently investigated as potential Cd-free buffer layers.

Buffer layers also enhance the durability of the cell as the absorber is usually sensitive and needs protection during the impact of ions while sputtering the intrinsic and doped TCO layers. Furthermore, the absorber film becomes better suited for air exposure when protected by a buffer layer.

1.2.2. The state of the art

The commercially available CdTe or CIGS solar cells use CdS as the buffer layer, deposited by chemical bath deposition [10,11] (CBD) technique. This provides a superior device performance compared to that deposited by physical vapour deposition (PVD) techniques partly due to the improvement in the interface chemistry between CdTe/CIGS and CdS during the chemical process.

In most laboratories, the standard device structure of Cu(In,Ga)Se2 (CIGS) based solar cells includes a very thin CdS buffer layer deposited using CBD technique between the CIGS absorber layer and the transparent front electrode. The beneficial effects of the buffer layer range from modifying the absorber (CIGS) surface chemistry to protecting the sensitive interface during the subsequent window deposition [12]. In the last decade, serious efforts to substitute the CdS buffer layer by other nontoxic low-absorbing materials have been made for the following reasons:

(a) The expected environmental risks arising from implementation of a CBD CdS process in a CIGS module production line. A risk assessment of the environmental implications is given in Ref. [11].

(b) The potential of increasing current generation in the spectral region of 350–550 nm thereby increasing the cell efficiency.

(c) The prohibition of cadmium in electrical or electronic equipment by legal regulations in different countries which can be a marketing problem for Cd-containing CIGS-based thin-film modules [13].

1. 2. 3. Bottle neck for thin film photovoltaics- Toxicity of cadmium

A non-toxic photovoltaic technology poses fewer issues than a toxic technology and would clearly be a superior choice provided other aspects are the same. The present strengths of CdTe in terms of its manufacturing robustness and low capital cost of deposition equipment are blinding the impact of toxicity. Recently "First Solar" the largest manufacturer of CdTe modules, announced an insurance policy approach for funding the estimated future costs of reclaiming and recycling their modules at the end of its use [14]. This addresses the concern about large number of disowned modules containing toxic materials getting accumulated in the environment [15].

Under present European legislation, thin film solar cells (both CISe/S and CdTe) containing Cd in concentration greater than 0.1% by weight of Cd in a unit (that cannot be mechanically disjointed) are banned from sale on the European market from 1 July, 2006. While photovoltaic consumer products are covered by the impending legislation, photovoltaic modules are exempted with the condition that such exemption to be reviewed at least every 4 years [16]. Exemptions may be given when it is likely that the elimination or substitution of the cadmium causes an increase in the environmental health and/or consumer safety impact [16].

Non-toxicity will ensure that the future progress of technology is not impeded by the increasingly stringent legislation relating to the use and disposal of toxic material. The potential of indium sulfide as an alternative to CdS buffer layer assumes greater significance under this scenario.

1.3. Alternative buffer layers

The development of Cd free devices which flagged of in 1992 with an efficiency level of about 9% has progressed to the current status of 18–19.9% efficiency. Comparing with CdS buffer layer, the initial difference of 4% absolute has been erased to the current negligible level. The present understanding is that candidates for alternative buffer material should hold four common properties:

i. The material should be n-type in order to form a p-n junction with the absorber layer.
ii. The bandgap should be wide for limited light absorption.
iii. The process for deposition should be low cost and suitable for wide area deposition. In addition the technique should have capability to passivate the surface states of the absorber layer.
iv. The process and material choice of the buffer layer should provide an alignment of the conduction band with the Cu(In,Ga)Se2 absorber with a *E*C of 0 – 0.4.

Further in this chapter, we report the technical progress that has occurred in the last decade in the development of Cd-free buffer layers for Cu(In,Ga)Se_2-based thin-film solar cells and modules. In different laboratories, films based on ZnS, ZnSe, ZnO, (Zn,Mg)O, $In(OH)_3$, In_2S_3, In_2Se_3 and $InZnSe_x$ were deposited on differently processed absorbers and tested as an alternative to the traditional CdS buffer. The deposition methods used were: chemical bath deposition (CBD), atomic layer deposition (ALD), metal organic chemical vapour deposition (MOCVD), ion layer gas reaction (ILGAR), sputtering, thermal evaporation, and electrodeposition (ED). Quite a number of processes demonstrated efficiency comparable to CBD CdS standard.

All materials and methods which were successfully tested as an alternative to the CdS buffer could be amalgamated to yield a new option for buffer layer. Ten materials by eight methods theoretically result in 80 different possibilities for alternative buffer layer deposition. A closer look reveals that the materials used in

different laboratories are mainly chalcogenides (oxides, sulfides, and selenides) of two elements, zinc and indium. The composition of a buffer layer often depends on the deposition method and the preparation conditions. For example, the chemical bath deposition of sulfides and selenides normally yield films containing hydroxides and/ or oxides.

1.3.1. The ZnS-based buffer layer

The ZnS-based buffer layer is one of the most popular candidates for replacing the CBD CdS. This buffer demonstrated the highest CIGS-based solar cell efficiencies, is nontoxic and is relatively less costly. So far, four different deposition techniques were used: ALD, ILGAR, evaporation and CBD with latter proving to be most successful.

Chemical bath deposition (CBD)

The development of the CBD ZnS-based buffer started at ENSCP (Ecole Nationale Supe´rieure de Chimie de Paris), Centre National de la Recherche Scientific Laboratoire d'Electrochimie et de Chimie Analytique (France) and IPE (Institut for Physikalische Elektronik, Stuttgart University ,Germany) in 1992 with an efficiency level of 9–10% [17, 18]. Years later, in 1996, "Showa Shell" demonstrated a 12.8% efficient cell with an oxide-containing ZnS buffer [19]. This result began a new wave in the development of the CBD ZnS buffer. Thereafter, two different deposition paths arose. One is based on the Showa Shell process and led to an efficiency level of 14–15%. The other path, developed at the Aoyama Gakuin University, Japan (AGU) led to an efficiency level of 17–19%. A comparison of the Showa and the Nakada process showed that discrepancy in the efficiency level between the two processes was due to the difference in the absorber layer used. Showa Shell absorbers are $Cu(In,Ga)(Se,S)_2$ prepared by selenization /sulfurization of sputtered precursor metal films and AGU absorbers are $Cu(In,Ga)Se_2$ prepared by the three-stage process. The latter process

generally results in higher cell efficiencies. Comparing the buffer layer deposition conditions, the most important difference is the ammonia concentration. While the Showa Shell concentration ranges between 1 and 3 M, the 8 M in the Nakada process is extremely high. Both processes led to world-record efficiencies. Showa Shell already introduced CBD-ZnS as the new standard. Several 30X30 cm^2 modules were fabricated and a record efficiency of 14.2% on 900 cm^2 was demonstrated. Later, National Renewable Energy Laboratory, USA (NREL) together with AGU, realized an 18.6% total-area world-record cell.

In earlier publications, both AGU [20] and Showa Shell [22] reported a light-soaking effect (LS) for cells with CBD ZnS-based buffer. Also the conducting band offset (CBO) of evaporated ZnS on $CuInSe_2$ was measured to be 1.58 eV [23]. This high value was considered as a problem for the realization of highly efficient cells

Atomic layer deposition (ALD)

First device with an ALD ZnS-based buffer was realized at ENSCP on standard in-line-evaporated absorbers from ZSW (Zentrum fqr Sonnenenergie- und Wasserstoff-Forschung, Germany) [24]. Using the precursors $(CH_3)_2Zn$, and H_2S and by varying the ratio between water and H_2S pulses ZnS_xO_{1-x} films with x=0–1 were grown. Pure ZnS buffer gives the highest V_{OC}, but the fill factor and current densities are low, resulting in poor overall efficiency. The best reproducibility and efficiencies of 10.4% were obtained for about 7% H_2S pulses. A total-area solar cell efficiency of 16% was demonstrated with a few-nanometer thin ZnS_xO_{1-x} buffer deposited with 20% H_2S pulses.

A very important parameter for the device performance is the absorber storage history before the ALD process, which also influences the incubation time for ZnS_xO_{1-x} growth. The highest-efficiency devices were obtained for CIGS samples stored in vacuum.

Ion layer gas reaction (ILGAR)

ILGAR is a comparatively novel deposition technique developed by HMI (Hahn Meitner Institut, Berlin, Germany) for the deposition of buffer layers on $Cu(In,Ga)(S,Se)_2$ absorbers from Siemens/Shell Solar [25]. A chemical pre-treatment of the absorber in a zinc salt bath is shown to significantly improve the solar cell device performance. The highest reported total-area cell efficiency with an ILGAR ZnS-based buffer is 14.2%.

The evaporation or co evaporation of ZnS-based buffers was very interesting from a technological point of view. However, initial results demonstrated poor device efficiencies of 9% [26].

1.3.2. The ZnSe-based buffer layer

The progress of the ZnSe-based buffer layer is dominated by the processes CBD and MOCVD or Metal Organic Vapour Phase Epitaxy (MOVPE). The CBD method was optimized at HMI using the chemicals Zn-salt/ammonia/selenourea and $Cu(In,Ga)(Se,S)_2$ absorbers from Siemens/Shell Solar. A maximum active-area efficiency of 15.7% [27] or a total area efficiency of 14.4% [28] was achieved. Regarding the technological implementation of the CBD ZnSe process, the limited stability of the selenourea (and its high price) could be a deterrent.

The MOCVD or MOVPE ZnSe buffer is being developed by DESR (Department of Energy and Semiconductor Research, Faculty of Physics, University of Oldenburg, Germany), IAP (Institute for Applied Physics, University of Regensburg, Germany), HMI and Shell Siemens Solar. The efficiency level is about 3% absolutely lower compared to CBD ZnSe. The best demonstrated cell efficiency is 12.6% [29, 30]. The ALD ZnSe buffer is developed by TIT (Tokyo Institute of Technology, Japan) and Showa Shell in 1995–1996, achieved a peak efficiency of 11.5% [31]. However, the work has been discontinued.

The evaporated or co-evaporated ZnSe buffer is limited by the low efficiencies of about 9% [26, 31]. The extremely low thickness needed for highly efficient devices is remarkable for the ZnSe buffer. In most publications, independent of the deposition technique, the reported optimum ZnSe thickness is in the range of 5–10 nm. It is not reported whether an ultra thin ZnSe buffer is an issue for the long-term stability of the CIGS-based cells.

1.3.3. The ZnO and the ZnMgO buffer layers

Devices with MOCVD or a sputtered ZnO buffer can also be interpreted as buffer-free cells when the ZnO window is directly deposited on CIGS by MOCVD or sputtering respectively. From a technological point of view, this is advantageous for reducing costs, because it eliminates an additional buffer layer deposition step by a different technology. Different techniques were used to grow a ZnO buffer layer [ALD, electrodeposition (ED), MOCVD, CBD, ILGAR, and sputtering] in the last decade. The results were not so promising.

A new development with a high potential to replace the CBD CdS buffer is the sputtered ZnMgO buffer. The best efficiency of 16.2% (active area) was achieved by Matsushita Electric Industrial [32]. At the moment, the potential of this high-band-gap material is under investigation [33, 34].

1.3.4. The $ZnInSe_x$ and $InSe_x$ buffer layers

Co-evaporation is the only reported method for the deposition of $InSe_x$ and $ZnInSe_x$. The buffer was continuously evaporated on CIGS. Most work is from Energy Photovoltaics and TIT. The maximum demonstrated cell efficiency is 13% for the $InSe_x$ buffer [35] and 15.3% for the $ZnInSe_x$ buffer [36, 37].

1.3.5. The In_2S_3 and $In(OH)_3$ based buffer layer

The high demonstrated efficiencies, comparable to the CBD CdS standard, make In-based buffers very interesting alternative. Progress achieved by the different growth methods (CBD, ALD, evaporation, and sputtering) are mentioned below.

Chemical bath deposition of $In(OH)_3/In_2S_3$

Development of the CBD In_2S_3-based buffer started at IPE with the $In(OH)_3$ deposition. The $In(OH)_3$ buffer grown in an $InCl_3$/thiourea solution led to a cell efficiency of 9.5% [38]. Replacing thiourea by thioacetamide caused the formation of an oxide hydroxide-containing indium sulfide buffer, and shifted the device efficiency to 15.7% (active area) [39].

Using the CBD In_2S_3-based buffer, 30X30 cm^2 modules were fabricated with efficiencies up to 9.7% [40]. Investigations on growth mechanism of CBD-In_2S_3 films were performed by CIEMAT (Departamento de Energı´as Renovables, Centro de Investigaciones Energe´ticas Medioambientales y Tecnolo´ gicas, Madrid, Spain) [41]. However, these cells and modules exhibited a light soaking effect. The highest efficiency was reached after annealing and illumination. After indoor storage, the fill factor dropped by around 30% and the cell required at least 30 minutes of further illumination to regain the initial fill factor value [42]. These metastability effects were examined by Nguyen et al. [43, 44]. The origin for this behavior was traced to the presence of acceptor defects at the CBD In_2S_3/ZnO interface. All cells with non- CdS buffer materials which are sensitive to light-soaking also exhibit the reverse bias effect [45].

The chemical bath deposition of $In(OH)_3$ buffers was carried out in an $InCl_3/ZnCl_2$/ thiourea solution, producing $In(OH)_3:Zn^{2+}$ films. These films were used as buffers on both sequentially grown $Cu(In,Ga)(Se,S)_2$ [46] and three-stage-process $Cu(In,Ga)Se_2$ absorbers [47] leading to cell efficiencies up to 14.0% without the light-soaking effect.

Atomic layer deposition (ALD) of In_2S_3

Development of the ALD In_2S_3 buffer began as cooperation between ENSCP and ASM Microchemistry, and was continued by ENSCP with ZSW. The best efficiencies realized with the ALD In_2S_3 buffer on in-line evaporated CIGS substrates from the ZSW or WS (Wqrth Solar GmbH and Co. KG, Germany) line were 16.4% for a laboratory cell [48] and 12.9% for a certified 30X30 cm^2 module [49].

Variation of deposition temperature during the ALD process and annealing experiments indicated a significant influence of temperature on the performance of the Cd-free devices. The initial efficiency was in the range of 11% and strongly improved to an efficiency level of 15.5% after post-annealing at 200 ^{0}C in air for 2 hours. The post-annealing time reduced with increased deposition temperature and was even eliminated when the intrinsic ZnO layer was deposited at the elevated temperature of 200 ^{0}C.

Depth profile analyses were performed on the CIGS/ALD In_2S_3 interface in order to investigate diffusion processes at different deposition temperatures. Significant interface diffusion of Cu, Na and Ga was observed for high deposition temperature (210 ^{0}C) and/or annealed devices [49]. XPS surface analysis on 50- nm ALD In_2S_3 layers on CIGS devices confirmed the diffusion of Cu and Na at high deposition temperatures. Abou-Ras et al. [50] analyzed the CIGS/ALD-In_2S_3 interface by means of high-resolution transmission electron microscopy. Cu diffusion from the CIGS into the In_2S_3 layer, and in addition, Cu depletion and In enrichment on the CIGS side of the interface were detected. These effects enhanced with increasing temperature and indicated the possibility of formation of a p–n homojunctions inside the CIGS.

The CIGS devices with ALD In_2S_3 did not show metastability behaviour [45]. No significant performance losses were observed for non-encapsulated 15X30 cm^2 modules even after a few months indoor storage. In addition, light-soaking did not affect the device performance [51]. Encapsulated 15X30 cm^2 modules were tested

according to the IEC 61646 in damp heat (1000 hr, 85 ^{0}C, and 85% relative humidity) the modules passed the test with less loss in the output power than the allowed limit of 5%.

Physical vapor deposition (PVD)

The vapour phase deposition technique can be easily upscaled for industrial production. Initial efforts were reported in 1997 on the In_2S_3 buffer layer deposition for CIGS devices by co evaporation of indium and sulphur. A cell efficiency of 11.2% was reached by the IPE at that time [52, 53, 54]. Cell efficiencies up to 12.4% were realized for a deposition temperature of 130 ^{0}C [55]. They found Cu diffusion into the buffer layer strongly depends on the deposition temperature, and infer the formation of an n-type $CuIn_5S_8$ phase in the buffer layer. For higher deposition temperatures (200 ^{0}C), the quality of the CIGS devices is much lower, an effect ascribed to the formation of a p-type $CuInS_2$ phase. A different approach was recently performed at the IPE by buffer deposition via direct evaporation of In_2S_3 powder. A cell efficiency of 14.8% could be realized with this technique [56]. The reason for the difference in the performance of CIGS devices with co evaporated or direct-evaporated buffer layers are not yet fully investigated. XRD data and SEM images indicate a distorted structure of the co evaporated In_xS_v layer, whereas the direct-evaporated layer was not distorted. Furthermore, XPS analyses detected a significant loss of S in the evaporated In_2S_3 powder, changing its stoichiometry after a few deposition runs.

1.4. Motivation for the present work

The contradiction of using heavy metals in environmentally benign energy systems and the hazardous handling of cadmium during manufacturing needle CIS solar cell industry provided the impetus to find a replacement for the CdS buffer material. Besides, the replacement of CdS by buffer material of larger bandgap is motivated by the reduced light absorption of these layers. The current loss of

$Cu(In,Ga)Se_2$ device caused by the CdS film is estimated to be in the order of 1 mA/cm^2 [57].

The standard $Cu(In,Ga)Se_2$ based solar cell contains about 50 nm thick CdS buffer layer between the absorber layer and the transparent front contact layer, to improve efficiency. Although a number of different wide bandgap materials have been investigated such as Zn(OS), Zn(OH,S), ZnO, ZnS, ZnSe, In_2S_3, $In(OH)_3$, $In(OH,S)_3$, etc. [29,30], best performance is achieved using the CdS buffer material. This is contrary to the fact that a performance gain is expected for wider bandgap material due to a lower light absorption. This strengthens the argument that the alternate buffer layers are not yet optimized to grab its full potential.

As the world of thin film solar cells started to look towards indium sulfide as the future buffer layer and potential competent to CdS, reservations have surfaced on the availability and the inflated price of indium. This futile concern was overruled by the data disclosed by Indium Corporation during 2007 European photovoltaic conference [58]. The availability of indium is estimated to be 0.05 ppm and 0.072ppm on the continental and oceanic crust respectively (Taylor and Mclennan 1985 [59]). This is higher than the concentration of silver. In addition, the annual output of silver is around 20,000 tons compared to 400 tons of indium. These suggest that supply limitations would hardly hinder the vast growth potential of indium [58].

For large-area, thin-film device fabrication becomes complex and requires proper control over the entire process sequence. Proper understanding of thin-film deposition processes can help in achieving high-efficiency devices. Research and development in new, exotic and simple materials and innovative as well as cost effective processes for the development of devices, are to be pursued in a focused manner. Which cell(s) and which technologies will ultimately succeed commercially continue to be anybody's guess, but it would surely be determined by the simplicity of manufacturing process and cost per reliable watt. Cheap and moderately efficient TFSC are expected to receive a due commercial place under the sun. In the present

study, indium sulfide films were prepared by chemical spray pyrolysis (CSP) technique which is benefited by low production cost. The upscaling of this technology for industrial implementation is possible due its lenience towards large area deposition. Compared to other thin film deposition techniques, input of energy for manufacturing is relatively low in CSP. This will shorten the energy pay back time, defined as the time it takes until the photo-generated energy output equals the energy that was consumed to produce the device. Specific advantages of the CSP and its wide possible adaptations towards compositional variations could be used to amend the properties of In_2S_3 as an ideal buffer layer.

1.4.1. Beyond 20% Efficiency

Summarizing the features of thin film solar cells, further improvements look obvious if we could incorporate the better understanding of the material into developing appropriate technologies.

The maximum efficiency one can reach with the conventional solar cell structure is given by the so-called single material or Schockley-Queisser [60] limit. Using a detailed balance approach, assuming that each photon above bandgap gives rise to just one electron-hole pair, while all photons with energy below the bandgap is lost, one comes to a theoretical maximum energy conversion efficiency of about 30 %. This is relatively low, mainly because of the thermalization and transmission losses, which account for around 56% loss of photon energy.

It would be erroneous to consider Shockley-Queisser limit as the ultimate achievable limit with photovoltaics. The physical limit Could be much higher. Considering the Sun as a black body at 5760 K and solar cell (another black body) at 300 K, the Carnot efficiency limit is 95%. Landsberg and Baruch [61] calculated energy conversion limit of 93.3%, in which radiative losses from the solar cell was also considered. Taking into account entropy generation during the energy conversion, one obtains a black body limit of about 86%. Efficiencies of this magnitude seems

possible by using monochromatic filter with an ideal solar cell wherein the cell band gap is matched with the non-filtered frequency.

The large difference between the Shockley-Queisser and the thermodynamic limit arises from the fact that a single material is characterized by only two energy levels, whereas the solar spectrum contains photons with a wide range of energies. Devices that rely on a single transition between energy levels are intrinsically ill-suited for the broad spectrum of sunlight. The need is to make more effective use of solar spectrum. Different concepts have been proposed to overcome the Shockley-Queisser limit of light conversion efficiency. The concepts are based on splitting of sun light in to beams of different energies which are then absorbed by many cells (e.g. multijunction solar cells) or by adopting solar spectrum for one host material (e.g. up and down-conversion of photon energy) or by the reduction in thermalisation losses (e.g. hot carrier cells).

The impurity photovoltaic (IPV) effect is the idea of exploiting two-step generation via impurity states within the band gap to utilize sub-band gap photons and thus enhance solar cell performance (see Fig. 1.1(a)). Three transitions available in that system, in principle, enable a better matching to the solar spectrum. High efficiencies have been predicted for IPV solar cells. The challenge is to find a suitable semiconductor with sufficiently wide band gap and having radiative efficient impurity [62]. A related concept is the so-called “intermediate-band (IB) solar cell”, characterized by the existence of a narrow band within the main band gap (see Fig. 1.1(b)). For this concept, experimental work has been carried out using the InAs quantum dots embedded in GaAs [63]. Evidence of generation from sub-band gap was found. However, the concept is still far from enabling an efficiency increase above conventional cells. The limiting solar cell efficiency for single impurity level and single intermediate band gap is above 63% [64, 65] which is same as the limiting efficiency of stacked solar cells (three). Main advantage in IPV and IB concepts is that

the same material is used throughout and the interconnection between cells occurs automatically.

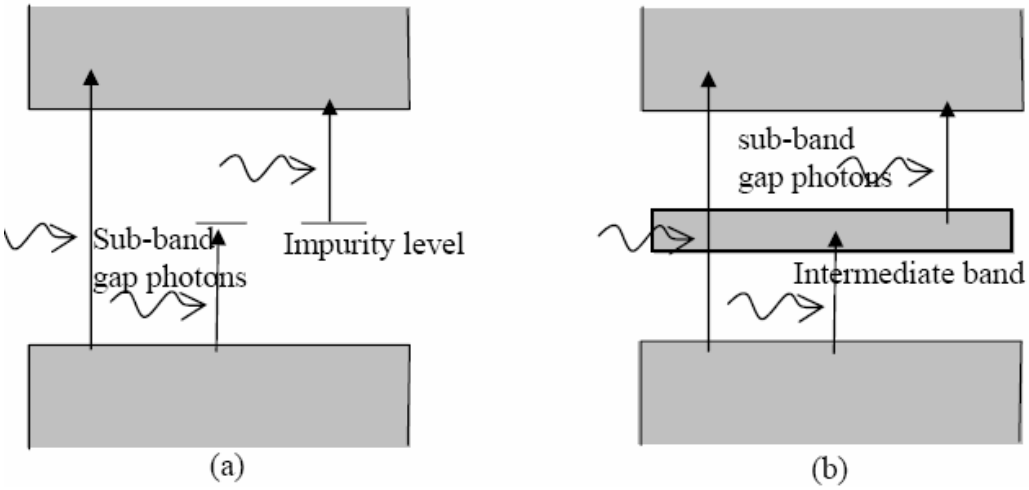

Fig.1.1: Schematic diagram showing absorption of above band gap and sub-band gap photons through, (a) impurity level, (b) intermediate band

Defective structure of indium sulfide has shown tolerance towards incorporation of dopants which provide space for the impurity photovoltaic effect in tuning the properties to realize an ideal buffer layer. This along with the environmental benefits achieved while using as the buffer layer, endowed the motivation to take all efforts in realizing an ideal Cd-free buffer layer for thin film solar cells, by tuning the properties of indium sulfide through doping.

References

[1] Chopra KL. Thin-Film Phenomena. McGraw-Hill: New York, (1969).

[2] K. L. Chopra, P. D. Paulson and V. Dutta, Prog. Photovolt: Res. Appl. **12** (2004) 69–92.

[3] Fahrenbruch AL, RH. Bube, Fundamentals of Solar Cells. Academic Press: New York, (1983).

[4] McCandless BE, Hegedus SS. Proc. of the 22th IEEE Photovoltaic Specialists Conference, (1991) 967–972.

[5] A. Niemegeers, M. Burgelman and A. De Vos, Appl. Phys. Lett. **67** (1995) 843.

[6] I. Konovalov and R. Szargan. Appl. Phys. Lett. **82** (2003) 2088.

[7] R. Klenk, Thin Solid Films **387** (2001) 135.

[8] U. Rau Appl. Phys. Lett. **74** (1999) 111.

[9] Jan Sterner, Comprehensive Summaries of Uppsala Dissertations from the Faculty of Science and Technology **942** (2004) 14.

[10] M. Powalla, B. Dimmler, R. Schaeffler, G. Voorwinden, U. Stein, H.-D. Mohring, F. Kessler, D. Hariskos, Proc. 19th European Photovoltaic Solar Energy Conference Paris, France, (2004).

[11] K.M. Hynes, J. Newham, Proc. 16th European Photovoltaic Solar Energy Conference, (2000) p. 2297.

[12] H.W. Schock, R. Noufi, Prog. Photovolt. Res. Appl. **8** (2000)151.

[13] Directive 2002/96/EC of the European parliament and of the council of 27 January 2003 on waste electrical and electronic equipment (WEEE), Official Journal of the European Union (2003) L37/24.

[14] First Solar Announces Insurance Policy to Fund Solar Module Reclamation and Recycling Expenses at End of Product Life in First Solar Press Release, May, 2005 (http://www.firstsolar.com.).

[15] D. Hariskos, S. Spiering, M. Powalla, Thin Solid Films **480–481** (2005) 99–109.

[16] de Wild MJ, Wamback K, Alsema EA, Ja¨ger-Waldau A. Conference Record, 20th European Photovoltaic Solar Energy Conference, Barcelona, (2005) 3143.

[17] R. Ortega Borges, D. Lincot, J. Vedel, Proc. 11th European Photovoltaic Solar Energy Conference, Montreux, Switzerland, (1992) 862.

[18] J. Kessler, M. Ruckh, D. Hariskos, U. Rqhle, R. Menner, H.W. Schock, Proc. 23rd IEEE Photovoltaic Specialist Conference, (1993) 447.

[19] K. Kushiya, T. Nii, I. Sugiyama, Y. Sata, Y. Inamori, H. Takeshita, Jpn. J. Appl. Phys. **35** (1996) 4383.

[20] T. Nakada, K. Furumi, A. Kunioka, IEEE Trans. Electron Devices **46** (1999) 2093.

[21] T. Nakada, M. Hongo, E. Hayashi, Thin Solid Films **431–432** (2003) 242.

[22] K. Kushiya, O. Yamase, Jpn. J. Appl. Phys. **39** (2000) 2577.

[23] D. Schmid, M. Ruckh, F. Grunwald, H.W. Schock, J. Appl. Phys. **73** (1993) 2902.

[24] E.B. Yousfi, T. Asikainen, V. Pietu, P. Cowache, M. Powalla, D. Lincot, Thin Solid Films **361–362** (2000) 183.

[25] H.-J. Muffler, M. Baer, C.-H. Fischer, R. Gay, F. Karg, M.C. Lux- Steiner, Proc. 28th IEEE Photovoltaic Specialist Conference, Anchorage, Alaska, USA, (2000) 610.

[26] A. Romeo, R. Gysel, S. Buzzi, D. Abou-Ras, D.L. B7tzner, D. Rudmann, H. Zogg, A.N. Tiwari, Proc. 14th Photovoltaic Science and Engineering Conference (PVSEC-14) (2004) 705.

[27] A. Ennaoui, S. Siebentritt, M.Ch. Lux-Steiner, W. Riedl, F. Karg, Sol. Energy Mater. Sol. Cells **67** (2001) 31.

[28] W. Eisele, A. Ennaoui, P. Schubert-Bischoff, M. Giersig, C. Pettenkofer, J. Krauser, M. Lux-Steiner, S. Zweigart, F. Karg, Sol. Energy Mater. Sol. Cells **75** (2003) 17.

[29] M. Munzel, C. Deibel, V. Dyakonov, J. Parisi, W. Riedl, F. Karg, Thin Solid Films **387** (2001) 231.

[30] F. Engelhardt, L. Bornemann, M. Kfntges, Th. Meyer, J. Parisi, E. Pschorr-Schoberer, B. Hahn, W. Gebhardt, W. Riedl, U. Rau, Prog. Photovolt. Res. Appl. **7** (1999) 423

[31] Y. Ohtake, K. Kushiya, M. Ichikawa, A. Yamada, M. Konagai, Jpn. J. Appl. Phys. **34** (1995) 5949.

[32] T. Negami, T. Aoyagi, T. Satoh, S. Shimakawa, S. Hayashi, Y. Hashimoto, Proc. 29th IEEE Photovoltaic Specialist Conference, New Orleans, USA, 2002, p. 656.

[33] Th. Glatzel, H. Steigert, R. Klenk, M.Ch. Lux-Steiner, T.P. Niesen, S. Visbeck, Proc. 14th Photovoltaic Science and Engineering Conference (PVSEC-14), (2004) 707.

[34] S. Visbeck, K. Stiegberger, T.P. Niesen, J. Palm, V. Probst, F. Karg, Presented at the EMRS Spring Meeting, Strasbourg, (2004).

[35] M. Konagai, Y. Ohtake, T. Okamoto, Mater. Res. Soc. Symp. Proc. **426** (1996) 153.

[36] S. Chaisitsak, Y. Tokita, H. Miyazaki, R. Mikami, A. Yamada, M. Konagai, Proc. 17th European Photovoltaic Solar Energy Conference, Munich, Germany, (2001) 1011.

[37] A. Yamada, S. Chaisitsak, Y. Othake, M. Konagai, Proc. 2nd World Conference of Photovoltaic Energy Conversion, Vienna, Austria, (1998) 1177.

[38] K.O. Velthaus, J. Kessler, M. Ruckh, D. Schmid, H.W. Schock, Proc. 11th European Photovoltaic Solar Energy Conference, Montreux, Switzerland, (1992) 842.

[39] D. Hariskos, M. Ruckh, U. Rqhle, T. Walter, H.W. Schock, J. Hedstrfm, L. Stolt, Sol. Energy Mater. Sol. Cells **41–42** (1996) 345.

[40] B. Dimmler, E. Gross, D. Hariskos, F. Kessler, E. Lotter, M. Powalla, J. Springer, U. Stein, G. Voorwinden, M. Gaeng, S. Schleicher, Proc. 2nd World Conference of Photovoltaic Energy Conversion, (1998) 419.

[41] Rocı´o Bayo´n, Jose´ Herrero, Res. Soc. Symp. Proc. **668** (2001) H8.3.1.

[42] D. Hariskos, R. Herberholz, M. Ruckh, U. Rqhle, R. Sch7ffler, H.W. Schock, Proc. 13th European Photovoltaic Solar Energy Conference, Nice, France (1995) 1995.

[43] Q. Nguyen, U. Rau, M. Mamor, K. Orgassa, H.W. Schock, J.H. Werner, Proc. 17th European Photovoltaic Solar Energy Conference, (2001) 1107.

[44] Q. Nguyen, K. Orgassa, I. Koetschau, U. Rau, H.W. Schock, Thin Solid Films **431–432** (2003) 330.

[45] U. Rau, K. Weinert, Q. Nguyen, M. Mamor, G. Hanna, A. Jasenek, H.W. Schock, Mater. Res. Soc. Proc. **668** (2001) H9.1.1.

[46] Y. Tokita, S. Chaisitsak, H. Miyazaki, R. Mikami, A. Yamada, M. Konagai, Jpn. J. Appl. Phys. **41** (2002) 7407.

[47] Y. Tokita, S. Chaisitsak, A. Yamada, M. Konagai, Sol. Energy Mater. Sol. Cells **75** (2003) 9.

[48] N. Naghavi, S. Spiering, M. Powalla, B. Cavana, D. Lincot, Prog. Photovolt. Res. Appl. **11** (2003) 437.

[49] S. Spiering, A. Eicke, D. Hariskos, M. Powalla, N. Naghavi, D. Lincot, Thin Solid Films **451–452** (2004) 562.

[50] D. Abou-Ras, H. Heinrich, G. Kostorz, M. Powalla, S. Spiering, A.N. Tiwari, Proc. 19th European Photovoltaic Solar Energy Conference, (2004).

[51] S. Spiering, D. Hariskos, S. Schrfder, M. Powalla, Proc. EMRS Spring Meeting, Strasbourg, (2004) .

[52] F. Karg, H.A. Aulich, W. Riedl, Proc. 14th European Photovoltaic Solar Energy Conference, Barcelona,(1997) 2012.

[53] N. Barreau, J.C. Bernede, S. Marsillac, C. Amory, W.N. Shafarman, Thin Solid Films **431–432** (2003) 326 .

[54] N. Barreau, S. Marsillac, D. Albertini, J.C. Bernede, Thin Solid Films **403–404** (2002) 331.

[55] S. Gall, N. Barreau, S. Harel, J.C. Berne`de, J. Kessler, Proc. EMRS Spring Meeting (2004).

[56] A. Strohm, L. Eisenmann, R.K. Gebhardt, A. Harding, T. Schlftzer, D. Abou-Ras, H.W. Schock, Proc. E-MRS Spring Meeting (2004).

[57] K. Orgassa, U. Rau, Q. Nguyen, H. W. Schock, and J. H. Werner, Progress in Photovoltaics: Research and Applications **10 (7)** (2002) 457.

[58] Gregory Phipps, Claire Mikolajczak, Terry Guckes, Indium Corporation Proc. 22nd European Photovoltaic Solar Energy Conference (2007) 3BV.5.20.

[59] Taylor SR and SM McLennan. The continental crust: its composition and Evolution. Blackwell, Oxford (1985).

[60] Shockley W., H. J. Queisser, J. Appl Phys., **32** (1961) 510-519.

[61] Beaucarne G., A. S. Brown, M. J. Keevers, R. Corkish, M. A. Green, Prog. Phot. Res. Appl. **10** (2002)345-353.

[62] Landsberg P.T., P. Baruch, J. Phys. A. **22** (1989)1911.

[63] Luque A., A. Marti, N. Lopez, E. Antolín, and E. Canovas, C. Stanley and C. Farmer, L.J. Caballero, L. Cuadra, J.L. Balenzategui, App.Phys. Letters **87** (2005) 083505.

[64] Luque A., A. Marti, Physical Rev. Lett. **78** (1997) 5014-5017.

[65] Green M.A., A.S. Brown, J. Appl. Phys. **92** (2002) 1329-1326.

Chapter 2
Indium Sulfide: A Review

2.1 Introduction

Indium sulfide (In_2S_3) is an important material for optoelectronic and photovoltaic applications and is a promising candidate for many technological applications due to its stability, wider band gap and photoconductive behavior [1]. This material is also having interesting photoluminescence properties [2], and hence finds large number of applications in optoelectronic devices [3]. It can be used as an effective nontoxic substitute for cadmium sulfide (CdS) in $Cu(In,Ga)Se_2$ based solar cells. This material not only eliminates toxic cadmium but also improve light transmission in the blue wavelength region on having band gap wider than that of CdS.

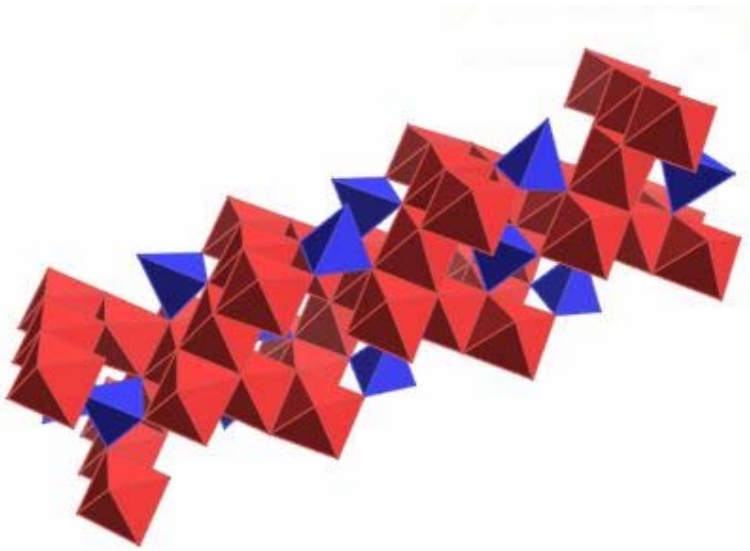

Fig. 2.1 Crystal structure of In_2S_3
(Indium atoms are in red colour and sulfur in blue colour)

The physical properties and structure of indium sulfide [Fig. 2.1] thin films are given below.

Structure	: Tetragonal
Colour	: Yellow
Appearance	: Crystalline solid
Melting Point	: 1050ºC
Density	: 4450 kg/m^3
Lattice Parameters	: a = b = 7.619 Å and c = 32.329 Å

2.2 Structure of In_2S_3

The structure of β-In_2S_3 has been determined by Hahn and Klinger [4] and was refined by Rooymans [5] and King [6].

Hahn and Klinger ascribed to it the cubic structure of a disordered cation deficient spinel. The structure of β-In_2S_3 has been studied by Rooymans using an x-ray powder technique. The powder pattern contained a large number of weak reflections which were attributed to a super-lattice based on a cation-deficient spinel structure. Rooymans found that the super-cell was body-centred tetragonal with $a = a'/\sqrt{2} = 7.62\ A^0$ and $c = 3a' = 32.32\ A^0$, a' being the parameter of the spinel-type cell from which the structure was derived. The absence of *00l* reflections with $l \neq 4n$ (*n* being an integer), and the assumption that the structure is essentially that of a spinel with 4 tetrahedrally coordinated cation vacancies per super-cell, suggested the four vacancies to be located at the equivalent positions of the 4_1 screw axes of the space group. However, Rooymans also mentioned that the structure might possibly have a lower symmetry because of the observation of a weak reflection at about 3.6 A^0 which was not reconcilable with a tetragonal lattice.

In order to maintain stoichiometry of In_2S_3, all interstices in the complete spinel are not occupied (occupancy of complete interstices would result in composition In_3S_4). This can be expressed by saying that vacancies are present in the lattice of tetrahedral interstices of the spinel structure. These vacancies are ordered along rows which are parallel to the close packed sulfur rows in the {111} planes [5]. As a result of the ordering, the cubic symmetry is lost making the crystal tetragonal with c/a = 3. The unit cell contains in fact three unit cells of the normal spinel, the [001] direction of the tetragonal lattice coinciding with one of the cube directions of the basic spinel. Thus the tetragonal unit cell was supposed to be formed by the superposition of three spinel blocks; a four-fold screw axis appeared as the result of indium vacancy ordering.

R.S Becker et al interpreted the ordered modification of β-In_2S_3 as a quasi-ternary compound consisting of In, S and 'vacancies'. Here eight of the twelve tetrahedral sites are occupied by indium and other four are empty (the latter are ordered). All octahedral sites are occupied by In and could be written as $In_6(In_2\square)S_{12}$, where □ indicates vacancies and parenthesis describes tetrahedral site [11]. J. Goodyear and G. A. Steigmann reported the twinning of the cation deficient spinel structure during redistribution of the tetrahedrally occupied sites [7].

C. Haas made theoretical predictions on phase transitions based on Landau's theory. Theoretically the transition was assumed to be first order [8]. H. Hatwell et al [9] owing to the observations in polarized light proposed that the lattice of tetrahedral indium ions undergoes some kind of "melting", [i.e. disordering], at 420 ° C [The actual melting point is 1100 °C] , whereas a second transition was noted at 750 ° C.. This second transition is presumably associated with the disordering of the octahedral indium ions. J. Van Landyut et al [10] reported that the indium ions in tetrahedral interstices disorder at 420° C whereas the indium ions in octahedral interstices disorder at 780° C. The order-disorder process was observed in the electron

microscope and different types of interfaces resulting from the ordering of indium ions (or indium vacancies) were studied.

Three well defined modifications of In_2S_3 have been reported in the literature. The cubic α-form [4] is stable above 693 K and crystallizes in the defect spinel structure (a = 10.77 Å). The stable room temperature phase is β-In_2S_3 [5]. A third modification (γ-In_2S_3) with trigonal symmetry has been reported above 1047 K [10].

2.3 Preparation Techniques

Variety of preparation techniques were reported for this material and some of them are discussed below.

2.3.1. Indium sulfide crystals

In_2S_3 crystals of α, β and γ form were synthesized by Diehl et al [12]. Ampoule was charged with elements of indium and sulfur in quantities corresponding to the stoichiometric composition. They found that growth temperature of 800ºC and sulfur vapour pressure of 4 atm were required to prevent dissociation of In_2S_3 and to maintain stoichiometry. This was achieved by adding 80 mg of extra sulfur in a volume of 25 cm^3. Iodine was used as the transport agent.

Kaito et al [13] prepared single crystals of β- In_2S_3 by the reaction of indium metal and sulfur vapour. Sulfur vapour was obtained by evaporating sulfur powder from quartz boat while Indium was evaporated from nichrom boat. β In_2S_3 particles grew as single crystal octahedra.

In_2S_3 crystals were grown by direct melting of stoichiometric mixtures of the components [14]. Stoichiometric quantities of high purity indium and sulfur were reacted in evacuated double-wall sealed silica tubes. Temperature of the furnace was raised to 800ºC in first step and then up to 1150ºC. Molten mixtures were held at this temperature for three days with occasional stirring for homogenization. The samples

were then cooled to about 10 K below the melting point (1050 ºC) and were kept at this temperature for a week. Two methods were used to cool the sample. In the first one, the tube was pulled out of the furnace progressively achieving a cooling rate of 0.5 K/h. Large surfaces of ordered crystals were obtained in this way. The second method of sample preparation consisted of rapid quenching of the ingot into ice water. Disordered crystals with random distribution of cation vacancies were produced by this procedure. Annealing in vacuum, to avoid oxidation, was performed for duration of three months at 400ºC just below the transformation temperature (420 ºC) between α and β- In_2S_3 modifications.

A novel layered indium sulfide material consisting of corner and edge shared InS_4 tetrahedra were synthesized under solvothermal conditions by Cahill et al [49]. DPA-InS-$SB_3$was synthesized by reacting elemental In and elemental S with the organic structure directing agent dypropylamine in the approximate molar ratio 1:2.3:3.5. Reactant slurries were sealed in pyrex tubes and held static at 180ºC under autogenous pressures for five days. The resultant product, a white powder, was then washed with ethanol and water and allowed to dry in air. Large single crystals up to 0.2 mm on edge were obtained. Qualitative electron probe microanalysis revealed the presence of In, S and N. The In-S bond lengths range from 2.42 to 2.534 Å with an average of 2.432 Å. Gorai et al [57] has also reported synthesis of Indium sulfide using a convenient solvothermal route. The X-ray diffraction analysis confirmed that 180 °C was the optimum temperature for the preparation. Scanning electron microscopic images showed that morphological patterns of the samples varied depending on the growth conditions.

2.3.2 Indium Sulfide Powder

Amorphous indium sulfide powder was prepared at relatively low temperatures (50 °C) from inorganic salts [16] using the reaction between acidified

(*pH* = 1.3) solution of indium chloride and sodium hydrosulfide (NaHS). Indium sulfide powder prepared by this process exhibited glass transition at 330 °C and a crystallization exotherm on heating at 390 °C in a DSC.

β-In_2S_3 powder with particles having an average size of 13 nm and spherical shape was successfully prepared through the hydrothermal treatment of an acidic sol (pH = 3) from indium trichloride and sodium sulfide at 140 ºC [3]. Hydrothermal treatment of alkaline sol gave amorphous In_2S_3 powder. The effects of temperature, time and the pH value of the solution on the formation of nanocrystalline β-In_2S_3 powder were investigated. Results showed that hydrothermal treatment of an acidic sol (pH = 3) at 140ºC for 6 to 12 h was the optimum condition for crystallization of amorphous In_2S_3.

Bulk indium sulfide was prepared by passing H_2S gas through a solution of indium chloride in water [39]. The precipitate, orange in colour, was washed several times with distilled water and then dried in desiccators. The powder thus formed was then vacuum deposited on different faces of rock salt, on the cleavage face of mica, polycrystalline NaCl tablets and also on the glass substrates at temperatures varying from 25 to 450ºC. X-ray diffraction showed that the material consisted of predominantly α phase of In_2S_3 mixed with little amount of β phase. The deposits were of β variety at high temperatures.

A novel in situ oxidation-sulfurization growth route via a self purification process was developed to synthesize β-In_2S_3 dendrites by Xiong et al [55]. The precursor of InSb dendrites was firstly obtained using “sonochemical coreduction” route. Subsequently , the mixtures of InSb dendrites (0.473 g, 2 mmol), CS_2 (0.18 mL, 3 mmol), NaOH (0.72 g, 18 mmol) and 30% H_2O_2 (0.60 mL, 6 mmol) were loaded into a 50 mL teflone-lined autoclave, which was then filled with distilled water up to 90% of the total volume. The autoclave was sealed and maintained at 180ºC for 24 h and was then cooled to room temperature naturally. Precipitate was filtered off,

washed with distilled water and absolute ethanol for several times, and then dried in vacuum at 60ºC for 4 h. The product obtained was pure In_2S_3.

2.3.3 Indium Sulfide Thin films

2.3.3.1 Thermal Evaporation

Indium monosulfide thin films were prepared by Seyam [17] by thermal evaporation onto quartz and glass substrates held at 473 K during deposition process. Deposition rate was held at 10 nm/sec keeping the pressure at 10^{-6} Torr. InS granules (99.999% pure) were evaporated. The films obtained were amorphous, and stoichiometric.

Stoichiometric thin films of In_2S_3 were prepared using thermal evaporation technique for the first time by Shazly et al [18]. The 'as deposited' films were amorphous and crystallinity was built in on annealing at 423 K. The crystal structure, as determined by both x-ray and electron diffraction, showed that tetragonal films of β-In_2S_3 phase were obtained. The degree of crystallinity increased with increasing either the film thickness or the annealing temperature.

Indium sulfide was synthesized and deposited by single source vacuum thermal evaporation method on glass substrates by A. Timoumi et al [19]. The X-ray diffraction analysis confirmed initial amorphous nature of the deposited InS film and phase transition into crystalline In_2S_3 occurred upon annealing in free air for 2 hr at a substrate temperature of 250 °C. Optical constants of the films were obtained from the analysis of the transmission and reflectance spectral data over the wavelength range of 300–1800 nm. Films annealed at 250 °C for 2 h show a good homogeneity with 80% transmission. Analysis of the optical absorption data of the deposited films revealed optical direct band gap energy in the range of 2.0–2.2 eV.

A. Timoumi et al also reported the effect of subsequent annealing of films deposited by single source vacuum thermal evaporation in nitrogen and free air atmosphere from 250 to 350 °C for different durations [20]. Experimental parameters

were adjusted in order to optimize the annealing conditions and to obtain high band gap energy at low deposition temperature, as required for photovoltaic applications. X-ray diffraction analysis revealed the initial amorphous nature of deposited In–S thin films and the phase transition into crystalline In_2S_3 upon thermal annealing. Films had an optical direct band gap of energy about 2.2 eV. Annealing temperature of 350 °C for 60 min in air atmosphere was the optimal condition.

Use of single source evaporation for the deposition of compound semiconductor films often leads to highly non-stoichiometric films. This was because of the decomposition of the solid when heated in vacuum and/or of preferential evaporation of the components. To avoid these difficulties George et al deposited indium sulfide by reactive evaporation of indium in a sulfur atmosphere by [21]. They used a glass crucible placed in a canonical basket of molybdenum wire to evaporate sulfur and a molybdenum boat to evaporate indium. The substrate (micro glass slides) temperature was varied between room temperature and 600 K. The source to substrate distance was 15 cm and the deposition rate was around 20 to 30 nm/min. Films showed β-In_2S_3 phase. They optimized the substrate temperature to be 425 ± 50 K ie, the films were smoother, had good transmission and the refractive index approached that of the bulk value at this temperature. They also found that this was in good agreement with the concept of critical optimization of Vincett [22]. He concluded from many experimental results that, when the substrate temperature approached about 0.33 of the boiling point of the material, the film qualities (surface smoothness, optical transmission, carrier mobility etc) improved considerably. Also the bulk diffusion was large at these temperatures, which helped the filling of gaps created by the evaporation of amorphous or disordered materials.

β-In_2S_3 films were obtained by solid-state reaction, induced by annealing for half an hour under constant argon flow, between the constituents sequentially deposited in thin layers by vacuum thermal evaporation [48]. The films obtained after

annealing at 623, 673 and 723 K were crystallized in β-In_2S_3 tetragonal structure without any preferential orientation. XPS study proved that the films were contaminated by oxygen during annealing. This contamination increased slightly with the annealing temperature but the oxygen atomic percentage never exceeded 3% in the samples annealed at 623 and 673 K. To obtain In_2S_3 films with the best crystalline properties and the best purity, the optimum temperature has been found to be 673 K.

2.3.3.2 Plasma-Assisted Co-Evaporation (PACE)

Sreenivas Kosaraju et al reported the development of plasma-assisted co-evaporation (PACE) for the formation of *β*-In_2S_3 thin films [47]. Indium was supplied by conventional thermal evaporation, while the chalcogen gas precursor (H_2S) was activated using inductively coupled plasma (ICP) source. With the help of optical emission spectroscopy and mass spectrometry it was shown that the ICP effectively dissociated H_2S, producing atomic sulfur. Transport modeling was used to quantify the flux distributions of the co-evaporated metal and the plasma-generated species impinging the substrate. Model predictions were validated by measurements of deposition rate and film properties. Substantial improvements in both materials utilization and substrate temperature reduction were realized with respect to conventional co-evaporation. *β*-In_2S_3 was formed at a temperature of 100 °C and the quality was a strong function of S/In ratio. The grain size decreased and the optical band gap increased as the substrate temperature was reduced.

2.3.3.3 Chemical Bath Deposition

Thin films of In_2S_3 were prepared by chemical precipitation onto glass substrates by Kitaev and Dvounin [24]. These films were amorphous regardless of their thickness (150 to 400 nm) and crystallized when heated to 773 K in vacuum.

R. Bayón et al used simple and low cost CBD technique for the preparation of indium hydroxy sulfide films [25]. Thin films of In $(OH)_xS_y$ were prepared from an

acidic bath (pH = 2.2-2.5) containing indium (III) chloride, acetic acid (AcOH) and thioacetamide (TA). Indium (III) chloride concentration was kept constant (0.025 M) while that of [TA] was varied from 0.05 M to 0.5 M and [AcOH] from 0 M to 0.3 M [bath temperature -70ºC]. Formation of In_2S_3 films was based on the slow release of In^{3+} and S^{2-} ions in an acidic medium and their subsequent condensation on the substrates when the ionic product exceeded the solubility product. Sulfide ions were provided by the hydrogen sulfide, produced during the thioacetamide hydrolysis, in dilute acid solutions. Finally the hydrogen sulfide dissociated to give rise the sulfide ions needed for the In_2S_3 precipitation. Acetic acid was added to the reaction mixture either to reduce the pH, which would favor the TA hydrolysis and avoid the formation of hydrolyzed species, or to complex the In^{3+} ions. Thickness of the films was 1800 Å after deposition of about 45 min. From XPS characterization, they proved that the films were mainly composed of indium hydroxyl sulfide, indium oxide and indium sulfate having absorbed on the surface, some contaminant species from the solution and also CO_2 from air. Samples annealed in air were found to have grater oxygen concentration. The unannealed samples had more than 80% indium hydroxy sulfide in their composition. Molecular formula of the as deposited film was close to In (OH) S.

They investigated the structure and surface morphology of CBD indium hydroxy sulfide thin films and found that films were polycrystalline and their structure depended on deposition conditions [26]. When low TA and AcOH concentrations were used, In_5S_4 was obtained; nevertheless, as these concentrations were increased, films were composed of mixture of cubic α- and β-In_2S_3 phases. The film composition obtained by energy-dispersive X-ray analysis (EDS) showed that samples were sulfur deficient (S/In ratios between 0.5 and 1.2). Surface morphology of the films suggested two different growth mechanisms. Which one took place seemed to be related to reactant concentrations, especially to AcOH concentration.

This group also probed reaction mechanism and kinetics of the chemical bath deposited $In(OH)_xS_y$ thin films [27]. They studied solution chemistry of $InCl_3$–

CH_3CSNH_2–CH_3COOH ($InCl_3$–TA–HAcO) system and the species distribution diagrams, solubility and precipitation curves. At an acidic pH (1–4), the ($InCl_3$–TA–HAcO) solution contains mainly indium–chloro-complexes and $In(OH)_3$ precipitation is not expected when HAcO is added. Kinetic calculations based on TA hydrolysis showed that indium hydroxide–sulfide($In(OH)_xS_y$) precipitation took place through a mechanism faster than TA hydrolysis, probably a direct reaction between TA and any indium–chloro-complex, leading to different products depending on the pH of the deposition solution.

Temperature of the bath and the concentration of the reactants were important parameters for films deposited using CBD. In_2S_3 thin films were successfully deposited using CBD technique by Lokhande et al [28]. The chemicals used were indium sulfate ($In_2(SO_4)_3$), 80% hydrazine hydrate, thioacetamide, triethanolamine (TEA) and ammonium chloride (NH_4Cl). For the deposition of In_2S_3 thin films, 10 ml of indium sulfate solution was taken in a glass vessel to which 1 ml of 7.4 M TEA and 10 ml of NH_4Cl solutions were added successively. Under continuous stirring, 0.2 ml of hydrazine hydrate (80%) was mixed and the reactant vessel was kept in a constant temperature water bath (± 0.5ºC). When the appropriate temperature (25 to 70ºC) was attained, 10 ml of thioacetamide solution was added to the bath. The resultant solution was transparent, which was stirred with a magnetic stirrer for a few seconds and cleaned glass substrates were immersed into it vertically. The solution colour changed to lemon yellow and finally to bright yellow. The presence of $In(OH)_3$ in the deposition bath was unavoidable due to the aqueous nature of the bath. For In_2S_3 films concentrations of the reactants taken in the solution were 0.1 M indium sulfate, 0.5 M thioacetamide, 1.4 M NH_4Cl, 14.7 M TEA and 80% hydrazine hydrate. Temperature increase favored homogeneous precipitation and lower film thickness. Samples deposited on FTO (F doped tin oxide) exhibited better crystallinity. Presence of oxygen in the film had been detected using RBS.

Indium sulfide thin films were deposited using CBD technique from aqueous solution containing $InCl_3$ and thioacetamide [29]. The pH of fresh solution was 3.1 and it could be adjusted by adding HCl to the reaction bath. Temperature of the bath was 50-90ºC and the reaction time was varied between 5 and 600 min to achieve required film thickness. The deposits consisted of nano-sized particles of β-In_2S_3 or its mixture with α-In_2S_3 as found by crystallographic study and TEM. EDAX and XPS analysis revealed presence of excess sulfur in the film. Chemical bath Deposition of indium sulfide thin films from aqueous mixtures containing indium chloride and thioacetamide under the two extreme reaction conditions 30 and 70ºC was examined by Yamaguchi et al [30]. X-ray analysis of the films indicated the formation of amorphous indium hydroxysulfide in the early stage, followed by the formation of nanocrystalline indium sulfide in the late stage of the film growth. The films deposited at 30ºC had a "cauli-flower-like" morphology, whereas the fibrous structure was obtained at 70ºC.

Properties of thermal-annealed In_2S_3 films prepared by using CBD technique were presented by M. G. Sandoval-Paz et al [31]. Polycrystalline In_2S_3 films were grown on glass substrates by means of this technique and were subsequently thermal-annealed in an Ar atmosphere at temperatures from 200 to 450 °C. Experimental results showed that the as-deposited films were composed of a mixture of both cubic α and β crystalline phases, with some fraction of tetragonal phase. Thermal annealing of the films caused the conversion of the cubic crystalline phases to the tetragonal β one and crystalline reorientation of the latter phase. Two energy band gaps were determined for all the films: one indirect and the other direct at higher energy. Structural modifications of the films were accompanied by changes in the two energy band gaps of the films. Annealing treatment of β-In_2S_3 thin films grown on glass substrate during t_D=60 min, and in nitrogen at 400 °C for 1 hr resulted in the

formation of well crystallized samples with cubic structure and preferential orientation along (610) [32].

N. Barreau et al compared the properties of indium sulfide thin films prepared using Chemical Bath Deposition (CBD) and Physical Vapor Deposition (PVD) and the influence of the synthesis conditions on the physico-chemical, optical and electrical properties were discussed [23]. In CBD, the deposition took place in aqueous solution containing indium chloride ($InCl_3$) and thioacetamide (CH_3CSNH_2). Temperature of the bath was 345 K. Substrates were immersed vertically in the stirred solution.

In PVD deposition of the constituents was carried out by vacuum thermal evaporation at a pressure of 5×10^{-4} Pa with the purities of indium and sulfur maintained at 99.99 and 99.98% respectively. In order to obtain films, indium and sulfur layers were sequentially deposited, their thickness and evaporation rate being controlled in situ by an rf quartz monitor. [S/In ratio was ≥ 3]. Structure obtained from this process was then annealed in a tubular oven for 30 min under a constant argon flow of 0.6 dm^3/min. They studied films annealed at five different temperatures 523, 573, 623, 673 and 723 K. The threshold temperature was found to be 623 K. Above this temperature, the films were wholly crystallized.

From the XPS analysis, they found that, for PVD deposited films, there was partial bond formation between In and S even before annealing. Film, after annealing, contained oxygen and Na in the bulk while there was no such contamination before annealing. However the films were amorphous, with large amount of excess sulfur. Best β- In_2S_3 thin films were obtained with heat treatment at 673 K. They had the same crystallization as those annealed at 723 K and they were lightly contaminated as those obtained at 623 K.

The CBD films were sulfur deficient and there was more oxygen than sulfur

in the film with the oxygen compensating sulfur deficiency. The major difference between the two kinds of films was in their crystalline properties; crystalline property of PVD film was far better than that of CBD.

2.3.3.4 Successive Ionic Layer Adsorption and Reaction (SILAR)

SILAR technique was used by Sankapal et al to deposit indium sulfide thin films [33]. This was achieved using indium sulfate ($In_2(SO_4)_3$)and thioacetamide solutions. Temperature of deposition was 25-70ºC and deposition time was 4-5 hours. The films were 0.2 μm thick. Films deposited on glass substrates showed poor crystallinity, but those on FTO samples were crystalline. TEM analysis revealed that the initial growth of film on glass substrate was the γ phase of In_2S_3 with particle size ranging from 20 - 40 Å. Presence of oxygen was detected by RBS analysis.

R. S. Mane and C. D. Lokhande used the versatile and simple SILAR method to deposit indium sulfide (In_2S_3) thin films [34]. Optical band gap of the In_2S_3 thin films was 2.3 eV. Films were highly resistive with resistivity of the order of 10^5 Ω cm. Utilization of triethanolamine and hydrazine hydrate complexed indium sulphate and sodium sulfide as precursors, resulted in nanocrystalline In_2S_3 thin films [35] and the optical band gap was found to be 2.7 eV.

Post-deposition annealing effects on In_2S_3 thin films deposited using SILAR technique was reported by R. Ranjith et al [36]. Samples were prepared by varying dipping and rinsing time, and those prepared at room temperature were found to be amorphous in nature. However, peaks corresponding to β-In_2S_3 were observed on annealing at 400 °C. Grain size increased with increase in the dipping times, either in the precursor solutions or in water. Band gap decreased considerably for samples annealed at 400 °C in vacuum.

2.3.3.5 Photochemical deposition technique (PCD)

Kumaresan et al deposited indium sulfide thin films by photochemical deposition technique (PCD) [37]. The $S_2O_3^{2-}$ ions present in the solution absorb UV radiation and release S according to the following equation

$S_2O_3^{2-} + h\nu = S + SO_3^{2-}$

This spontaneous release of S in a more acidic medium takes place according to the equation

$S_2O_3^{2-} + 2\ H^+ = S + H_2SO_3$

Also the $S_2O_3^{2-}$ ions get excited by absorbing the UV radiation and release electrons according to the equations

$2S_2O_3^{2-} + h\nu = S_4O_6^{2-} + 2e^-$

$SO_3^{2-} + S_2O_3^{2-} + h\nu = S_3O_6^{2-} + 2e^-$

Sulfur atoms and electrons combine with the In^+ metal ions present in the solution of $In_2(SO_4)_3$ to form InS according to the relation

$In^+ + S + e^- = InS$

The as-deposited InS films were amorphous in nature and phase transition to crystalline In_2S_3 occurred upon annealing at 500ºC. Raman analysis of the as-deposited film confirmed the formation of In-S phase. The films had 3 μm thickness over a deposition period of 90 min. Thickness decreased to 1 μm upon annealing at 500ºC. Presence of oxygen in the film was detected using AES analysis and the sulfur to oxygen ratio was 6:1. Even after annealing at 500ºC, oxygen was present in the film and there was a possibility for the formation of $In_2S_{3-3x}O_{3x}$ and the S to O ratio was about 9:1. The as-deposited films did not show clear absorption edge, possibly because of the amorphous nature of the film, while on annealing, clear absorption edge was observed. Annealed samples exhibited a direct band gap of 2.1 eV.

2.3.3.6 Electrosynthesis

A new approach for the electro-synthesis of indium sulfide thin films (In_2S_3) was described by Tacconi et al [38]. Electro-synthesis using sulfur modified gold electrode and alternative exposure to indium and sulfur ion containing aqueous bath consisted of four steps (a) A polycrystalline gold surface was first modified with a sulfur layer (b) indium was placed onto this layer forming indium sulfide (c) indium continues to deposit atop the indium sulfide layer (d) transfer back to a sulfide ion containing bath resulted in the sulfurization of the residual indium sites. $In_2(SO_4)_3$ was used as the indium containing electrolyte and Na_2SO_4 as sulfur containing medium. Raman active modes present at 235, 268 and 309 cm^{-1} indicated presence of the β-In_2S_3 defect spinel structure. Combined cyclic voltammetry and electrochemical quartz crystal microgravimetry scans demonstrated the veracity of this film growth approach. Photo-electrochemical measurements in a polysulfide redox medium showed that the In_2S_3 layers thus grown were photoactive and behave as an n-type semiconductor.

2.3.3.7 Atomic layer deposition

Thin films of In_2S_3 were deposited on soda lime glass and SnO_2 coated glass using indium acetyl acetonate and H_2S precursors by atomic layer deposition (ALD), a sequential deposition technique allowing the formation of dense and homogeneous films [41]. ALD is based on alternate saturative surface reactions. Each precursor is pulsed into the reaction chamber alternately, one at a time, and the pulses are separated by inert gas purging periods. With properly chosen growth conditions, the reactions are surface saturated and the film growth is thereby self limiting. In that case, each ALD cycle deposits maximum one monolayer of the desired material. However the amount of material deposited per cycle depends on the temperature, precursor combination and the reactive sites on the surface and therefore only rarely is

a full monolayer growth per cycle obtained. The required thickness can be obtained simply by repeating these ALD cycles. The precursors must be volatile and thermally stable up to the reaction temperature. They should chemisorb on the surface and react rapidly at the absorbed state with the other precursors. To obtain In_2S_3, the pulsing orders were

1. indium acetyl acetonate 0.7 s
2. nitrogen (purge 1) 1 s
3. hydrogen sulfide 0.5 s
4. nitrogen (purge 2) 0.8 s

The surface chemical reactions were

Step 1 Indium pulse

$2\ In(CH_3COCHCOCH_3)_3\ (g) + surface \longrightarrow 2\ In(CH_3COCHCOCH_3)_3\ (adsorbed)$

Step 2 Sulfur pulse

$3H_2S\ (g) + 2\ In(CH_3COCHCOCH_3)_3\ (adsorbed) \longrightarrow In_2S_3 + 6\ CH_3COCH_2COCH_3$

In a temperature window between 130 and 260ºC, a maximum growth rate of about 0.7 Å per cycle was obtained at 180ºC.

Yousfi et al [42] also employed Atomic Layer Deposition (ALD) for depositing In_2S_3 thin films. Depositions were carried out in an ALD machine. Indium sulfide layers were prepared from indium acetylacetonate at 130ºC and hydrogen sulfide. Deposition temperature was approximately 150-160ºC. The purging gas was nitrogen with 300/500/300/500 ms. Composition measurements were made using RBS technique, on film deposited on silicon substrates. In/S ratio was found to be 0.66 indicating the film to be In_2S_3. As the composition of the films did not change with annealing, they related the high band gap value to structural effects like quantum size effects.

Asikainen et al described the growth of In_2S_3 thin films by Atomic Layer Epitaxy (ALE) [50]. $InCl_3$ and H_2S were employed as the reactants. Nitrogen was used as the carrier and purging gas. The reactor pressure was about 10 mbar. $InCl_3$

was evaporated inside the reactor from a crucible held at 275ºC. H_2S flow rate was 9 cm^3/min. The films were deposited on glass substrates at 300-400ºC. The films were cooled to about 200ºC under nitrogen flow before removing from the reactor. The highest growth rate obtained was 1.4 Å/cycle at 300ºC. Resulting films were polycrystalline β-In_2S_3. SEM analysis showed that the film consisted of densely packed particles with a diameter of about 100-150 nm. RBS analysis revealed the composition of the film grown at 300ºC as $In_{0.40}S_{0.57}Cl_{0.03}$.

2.3.3.8. Metal Organic Chemical Vapor Deposition (MOCVD)

Indium sulfide films were prepared using MOCVD by Barron [43]. The majority of studies have employed the thiolate compounds prepared from the parent trialkyl indium:

$InR_3 + HSR' \longrightarrow ½ [(R)_2 In(R')]_2 + RH$

$InMe_3 + 2HS'Bu \longrightarrow ½ [('BuS) (Me) In(S'Bu)]_2 + 'BuH$

Films grown using either $[('Bu)_2In(S'Bu)]_2$ or $[(^nBu)_2In(S'Bu)]_2$ as the precursor at each of the temperatures 300, 350 and 400ºC were essentially independent of the precursor in terms of morphology and phase present. The micro-structural features and chemical composition of the deposited films were, however, observed to have significant dependence on the deposition temperature. Films deposited from methyl substituted precursor $[(Me)_2In(S'Bu)]_2$ exhibited marked difference from those grown using either $[('Bu)_2In(S'Bu)]_2$ or $[(^nBu)_2In(S'Bu)]_2$. Films deposited from the methyl precursor at 400ºC yielded a crystalline diffraction pattern.

Single-source organo-metallic chemical vapour deposition was reported by R. Nomura et al using $Bu^nIn(SPr^i)_2$ as the precursor molecule [46]. Tetragonal β-In_2S_3 thin layers with strongly preferred (103) growth orientation were obtained on Si(111) and quartz substrates at a substrate temperature T_{sub} of 300–400°C. β-In_2S_3 thin films

thus obtained were photo-responsive, with optical band gap energies and dark conductivity estimated as 1.98 eV and 2.0×10^{-4} S cm^{-1} respectively.

P. O. Brien et al [44] reported cubic α-In_2S_3 deposited on glass, GaAs(100) and InP(111) by low-pressure metal-organic chemical vapour deposition (LP-MOCVD), using novel air-stable precursors of general formulae $In(S_2CNMeR)_3$ [where R=*n*-Butyl (compound (**1**)), *n*-Hexyl (compound (**2**))]. The predominant phase in all films grown was found to be α-In_2S_3, regardless of substrate or growth temperature. Andrew N. MacInnes et al also reported deposition of indium sulfide films using MOCVD which yielded amorphous films of stoichiometry which turned crystalline (β-In_2S_3) upon annealing [45].

2.3.3.9 Modulated flux deposition

Indium sulfide thin films had been prepared by a novel modulated flux deposition technique [53]. Experimental parameters were adjusted to obtain high band gap and low absorption material at low deposition temperature as required for photovoltaic applications. Films were deposited in a 'home-made' evaporation chamber containing a rotating holder that transported standard soda-lime glass substrates cyclically around three different areas: indium source beam, heating lamps and reactive sulfur region. Parameters that had been controlled in the film deposition were the evaporation source temperatures, the substrate temperature and the angular velocity of the rotating substrate holder. Substrates were rotated at 30 rev/min and maintained at 200ºC. Samples showed tetragonal β-In_2S_3 phase. Layer thickness did not affect the crystalline phase, but influenced the average crystallite size.

C. Guillén et al also reported that indium sulfide thin films were prepared using a 'novel modulated flux deposition' procedure. All samples showed tetragonal β-In_2S_3 structure with random or preferential (103) plane orientation, depending mainly on the sulfur availability during the growth process. The sulfur availability was

optimized to achieve smooth surfaces and low scattering/absorption in the films. The average crystallite size decreased and the energy gap increased as the layer thickness decreased from 250 to 60 nm. Energy gap values of 3.02 eV was obtained for the thinnest In_2S_3 films.

Indium sulfide (In_2S_3) polycrystalline thin films were deposited on amorphous glass substrates employing modulated flux deposition (MFD) by C. Sanz et al [54]. Influence of different deposition parameters (elemental sources temperatures, substrate temperature, and substrate angular velocity) was studied. All the samples had tetragonal structure (β-In_2S_3) with high (103) preferential orientation. Optimized samples showed good coverage and small-grain homogeneous microstructure. A direct optical transition was observed, suggesting band gap energy (E_g) of 2.75 eV for 100-nm-thick films.

B. Asenjo et al reported indium sulfide (In_2S_3) thin films deposited on amorphous glass, glass coated by tin oxide (TCO) and crystalline silicon substrates by two different methods: modulated flux deposition (MFD) and CBD [62]. In_2S_3 films prepared using MFD were more compact and having homogeneous surface than those prepared using CBD. Films deposited employing CBD contained indium oxide in their composition and exhibited higher absorption edge values when deposited on glass.

2.3.3.10 Electrochemical deposition

The electrochemical deposition of In_2S_3 from an aqueous solution of $In_2(SO_4)_3$ and Na_2SO_3 was reported by B.Asenjo et al. In_2S_3 films with good adherence and uniformity were obtained by cycling the potential in the range for cathodic deposition of In and S [59]. A secondary In_2O_3 phase was detected in thin films, possibly arising from reduction of residual oxygen in solution and/or by an electrochemically induced precipitation reaction.

2.3.3.11 Spin Coating

In_2S_3 colloidal thin films with various thicknesses were prepared by the spin coating method [60]. In this work interestingly band gap of the thin films depended on the thickness and decreased with heat treatment. Dependence of the band gap on the thickness and heat treatment was explained well using the 'size quantization effect' of In_2S_3 colloidal particles in the film. In_2S_3 colloidal thin films prepared on wide gap semiconductors such as TiO_2 and ZnO showed an anodic photocurrent under visible light irradiation.

.

2.3.3.12 Chemical Spray Pyrolysis (CSP)

CSP is a simple and cost effective method for the fabrication of In_2S_3 thin films.This technique is used in the present work due to its low cost and its adaptability for large area deposition. Review of the earlier works done on indium sulfide films prepared using spray technique is given below.

Indium sulfide films deposited on glass substrate by spray method was studied by Bouguila et al [67]. In_2S_3 was formed from the chemical reaction

$$2InCl_3 + 3\,CS(NH_2)_2 + 6\,H_2O \longrightarrow In_2S_3 + 3CO_2 + 6\,NH_4Cl$$

X-ray diffraction showed that In_2S_3 was the main phase present in these films and that the structure and the allotropic form of this phase were affected by substrate temperature. Analysis of the layers by SEM and AFM revealed that best crystallinity and homogeneity were obtained for the substrate temperature 613 K.

In_2S_x thin films grown using spray solution composition from x = 2.0 to x = 3.9 was studied by Kim et al [66]. Films exhibited β-In_2S_3 phase with tetragonal structure. They also found that the band gap increased from 2.15 eV to 2.43 eV on increasing the *x* composition.

Bhira et al prepared In_2S_3 thin films using spray pyrolysis technique. Films were deposited on pyrex glass by spraying a solution of 10^{-3} M indium chloride and $2x10^{-3}$ M thiourea [1]. Here substrate temperature was kept at 340ºC. They used

nitrogen as 'carrier gas' keeping the solution and gas flow rates at 2 cm^3/min and 4 l/min. Well crystallized films showed β-In_2S_3 phase with preferential orientation along (400) plane. Microanalysis of the films pointed out a deficit of chalcogen (46%) and using XPS analysis, they confirmed that this deficit was compensated by oxygen bonded to indium, in addition to that as a surface contaminant. They detected traces of chlorine also in the bulk of the sample. Photoconductivity measurements were carried out within the range of wavelengths in the visible spectrum at different modulation frequencies and bias voltages ranging from 5 to 300 Hz and from 3 to 25 V respectively. They observed a fast increase of photocurrent signal toward 2 eV connected with a progressive decrease in the high absorption region. They attributed this to the presence of trap centers at the grain boundaries or to the presence of structural defects or secondary phases in the film. The response increased with increase in illumination time and bias voltage. They found out the mean absorption edge from the photocurrent measurements using Devore's model [64]. Band gap value (2.05 eV) was found to be in close agreement with that obtained from optical absorption measurements (2.08 eV).

InS films with composition close to that of In_2S_3, prepared using airless spray technique was studied by Kamoun et al [65]. Samples were prepared with different In/S ratio. They observed broadening and/or shift of the short wavelength absorption edge for smaller In/S values which was ascribed to the presence of secondary phases and to a more disordered structure. They performed spectroscopic ellipsometric measurements over the 0.5eV to 4 eV spectral ranges. It was found that the refractive index (n) and absorption coefficient (α) decreased with increase in In/S value. Annealing of the films at high temperature (500ºC) resulted in strong decrease in the value of both n and α which was explained by an improvement in sample crystallinity, while annealing at rather low temperatures (300ºC) had little effect on the optical constants.

Teny et al had done an extensive study on indium sulfide films deposited using this technique. Indium sulfide thin films prepared using chloride based precursor solutions showed β-In_2S_3 phase with preferential orientation along (220) plane [68]. Indium sulfide thin films were prepared systematically, by varying the In/S ratio in the spray solution as well as the substrate temperatures. Band gap was found to be 2.67 eV for In/S ratio 2/3. XPS analysis of the samples revealed presence of oxygen as just the surface contamination only [for a thickness of ~ 100 A] for the samples prepared using solution having higher sulfur concentration. They could get good control over the stoichiometry of the films by varying the substrate temperature or In/S ratio in the film. Samples having In/S ratio 1.2/8 showed maximum photosensitivity ($\Delta I/I_D$ = 949.97). However these were highly resistive. On increasing the indium concentration resistivity as well as photosensitivity of the samples decreased. Teny et al had also studied the post annealing effects on indium sulfide thin films prepared using spray pyrolysis [69]. Films were annealed in vacuum at 300 and 400 °C. Annealing did not affect the optical properties of the film much, but the resistivity of the films drastically decreased while grain size increased. It was observed through these studies that In_2S_3 thin films have potential use as buffer layer in photovoltaic heterojunction devices.

Ratheesh et al studied the SHI induced modifications in spray pyrolysed β-In_2S_3 thin films [70]. In this work the films, were irradiated using 100 MeV Au ions with different fluences. XRD analysis showed that, on irradiation, crystallinity became poor. Mean crystallite size decreased from 17 nm to 10 nm, as the fluence increased up to 3×10^{12} ions/cm^2. XRD pattern revealed that, for ion fluence 1×10^{13} ions/cm^2, the sample became amorphous. However, when ion fluence increased to 3×10^{13} ions/cm^2, recrystallization was observed and the grain size also increased to 16.5 nm. A red shift in absorption edge was observed in the case of irradiated samples

Preparation of indium sulfide thin films employing spray pyrolysis using a new precursor [indium nitrate] was done by Teny et al [71]. In this work, Indium nitrate and thiourea were used as the precursor solutions. Samples having In/S ratio 2/3 showed better crystallinity with the band gap of 2.66 eV. XPS analysis of the sample proved the formation of indium sulfide. It was also observed that In/S ratio in the initial precursor solution determined the composition as well as electrical properties of the films. Maximum photosensitivity was observed for the sample prepared using solution having In/S ratio 2/4.

Indium sulfide (In_2S_3) thin films were prepared through the spray pyrolysis (SP) technique using indium acetate and *N*-*N* dimethyl thiourea as precursor compounds [72]. Samples prepared at different temperatures and atomic ratio of In to S in the starting solution, were characterized using several techniques. X-ray diffraction studies indicated that the preparation temperature (T_p) affects the crystallinity of the deposited materials as well as the optoelectronic properties. For $(In/S)_{sol}$=1/8, the optical band gap (E_g) increased from 2.2 up to 2.67 eV when T_p increased from 250 to 450 °C. For $(In/S)_{sol}$=1 and T_p=450 °C, the deposited material showed *n*-type electrical conductivity with a resistivity [in dark condition] of 1 $(\Omega cm)^{-1}$, and E_g=2.04 eV.

2.3.3.13 Spray Ion Layer Gas Reaction Technique (Spray-ILGAR)

N.A. Allosop et al reported a new technique for the preparation of indium sulfide thin films on large area [73]. The was claimed to be a modification of the ILGAR technique used to prepare chalcogenide thin films. These samples were having high suitability for buffer layer applications in chalcopyrite solar cells. The process involved cyclical spray deposition of an indium containing precursor layer followed by its conversion to sulfide using hydrogen sulfide gas. Analysis of the deposition revealed that the indium chloride based precursor was transported via the vapor phase from the spray droplets to the substrate surface.

2.3.3.14. Miscellaneous methods

In_2S_3 films were grown using indium (III) isopropyl xanthate, $In(S_2COC_3H_7\text{-}iso)_3$, a readily available chelate, which volatized when heated in vacuum and yielded β-In_2S_3 when thermally decomposed in an inert atmosphere [51]. Resistivity of In_2S_3 films (~ 200 nm thick) increased from 10^{-1} to 5 x 10^2 Ω-cm as the deposition temperature was raised from 230 to 450ºC. It was suggested that the lower resistivity of films deposited at lower temperatures might be due to a higher degree of disordering in the structure of In_2S_3. Analysis of film composition using AES revealed presence of In, S and O. The average ratios were I_S/I_{In} = 3 and I_O/I_{In} = 0.55. Triangular features were seen from SEM analysis, which were indicative of film growth along (111) direction.

Rahana et al has prepared β-In_2S_3 films on glass and on quartz substrates by rapid heating of metallic indium films in H_2S atmosphere [58]. Effect of sulfurization temperature and time on the growth of β-In_2S_3 films were investigated in this work. Highly oriented single-phase β-In_2S_3 films were grown by the sulfurization technique. A high photo-response was obtained for films prepared at a sulfurizing temperature of 600 °C.

Herrero et al prepared thin films by chalcogenization of electroplated metallic indium films onto Ti substrates, in a flowing stream of H_2S, at about 350ºC for 1 hour with a pretreatment of 3 hour at 130ºC [15]. X- ray diffraction patterns showed that β-In_2S_3 thin films were grown with good crystallinity. This material in a photo-electrochemical cell with polysulfide solution, showed low dark current, a noticeable photocurrent characteristic of n-type semiconductors. Photostability tests of the semiconductor in aqueous polysulfide showed that it was photo-degraded, and from the band scheme of In_2S_3 it was inferred that the photo-corrosion was a kinetic process and that its stability in this electrolyte was, at least thermodynamically possible.

Growth of indium sulfide by deposition of indium onto MoS_2 surface was studied [56]. Topotactical growth of indium sulfide at the initial stages of the film growth had been observed. From the electron microscopic images of the film, it was found that by the increment of In_2S_3 particle size, InS was also produced. On increasing the film thickness to more than 20 nm, indium crystals predominantly grew.

2.4. Nano Indium Sulfide

Semiconductor nanoparticles (NPs) offer a rich palette of optical, electronic, and catalytic properties, which can be tuned by their size. Their uniqueness, as compared to the bulk materials, stems from their large surface area and size quantization effect.[74, 75, 76] For the past decade, a large variety of semiconductors have been prepared in nanocrystalline form. Among others, metal chalcogenides are the materials for which the quantum confinement effect is most pronounced. Properties of NPs (quantum dots) have been extensively investigated for the II-VI class of compounds (CdS, CdSe, etc.) [77].All nanocrystalline materials usually have 1:1 or greater stoichiometric ratio of metal atoms to atoms of chalcogenide in the unit cell. There are a large number of other semiconductors for which the total number of chalcogen atoms in the unit cell is greater than the number of metal atoms, such as MoS_2, WS_2, ReS_2, FeS_2, Sb_2S_3, In_2S_3, Bi_2S_3, with special optical, mechanical, and catalytic properties. For most of them, the nanocrystalline form was reported only in the presence of polymers [78-83] or in a physically constrained environment, such as porous solids and reverse micelles, where the growth of the NPs is arrested by the phase boundaries [84,85].

In addition to properties mentioned above, In_2S_3 has mainly three more special qualities making it an interesting candidate for both fundamental and practical aspects of NP research [86]:

1. In_2S_3 is a rare case of ordered crystalline material with a large amount of vacancies. Owing to tetragonal sites formed by incompletely coordinated sulfur atoms, indium sulfide can serve as a host for a number of metal ions to form semiconducting and/or magnetic materials [87, 88, 89] Doping In_2S_3 produces materials with exceptional optical, electrical, and magnetic properties, which can be adjusted not only by the NP diameter, but also by the concentration of the guest ion.[90, 91] This is in contrast to II-VI NPs, which tend to expel guest ions.[92, 93]
2. Unlike most of the semiconductors currently being used for nanocolloids, In_2S_3 and related materials display both direct and indirect conduction-to-valence band transitions, which can be observed by different modalities of UV-vis spectroscopy at 2.0-2.2 and 1.0-1.1 eV, respectively. This opens the door for the investigation of the effect of quantum confinement on direct and indirect excitonic transitions.
3. In_2S_3 NP bioconjugates can have medical applications such as cancer diagnosis.

Several authors have reported nano structured indium sulfide obtained by different deposition techniques.

Uniform nanocrystalline β-In_2S_3 powders were prepared using organothermal synthesis by S. H. Yu et al [94]. The reaction was

$$2\ InCl_3 + 3\ Na_2S_3 \xrightarrow{\text{solvent}} In_2S_3 + 6\ NaCl + 6\ S$$

This was conducted in a glove box filled with argon gas. Toluene and 1, 2-dimethoxy ethane (DME) were used as the solvents. An appropriate amount of analytical grade $InCl_3$ and 0.01M of Na_2S_3 were added into a teflone-lined autoclave of 100 ml capacity, which was filled with organic solvent up to 80% of the total volume. The air dissolved in the solution was driven off by passing argon gas through it. The autoclave was sealed and maintained at 140^oC for 12 hours and cooled to room temperature

naturally. The yellow precipitate was filtered and washed respectively with CS_2, acetone, distilled water and absolute ethanol several times to remove the byproducts of S, NaCl and other impurities. The product was then dried under vacuum at 80ºC for 4 hours. The broad nature of diffraction peaks indicated formation of nanocrystalline β-In_2S_3. They found that the particle size of nanocrystalline β-In_2S_3 could be controlled by choosing different solvents. Particle size in Toluene was smaller than that in DME (8 and 16 nm respectively). They also studied the influence of water content, organothermal time and temperature on the samples. No evidence for organic impurities in the samples was obtained from IR spectrum.

Qichun Zhang et al have reported two-dimensional indium sulfide framework constructed from penta supertetrahedral p1 and supertetrahedral t2 clusters [95]. They could construct new open-framework indium sulfide ($[In_{12}S_{24}H_2]^{10-}$) from penta super tetrahedral sulfide clusters ($[In_8S_{17}H]$,$^{9-}$ P1) and supertetrahedral sulfide clusters ($[In_4S_{10}H]$,$^{7-}$ T2) through hydrothermal synthesis. The P1 cluster reported consisted of only trivalent ions (In^{3+}) and was the only known example of tetrahedral clusters with a core sulfur site bonded to four trivalent ions. Each P1 cluster was joined to three T2 clusters (vice versa) to form an infinite two-dimensional sheet stacked along the crystallographic *c*-axis. The UV-vis diffuse reflectance spectrum showed this material to be a wide band gap semiconductor.

Mohammmad Afzaal et al could obtain indium sulfide nanorods from single-source precursor [96]. Thin films comprised of In_2S_3 nanorods had been prepared on glass substrates by metal-organic chemical vapour deposition using [$Et_2In(S_2CNMe^nBu)$] without either template or catalyst.

Changhao Liang et al [97] utilized a high temperature approach for the mass production of ultra-long, straight silica nanotubes and indium sulfide filled cable-like structures by heating Si wafer and In_2S_3 powder under a stream of hydrogen/argon gases at 950 °C. Transmission electron microscopy, scanning electron microscopy and

X-ray diffraction analysis demonstrated the formation of hollow cylindrical amorphous silica tubes with lengths up to hundreds of micrometers and outer diameters in the range of 70 to 300 nm, silica tubes encapsulating indium sulfide nanorods with a cubic structure and S-filled silica tubes with high sensitivity to a focused electron beam.

Koichi Yamaguchi et al [30] reported chemical bath deposition of indium sulfide thin films from aqueous mixtures containing indium chloride and thioacetamide under the two extreme reaction conditions, namely, at 30 and 70 °C. The films deposited at 30 °C had a 'cauliflower-like' morphology, whereas the fibrous structure was observed at 70 °C.

Anuja et al could realize indium sulfide (In_2S_3) micro- and nanorods by sulfurization of electrodeposited metal indium layers at room temperature [99]. From XRD and TEM observations, it was concluded that the In_2S_3 nanorods and microrods had ~50 nm and ~0.5 μm diameter, respectively. A plausible top-growth mechanism was proposed for the formation of the nanorods in which the hydroxide layer was found to play an important role. The micro- and nanorods showed optical band gap of ~2.2 and ~2.54 eV, respectively.

This group also reported surfactant assisted synthesis of In_2S_3 dendrites and their characterization [100]. Partially crystalline indium sulfide dendrites were obtained via precipitation in presence of CTAB. In absence of CTAB, crude self-assembly of particles was observed. With increasing CTAB concentration and aging time of the solutions, particles were found to self-assemble in a progressive manner to extended hierarchical dendrites. Unlike in commonly known cases where dendrites are unstable but well crystallized; partially crystallized particles can also self-assemble to well-formed dendrites especially when assisted by the surfactant molecules. X-ay analysis and TEM studies confirmed the partially crystallized nature of the samples. Optical properties of the dendrites were found to show quantum confinement effects.

A template-free route to the preparation of hollow In_2S_3 nanospheres was demonstrated by Xuebo Cao et al [101]. This was achieved by solvothermally treating solid In_2S_3 spheres comprised of small particles at 180 °C, for 24 h. The well crystalline hollow nanospheres had diameter in the range 40–70 nm and an average wall thickness of 7 nm. Hollow In_2S_3 nanospheres showed an intense absorption between 318 and 512 nm, which was blue-shifted to shorter wavelengths relative to that of bulk In_2S_3. Hollow In_2S_3 nanospheres also exhibit a strong photoluminescence. The green band, centered 518 nm, was due to the band-band transitions and the orange emission centered at 624 nm originates from the indium interstitial defect. These hollow In_2S_3 nanospheres could be used as a distinctive multicolored phosphor and material for producing photo electrochemical devices.

D.P. Dutta et al accounted the preparation of nanocrystalline indium sulfide (In_2S_3) by a two-step process [102]. The first step involved metathesis reaction of trimethyl indium ether adduct ($Me_3In{\cdot}OEt_2$) with 1,2-ethanedithiol ($HSCH_2CH_2SH$), resulting in the formation of a polymeric precursor. In the second step, these precursor complexes were pyrolysed in furnace under flowing nitrogen atmosphere where they undergo thermo-destruction to yield nanometer-sized particles of indium sulfide. The average size of the nanoparticles ranged from 20 to 22 nm.

Paz Vaqueiro [103] has reported solvothermal synthesis and characterization of new one-dimensional indium sulfides: $[C_{10}N_4H_{26}]_{0.5}[InS_2]$. Two new main group metal sulfides were prepared solvothermally in the presence of 1,4-bis(3-aminopropyl) piperazine and their crystal structures determined by single-crystal X-ray diffraction.

S. Gorai and S. Chaudhuri could synthesize β-indium sulfide (In_2S_3) sub-micron particles with cage-like network structures via the sonochemical route [104]. Time for ultrasonic treatment of the alcoholic solution of indium chloride and thioacetamide was found to be the prime factor for the formation of a cage-like network structure.

This group has also reported the synthesis of In_2S_3–SiO_2 nanocomposite films (with molar ratios of In_2S_3:SiO_2 = 15:85, 10:90 and 5:95) on quartz substrates by sol–gel method [105]. Highly confined nanoparticles of In_2S_3 (radius ~ 1.8–7 nm) were obtained in SiO_2 matrix, indicating SiO_2 to be a good capping agent for the nanoparticles.

Yujie Xiong et al report a novel in situ oxidization–sulfurization growth route via a self-purification process to synthesize β-In_2S_3 dendrites [106]. It was found that the product was pure In_2S_3 with strong quantum confinement of the excitonic transition expected for the In_2S_3 dendrites.

β-In_2S_3 powder with particles having an average size of 13 nm and spherical shape, had been successfully prepared by S.Yu et al through the hydrothermal treatment of a sol from indium trichloride and sodium sulfide at 140°C [3].

β-In_2S_3 nanofibers were successfully synthesized by Xiaoyi Zhu et al via a hydrothermal method with AAO membrane as a template at 150 °C for 15 h [108]. XRD patterns indicated perfect crystallization of β-In_2S_3. SEM images proved the presence of nanofibers grown up from the channel ends of the AAO template. TEM images confirmed that the nanofibers had high aspect ratio of ca. 40–50 and diameters of about 10 nm. Room temperature photoluminescence (PL) spectrum of the β-In_2S_3 nanofibers indicated its potential applications in light-emission devices.

Shaohua Shen and Liejin Guo have presented the structural, textural and photocatalytic properties of quantum-sized In_2S_3-sensitized Ti-MCM-41 prepared by ion-exchange and sulfurization methods [109]. In_2S_3 nanocrystallites were successfully encapsulated into the mesopores of Ti-MCM-41 by a two-step method involving ion-exchange and sulfurization. The In_2S_3 nanocrystallites inside the Ti-MCM-41 host showed a significant blue-shift in the UV-vis absorption spectra. Under irradiation using visible light, the composite material showed much higher photocatalytic activity for hydrogen evolution than bulk In_2S_3. It can be explained by the effective charge-separation in the quantum-sized In_2S_3-sensitized Ti-MCM-41.

2.5 Characterization

Structural, optical and electrical properties of indium sulfide prepared through different methods were characterized using different techniques.

2.5.1 Structure and growth

Crystal structure of In_2S_3 thin films obtained by the chemical vapor deposition from the volatile complex compounds [indium (III) isopropyl xanthate and indium (III) diethyl dithiocarbonate] was studied with the help of synchrotron radiation diffraction [110]. High photon beam intensity ($3x10^{10}$ photons/mm^2s) and high angular resolution (0.02º) of the reflexes made it possible to study weak reflexes to analyze the phase composition of the samples in more detail, to determine the size of the particles and to evaluate stress at the microscopic level. They showed that the films obtained at T= 230ºC crystallized as cubic α-In_2S_3. At the deposition temperature T > 250ºC, the films crystallized in the tetragonal β phase. Annealing of the films synthesized at 230ºC, lead to β-In_2S_3 phase formation as well. Size of the particles increased as the deposition temperature increased. Values of the inter-planar spacing *d*, for close packed planes, were almost the same for all the samples deposited at temperatures, in the range, 230 - 370ºC and practically did not depend on crystal modification, deposition temperature and thickness of the samples. They also showed that microstress decreased after annealing or for higher deposition temperatures. For the sample deposited at 430ºC, splitting of the reflex (5,0,15) was observed, which could be explained as a monoclinic or hexagonal distortion of β-In_2S_3.

Powder neutron and X-ray diffraction data for indium sulfide were reported by N. S. Rampersadh et al [111]. The lattice parameters obtained from a Rietveld refinement for the neutron data are: a=7.5937 (6) Å; c=32.352 (3) Å; V=1865.6 (3) $Å^3$ and for X-ray data are: a=7.6172 (1) Å; c=32.3307 (8) Å; V=1875.86 (6) $Å^3$. The crystal system was taken to be tetragonal (space group $I4_1/amd$).

Growth of indium (III) sulfide thin films from aqueous thioacetamide (TA)–In(III) solution was monitored with a quartz crystal microbalance (QCM) [112]. It was found that growth of the film consists of parallel deposition of In_2S_3 and In_2O_3. Both the processes were induced by sulfide anions (S^{2-}) produced after decomposition of thioacetamide. In_2S_3 was deposited by precipitation of crystallites formed in the bulk solution. When the solutions were stirred, this reaction was hindered due to the disruption of the nucleation centres.

Amlouk et al [129] showed that acoustic techniques, more specifically acoustic signature V(z), are very powerful non destructive methods to characterize β-In_2S_3 thin films prepared using CSP technique. Young's modulus of the order of 443 GPa, was consistent with the assumption of the β-In_2S_3 material to be in ceramics group. Acoustic microscopy study revealed the possibility of presence of surface and bulk defects in this thin film.

In almost all the reports the crystal structure of β-In_2S_3 is analyzed with the help of X-ray diffraction technique. The crystal structure is found to depend on different deposition parameters and post deposition treatments. The crystal structure of annealed β-In_2S_3 thin films with different thickness was investigated by X-ray diffraction technique [113]. Lattice parameters, crystallite size and microstrain were calculated. It was found that the lattice parameters were independent on film thickness, while annealing in an increase of these parameters. Crystallite size increased with the increase of the film thickness and annealing temperature. In all cases, the microstrain decreased gradually with the increase in both film thickness and annealing temperatures.

2.5.2 Optical

The first optical measurements of In_2S_3 were reported by Kauer and Rabenau [114]. Investigations by Bube and McCarroll [115] and Gilles et al[116] were mainly concerned with photoconduction in indium sulfide. Garlick et al [117] reported on the

IR emission and luminescence properties. Rehwald and Harbeke [118] reported on the electrical and optical properties. All the studies were done on single crystals or polycrystalline bulk materials. For β-In_2S_3 the absorption edge was mainly due to direct transitions [119] and weak indirect transition was also reported [118].

George et al [21] calculated refractive index from the optical transmission spectra of the samples prepared using reactive evaporation of indium in sulfur atmosphere. They used the method given by Manifacier et al [120]. The value was found to be 2.56. Band gap was found to be 2.01 eV corresponding to a direct forbidden transition. They attributed the unresolved absorption peaks just before the onset of band-to-band transition from the plot of α vs hν as due to different energy levels (sulfur vacancies) in the forbidden gap to which transition may take place.

Indium monosulfide thin films prepared using thermal evaporation by Seyam [17] exhibited absorption coefficient of the order of 10^5 cm^{-1} and the band gap was 1.94 eV. He calculated the refractive index (*n*) and extinction coefficient (*k*) from the transmittance and reflectance spectra and the values were estimated to be 2.2 and 2.3 respectively. The high frequency dielectric constant was calculated from the plot of $(n^2-1)^{-1}$ vs $\lambda^{-1}$and the value was found to be 5.76.

Optical band gap (E_g) of indium sulfide thin films prepared using CBD technique by Lokhande et al [28] was found to be 2.75 eV. The 'as prepared' samples were photoactive as observed from Time Resolved Microwave Conductivity (TMRC) studies. The same value of band gap was obtained for SILAR samples also [33]. Band gap value could be tuned between 2.3 and 2.7 eV by changing the reaction temperature or pH of the aqueous chemical bath as shown by Yoshida et al [29]. Variation of E_g values was discussed in terms of the change of chemical composition, crystal modification and crystal size.

Refractive indices of the films prepared using Atomic Layer Epitaxy was found to be of the order of 2.5-2.7 and the band gap was 2.3 eV [50]. Samples were

highly resistive and they showed photo response when exposed to daylight. The photo response was reversible and fast.

Barreau et al studied the optical properties of In_2S_3 thin films grown using PVD [122]. Optical properties of indium sulfide thin film depended on their synthesis process and composition. High homogeneity and excellent surface state of the films were confirmed by the presence of interference fringes on transmission and reflectivity spectra. Band gap was found to be independent of the annealing temperature and the value was about 2.8 eV, higher than that of β-In_2S_3 single crystal, due to the presence of oxygen in the film. Refractive index (*n*) and the extinction coefficient (*k*) were also found to be independent of annealing temperature. The values were in the range 2.1- 2.8 and 0.01 – 0.3 for wavelengths in the range 250 nm to 2500 nm.

Absorption onset indicated a band gap value above 2.5 eV for indium sulfide thin films, prepared using a novel modulated flux deposition technique [53]. Energy band gap increased for indium sulfide layers of lower thickness, which was related to a reduction of the average crystallite size of the films.

ALD In_2S_3 thin films, deposited by Yousfi et al [42] were amorphous and the band gap was approximately 3.3 eV which was much greater than that of the bulk value. Band gap reduced to 2.25 eV after annealing, while those deposited by Naghavi et al [41] were crystallized in tetragonal form with band gap vales of about 2.7 eV. Quantum size effect was considered as the possible reason for wide band gap. A shift of 0.7 eV was expected for grain size of about 3 nm.

Mane et al deposited indium sulfide thin films by SILAR technique using indium chloride and sodium sulfide as cation and anion source in an aqueous medium [123]. The films were amorphous. Optical band gap was 2.3 eV and the films were highly resistive [~ 10^5 Ω-cm].

Optical band gap of the prepared by rapid heating of metallic indium films in H_2S atmosphere [58] was found to vary from 1.9 to 2.5 eV when the sulfurization temperature was varied from 300 to 600 °C or by increasing the sulfurization time. Indium sulfide thin films were prepared using Spray-ILGAR pocess an indirect bandgap of 2.2 eV [73].

Bhira et al. found out the mean absorption edge from the photocurrent measurements using Devore's model [64] for samples prepared using spray pyrolysis technique on pyrex glass by spraying a solution of 10^{-3} M indium chloride and $2x10^{-3}$ M thiourea [1]. Band gap value (2.05 eV) was found to be in close agreement with that obtained from optical absorption measurements (2.08 eV). In_2S_x thin films grown using spray solution composition from x = 2.0 to x = 3.9 was studied by Kim et al [66]. Films exhibited β-In_2S_3 phase with tetragonal structure. They also found that the band gap increased from 2.15 eV to 2.43 eV on increasing the *x* composition. Teny et al reported bandgap of be 2.67 eV for In/S ratio 2/3 for indium sulfide thin films prepared using chloride based precursor solutions. Indium sulfide thin films prepared through the spray pyrolysis (SP) technique using indium acetate and *N*-*N* dimethyl thiourea as precursor compounds [72] showed that the optical band gap (E_g) increased from 2.2 up to 2.67 eV for $(In/S)_{sol}$=1/8, when T_p increased from 250 to 450 °C. New precursor indium nitrate gave crystalline indium sulfide films having band gap of 2.66 eV [71].

For indium sulfide polycrystalline thin films deposited on amorphous glass substrate employing modulated flux deposition direct optical transition was observed, suggesting band gap energy (E_g) of 2.75 eV for 100-nm-thick films.

Electro reflectance measurements on indium sulfide grown from indium melt was done by T. Nishimo et al [124]. Electro reflectance spectra of InS grown from In melt was measured in the photon energy range from 2.0 to 4.0 eV. The spectra revealed structures associated with the E_0 fundamental edge due to direct transitions and some higher interband transition edges. Analysis of the E_0 structure indicated

characteristic features of low-field electro reflectance spectra which enabled to determine the direct band gap of this material.

Widening of bandgap is usually observed in indium sulfide thin films. Some authors attribute the widening of band gap of indium sulfide films to quantum size effect [125] while some authors explained this due to excess sulfur [66]. Recently presence of oxygen and sodium were also reported to increase the band gap markedly [23]. Optical band gap varied from 2.1 eV to 2.9 eV for samples, which contained 8.5 at% oxygen as reported by Barreau et al [121]. They found that the electronic structure of indium sulfide was very much disturbed due to the presence of even a few oxygen atoms that substituted sulfur in the crystalline matrix, which induced the high increase of optical band gap. Electrical conductivity of the oxygen containing samples was found to be greater by approximately 2 orders than that of pure In_2S_3 films. They attributed this effect to the modification of the properties of the grains or their grain boundaries when oxygen was introduced in the films. The films showed n-type conductivity indicating that the introduction of oxygen did not change the type of majority carriers.

Temperature dependence of band gap of β-In_2S_3 thin films was studied by Kambas et al [119]. They found that the transition was direct and the E_g dependence on T was linear. Band gap increased with decrease in temperature and the value was found to be 2 eV at room temperature.

Optical properties annealed β-In_2S_3 thin films with different thickness were studied in the spectral range from 400 to 2500 nm to determine the optical constants (*n* and *k*), the high frequency dielectric constant, ε_∞, the lattice dielectric constant, ε_L, and the energy gap [113]. The optical constants were found to be independent on film thickness in the range from 200 to 630 nm. High frequency dielectric and lattice dielectric constants of the as-deposited films increased on annealing. The energy gap for the as-deposited In_2S_3 was found to be 2.60 eV and increased to 2.70 and 2.75 eV by annealing at 423 and 473 K for 1 h, respectively

Band gap of PVD β-In_2S_3 films increased with annealing temperature until 623 K, whereas for higher annealing temperature, the absorption threshold was stable [23]. Band gap was found to be in the range, 2.8 eV to 2.9 eV, which was greater than that of earlier reports. They observed that, when oxygen was introduced into the films, the band gap values were far higher than that of the single crystals. The wide band gap of PVD films was attributed to the presence of In-O bonds. Substitution of indium by Na was also found to increase the band gap. When heating rate was increased, the band gap was not as broad, because of the fast crystallization. They found that oxygen contamination had a positive effect to obtain layers with properties matching well with the specification of solar cell buffer layers.

PL spectra of InS single crystals were investigated in the wavelength region 477.5-860 nm and in the temperature range 8.5-293 K [126]. There were three PL bands centered at 605 nm, 626 nm and 820 nm. The first two bands were due to radiative transitions from the donor level at 0.01 eV below the bottom of the conduction band to the valence band and from the donor level at 0.06 eV below the bottom of the conduction band to the acceptor level at 0.12 eV above the top of the valence band respectively.

PL study done by R. Jayakrishnan et al on β- In_2S_3 thin films prepared using CSP technique revealed presence of two emission bands (named A and B) with peaks at 568nm and 663nm [2]. Based on the PL peak energy dependence on composition the A-band emission was found to be due to transition from sulphur vacancy (0.43eV) to Indium vacancy (0.1eV), (V_S-V_{In}), and the B-band was assigned to be due to transition from Indium interstitial, [acting as donor level 59meV] to oxygen replacing sulphur vacancy level (0.82eV above the valence band). Dependence of FWHM and PL peak energy on temperature of both the bands confirmed the assignments.

Fifteen normal modes of vibrations were observed for β-In_2S_3 dendrites from Raman spectra, which exactly correspond to those given by a sample of β-In_2S_3 with

unpolarised light [55]. The sample showed strong quantum confinement of excitonic transition, which was expected for In_2S_3 dendrites. Under PL excitation at 330 nm, the In_2S_3 dendrites emitted blue light at 358 nm, which clearly indicated the existence of electronic transition at particular wavelength (358 nm), and was stronger than in the bulk In_2S_3.

Temperature dependence of the Raman-active mode frequencies in indium sulfide was measured in the range from 10 to 300 K [127]. Temperature dependence of the A_g intralayer optical modes showed that Raman frequency shift resulted from the change of harmonic frequency with volume expansion and anharmonic coupling to phonons of other branches. The pure-temperature contribution (phonon–phonon coupling) was due to three- and four-phonon processes.

Raman spectra of InS single crystals was studied at different hydrostatic pressures up to 1.2 GPa [128]. Mode-Grüneisen parameters were obtained for Raman-active normal modes. It was shown that the variations observed in Raman spectra with growing pressure could be interpreted from the standpoint of the structural phase transition $D^{12}_{2h} \rightarrow D^{17}_{4h}$ in InS as the hydrostatic pressure continues to increase. The transition pressure was evaluated at (7 ± 1) GPa.

IR reflectivity of In_2S_3 crystals was studied and higher reflectivity was observed for quenched sample at low frequencies [14]. The peaks for the annealed samples were sharper and well resolved. There were 12 reflectivity bands for polarized light having E ⊥c case and eight bands for E || c case.

2.5.3. Electrical

The electrical property of single crystal indium sulfide was studied by Rehwald et al [118].The range of electrical resistivity and Hall coefficient at room temperature and it variance with temperature was presented. When these parameters were low, it changed slightly with temperature or even remained constant down to

liquid nitrogen temperature, whereas higher values had strong dependence on temperature. By heat and sulfur vapour treatment, it was demonstrated that this large variation had its origin in the deviations from stoichiometric composition of the material. The nearly exponential dependence of the measured Hall mobility on temperature, observed in specimens of high resistivity, was explained by different scattering mechanisms for electrons and hole in the same temperature region. All crystals were found to be n-type, regardless of doping during growth. Impurities, which otherwise produce p-type conductivity in similar materials, did not have the effect of changing the sign of charge carriers in In_2S_3. The main effect on concentration and sign of charge carriers come from the deficiency in sulfur, which could not be completely avoided during growth. The cation vacancies, forming a constituent of the lattice due to the chemical formula, were assumed to be mainly ordered in indium sulfide. The small fractions of disordered cations and cation vacancies acted as donors and acceptors nearly compensating each other. Their difference in concentration was determined by the lack of sulfur. They also suggested that high resistivity material might be useful as a photoconductor.

Gilles et al [116] studied the photoconduction in In_2S_3 prepared by the direct synthesis under a pressure of sulfur of the order of 5 to 10 atmospheres. They found that under an illumination of nearly 1000 lux, conductivity of this material increased by five orders of magnitude. Traces of copper increased the photosensitivity of the compound markedly. Diffusion length was found to be of the order of few millimeters. They observed a correlation between the reciprocal of the diffusion length and the photosensitivity of copper doped samples: the maximum photocurrent was obtained in samples where the reciprocal of the diffusion length was a maximum. From the thermal analysis, they found two-phase transitions in indium sulfide. The first one was in the temperature range between 414ºC and 421ºC while the second one was around 738ºC. Thermal activation energy was determined from the measurements

of resistivity as a function of temperature and was found to be 0.56 eV below first transition point and 0.63 eV above 420ºC.

Electrical properties In_2S_3 thin films deposited by ALD [41] had been addressed by using impedance measurements on semiconductor-electrolyte junctions. The films were n-type with doping concentration around 10^{16}-10^{17} cm^{-3} and possessed good blocking behaviour under reverse bias. The doping concentration increased with increase in the deposition temperature. Their flat band potential was close to -1.1 V versus MSE.

George et al [21] also found that for samples prepared using reactive evaporation of indium in sulfur atmosphere above a substrate temperature of 350 K were low resistive and indium made good ohmic contact to these films while films prepared below this temperature showed high resistivity and indium did not make ohmic contact to these films. From the temperature dependant resistance measurements of these films, the activation energy for electronic conduction was obtained as 0.26 ± 0.02 eV.

Both dark electrical resistivity and thermoelectric power (Seebeck coefficient S) were measured for films prepared using thermal evaporation technique, the measurements were carried out before and after annealing [13]. Dark electrical resistivity decreased exponentially with increasing film thickness. Resistivity decreased after annealing also. Thermoelectric power of all films decreased on increasing the sample temperature. The films showed n-type conduction. Existence of two distinct activation energies ΔE_1 and ΔE_2 belongs to two types of level: a shallow level of $\Delta E_1 = 0.319$ eV before annealing and $\Delta E_1 = 0.166$ eV after annealing and deep level of $\Delta E_2 = 0.61$ eV for as deposited films and $\Delta E_2 = 0.515$ eV for annealed films. The deep level was also detected by the 'space charge limited current' technique and the trap density was found to be 3.92×10^{22} m^{-3}. The decrease in ΔE_1

for the shallow levels as a result of annealing indicated that these levels were structure defect levels.

Dark resistivity of Indium monosulfide thin films prepared using thermal evaporation was reported by Seyam [17]. the dark resistivity of the samples decreased with increasing temperature and film thickness. Thermal activation energy of the charge carriers, from the electrical resistivity measurements, was found to be 0.84 eV. Density of charge carriers was found to be 10^{21} m^{-3} from the space charge limited current analysis.

Thermally stimulated current measurements were carried out on as grown n-InS single crystals having orthorhombic structure in the temperature range 10-125 K by Gasanly et al [131]. They identified four trap levels located at 20, 35, 60 and 130 meV and suggested that these levels in undoped layered crystals might be associated with structural defects and/or unintentional impurities. Trap parameters were determined by curve fitting method, peak shape method and initial rise method and found that they agreed well with each other. The re-trapping process was negligible for these levels, as confirmed by the good agreement between the experimental results and the theoretical predictions of the model that assumed slow re-trapping.

Defect characterization of the semiconducting thin films of β-In_2S_3 was done by Rupa et al using thermally stimulated conductivity studies and this work revealed four trap levels with activation energies 0.1 eV, 0.26 eV, 0.43 eV and 0.82 eV in the band gap of this material [132]. Variation of their prominence was studied with different stoichiometric ratios of In:S. Samples with lower In concentration showed the presence and prominence of Indium Vacancy (0.1 eV). Irrespective of the variation of In:S concentration ratio, chlorine impurity level (0.26 eV) and sulphur vacancy (0.43 eV) existed in almost all the samples. A high temperature defect level attributed to the replacement of sulphur by oxygen is also detected at 0.82 eV. Variation in the prominence of these traps with rate of heating and duration of

illumination was also observed. It is relevant from the observation that no single trap gained prominence, as the material possessed a multiple distribution of traps rather than a single trap. But the trap level at 0.82 eV was prominent in all measurements and was not affected by the change in heating rate. Effect of re-trapping of the carriers by the traps was also detected. Comparing the capture cross sections of these levels with the earlier theoretical results the authors concluded three centers (0.1 eV, 0.266 eV and 0.43 eV) to be coulomb repulsive while the fourth one (at 0.82 eV) to be a neutral center, which is mostly responsible for the electrical property of β-In_2S_3.

2.6 Doping in In_2S_3

High-temperature modification of In_2S_3 called γ-In_2S_3, (which exist above 754 °C), was stabilized at room temperature by replacing about 5 to 10% of the In atoms by the elements As, Sb or Bi [12]. Single crystals of In_2S_3 is doped with As (γ-In_2S_3 (As)) (red, hexagonal plates up to 1.5 cm^2, P m1, a = 3.800 ± 0.001 Å, c = 9.044 ± 0.005 Å) formed a layer structure in a closed system by iodine transport in the presence of As_2S_3 vapor. From the measured As_2S_3 equilibrium pressures over γ-In_2S_3 (As) and the thermodynamics of the vapor transport of In_2S_3 with iodine, the optimal growth conditions were derived. Crystals of In_2S_3 is doped with Sb (γ-In_2S_3 (Sb)) were also prepared in a similar way. The compositions of these materials were $In_{1.9}As_{0.1}S_3$ and $In_{1.8}Sb_{0.2}S_3$. These were characterized by measuring absorption spectra, thermoelectric power and temperature dependence of the conductivity between 20 and 500 °C. Both were n-type semiconductors. The phase diagram As_2S_3-In_2S_3, which was evaluated using DTA, indicated that γ-In_2S_3 (As) is soluble in molten As_2S_3. Single crystals were obtained by cooling solution of 7 mole% In_2S_3 from 850 to 300 °C. The potential of As_2S_3 as the flux for other sulfide materials is emphasized.

A variety of differently doped samples of In_2S_3 were prepared by chemical vapor phase transport (CVT) and gradient freeze techniques by Becker et al [11]. For

CVT, I_2 was used as the transport agent. X-ray diffraction of pure, tin doped, samples with excess sulfur and those with P and InP doping were shown to be single-phase β-In_2S_3. They found that if a sample with excess sulfur, having n- and p-type responses, was heated at 750ºC for 0.5 hour, the resistivity dropped by ~ 5 orders of magnitude and the n- and p-type responses were then replaced solely by the n-type response. The result was explained by the removal of S giving excess interstitial In donors. Doping of phosphorous and indium phosphide resulted in a weak p- response but n-response was also present. In the case of Sn doping, low resistance n-type material resulted. Whether this was due to true Sn^{4+} substitution for In^{3+} or whether Sn disrupted the lattice order such that the concentration of interstitial In was greater than In vacancies was not known.

Studies of conduction mechanism in single crystal β-In_2S_3 [118] showed that the conductivity is always n-type and p-type is not observed when the samples are doped with copper or cadmium. Becker [11] obtained p-response when single crystals were prepared with an excess of sulfur or InP, but n- response was also present.

β-In_2S_3 and β-In_2S_3:Co^{2+} (cobalt doped β-In_2S_3) single crystals were produced using chemical transport reaction method employing $ZnCl_2$+I_2 as a transport agent by Choe et al [134]. For In_2S_3 single crystal, In_2S_3 powder (purity 99.999%), 15 mol% of excess sulfur (purity 99. 9999%) and 5 mol% of ZnS (purity 99.999%) were used as starting materials. For β-In_2S_3:Co^{2+} single crystal, 2 mol% of Co (purity 99.99%) was added to the starting materials. Temperatures of the growth and source-zones were maintained at 670ºC and 830ºC respectively for 7 days. Dimension of the single crystals were approximately 6 x 5 x 3 mm^3 and they crystallized into tetragonal structure. Optical absorption spectra were measured in the temperature range 5 K to 300 K. At 290 K, they obtained an indirect optical energy band gap of 2.24 eV for β-In_2S_3 and 1.814 eV for β-In_2S_3:Co^{2+} while the direct energy band gap was 2.639 eV for β-In_2S_3 and 2.175 eV for β-In_2S_3:Co^{2+}. Three groups of impurity optical absorption peaks for β-In_2S_3:Co^{2+} single crystal were observed in the wavelength ranges of 675-

830 nm, 1300- 1900 nm and 2800- 3200 nm. These peaks could be attributed to the electron transition between the energy levels of Co^{2+} ions sited in the Td symmetry point. Polycrystalline thin films of Co-doped In_2S_3 were grown by the spray pyrolysis method and flash evaporation method [135]. The optical absorption spectra of these thin films were investigated in the wavelength region from 500 to 2500 nm at 298 K.

Kim et al has reported the preparation of $CoIn_2S_{3+x}$ thin films [136] by spraying a solution prepared by dissolving $CoCl_2$, $InCl_3$ and thiourea in solvent composed of methanol and distilled water (ratio of 1:1) to give 0.2 molar solutions of each solute, and then by mixing these solutions in appropriate volume ratio to give the desired x composition. An additional 20% in volume of thiourea solution compensated for the loss of sulfur caused by vapourisation. Rate of spray was 6 ml/min and the substrate was maintained at 270ºC. They found that, β-In_2S_3 thin films were grown over the range x = 0 to 0.4 and amorphous thin films over the range 0.6 to 1. Band gap was found to be decreasing with increasing x composition. The samples showed impurity absorption corresponding to wavelengths 695 nm, 750 nm and 802 nm. Intensities of these peaks increased with increasing x composition and they found that the Cobalt atoms in $Co_xIn_2S_{3+x}$ existed as Co^{2+} ions.

Kim et al also found that, as Cobalt was introduced into In_2S_3 single crystals, the structural defects were decreased [137]. The Cobalt atoms were located at the Td symmetry site of the β-In_2S_3 host lattice as Co^{2+} ion. Three peaks at 752 nm, 802 nm and 825 nm in the absorption spectrum of Co doped crystals were ascribed to Cobalt impurities. The photo acoustic spectrum of β-In_2S_3:Co^{2+} crystal, when compared with that of β-In_2S_3 single crystal in the wavelength region 500 to 2500 nm, possessed four peaks at 650, 760, 1700 and 2130 nm. First peak was ascribed to crystal defect and the rest to Cobalt impurities. Photoconductivity spectra of β-In_2S_3 single crystal at 286 K showed a broad peak centered at 663 nm and a tail in the long wavelength region. As ambient temperature decreased to 28 K, the broad peak also appeared at 626 nm and

the tailing phenomenon in the long wavelength region was not reduced. Photoconductivity spectrum of β-In_2S_3:Co^{2+} single crystal at 284 K had two peaks centered at 620 and 705 nm. The long wavelength tail in the spectrum was reduced when compared to that of β-In_2S_3 single crystals. When the temperature was reduced to 21 K, the spectrum showed two peaks at 585 and 655 nm and the tail in the long wavelength region was rapidly reduced.

Structural and optical properties of $In_{2-2x}Al_{2x}S_{3-3y}O_{3y}$ alloys obtained by the spray pyrolysis technique were studied by L.Bhira et al [138]. X-ray diffraction (XRD) showed well crystallized films preferentially oriented towards (4 0 0) direction corresponding to β-In_2S_3 phase for low compositions ($x \leq 0.2$); for $x > 0.2$, the structure became amorphous as confirmed by scanning electron microscopy (SEM). Moreover, microanalysis and X-ray photoelectron spectroscopy (XPS) measurements detected oxygen in the films, present in Al_2O_3 and In_2O_3 oxides and $Al(OH)_3$ hydroxides forms. The study of the absorption coefficient of thin layers versus incident light energy revealed that the value of the band gap energy increased with the composition *x* according to a parabolic profile.

β-In_2S_3 and β-$In_{2-x}Al_xS_3$ thin films were deposited on different substrates (pyrex glass, SnO_2/pyrex and steel) using spray pyrolysis technique at 320ºC [139]. In the case of the growth on a steel substrate, crystallography of the film was good and introduction of Al did not noticeably change the spectrum. In the case of deposition on pyrex, the structure of β-In_2S_3 was of poor quality. Al improved the crystallinity. On SnO_2/pyrex substrate, presence of Al resulted in broader and smaller diffraction peaks. The surface structure was studied using AFM and SEM. Crystallite size increased on going from steel to SnO_2. For steel substrates, characterized by a poor structural quality and a lattice disorder, the impinging atoms strongly interacted with the surface but with little surface migration. The layers were having good stability; Work function and surface photovoltage did not change with time. They used Auger studies to get

information on the surface layer composition. They also studied effect of heat treatment and substitution of a few indium atoms by aluminium atoms to this composition. In all the cases, the work function topographies were flat and variation of $\Delta\phi$ along the surface was small indicating uniformity of the surface layer of the films.

$In_{2-2x}Al_{2x}S_{3-3y}O_{3y}$ alloys were prepared on pyrex glass substrates by spray pyrolysis technique and their photoelectrical properties were studied by Bhira et al [140]. The spraying solution contained $InCl_3$, $AlCl_3$ and $CS(NH_2)_2$ as starting materials. The Al/In ratio (x) was varied from 0 to 1. Solution and gas flow rates were kept at 2 cm^3/min and 4 l/min respectively. Nitrogen was used as the carrier gas and the substrate temperature was 340ºC. Shape of the photoconductivity spectra I_{ph} ($h\nu$) and the variations I_{ph} (f) and I_{ph} (V) helped them to understand the conduction mechanism and the photo carrier recombination. For low compositions ($x \leq 0.2$), I_{ph} (V) parabolic variation showed that this conduction was limited by the space charge zone in accordance with Child's law ($I_{ph} \propto V^2$). This showed that the density of trap centers increased with the composition. As percentage of Al doping was increased, the photoconductivity measurements depended on the photo carrier recombination mechanism due to the presence of trap centers at grain boundaries. For $x \geq 0.4$, the electrical conduction followed Ohm's law. Band gap showed a parabolic profile with x, varied in the range from 2.05 to 2.42 eV. For low compositions (x = 0, 0.05, 0.1, 0.2) the conductivity study, as a function of temperature, presented a deviation to Arrhenius law in the temperature domain 80 to 330 K. At very high temperatures, ranging from 330 to 575 K, a quasi-linear variation of σ as a function of temperature according to Arrhenius law was observed. They found that for higher Al compositions, films were amorphous having poor electrical and photoelectrical properties.

Kulińska et al prepared $Li_xIn_2S_3$ electrochemically with different amounts of Lithium ($0 \leq x \leq 0.13$) [141]. They applied Perturbed Angular Correlation (PAC) to understand the mechanisms that occur during Li insertion. PAC experiments could measure the hyperfine interaction between a radioactive probe and the Electric Field Gradient (EFG) generated by direct neighborhood at the site of the probe atom. At lower temperatures undoped material showed a strong damping of the PAC spectra while after doping (with electron donor Li) the higher concentration of mobile charge carriers repaired this damping. PAC spectra showed a new dynamic behavior, which increased with increasing Li content. They proposed that for higher temperatures ($T \geq$ 500 K) migration of indium atoms from the tetrahedral site started and this was favored by the presence of empty sites in the direct neighborhood of a tetrahedral site, in contrast to the octahedral sites. They also proposed that the Li insertion lowered the threshold which confined the indium ions to the tetrahedral sites. The dynamic behavior between room temperature and 500 K was caused by the mobile Li ions, because the dynamic fraction was proportional to the Li content.

β-$In_2S_{3-3x}O_{3x}$ thin films were prepared using a dry physical process on glass substrate [121]. The temperature during the synthesis process was 473 K. Na free substrates were used to avoid diffusion of Na. They found that the films were smooth, continuous and homogeneous from SEM analysis and the grain size was 50 nm as obtained from AFM. N. Barreau et al investigated the evolution of the conduction and valence band levels with the increase in optical band gap. The results obtained are discussed first in terms of β-$In_2S_{3-3x}O_{3x}$ intrinsic property, then in terms of its application as buffer layer in Cu(InGa)Se_2-based solar cell. The valance band discontinuity measurements suggested that the substitution of sulphur atoms by oxygen atoms in the crystalline matrix of β-In_2S_3 has only a small influence on the position of the valence band level of the material. Robles et al.[143] had shown that the sulfur orbitals participate in both conduction and valence bands of β-In_2S_3 . On the another hand, Matar et al.[144] had shown that the oxygen orbitals also contribute to

both conduction and valence bands of β-In_2O_3 . Therefore, in the case of an increase of the optical band gap due to an electronic effect, both valence and conduction bands should shift, contrary to what is usually observed [142]. Robles *et al*. have also shown that the compression of the β-In2S3 lattice induced an increase in its optical band gap. In the case of the BISO thin films, we observed that the introduction of oxygen, substituted for sulfur in the crystalline matrix of β-In_2S_3, induces a decrease of its lattice parameters.[145] From these results, it seems that the increase of the optical band gap of the BISO thin films with *x* is not due to the presence of oxygen orbitals, but instead it is simply due to the decrease of the lattice parameter induced by its introduction.

Thin films of In_2S_3 containing different quantities of sodium were synthesized by annealing at 400°C of structures composed of thin indium, sulphur and indium fluoride layers sequentially evaporated on sodium-free glass substrates [146]. They exhibited *β*-In_2S_3-like structure and the sodium atoms are homogeneously distributed in the whole films. To determine the structure of the material and particularly the position of the sodium atoms in the *β*-In_2S_3 spinel matrix, single crystal of the same compound was synthesized and then studied using XRD and transmission electron microscopy. These studies showed that the materials obtained could be described using the general formulation $[In_{16}]_{Oh}[In_{5.33-x}Na_{3x}\square_{2.66-2x}]_{Td}S_{32}$ (0*x*1.33), where Oh and Td, respectively, represented the octahedral and tetrahedral sites of the spinel structure. In thin film form, the maximum of sodium which could be introduced in the crystalline matrix corresponded to *x*=0.9. This new material family was named as BINS

Optical and electrical properties of β-In_2S_3 thin films containing Na ($[In_{16}]_{Oh}[In_{5.33-x}Na_{3x}\square_{2.66-2x}]_{Td}S_{32}$) were studied by Barreau et al [147]. Both transmission and reflectivity curves showed interference fringes, which proved the homogeneity of the morphology of the films. They found that the band gap linearly

increased from 2.1 eV (when the films were pure) to 2.95 eV (when their Na content was 8.4 at%). The electro-negativity of Na is 0.9 while that of In is 1.7. Therefore when it was substituted for indium, the sodium increased the ionicity of the tetrahedral cationic-sulfur bonds, which could be an explanation of the increase of the optical band gap. They also suggested that incorporation of Na in the tetrahedral vacant sites, attracted electrons of sulfur, inducing an increase of In-S bond length which in turn produced perturbation of the electronic structure of the material resulting in the increase of band gap. All the films had n-type conductivity. Incorporation of Na was found to increase the conductivity of In_2S_3 films. But when the Na content was increased from 0.2 at% to 5 at% the conductivity decreased, while on further increasing (above 6 at%) conductivity drastically increased.

F. Py, M. Womes et al have worked on In_2S_3 containing copper. A study of the In_2S_3---Cu_2S---CuS system indicated the existence of a solid solution range with the In_2S_3 vacant spinel crystal structure. An X-ray diffraction study has allowed the identification of two redox processes in the formation of solid solutions with CuS, which is a mixed valency copper sulfide, $Cu_2^{1}Cu^{11}(S_2)^{2-}S^{-}$. At low CuS concentrations all copper (I) is oxidized to copper (II) and the substitution of indium (III) by copper (II) proceeds without sulphur loss. At higher CuS concentrations the redox reaction is restricted to the sulphur atoms and the substitution of indium (III) by copper (I) and copper (II) is accompanied by sulphur losses. Presence of copper in two oxidation states has been confirmed by diffuse reflectance and X-ray absorption at the Cu K edge.

2.7 Indium sulfide in solar cells

Naghavi et al [149,150], through a systematic study of the deposition parameters of In_2S_3 buffer layers on CIGS solar cells, achieved a high efficiency of about 16.4% without anti-reflection coating. These studies demonstrate the considerable potential in the fabrication of cadmium-free CIGS thin-film solar cells

without the CBD method and using indium sulfide buffer layers. The highest efficiency of 16.4% has been obtained at 220 ^{0}C for a layer thickness of 30 nm. However the temperature of deposition and the thickness of the films are compromised to yield out good efficiency. Analysis of the device showed that indium sulfide layers were characterised by an improvement of the blue response of the cells compared with a standard CdS-processed cell, due to a high apparent band gap (2.7–2.8 eV), higher open-circuit voltages (up to 665 mV) and fill factor (78%). The high values of the open-circuit voltage and the fill factor of the best cells show that the interface quality between CIGS and In_2S_3 was high. Preliminary XPS measurements indicated the presence of a small amount of Cu and Na in these films, meaning that inter-diffusion processes had taken place during film formation, which is supposed to have positive role in the junction formation processes and the cell performance. For instance, indium sulfide might have acted as a sink for copper from CIGS up to a certain level at higher temperatures, which could have improved the properties of the cells. It seems that the indium sulfide buffer layers allow higher temperature device preparation compared with classical CdS.

Spiering et al presented the results of large area CIGS modules with indium sulfide (In_2S_3) as buffer layer deposited by the atomic layer chemical vapor deposition technique [152, 153]. This work is interesting regarding environmental aspects and the implementation in industrial production. Module efficiency close to 13% was realized on the area of 30×30 cm^2 (η=12.9%, V_{OC}=27.8 V, FF=72.6%, I_{SC}=0.457 A, aperture area: 714 cm^2 and 42 cells). Diffusion processes at the buffer layer interfaces, dependent on deposition temperature and post annealing, have been investigated by X-ray photoelectron spectroscopy, secondary ion mass spectrometry and sputtered neutral mass spectrometry analysis. Diffusion of Cu and Na into the buffer layer and intermixing of S and Se at the In_2S_3/CIGS interface was detected.

In yet another work Spiering et al reported lifetime measurements of these solar modules [154] which are very important for its implementation in industrial

production. The results from long-term stability testing of Cd-free devices are presented in comparison with reference devices with the CdS buffer layer. Indoor tests were performed at the ZSW laboratories, including damp heat and thermal cycling tests and the I–V performance under light soaking and under different irradiances were investigated. The outdoor testing was performed at the Widderstall solar test field in Germany. The results showed comparable stability behavior of the CIGS modules with different buffer layers and thus reinforced the qualification of In_2S_3 as buffer material for high-efficiency CIGS thin-film solar modules.

D. Hariskos et al reported Solar cells based on Cu(In,Ga)Se_2 by replacing the "standard buffer layer" CdS with a Inx(OH,S)y thin film [155]. The buffer layer was deposited using chemical bath (CBD) process using an aqueous solution containing $InCl_3$ and thioacetamide. The achieved conversion efficiency of 15.7% (active area) using the cadmium free Inx(OH,S)y buffer demonstrated the potential of this process as an alternative to the standard chemical bath deposition of CdS. X-ray photoemission spectroscopy measurements were performed in order to characterize the growth kinetics and the chemical composition. Influence of different concentrations of $InC1_3$ and thioacetamide in the solution on the electrical properties of the solar cells was studied by measuring the *j-V* characteristics and the spectral quantum efficiencies. Capacitance-voltage *(C-V)* measurements indicated that the high V_{oc}, values of devices with the novel buffer layer were correlated with narrower space charge widths and higher effective carrier concentrations in the absorber materials.

Solar cells with ALD deposited ZnO and indium sulfide layers has been investigated by E. B. Yousfi et al [42]. In situ monitoring at the monolayer level was done using quartz crystal microgravimetry (QCM), with a special focus on extrinsic doping of ZnO with Al. Cu(In,Ga)Se_2/In_2S_3 (ALE)/ZnO (ALE) cells present efficiencies up to 13.5%. Indium sulfide layers used in these cells were characterized by a high band-gap value (up to 3.3 eV). They possessed an ‘amorphous-like’ structure and a composition close to In_2S_3 as determined by Rutherford Back

Scattering measurements. Lowering of the band-gap and crystallization took place under annealing; they suggest that the high band-gap value of ALE indium sulfide layer to be related to the structural effects.

Indium sulfide buffer layers deposited with the help of the Spray-Ion Layer Gas Reaction (Spray-ILGAR) technique had recently been used with $Cu(In,Ga)(S,Se)_2$ absorbers resulting in cells with an efficiency equal to that of cadmium sulfide references was reported by Nicholas A. Allsop et al [157]. In this paper they show that cells prepared with $Cu(In,Ga)Se_2$ absorbers (sulfur free) having indium sulfide buffer layers reached an efficiency of 13.1% which was slightly below the efficiency of the cadmium sulfide reference. However, temperature dependant current-voltage measurements revealed that the activation energy of the dominant recombination mechanism remained unchanged from the cadmium sulfide buffered cells indicating that recombination was within the space charge region. They also reported the results of manipulating the absorber/buffer interface between the chalcopyrite $Cu(In,Ga)(S,Se)_2$ absorber (CIGSSe) and the indium sulfide buffer [158]. It was shown that the deposition of a small amount of zinc sulfide at the absorber/buffer interface could be used to increase the open circuit voltage. A small but significant increase of 20 mV (up to 580 mV), as compared to the pure indium sulfide buffered cells was possible leading to an increase in the overall efficiency.

They also carried out dry and damp heat stability of chalcopyrite solar cells prepared with an indium sulfide buffer deposited by the spray-ILGAR technique [159]**.** These cells were subjected to dry and damp heat conditions of 85 °C and 85% humidity for 100 h without encapsulation. The resulting cell parameters were measured and compared to cells prepared using a standard cadmium sulfide layer deposited by chemical bath deposition. Two different zinc oxide window processes were used for both buffers and the effect of changing the zinc oxide process was discussed. Before the damp heat tests, using an rf-sputtered zinc oxide process the indium sulfide buffers had an efficiency equal to the cadmium sulfide buffered cells

and on using a second rf/dc-sputtered zinc oxide process, a superior efficiency was obtained with the indium sulfide. The biggest loss in efficiency after damp heat testing was shown to arise from shunt paths at the scribe lines. The indium sulfide buffered cells degraded by only 11% under damp heat conditions when measured after re-scribing. A difference between the cell efficiencies using two different zinc oxide windows highlighted the interdependence of the process steps.

S.Gall et al conducted XPS studies of $Cu(In,Ga)Se_2$ (CIGSe)/In_2S_3 structures [160]. The indium sulfide layers were grown using physical vapor deposition (PVD) in which indium and sulfur were evaporated on the substrates at a temperature T_s. These as-deposited thin films were then heated at 200 °C for 1 min. A 12.4% efficiency was achieved using this process. The XPS study revealed that copper diffused from the chalcopyrite absorber towards the indium sulfide layer during this synthesis process. The quantity of copper strongly depended on synthesis temperature (T_s); the higher T_s, the more was the copper diffused. This observation was correlated with the solar cell performance to conclude that a significant Cu-diffusion inhibited the formation of a high-quality junction between the $Cu(In,Ga)Se_2$ and the buffer layer.

S. Gall et al also reported the influence of sodium compounds at the $Cu(In,Ga)Se_2$/(PVD)In_2S_3 interface on solar cell properties [161]. This work dealt with indium sulfide buffer layers grown by thermal co-evaporation of elemental indium and sulfur. It was found necessary to deposit these buffer layers at low substrate temperatures in order to reach V_{oc} values similar to those with (CBD) CdS. However, such deposition conditions lead to high recombination at the $Cu(In,Ga)Se_2$/ indium sulfide interface. Even though the $Cu(In,Ga)Se_2$ surface was cleaned in NH_3 (1 M, room temperature) prior to the indium sulfide deposition, this behavior was associated to the presence of sodium carbonates/oxides at the interface. An explanation is that, despite the chemical etch, sodium carbonates/oxides remain in the air exposed $Cu(In,Ga)Se_2$ grain boundaries and can migrate towards the surface when

the $Cu(In,Ga)Se_2$ is heated under vacuum. These polluted interface areas acted as recombination zones and this might have lead to the inferior devices. The device performance was improved by (i.e. improve the interface quality) sulfurizing the remaining sodium carbonates/oxides. The resulting Na_2S could then leave the interface by formation of a solid solution with the indium sulfide. By adapting this buffer layer deposition process, device with an efficiency of 13.3% was realized.

Lafond et al reported investigations on In_2S_3 containing Cu and/or Na compounds [151], which were expected to be formed at the $Cu(In, Ga)Se_2/In_2S_3$ interface. It was observed that a solid solution $Na_{(x)}Cu_{(1-x)}ln_{(5)}S_{(8)}$ existed from $CuIn_5S_8$ (x=0) to $NaIn_5S_8$ (x= 1) with a spinel-like structure. The single crystal structure determination showed that indium, copper and sodium atoms are statistically distributed on the tetrahedral sites. XPS investigations on the $CuIn_5S_8$, $Na_{0.5}Cu_{0.5}In_5S_8$ and $NaIn_5S_8$ compounds combined with the band gap changes are mainly due to valence band maximum shift; it is moved downward when x increases from 0 to 1. These observations are confirmed by the electron structure calculations based on the density functional theory, which additionally demonstrate that the pure sodium compound has direct gap whereas the copper-containing compounds have indirect gaps.

N. Barreau et al showed the potential of In_2S_3 containing sodium (BINS) thin films which can be grown on glass substrates heated at 200 °C [162]. The films had n-type electrical conductivity and their optical band gap could be managed between 2.15 and 2.90 eV by controlling their sodium content. In the aim of realizing efficient solar cells, the physico-chemical and electrical properties of Mo/CIGS/BINS structures and solar cells were studied. An efficiency of 8.2% was been reached with a 100 nm thick BINS buffer having a band gap of 2.8 eV.

The impact of $Na_xCu_{1-x}In_5S_8$ compounds formed at the $Cu(In,Ga)Se_2/In_2S_3$ interface of these thin film solar cells is also discussed by Barreau et al [163] in yet another work. Structural and optical properties of $Na_xCu_{1-x}In_5S_8$ powders, with x=0,

0.25, 0.5, 0.75 and 1, are determined. It is shown that all of the samples have the same crystalline structure, which indicates the existence of a solid solution over the whole range of *x* (i.e. 0-1). Increase of the optical band gap of these compounds is found to be linear between *x*=0 and *x*=0.75 (1.85 eV), whereas for *x*=1 (i.e. $NaIn_5S_8$) E_g is found to be 2.40 eV, which is much higher than the value expected from the linear slope. Such an evolution shows that the copper and the sodium weigh differently on the optical properties of the material.

F. Jacob et al presented the influence of the Ga content (x = Ga / (Ga + In)) in the absorber on the solar cell performance for devices using (PVD) In_2S_3-based buffers [164]. For experiments with *x* between 0 and 0.5, devices using (PVD) In_2S_3-based buffers were compared to reference devices using (CBD) CdS. Both buffers showed similar cell characteristics for narrow band gap absorbers, typically $E_{gCIGSe} < 1.1$ eV. However, the parameters of the cells buffered with (PVD) In_2S_3 are degraded when the absorber gap was widened. These evolutions were coherent with the existence of a conduction band cliff at the CIGSe/(PVD)In_2S_3 interface.

Our group reported Copper indium sulfide ($CuInS_2$)/In_2S_3 solar cells fabricated using spray pyrolysis method [165]. High short circuit current density and moderate open circuit voltage were obtained by adjusting the condition of deposition and thickness of both the layers. Consequently, a relatively high efficiency of 9.5% (active area) was obtained without any anti-reflection coating. The cell structure was ITO/$CuInS_2$/In_2S_3/Ag. We avoided the usual cyanide etching and CdS buffer layer, both toxic, for the fabrication of the cell.

K. Ernits et al presented In_xS_y thin-film buffer layers prepared by ultrasonic spray pyrolysis in the CIGS solar cell configuration, reaching an efficiency of 8.9% [166]. Light soaking enhanced the efficiency of In_xS_y/CIGS cells primarily by improvements in fill factor and open circuit voltage.

D. Ohashi et al reported the improvement of CIGS thin-film solar cells by surface sulfurization using In_2S_3 and sulfur vapor [167]. Surface sulfurization of

$Cu(In,Ga)Se_2$ (CIGS) thin films was carried out using two alternative techniques that did not utilize toxic H_2S gas; a sequential evaporation of In_2S_3 after CIGS deposition and the annealing of CIGS thin films in sulfur vapor. A $Cu(In,Ga)(S,Se)_2$ thin layer was grown on the surface of the CIGS thin film after sulfurization using In_2S_3, whereas this layer was not observed for CIGS thin films after sulfurization using sulfur vapor, although a trace quantity of S was confirmed by AES analysis. In spite of the difference in the surface modification techniques, the cell performance and process yield of the ZnO:Al/CdS/CIGS/Mo/glass thin-film solar cells were remarkably improved by using both surface sulfurization techniques.

Solar cells of $CuInS_2/In_2S_3$/ZnO type are studied by B. Asenjo et al [168] as a function of the In_2S_3 buffer deposition conditions. In_2S_3 was deposited from an aqueous solution containing thioacetamide (TA), as sulfur precursor and In^{3+}. In parallel, variable amounts of In_2O_3 are deposited that have an important influence on the buffer layer behavior. Higher efficiency was attained with buffer deposited at high temperature (70 °C) and [TA] (0.3 M). These conditions were characterized by short induction time, high deposition rate and low In_2O_3 content in the buffer. For films having higher In_2O_3 content (deposited at lower temperature), the efficiency of the cells decreased with buffer thickness.

K. C. Wilson et al of our group reported a novel route of preparing copper indium sulfide thin films on In_2S_3 thin films [156]. Copper indium sulfide thin films were prepared by copper diffusion into argon ion implanted In_2S_3 thin films. Copper diffusion in implanted samples enabled to prepare an $In_2S_3/CuInS_2$ solar cell.

The conduction band offset between the absorber and the buffer layer is an important parameter influencing conversion efficiency of solar cells. The evolution of the electronic affinity difference, $\chi(CuIn_{0.7}Ga_{0.3}Se_2)$-$\chi$(BISO- β-$In_2S_{3)}$ containing oxygen), versus the optical band of the BISO thin film has been reported [150], from which we can observe that at the conduction band offset between BISO and

$CuIn_{0.7}Ga_{0.3}Se_2$ is well adapted when the optical band gap of the BISO thin film is between 2.50 and 2.90 eV. The value for the CBD-CdS buffer layer is also reported; its electronic affinity corresponds to a 2.70-eV BISO film. For the same conduction band offset (0.20 eV), BISO films induced less absorption losses in the blue region due to their wider band gap. BISO thin films as buffer layer may allow an improvement in the performance of high band gap $Cu(InGa)Se_2$-based solar cells due to a better conduction band offset matching.

Band alignment at the interface of the heterostructure β-In_2S_3/SnO_2 was studied using XPS by Bernède et al [130]. They observed that the conduction band discontinuity (ΔE_c) between β-In_2S_3 and SnO_2 was -0.45 eV. From this value and using SnO_2 work function and the $Cu(In,Ga)Se_2$ electronic affinity values reported in the literature, they estimated the conduction band discontinuity at the interface $Cu(In,Ga)Se_2/\beta$-In_2S_3 to be about 0 eV.

H. Ihara et al has carried out XPS analysis of the valence band of $CdIn_2S_4$ and In_2S_3 single crystals [107]. The spectrum of $CdIn_2S_4$ had a strong resemblance to its synthesized spectrum from the In_2S_3 and CdS spectra, which was in good agreement with the theoretical density of states (DOS). The contribution of constituent atoms to the valence band DOS in $CdIn_2S_4$ was corresponding to those in In_2S_3 and CdS.

A comparative photo-electrochemical study of compact In_2O_3/In_2S_3 multilayer thin films was conducted by S.S. Kale et al. [98] Indium sulfide (In_2S_3) thin films were successfully deposited using chemical bath deposition (CBD) onto indium-doped-tin-oxide (ITO) substrates from an aqueous mixture containing indium chloride and thioacetamide at 343 K. As-deposited films were annealed at 673 K to convert into In_2O_3 and were confirmed through the measurement of energy dispersive X-ray analysis (EDAX). Over In_2O_3, again In_2S_3 film was deposited using CBD to form In_2O_3/In_2S_3 bilayer, where In_2O_3 served as an effective window and/or hole blocking layer and In_2S_3 as a sensitizing layer. Enhanced photochemistry was confirmed from

photo-electrochemical (PEC) measurement, where multilayer thin films showed better performance with solar conversion efficiency (η%) of 0.17% than In_2O_3 and In_2S_3.

Nanocrystalline In_2S_3 modified In_2O_3 electrodes were prepared with sulfidation of In_2O_3 thin film electrodes under H_2S atmosphere by Hara et al [63]. The aqueous slurry of In_2O_3 was prepared from 2 g of commercial In_2O_3 powder, 10 μl of acetylacetone, 50 μl of Triton X-100 (as a surfactant) and distilled water (4 ml). This slurry was deposited on fluorine doped SnO_2 transparent conducting glass using a scotch tape as the spacer with 'doctor blade painting' and calcinated at 500ºC for 1 hour under air. The In_2O_3 thin films were treated under H_2S at 200-300ºC for 10-30 min, resulting in the formation of an In_2S_3/In_2O_3 thin film electrode. Band gap of In_2S_3 estimated from the onset of absorption spectra was 2 eV. This photo-electrochemical cell could convert visible light of 400-700 nm to electrical energy. A highly efficient incident photon to electron conversion efficiency of 33% was obtained at 410 nm. The solar conversion efficiency [η], under AM 1.5 was 0.31% with J_{sc} = 3.1 mA/cm^2, V_{oc} = 0.26 V and FF = 38%.

P. M.Sirimanne has done a comparative study of semiconductor sensitization by micro-crystals of indium sulfide on various porous wide band gap semiconductor substrates [52]. Semiconductor sensitization on various n-type wide band gap semiconductors was studied by using micro-crystals of n-type indium sulfide. The generation of an anodic photocurrent on the electrode was explained from the viewpoint of semiconductor sensitization. A very high incident photon-to-current conversion efficiency (IPCE) of more than 80% was achieved on In_2S_3/In_2O_3 electrodes in a polysulfide electrolyte. The observed values of the IPCE for In_2S_3/TiO_2 and In_2S_3/ZnO electrodes were rather low compared to that of In_2S_3/In_2O_3 electrodes, in the same electrolyte. Semiconductor sensitization process was not observed on In_2S_3/ZnS electrodes. . A very high incident photon to current conversion efficiency of 80% was achieved at an $In_2S_3|In_2O_3$ electrode in a polysulfide electrolyte [40].

Conclusion

A review of the studies carried out on indium sulfide demostrates it to be an ideal buffer layer for PV applications. It could be prepared by a variety of techniques. Simple low cost chemical methods also yield good films and the impurities like oxygen, hydroxides and Na getting incorporated during these processes finds to be beneficial in the case of indium sulfide. Doping could beneficially alter the properties of indium sulfide but only a few studies are reported in this perceptive.

Studies prove that indium sulfide buffer layers allow higher temperature device preparation compared with classical CdS. The Long term stability test qualifies In_2S_3 as buffer material for high-efficiency CIGS thin-film solar modules. The highest efficiency value reported for cell with indium sulfide is slightly lower than value achieved by using CdS buffer layer, this contradicts the expectation of better efficiency for In_2S_3 as it posses a wider band gap. So to grab its potential fully, better optimization has to be done.

References

[1] L. Bhira, H. Essaidi, S. Belgacem, G. Couturier, J. Salardenne, N. Barreau and J. C. Bernede, Phys. Status Solidi A. **181**(2000) 427.

[2] R.Jayakrishnan, Teny Theresa John, C. Sudha Kartha, K. P. Vijayakumar, T. Abe, Y. Kashiwaba, Semicond. Sci. and Technol. **20** (2005) 1162.

[3] S. Yu, L. Shu, Y. Qian, Y. Xie, J. Yang, and L. Yang, Mater. Res. Bull. **33(5)** (1998) 717.

[4] H. Hahn and W. Klinger Z, Inorg. Chem. **260** (1949) 97.

[5] C. J. X. Rooymans J. Inorg, Nucl. Chem. **260** (1959) 78.

[6] G.D.S. King, Acta Cryst. 15, 512 (1962).

[7] J. Goodyear and G. A. Steigmann, Proc. PHYS.SOC. **78** (1961) 491.

[8] C. Haas, J. Phys. Chem. Solids, **26** (1965) 1225-1232.

[9] H. Hatwell, G. Offergeld, C. Herinckx and J. Van Cakenberghe, C.R. Acad. Sc. **258** (1962) 553.

[10] J. V. Landuyt, H. Hatwell and S. Amelinckx, Mater. Res. Bull. **3** (1968) 519.

[11] R S Becker, T Zheng, J Elton and M Saeki, Solar Energy Mater. **13** (1986) 97.

[12] R. Diehl and R. Nische, J. Cryst. Growth **28** (1975) 306.

[13] C. Kaito, Y. Saito and K. Fujita, J. Cryst. Growth **94** (1989) 967.

[14] M. Kambas, J. Spyridelis and M. Balkanski, Phys. Stat. Sol. (a) **105** (1981) 291.

[15] J. Herrero and J. Ortega, Sol. Energy Mater. **17** (1988) 357.

[16] P. N. Kumta, P. P. Phule and S. H. Risbud, Materials Letters, **5(10)** (1987) 401.

[17] M. A. M. Seyam Vacuum **63** (2001) 445.

[18] A. A. El Shazly, D. Abd Elhady, H. S. Metwally and M. A. M. Seyam, J. Phys.:Condens. Mater. **10** (1998) 5943.

[19] A. Timoumi, H. Bouzouita' , M. Kanzari and B. Rezig, Thin Solid Films, **480-481** (2005) 124-128.

[20] A. Timoumi, H. Bouzouita, R. Brini, M. Kanzari and B. Rezig**,** Applied Surface Science **253** (2006) 306.

[21] J. George, K. S. Joseph. B. Pradeep and T. I. Palson, Phys. Stat. Sol. (a) **106** (1988) 123.

[22] P. S. Vincett, Thin Solid Films **100** (1983) 371.

[23] N. Barreau, J. C. Bernède, H. E. Maliki, S. Marsillac, X. Castel and J. Pinel, Solid State Comun. **110** (1999) 231.

[24] G. A. Kitaev and U. T. Dvounin, Inorg. Mater. **12** (1976) 1448.

[25] R. Bayón, C. Maffiotte and J. Herrero, Thin Solid Films **353** (1999) 100.

[26] R. Bayón' and J. Herrero, Applied Surface Science, **158(1-2)** (2000) 49.

[27] R. Bayón' and J. Herrero, Thin Solid Films, **387(1-2)** (2001) 111.

[28] C. D. Lokhande, A. Ennaoui, D. S. Patil, M. Giersig, K. Diesner, M. Muller and H. Tributsch, Thin Solid Films **340** (1999) 18.

[29] T. Yoshida, K. Yamaguchi, H. Toyoda, K. Akao, T. Sugiura, H. Minoura and Y. Nosaka, Proc. Electrochem. Soc. **PV 97-20** (1997) 37.

[30] K. Yamaguchi, T. Yoshida and A. Minoura, Thin Solid Films **431-432** (2003) 354.

[31] M. G. Sandoval-Paz, M. Sotelo-Lerma, J. J. Valenzuela-Jáuregui, M. Flores-Acosta, and R. Ramírez-Bon, Thin Solid Films **472(1-2) (**2005) 5.

[32] B. Yahmadi, N. Kamoun' , R. Bennaceur, M. Mnari, M. Dachraoui and K. Abdelkrim Thin Solid Films, **473(2)** (2005) 201.

[33] B. R. Sankapal, S. D. Sartale, C. D. Lokhande and A. Ennaoui, Sol. Energy Mater. Sol. Cells **83** (2004) 447.

[34] R. S. Mane and C. D. Lokhande, Materials Chemistry and Physics, **78(1)** (2003) 15.

[35] H.M. Pathan, C.D. Lokhande, S.S. Kulkarni, D.P. Amalnerkar, T. Seth and Sung-Hwan Han, Materials Research Bulletin, 40(6) (2005) 1018.

[36] R. Ranjith, Teny Theresa John, C. Sudha Kartha, K.P. Vijayakumar , T. Abe and Y. Kashiwaba,, Materials Science in Semiconductor Processing, 10(1) (2007) 49.

[37] R. Kumaresan, M. Ichimura, N. Sato and P. Ramasamy, Mat. Sci. Eng. **B96** (2002) 37.

[38] N. R. de Tacconi and K. Rajeshwar, J. Electro. Anal. Chem. **444** (1998) 7.

[39] A. Goswami, G. D. Talele and S. B. Badachhape, Indian J. Pure Appl. Phys. **14** (1976) 716.

[40] P. M. Sirimanne' , N. Sonoyama and T. Sakata, Chemical Physics Letters , **350(3-4)** (2001) 211.

[41] N. Naghavi, R. Henriquez, V. Latev and D. Lincot, Appl. Surf. Sci. **222** (2004) 65.

[42] E. B. Yousfi, B. Weinberger, F. Donsanti, P. Cowache and D. Lincot, Thin Solid Films **387** (2001) 29.

[43] A. R. Barron, Adv. Mat. Opt. Elec. **5** (1995) 245.

[44] P. O'Brien, D. J. Otway and J. R. Walsh, Thin Solid Films, **315(1-2)** (1998) 57.

[45] A. N. MacInnes, M. B. Power, A. F. Hepp and A. R. Barron, Journal of Organometallic Chemistry**, 449(1-2)** (1993) 95.

[46] R. Nomura, K. Konishi and H. Matsuda, Thin Solid Films,Volume **198(1-2)** (1991) 339.

[47] S. Kosaraju, J. A. Marino, J. A. Harvey and C. A. Wolden, Solar Energy Materials and Solar Cells, **90(7-8)** (2006) 1121.

[48] N. Barreau, S. Marsillac and J. C. Bernède, Vacuum, **56(2)** (2000) 101.

[49] C. L. Cahill, B. Guliotta and J. B. Parise, Chem. Commun. (1998) 1715.

[50] T. Asikainen, M. Ritala and M. Leskelä, Appl. Surf. Sci. **82-83** (1994) 122.

[51] V. G. Bassergenev, E. N. Ivanova, Y. A. Kovalevskaya, S. A. Gromilov, V. N. Kirichenko and S. V. Larionov, J. Inorg. Mat. **32 (6)** (1996) 592.

[52] P. M. Sirimanne' , Y. Yasaki, N. Sonoyama and T. Sakata, Materials Chemistry and Physics, **78(1)** (2003) 234.

[53] C. Guillén, T. García, J. Herrero, M. T. Gutiérrez and F. Briones, Thin Solid Films, **451-452** (2004)112-115.

[54] C. Sanz , C. Guillén and M.T. Gutiérrez**,** Thin Solid Films, **511-512** (2006) 121-124.

[55] Y. Xiong, Y. Xie, G. Du, X. Tian and Y. Qian, J. Solid state Chem. **166** (2002) 336.

[56] C. Kaito, A. Ito, S. Kimura, Y. Kimura, Y. Saito and T. Nakada, J. Cryst. Growth **218** (2000) 259.

[57] S. Gorai, A. Datta and S. Chaudhuri, Materials Letters, **59(24-25)** (2005) 3050.

[58] Rahana Yoosuf and M.K. Jayaraj, Solar Energy Materials and Solar Cells, **89(1)** (2005) 85.

[59] B. Asenjo, A.M. Chaparro' , M.T. Gutiérrez, J. Herrero and C. Maffiotte, Thin Solid Films, **480-481** (2005) 151.

[60] Yoichi Yasaki, Noriyuki Sonoyama and Tadayoshi Sakata, Journal of Electroanalytical Chemistry, **469(2)** (1999) 116.

[61] Norma R. de Tacconi and Krishnan Rajeshwar, Journal of Electroanalytical Chemistry, **444(1)** (1998) 7.

[62] B. Asenjo, C. Sanz, C. Guillén, A.M. Chaparro, M.T. Gutiérrez and J. Herrero, Thin Solid Films, **515(15)** (2007) 6041-6044.

[63] K. Hara, K. Sayama and H. Arakawa, Sol. Energy Mater. Sol. Cells **62** (2000) 441.

[64] H. B. Devore, Phys Rev. **102** (1956) 1.

[65] N. Kamoun, R. Bennaceur, M. Amlouk, S. Belgacem, N. Milki, J. M. Frigerio and M. L. Theye, Phys. Stat. Sol (a) **169** (1998) 97.

[66] W. T. Kim and C.D. Kim, J. Appl. Phys. **60(7)** (1986) 2631.

[67] N. Bouguila, H. Bouzouita, E. Lecaze, A. B. Amara, H. Bouchriha and A. Dhouib, J. Phys. III **7** (1997) 1647.

[68] Teny Theresa John, S. Bini, Y. Kashiwaba, T. Abe, Y. Yasuhiro, C. Sudha Kartha, K. P. Vijayakumar, Semicond. Sci. and Tech. **18**, (2003)491.

[69] Teny Theresa John, C. Sudha Kartha, K.P. Vijayakumar, T. Abe and Y. Kashiwaba Vacuum, **80(8)** (2006) 870.

[70] P.M. Ratheesh Kumar, Teny Theresa John, C. Sudha Kartha and K.P. Vijayakumar, Nuclear Instruments and Methods in Physics Research Section B: Beam Interactions with Materials and Atoms, **244(1)** (2006) 171.

[71] Teny Theresa John, C. Sudha Kartha, K.P. Vijayakumar , T. Abe and Y. Kashiwaba, Applied Surface Science, **252(5)** (2005) 1360.

[72] M. Calixto-Rodriguez, A. Tiburcio-Silver , A. Ortiz and A. Sanchez-Juarez, Thin Solid Films, **480-481** (2005) 133.

[73] N.A. Allsop, A. Schönmann, A. Belaidi, H.-J. Muffler, B. Mertesacker, W. Bohne, E. Strub, J. Röhrich, M.C. Lux-Steiner and Ch.-H. Fischer Thin Solid Films, **513(1-2)** (2006) 52

[74] L. E.Brus, J. Chem. Phys. **79** (1983) 5566-5571.

[75] L. E.Brus, Jerusalem Symp. Quantum Chem. Biochem. **17** (1984) 431-435.

[76] A. L.Efros,; Efros, A. L. Fiz. Tekh. PoluproVodn. (Leningrad) **1982**, 16, 1209-1214.

[77] A. P. Alivisatos, J. Phys. Chem. **100** (1996) 13226-13239; Weller, H. Philos. Trans. R. Soc. London A **1996**, 354, 757-766; Brus, L. E.; Trautman, J. K. Philos. Trans. R. Soc. London A **1995**, 353, 313-321; Bawendi, M. G. Solid State Commun. **1998**, 107, 09-709.

[78] P.Kamat, N. M.Dimitrievich, R. W Fessenden, J. Phys. Chem **92** (1988) 2324-2329.

[79] R.Suarez, P. K Nair, P.Kamat, Langmuir **14** (1998) 3236-3241.

[80] N.Dimitrievich, P.Kamat, Langmuir **3 (**1987) 1004-1009.

[81] Y.Nosaka, N.Ohta, H.Miyama, J. Phys. Chem. **94** (1990) 3752- 3755.

[82] R.Vogel, P.Hoyer, H.Weller, J. Phys. Chem. **98** (1994) 3183- 3188.

[83] Y.Yuan, I.Cabasso, Fendler, J. Chem. Mater. **2** (1990) 226- 229.

[84] J. P.Wilcoxon, P. P.Newcomer, G. A.Samara, J. Appl. Phys. **81** (1997) 7934-7944.

[85] J. P.Wilcoxon, P. P.Newcomer, G. A. Samara, Solid State Commun. **98** (1996) 581-585.

[86] K.Dattatri Nagesha, Xiaorong Liang, Arif A. Mamedov, Gordon Gainer, Margaret A. Eastman, Michael Giersig, Jin-Joo Song, Tong Ni, and Nicholas A. Kotov., J. Phys. Chem. B **105** (2001**)** 7490-7498

[87] P.Lianos, J. K.Thomas, Mater. Sci. Forum 25-29 (1988) 369.

[88] S. I.Radautsan, N. N.Syrbu, V. E.Tezlevan, K. F.Sherban, N. P. Baran, Phys. Status Solidi B **57** (1973) K93-K97; Nakanishi, H. Jpn. J. Appl. Phys. **19 (**1980) 103-108,

[89] D. T. Kim, K. S.Yu,; W. T.Kim, Sae Mulli **31** (1991) 477-481.

[90] J.Cizeron, M. P.Pileni, J. Phys. Chem. B **101** (1997) 8887-8891.

[91] Y.Tian,; T.Newton; N. A.Kotov; D.Guldi, J.Fendler, J. Phys. Chem. **100** (1996) 8927.

[92] F. V.Mikulec, M.Kuno, M.Bennati, D. A.Hall, R. G.Griffin, M. G.Bawendi, J. Am. Chem. Soc. **122** (2002) 532.

[93] D. J.Norris, N.Yao, F. T.Charnock, T. A. Kennedy, Nano Lett. **1** (2001) 3-7.

[94] S. H. Yu, L. Shu, Y. S. Wu, J. Yang, Y. Xie and Y. T. Qian J. Am. Ceram. Soc **82 (2)** (1999) 457

[95] Qichun Zhang, Xianhui Bu , Lei Han , Pingyun Feng, Inorg. Chem., **45 (17)** (2006) 6684 -6687.

[96] Mohammmad Afzaal, Mohammad A. Malik and Paul O'Brien, Chem. Commun., 2004, 334.

[97] Changhao Liang, Yoshiki Shimizu, Takeshi Sasaki, Hiroyuki Umehara and Naoto Koshizaki, J. Mater. Chem., **14** (2004) 248.

[98] S. S. Kale, R.S. Mane, C.D. Lokhande, K.C. Nandi and Sung-Hwan Han, Materials Science and Engineering: B, **133(1-3)** (2006) 222-225.

[99] Anuja Datta, Subhendu K. Panda, Soma Gorai, Dibyendu Ganguli and Subhadra Chaudhuri, Materials Research Bulletin (Article in Press).

[100] A. Datta, S. Gorai, D. Ganguli and S. Chaudhuri**,** Materials Chemistry and Physics, Volume **102(2-3)** (2007) 195.

[101] Xuebo Cao, Li Gu, Lanjian Zhuge, Wenhu Qian, Cui Zhao, Xianmei Lan, Wenjun Sheng and Dan Yao, Colloids and Surfaces A: Physicochemical and Engineering Aspects**, 297 (1-3)** (2007) 183.

[102] D.P. Dutta, G. Sharma, A.K. Tyagi and S.K. Kulshreshtha, Materials Science and Engineering: B, **138(1)** (2007) 60-64.

[103] Paz Vaqueiro, Journal of Solid State Chemistry, **179(1)** (2006) 302-307.

[104] S. Gorai and S. Chaudhuri**,** Materials Chemistry and Physics, **89(2-3)** (2005) 332.

[105] S. Gorai and S. Chaudhuri, Materials Science and Engineering: B, **126(1)** (2006) 97.

[106] Yujie Xiong, Yi Xie, Guoan Du, Xiaobo Tian and Yitai Qian, Journal of Solid State Chemistry, **166(2)** (2002) 336.

[107] H. Ihara, H. Abe, S. Endo and T. Irie, Solid State Communications, **28(7)** (1978) 563-565.

[108] Xiaoyi Zhu, Junfeng Ma, Yonggang Wang, Jiantao Tao, Jun Zhou, Zhongqiang Zhao, Lijin Xie and Hua Tian, Materials Research Bulletin **41(8)** (2006) 1584.

[109] Shaohua Shen and Liejin Guo, Journal of Solid State Chemistry **179(8)** (2006) 2629-2635.

[110] V. G. Bessergenev, A. V. Bessergenev, E .N. Ivanova and Y. A. Kovaevskaya, J. Solid State Chem. **137** (1998) 6.

[111] Niyum S. Rampersadh , Andrew M. Venter and David G. Billing, Physica B: Condensed Matter, **350(1-3) 1** (2004) E383.

[112] B. Asenjo, A. M. Chaparro' , M. T. Gutiérrez, J. Herrero and C. Maffiotte, Electrochimica Acta, Volume 49, Issue 5, 25 February 2004, Pages 737.

[113] M.M. El-Nahass, B.A. Khalifa, H.S. Soliman and M. A.M. Seyam, Thin Solid Films, **515(4, 5)** (2006) 1796.

[114] E. Kauer and A. Rabenau Z, Naturef **13a** (1958) 531.

[115] R. H. Bube and W. Mc Carroll, J. Phys. Chem. Solids **10** (1959) 333.

[116] J. M. Gilles, H. Hatwell, G. Offergeld and J. Van Cakenberghe, Phys. Stat. Sol. **2** (1962) K73.

[117] G. F. Garlick, M. Springford and H. Checinska, Proc. Phys. Soc. **82** (1963) 16.

[118] M. Rehwald and G. Harbeke, J. Phys. Chem. Solids **26** (1965) 1309.

[119] M. Kambas, A. Anagnostopoulos, S. Ves, B. Ploss and J. Spyridelis, Phys. Stat. Sol. (a) **127** (1985) 201.

[120] J. C. Manifacier, J. Gasiot and J. P. Fillard, J. Phys. E **9** (1976) 1002.

[121] N. Barreau, S. Marsillac, D. Albertini and J. C. Bernède, Thin Solid Films **403-404** (2002) 331.

[122] N. Barreau, S. Marsillac, J. C. Bernède, T. B. Nasrallah and S. Belgacem, Phys. Stat. Sol (a) **184 (1)** (2001) 179.

[123] R. S. Mane and C. D. Lokhande Mat. Chem. Phys. **82** (2003) 1

[124] T. Nishimo, K. Taniguchi and Y. Hamakawa, Solid State Communications, **19 (7)** (1976) 635.

[125] S. Chaisitsak, T. Sugiyama, A. Shimizu, A. Yamada and M. Konagi, Proc. PVSEC **11** (1999) 34.

[126] N. M. Gasanly and A. Aydinli, Solid State Commun. **101 (11)** (1997) 797.

[127] N. M. Gasanly , H. Özkan, A. Aydinli and. Yilmaz, Solid State Communications, **110(4)** (1999) 231.

[128] F. E. Faradzhev, N. M. Gasanly and A. S. Ragimov, A. F. Goncharov, S. I. Subbotin, Solid State Communications, **39(4)** (1981) 587.

[129] M. Amlouk, M. A. Ben Said, N. Kamoun, S. Belgacem, N. Brunet and D. Barjon, Jpn. J. Appl. Phys. **38** (1999) 26.

[130] J. C. Bernède, N. Barreau, S. Marsillac and L. Assmann, Appl. Surf. Sci. **195** (2002) 222.

[131] N. M. Gasanly, A. Aydinli, N. S. Yaksek, Mat. Res. Bull. **38** (2003) 699.

[132] Rupa R Pai, Teny Theresa John, Y. Kashiwaba, T. Abe, K. P. Vijayakumar and C. Sudha Kartha, J. Mater. Sci. **39** (2004) 1.

[133] R. Diehl and R. Nische , Journal of Crystal Growth, **20(1)** (1973) 38.

[134] S. H. Choe, T. H. Bang, N. O. Kim, H. G. Kim, C. I. Lee, M. S. Jim, S. K. Oh and W. T. Kim, Semicond. Sci. Technol. **16** (2001) 98

[135] C. D. Kim, H. Lim, H. L. Park, H. Y. Park, J. E. Kim, H. G. Kim, Y. G. Kim and W. T. Kim, Thin Solid Films , **224(1)** (1993) 69.

[136] W. T. Kim, C. S. Yun, H. M. Jong and C. D. Kim, J. Appl. Phys. **60(7)** (1986) 2357.

[137] W. T. Kim, W. S. Lee, C. S. Chung and C. D. Kim, J. Appl. Phys. **63 (11)** (1988) 5472.

[138] L. Bhira, T. Ben Nasrallah, J. C. Bernède and S. Belgacem, Materials Chemistry and Physics, **72(3)** (2001) 320.

[139] N. Kamoun, S. Belgacem, M. Amlouk, R. Bennaceur, J. Bonnet, F. Touhari, M. Nouaoura and L. Lassabatere, J. Appl. Phys. **89(5)** (2001) 2766.

[140] L. Bhira, S. Belgacem and J. C. Bernède, J. Appl. Phys **92(19)** (2002) 5327.

[141] A. Kulińska, M. Uhrmacher, R. Dedryvère, A. Lohstroh, H. Hofsäss, K. P. Lieb, A. P. Garcia and J. C. Jumas, J. Solid State Chem. **177** (2004) 109.

[142] N. Barreau, S. Marsillac, J. C. Berne`de,a) and L. Assmann, J. Appl. Phys **93(9)** (2003).

[143] R. Robles, A. Vega, and A. Mokrani, Opt. Mater. **17** (2001) 497.

[144] S. F. Matar, A. Villesuzanne, G. Campet, J. Portier, and Y. Saikali, C.R. Acad. Sci., Ser. IIc: Chim **4** (2001) 367.

[145] N. Barreau, J. C. Berne`de, S. Marsillac, and A. Mokrani, J. Cryst. Growth **235** (2002) 439.

[146] N. Barreau , J. C. Bernède, C. Deudon, L. Brohan and S. Marsillac, Journal of Crystal Growth, **241(1-2)** (2002) 4.

[147] N. Barreau, J. C. Bernède and S. Marsillac, J. Cryst. Growth **241** (2002) 51.

[148] F. Py, M. Womes, J. M. Durand, J. Olivier-Fourcade and J. C. Jumas, J. M. Esteva and R. C. Karnatak, Journal of Alloys and Compounds , **178(1-2)** (1992), 297.

[149] N. Naghavi, S. Spiering, M. Powalla, B. Cavana3and D. Lincot, Prog. Photovolt: Res. Appl. **11** (2003) 437–443.

[150] N. Naghavi, S.Spiering, M. Powalla, D. Lincot, Proceedings of 3rd World Conference on Photovoltaic Energy Conversion, **1** (2003) 340 - 343.

[151] A. Lafond, C. Guillot-Deudon, S. Harel, A. Mokrani, N. Barreau, S. Gall and J. Kessler, Thin Solid Films , **515(15)** (2007) 6020-6023.

[152] S. Spiering, A. Eicke, D. Hariskos, M. Powalla, N. Naghavi and D. Lincot, Thin Solid Films**, 451-452** (2004) 562-566.

[153] S. Spiering, D. Hariskos, M. Powalla, N. Naghavi and D. Lincot, Thin Solid Films**, 431-432** (2003) 359-363.

[154] S. Spiering, D. Hariskos, S. Schröder and M. Powalla, Thin Solid Films **480-481** (2005) 195-198.

[155] Dimitri Hariskos, Martin Ruckh, Ulfert Riihle, Thomas Walter, Hans Werner Schock, Jonas Hedstrom, Lars Stolt, Solar Energy Materials and Solar Cells **41-42** (1996) 345-353.

[156] K. C. Wilson, Tina Sebastian, Teny Theresa John, C. Sudha Kartha, K. P. Vijayakumar, P. Magudapathi and K. G. M. Nair, Appl. Phys. Lett. **89**, (2006) 013510.

[157] N. A. Allsop, Christian A. Kaufmann, Axel Neisser, Marin Rusu, Andreas Hänsel, Martha C. Lux-Steiner, Christian-H. Fischer, MRS Proceedings **865** (2005) F14.23.

[158] N. A. Allsop, C. Camus, A. Hänsel, S.E. Gledhill, I. Lauermann, M.C. Lux-Steiner and Ch.-H. Fischer, Thin Solid Films, **515(15)** (2007) 6068-6072.

[159] N. A. Allsop, A. Hänsel, S. Visbeck, T.P. Niesen, M.C. Lux-Steiner and Ch.-H. Fischer, Thin Solid Films, **511-512** (2006) 55-59.

[160] S. Gall' , N. Barreau, S. Harel, J.C. Bernède and J. Kessler, Thin Solid Films, **480-481** (2005) 138-141.

[161] S. Gall, N. Barreau' , F. Jacob, S. Harel and J. Kessler, Thin Solid Films, **515(15)** (2007) 6076-6079.

[162] N. Barreau, J. C. Bernède, S. Marsillac, C. Amory and W. N. Shafarman, Thin Solid Films**, 431-432** (2003) 326-329.

[163] N. Barreau, C. Deudon, A. Lafond, S. Gall and J. Kessler, Solar Energy Materials and Solar Cells, **90(12)** (2006) 1840-1848.

[164] F. Jacob, N. Barreau , S. Gall and J. Kessler, Thin Solid Films, **515(15)** (2007) 6028-6031

[165] Teny Theresa John , Meril Mathew, C. Sudha Kartha, K.P. Vijayakumar' , T. Abe and Y. Kashiwaba, Solar Energy Materials and Solar Cells, **89(1)** (2005) 27-36

[166] K. Ernits, D. Brémaud, S. Buecheler, C.J. Hibberd[c], M. Kaelin, G. Khrypunov, U. Müller, E. Mellikov and A.N. Tiwari, Thin Solid Films, **515(15)** (2007) 6051-6054.

[167] D. Ohashi, T. Nakada and A. Kunioka, Solar Energy Materials and Solar Cells, **67(1-4)** (2001) 261-265

[168] B. Asenjo, A.M. Chaparro, M.T. Gutierrez, J. Herrero and J. Klaer, Solar Energy Materials and Solar Cells, **87(1-4)** (2005) 647-656

Chapter 3
Silver Doped Indium Sulfide Thin Films

3.1 Introduction

Addition of 'impurities' to a semiconductor often induces dramatic changes in electrical and optical properties. Effect of the dopant elements depends on its electro negativity and the difference in ionic radii with the lattice atoms. A precise study on the doped film is essential to get controlled variations in the properties of the doped sample through doping and this is indispensable for optoelectronic device applications.

β-In_2S_3, the stable phase of In_2S_3 at room temperature, crystallizes in a defect spinel lattice, with high degree of vacancies, ordering at tetrahedral cation sites [1]. The ordered modification can therefore be interpreted as a quasi-ternary compound consisting of In, S and vacancies. Here eight of the twelve tetrahedral sites are occupied by indium and the remaining four are empty (the latter are ordered). All octahedral sites are occupied by In and could be written as $In_6(In_2\square)S_{12}$, where □ indicates vacancies and parenthesis describes tetrahedral site [2]. However, a small fraction of indium atoms may leave their ordered positions and occupy crystallographically ordered vacancies. This results in a number of quasi-interstitial cations and an equal number of cation vacancies, so that in a stoichiometric crystal of β-In_2S_3, considerable degree of disorder is always present [3]. These vacancies act as host to the foreign elements, making In_2S_3 a suitable compound for doping. Because of its high defect structure, this material finds several applications in preparing red and green phosphors for television picture tubes [4], dry cells [5], and photochemical cells [6], in addition to photovoltaic applications.

There are only few reports on doping of In_2S_3 films, so as to modify its structural and electrical properties. Becker et al. found that doping of In_2S_3 films with

Sn resulted in samples with low resistance [2]. Doping of indium sulfide single crystals with cobalt, lead to the decrease of structural defects [7]. N. Kamoun et al. reported that presence of Al caused an increase in adsorption of oxygen in the sample [8]. Roland Diehl and Rudolf Nitsche [9], presented stabilization of γ-In_2S_3, (which is the high temperature phase of In_2S_3) at room temperature by replacing about 5 to 10% of In atoms by As, Sb or Bi. Barreau et al. reported that incorporation of Na resulted in wider band gap and better conductivity [10].

During the course of investigations to produce low resistive ohmic contact to ITO/$CuInS_2$/In_2S_3 cell structure, it was observed that the efficiency of the cell enhanced significantly by the use of silver electrodes over In_2S_3. The cell could attain an efficiency of 9.5% [11]. But with aluminum electrodes, the efficiency was very low. Hence it was strongly suspected that the increase in efficiency might be due to the effect of silver on indium sulfide (In_2S_3). Present studies were carried out on this observation and the results revealed that Ag changed the properties of In_2S_3 favorably. In this chapter, the variations induced by Ag doping in structural, electrical and optical properties of spray pyrolysed β-In_2S_3 thin films are described.

3.2 Experimental Details

In_2S_3 thin films were deposited on soda lime glass substrate, using chemical spray pyrolysis (CSP) technique. In the spray deposition process, a precursor solution, (usually aqueous) containing soluble salts of constituents of the desired compound is pulverised by means of gas so that it arrives at the heated substrate in the form of very fine droplets. The constituents react to form a chemical compound onto the substrate. The chemical reactants are selected such that the products other than the desired compound are volatile at the temperature of deposition.

A typical spraying system mainly consists of spray nozzle, precursor solution, substrate heater, temperature controller and air compressor or gas propellant. To

measure flow of precursor solution and air, liquid and gas flow meters are used respectively. Vertical and slanted spray deposition arrangements with stationary or linearly moving spray nozzle are frequently used. To achieve uniform deposition the moving arrangements (either nozzle or substrates or both) have been used. Properties of the film depend on the anion to cation ratio, spray rate, substrate temperature, ambient atmosphere, carrier gas, droplet size and also the cooling rate after deposition. The film thickness depends upon the distance between the spray nozzle and substrate, the substrate temperature, the concentration of the precursor solution and the quantity of the precursor solution sprayed [i.e. spray rate]. The film formation depends on the process of droplet landing, reaction and solvent evaporation, which in turn are related to droplet size and momentum. Lampkin [12] showed that depending on droplet velocity and flow direction, a droplet may flatten, skip along the surface or hover motionless.

Since the pioneering work by Chamberlin and Skarman [13] in 1966 on cadmium sulfide (CdS) films for solar cells, several studies have been done during the last three decades on chemical spray pyrolysis (CSP) processing and preparation of thin films. Due to simplicity of the apparatus and good productivity of this technique on a large scale, it offered the most attractive way to produce thin films of noble metals, metal oxides, spinel oxides, chalcogenides and superconducting compounds. In addition to its simplicity, CSP has a number of advantages.

It offers an extremely easy way to dope films with any element in any proportion, provided it forms solution in a solvent. Then it can be added to the spray solution.

1. Unlike closed vapour deposition methods, CSP does not require high quality targets and/or substrates nor does it require vacuum at any stage, which is a great advantage especially for scaling up for industrial applications.

2. Deposition rate and thickness of the films can be easily controlled over a wide range by changing the spray parameters; this eliminates the major drawbacks of chemical methods such as sol-gel which produces films of limited thickness.
3. Operating at moderate temperatures (in the range, 300 to 400^0C), CSP can produce films on less robust materials.
4. Unlike high-power methods such as radio frequency magnetron sputtering (RFMS), it does not cause local overheating that can be detrimental for materials to be deposited. There are virtually no restrictions on substrate material, dimension or its surface profile.
5. By changing composition of the spray solution during the spray process, it can be used to make layered films and films having composition gradients along the thickness.
6. It is believed that reliable fundamental kinetic data are more likely to be obtained on particularly well characterized film surfaces, provided the films are compact, uniform with no side effects from the substrate.
7. It is very much suitable for depositing large area thin films using simple apparatus with good reproducibility.

Experimental set-up we used for the deposition of indium sulfide film is schematically shown in figure 3.1. Cleaned glass slides (37 x 12 x 1.4 mm^3) were placed on a thick iron block (15 x 9 x 1 cm^3), which could be heated to the required temperature with a controlled heater. Temperature of substrate holder was measured using a digital thermometer (Thermis, series 4000) and temperature control was achieved using a variable transformer. Spray head and heater with substrate were kept inside a chamber having an exhaust fan for removing gaseous by- products and vapor of the solvent (here water). During spray, the temperature of substrate was kept constant with an accuracy of ± 5º C. Pressure of carrier gas was noted using a

manometer and was kept at 90 ± 0.5 cm of Hg. Spray rate was 20 ml/min and the distance between spray head and substrate was ~ 15 cm. In order to get uniform composition and thickness, the spray head was moved to either side manually with uniform speed. At a time we kept three substrates spread over the heater for sample preparation. All these samples were found to be good for further studies.

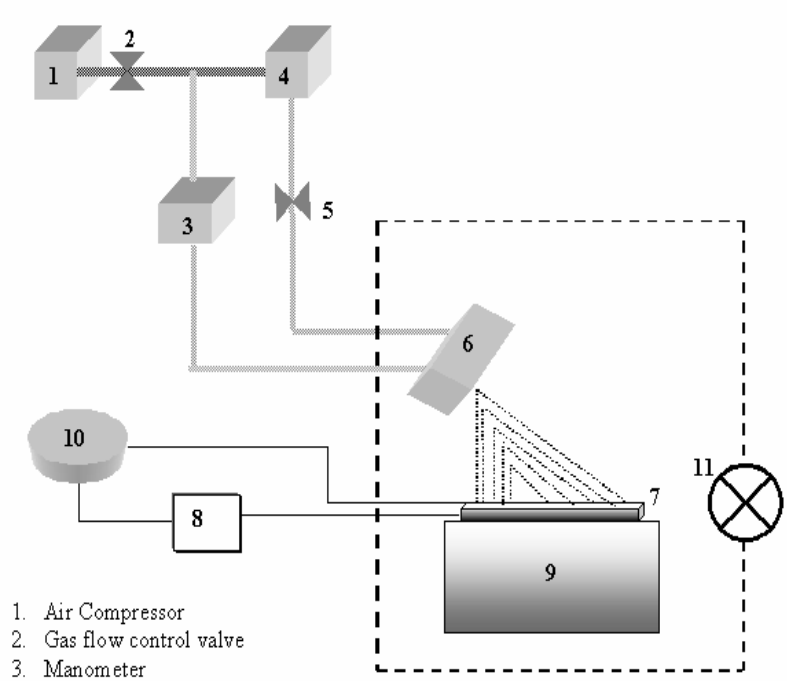

Fig. 3.1 Experimental set-up for spray pyrolysis system

In_2S_3 thin films were deposited by spraying aqueous solutions of indium chloride ($InCl_3$) and thio-urea ($CS(NH_2)_2$) using compressed air as carrier gas.

Thiourea was chosen as the source of sulfur ions in spray solution because it avoids precipitation of metallic sulfides and hydroxides by forming complexes with indium ions [14]. Aqueous solutions of these salts were prepared in distilled water. Indium to sulfur ratio in the solution was varied by varying molar concentration of $InCl_3$ and CS $(NH_2)_2$. Formation of In_2S_3 results from the chemical reaction:

$$2\ InCl_3 + 3\ CS(NH_2)_2 + 6\ H_2O \rightarrow In_2S_3 + 3\ CO_2 + 6\ NH_4Cl$$ [15].

The ratio of the compounds in the solution was varied to change the atomic ratio of In and S in the resulting films. In the present studies the ratio of $InCl_3$ and $(CS(NH_2)_2)$ was selected to be 1.2:8 as this ratio yielded nearly stoichiometric films and exhibited high photosensitivity [16]. 200 ml of the solution was sprayed at a rate of 20 ml/min on to the glass substrate kept at a temperature of 573 ± 5 K. Thickness of the film was 0.5μm. Experiment was also done with indium rich and sulfur rich films. This was achieved by preparing the films using solutions having In to S ratio 2.5:3 and 1.2:10 respectively.

To dope these samples with silver, thin layer of silver was deposited over the In_2S_3 layer using vacuum evaporation technique (pressure during evaporation ~$2x10^{-5}$ m bar). A minor rise in temperature of 12 K was observed during the silver deposition. Studies were conducted on these samples without any post deposition annealing. Different masses of silver (3, 5, 10, 12 and 15 mg) were evaporated for doping different sets of In_2S_3 films. The doped samples were named as IS:3Ag, IS:5Ag, IS:10Ag, IS:12Ag, IS:15Ag respectively and pristine sample was named as IS.

3.3 Results and Discussion

For In_2S_3 samples prepared using CSP technique when coated with a thin layer of Ag, it was found that silver diffused without any thermal assistance i.e. post deposition annealing. Thickness of the films and In to S ratio of the films was varied to optimize the doping parameters.

3.3.1. Structure and Morphology

3.3.1.1. X-Ray Diffraction (XRD)

XRD is an extremely important technique in the field of material characterization to obtain information on an atomic scale from both crystalline and non crystalline (amorphous) materials. It can be used to determine the phase content in many minerals and materials. It requires no elaborate sample preparation and is essentially non-destructive. Generally, it gives a whole range of information about the crystal structure, orientation, crystallite size, composition (with the help of standards), defects and stresses in thin films. Experimentally obtained diffraction pattern of the sample is compared with Joint Council Powder Diffraction (JCPDS) data for Standards. This gives information of different crystallographic phases, the relative abundance and preferred orientations. From the width of the diffraction peak, average grain size in the film can also be estimated.

Inter-planar spacing *d* was calculated from the X-ray diffraction profiles using the formula,

$$2d \sin\theta = n\lambda \quad \text{..... (3.1)}$$

where θ is the Bragg angle, *n* is the order of the spectrum and λ is the wavelength of X-rays. Using the *d*-values the set of lattice planes (h k l) were identified from the standard data and the lattice parameters were calculated using the following relations. For the tetragonal systems,

$$\frac{1}{d^2} = \frac{(h^2 + k^2)}{a^2} + \frac{l^2}{c^2} \quad \text{..... (3.2)}$$

and for hexagonal systems, [17]

$$\frac{1}{d^2} = \frac{4(h^2 + hk + k^2)}{3a^2} + \frac{l^2}{c^2} \quad \text{.....(3.3)}$$

where *a* and *c* are lattice parameters. The grain size (*D*) can be evaluated using Scherrer's formula,

$$D = \frac{k\lambda}{\beta \cos\theta} \quad \text{..... (3.4)}$$

where *k* is a constant which is nearly equal to one and β is the "full width at half maximum (FWHM)", usually measured in radians.

In the present study, XRD analysis was done using Rigaku (D.Max.C) X-Ray Diffractometer, with Cu K_α (λ = 1.5405 Å) radiation and a Ni filter operated at 30 kV and 20 mA.

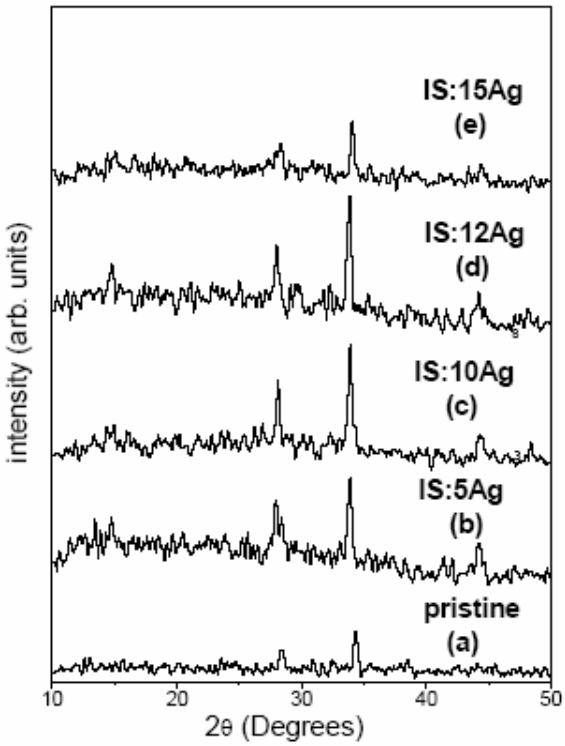

Fig. 3.2 Variation of XRD just after deposition of Ag

Figure 3.2(a) shows X-ray diffraction (XRD) pattern of pristine In_2S_3 thin film (all figures have the same scale on Y-axis). Figures 3.2(b)-(e) depict XRD patterns of

In_2S_3 samples just after silver deposition. The *d*-values of all samples coincided with that of β-In_2S_3 in standard JCPDS data card (25-390). For silver doped samples, it was very clear that the Bragg peaks in XRD pattern became more intense, indicating a clear improvement in crystallinity. However it was also evident that there was an optimum value of doping, up to which the crystallinity increased and after that a retracing phenomenon was observed. In this case, the crystallinity increased up to sample IS:12Ag and started decreasing from IS:15Ag. It was also noted that no new phase was observed even for the sample which had 15 mg of silver deposited, indicating that silver incorporation did not change the structure of In_2S_3 nor resulted in the formation of any new compounds.

Table 3.1. Grain size, lattice parameters and *c/a* as a function of Ag concentration

Sample	d (A^o)	Grain size (nm)	**Lattice parameters**		*c/a*
			a	*c*	
IS	2.675	16.28	7.567	32.14	4.247
IS:5Ag	2.699	26.24	7.634	32.41	4.245
IS:10Ag	2.699	28.82	7.634	32.41	4.245
IS:12Ag	2.699	36.87	7.634	32.41	4.245
IS:15Ag	2.695	28.26	7.623	32.28	4.234
Standard JCPDS (25-390)	2.694	-	7.619	32.33	4.24

From XRD studies (Fig. 3.2), it was also clear that after diffusion of silver the peak positions shifted slightly to lower values of 2θ. Correspondingly, value of lattice spacing (*d*) increased, (Table 3.1). Lattice constants were calculated for tetragonal β-In_2S_3 and it was found that with silver deposition, lattice constant '*a*' increased from 7.567 Å to 7.634 Å (nearer to standard value) and *c*-value increased above the

standard value. This observation proved that lattice parameters increased with silver deposition. The *c/a* ratio was nearly constant for all samples. Grain size calculated using Debye Scherrer formula, also showed a considerable increase with silver deposition (Table 3.1). But there was a decrease in grain size after optimum value of doping.

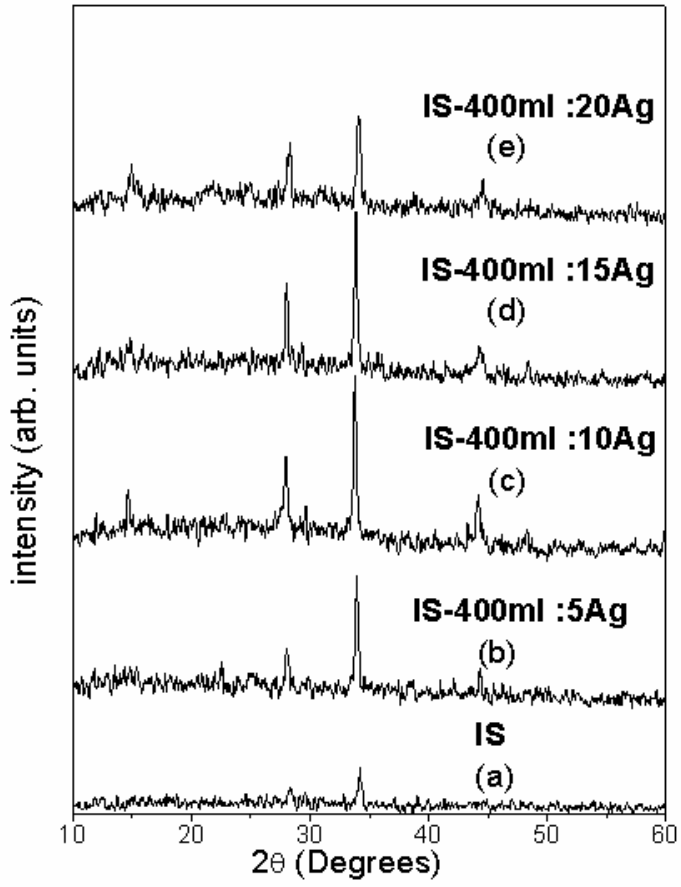

Fig. 3.3. Variation of XRD with doping, for film of 1μm thickness.

In order to understand the effect of variation of film thickness on optimum quantity of silver, volume of solution sprayed was varied from 200 ml to 400 ml keeping the In:S ratio constant at 1.2:8, so that the thickness of the film varied from

0.5µm to 1µm (measured using stylus technique). The samples were named as IS-400ml:(amount of silver deposited). It was seen that the optimum quantity of silver up to which crystallinity enhanced increased from 12 mg to 15 mg with thickness (Fig. 3.3)

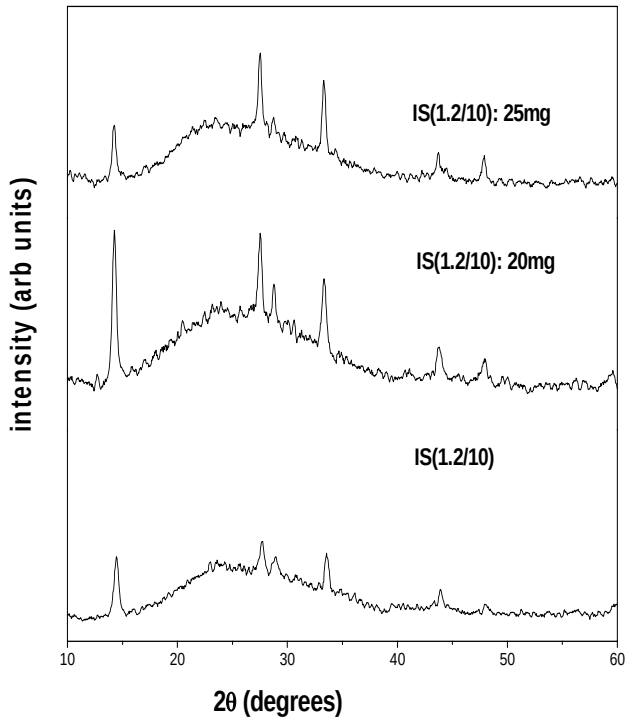

Fig. 3.4(a) Variation in XRD with doping for the ratio (in solution) 1.2:10

Next set of studies were carried out to understand the effect of variation in indium to sulfur ratio on the optimum quantity of silver. For this, samples were prepared with different In:S ratio (in the precursor solution). Indium and sulfur rich films were prepared by keeping indium to sulfur ratio in the precursor solution at 2.5:3 and 1.2: 10 respectively; the thickness of film remaining constant [0.5 µm].The sulfur

rich films showed a change in preferential orientation. The optimum value of silver required for good crystallinity decreased to 8 mg for indium rich sample while the same increased to 20 mg for sulfur rich sample (Fig. 3.4). Thus it could be inferred that the quantity of silver required to improve crystallinity of In_2S_3 was inversely related to concentration of indium in the films.

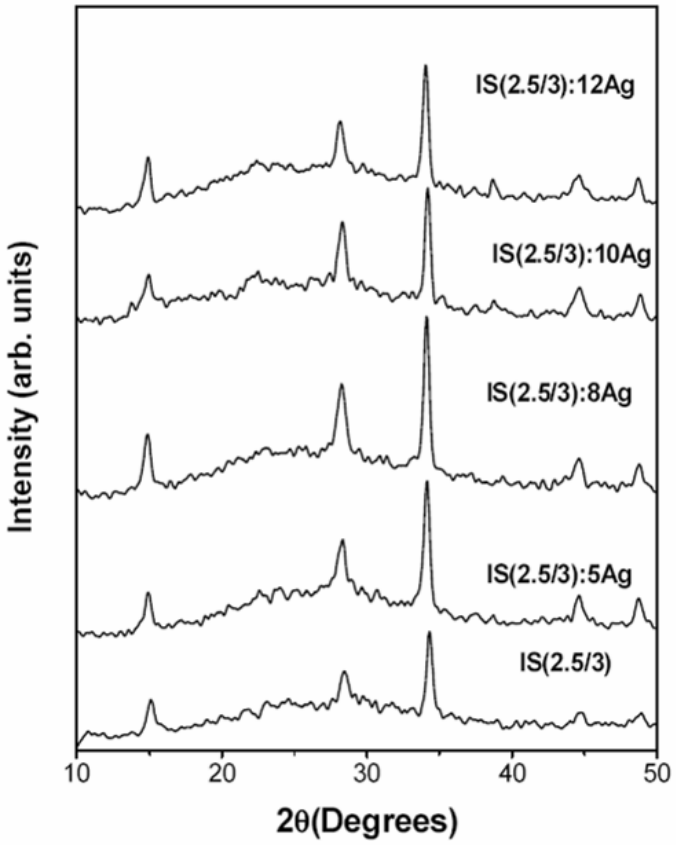

Fig. 3.4(b) Variation in XRD with doping for the ratio (in solution) 2.5:3

Studies were also done on β-In_2S_3 films prepared using vacuum evaporation technique. From EDAX measurements, atomic concentration of indium and sulfur in these samples were found to be 44.84 and 55.16 respectively i.e. nearly stoichiometric. However these films were amorphous in nature. The structural properties of these stoichiometric films did not vary with deposition of silver layer. Doped films remained amorphous even on annealing at 100^0C for one hour after silver deposition (see Fig. 3.5). Thus it was implicit that silver diffusion is pronounced in films made by CSP.

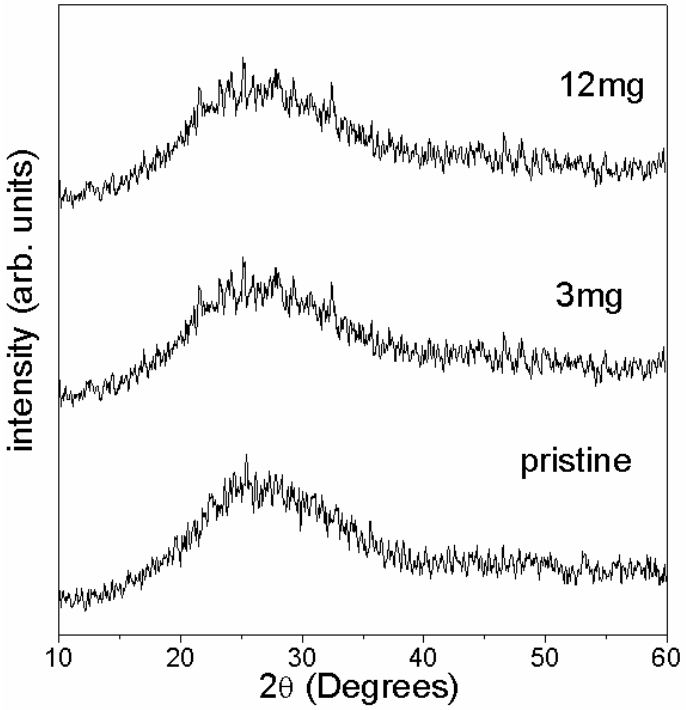

Fig. 3.5 XRD of vacuum evaporated samples, annealed at 100^0C after Ag deposition.

3.3.1.2. SEM and EDAX

Scanning Electron Micrograph **(**SEM**)** is a method for high resolution imaging of surfaces. It is the most widely used instrument for obtaining micro structural and surface features of thin films. The SEM uses electrons for imaging, much as optical microscope uses visible light. The advantages of SEM include magnification (>100,000X) and depth of field up to 100 times that of optical microscopy. A finely focused electron beam is scattered over the specimen surface and the secondary electrons emanating it are captured and used for imaging the surface. Since secondary electrons come from the surface layer, the picture obtained is a true reproduction of the surface features. Secondary electron imaging can provide high-resolution imaging the fine surface morphology. Quantitative and qualitative chemical analysis information can also be obtained using Energy Dispersive X-ray spectrometer (EDAX) with the SEM [17]. Morphological studies were done with Scanning Electron Microscope (SEM) (Cambridge Model). Atomic concentration of elements present in the samples was determined using Energy Dispersive X-Ray Analysis (EDAX) (Oxford Model 7060).

Figures 3.6(a) and 3.6(b) exhibit the scanning electron micrographs of IS:5Ag and IS:12Ag. Increase in grain size could be clearly observed, which supported the results obtained from XRD analysis. It was also seen that the samples were devoid of pinholes and cracks.

Atomic concentration of In, S, Ag and Cl in doped and pristine samples obtained from EDAX analysis are given in Table 3.2. Concentration of In either remained constant or showed only a slight decline. Even though the concentration of sulfur in the spray solution was high, its atomic concentration in pristine film was less than the stoichiometric composition of 60%. Doping with Ag further decreased the atomic concentration of sulfur. Chlorine present in the sample was from $InCl_3$, used in the spray solution.

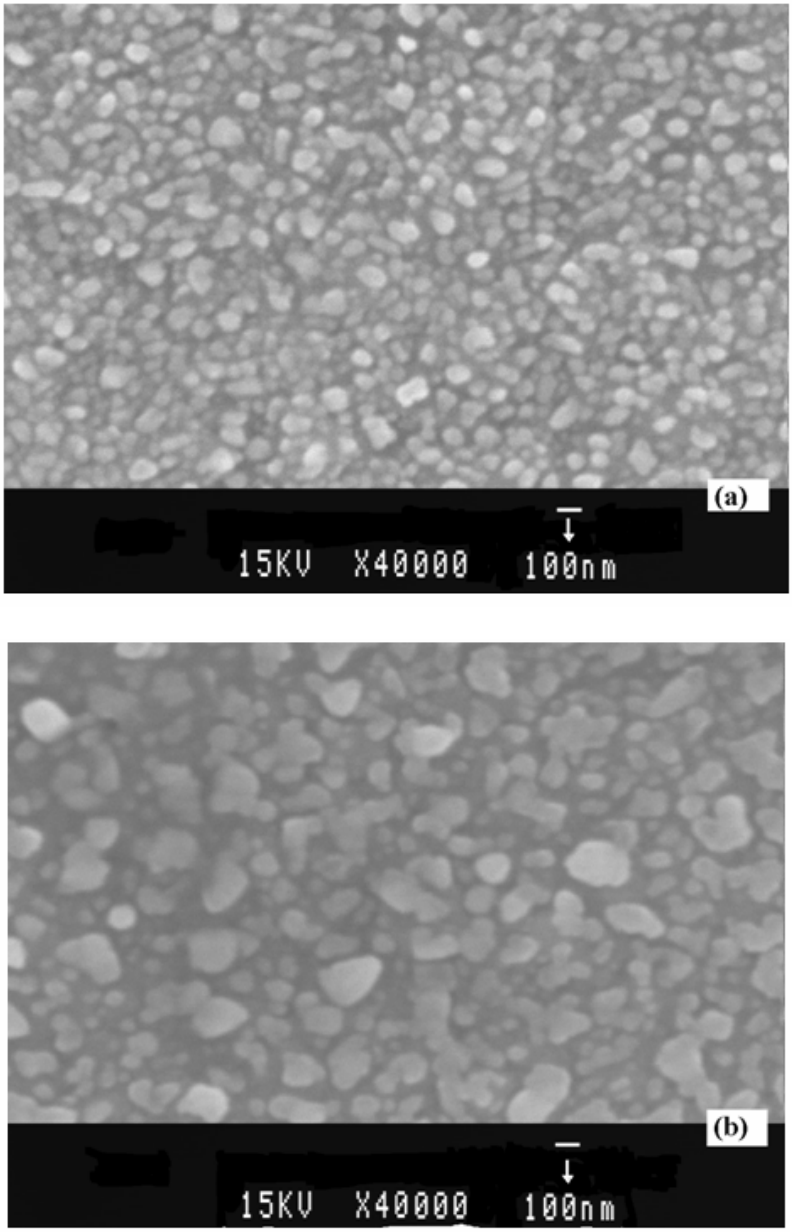

Fig. 3.6 (a). SEM micrograph of IS:5Ag, (b). SEM micrograph of IS:12Ag

Table. 3.2. Atomic concentration of the elements from EDAX measurements

Sample	In (%)	S (%)	Ag (%)	Cl (%)
IS	38.01	56.29	-	6.48
IS:5Ag	37.27	51.29	3.31	8.12
IS:10Ag	36.07	51.65	3.25	9.03
IS:12Ag	35.4	51.51	4.57	8.52
IS:15Ag	35.85	50.19	7.51	6.45

3.3.1.3. XPS Analysis

To understand the variation in stoichiometry as well as the chemical state of the elements along the thickness of the samples, we performed X-Ray Photoelectron Spectroscopy (XPS) [Electron Spectroscopy for Chemical Analysis (ESCA)] depth profile. It provides information on the elemental composition of sample as well as the chemical state of observed atoms.

In this technique, the sample is irradiated using electromagnetic radiation of energy hν. Due to the photoelectric effect, electrons are emitted with kinetic energy

$$E_{kin} = h\nu - E_B - \phi \quad \text{.....(3.5)}$$

where E_B is the binding energy (BE) of a particular electron shell and Φ is the sample work function. Photoelectrons are energy-analyzed in the spectrometer and, since the photon energy is known, one can determine characteristic binding energies of valence electrons coming from different elements present in the sample. Depending on the energy of the incident radiation, this technique is called either “Ultra Violet

Photoelectron Spectroscopy (UPS)" for lower photon energies (≤ 50 eV) or "X-ray Photoelectron Spectroscopy (XPS)" for higher photon energies (≥1 k eV) [18].

The chemical compositions of the films were evaluated using XPS technique in the present work. XPS spectra of the samples were recorded using an ULVAC-PHI unit (model: ESCA 5600 CIM) employing argon ion sputtering (Voltage = 3 kV, Raster size = 3 x 3 mm^2, pressure 10^{-8} m bar). Al K_α X-ray (1486.6 eV) with a beam diameter of 0.8 mm and power of 400 W was used as the incident beam.

Table 3.3 Binding energies of indium and sulfur in β-In_2S_3 film

Element	Binding Energy (eV)
In $3d_{5/2}$	444.99
In $3d_{3/2}$	453.06
S 2p	162.23

Here the presence of the elements In, S, O, Ag, Cl, Na and Si was checked along the sample thickness (depth profiling). In order to get this information, first XPS analysis was done on surface of the sample. After this the sample was etched using Ar ion sputtering and the analysis was repeated. Each line in the spectra shown in figure 3.7 represents the result of such analysis and one line is called 'one cycle'. The spectra were calibrated against shifts due to machine errors, using the C 1s line of the hydrocarbon contamination on the films as the standard (Binding energy of C 1s is 284.5 eV). The bottom portion of the spectra represented the surface of the film and the top, the substrate. After 7 cycles, peaks corresponding to O and Si could be seen indicating the beginning of the glass substrate (SiO_2). The binding energy values [Table 3.3] were in agreement with the reported values [19].

XPS depth profile showed the presence of silver throughout the depth of the doped sample (Figs. 3.7, 3.8). It is worth mentioning that this was taking place in as-

deposited condition and proved the diffusion of silver even before annealing. Binding energies were corresponding to that of elemental form of Ag (368 eV for $Ag3d_{5/2}$, 374 eV for $Ag3d_{3/2}$ and 98eV for 4s). Depth profile of the sample indicated that indium and sulfur were also uniformly distributed throughout the depth of the sample. Binding energies of indium and sulfur indicated the formation of indium sulfide (162.5 eV for S2p, 444.9 eV and 452.9 eV for $In3d_{5/2}$ and $In3d_{3/2}$ respectively) and were in agreement with the reported values [20]. At the surface binding energy of oxygen (532.5 eV) corresponded to surface contamination [21].

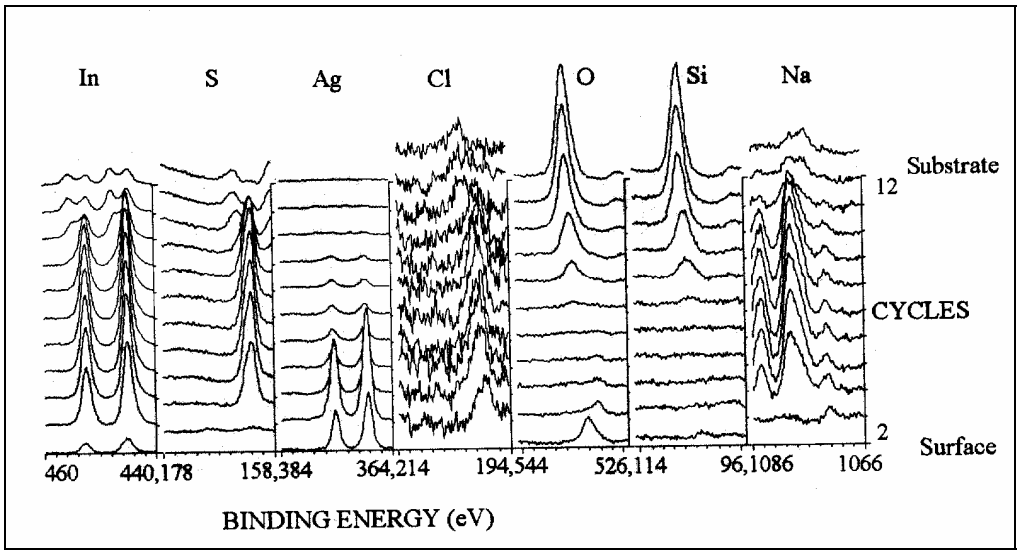

Fig. 3.7 . XPS depth profile of sample IS:12Ag.

Towards the interior of the film, intensity of the peak corresponding to oxygen decreased. Moreover there was a shift in peak position, indicating the presence of indium oxide (530.5 eV for O 1s in In_2O_3) [21]. Atomic concentration of oxygen present near the surface showed a drastic increase (from 56% to 61% for samples IS:12Ag and IS:15Ag respectively) after the optimum value of doping (Figs.

3.7, 3.8). However there was a decrease in the peak height of sulfur at the surface of the doped samples indicating a decrease in atomic percentage. EDAX measurements also showed a decrease in sulfur concentration in doped films. This could be explained by considering the substitution of sulfur by oxygen. Corresponding nature of oxygen and sulfur was observed in In_2S_3 films containing sodium [10]. Chlorine was also present throughout the depth of the sample. Presence of sodium is caused by diffusion from glass substrate during spraying, as it was done at 573 K.

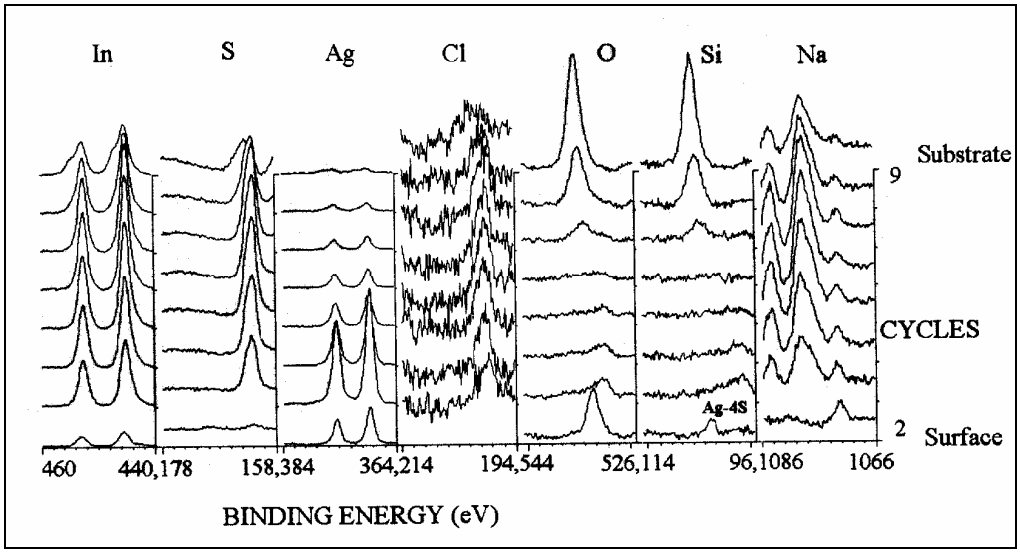

Fig 3.8 XPS depth profile of sample IS:15Ag.

Structural analysis proved that the doped silver helped to form a crystallized compound in β-In_2S_3 structure. The four cation vacancies per unit cell of β -In_2S_3 were ordered along the fourfold screw axis parallel to c axis. Thus the silver atoms introduced into the β-In_2S_3 matrix could be intercalated in the vacant tetrahedral cationic sites. This could be the reason for lower incorporation of silver in indium rich

films (In:S ratio2.5:3) and vise versa (In:S ratio 1.2:10). Further increase in doping concentration could have substituted the indium in the indium sulfide matrix.

3.3.2. Optical studies

3.3.2.1. Optical absorption

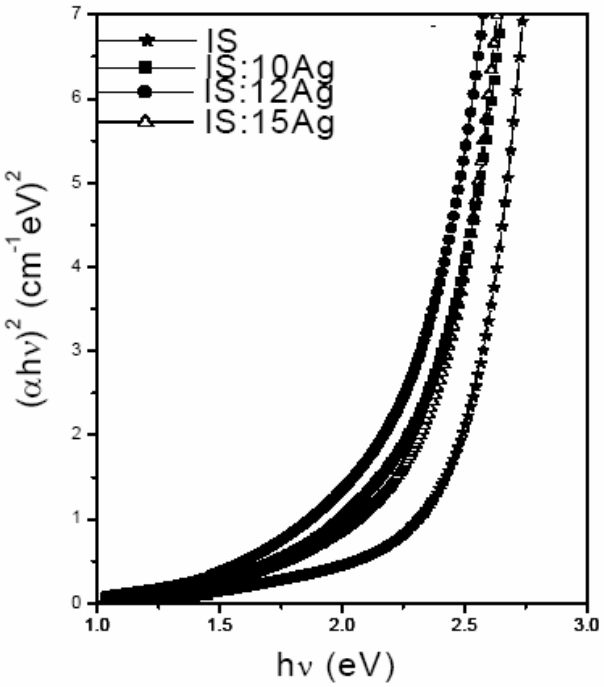

Fig. 3.9 Variation of band gap with doping.

The simplest and most direct method for probing the band structure of semiconductors is by measuring the absorption spectrum. Absorption is expressed in terms of a coefficient *α(hv)* defined as the relative rate of decrease in light energy *L(hv)* along its propagation path: [22]

$$\alpha = \frac{1}{L(h\nu)} \frac{d[L(h\nu)]}{dx} \quad \text{.....(3.6)}$$

the absorption coefficient α is related to the energy gap E_g according to the equation

$$\alpha h\nu = A(h\nu - E_g)^n \quad \text{.....(3.7)}$$

where A is a constant, h is the Plank's constant, v the frequency of the incident beam and n is equal to ½ for a direct gap and 2 for an indirect gap.

Optical absorption spectra were recorded in the wavelength region 190 -1200 nm using UV-VIS-NIR spectrophotometer (JASCO V-570 model) In order to determine the optical band gap, graph was plotted with $(\alpha h\nu)^2$ against $h\nu$ (Fig. 3.9) [16]. Optical band gap was determined from this plot for all films by the linear fit in the straight portion of the graph. Band gap of pristine sample was 2.51 eV. This decreased with doping concentration and became 2.24 eV for IS:12Ag. Increase in crystallinity and decrease in sulfur concentration [23], could have resulted in this shift.

Table 3.4. Band gap, Resistivity and Photosensitivity of the samples

Sample	Band gap (eV)	Resistivity (Ω cm)	Photosensitivity
IS	2.51	1266	450.34
IS:3Ag	2.482	86	102.6
IS:5Ag	2.406	36	89.81
IS:10Ag	2.32	138.15	148.33
IS:12Ag	2.24	50.5	538.88
IS:15Ag	2.33	.06	2.46

But on increasing the doping concentration above the optimum value, the band gap showed a retracing effect (i.e. increasing). This could be due to the decrease

in crystallinity and presence of oxygen in the sample, forming indium oxide. XPS studies revealed a sudden increase in oxygen concentration and formation of indium oxide when doping concentration increased beyond the optimum value. N. Barreau et al [24] has reported increase in band gap with oxygen concentration. Band gap variation of the samples is reported in Table. 3.4.

3.3.2.2. Photoluminescence (PL)

Photoluminescence (PL) is a contactless, non-destructive technique for the determination of certain impurities in semiconductors. It is particularly suitable for detecting shallow level impurities, provided the radiative recombination events dominate non-radiative recombination. Identification of impurities is easy with PL; but measurements of the concentration of impurities are more difficult. PL can provide simultaneous information on different types of impurities.

Photoluminescence in solids can be classified according to the nature of the electronic transitions producing it. Mainly we can have intrinsic and extrinsic emission. Intrinsic luminescence is further divided into i) band to band luminescence, ii) exciton luminescence and iii) cross luminescence. In band-to-band luminescence, emission occurs when an electron in the conduction band recombine with a hole in the valence band. This emission can be observed in very pure crystal at higher temperatures while at lower temperature, this gets transformed into 'exciton luminescence'. If there are some impurities having their level in the forbidden gap, electrons or holes are trapped by them and these recombine with each other via such level, either radiatively or non radiatively. 'Cross luminescence' is usually observed in alkaline and alkaline earth halides. Luminescence caused by intentionally incorporated impurities (in most cases metallic impurities) is classified as "extrinsic luminescence". In semiconductors, most important impurities are donors and acceptors that dominate semiconductor property and also act as luminescence activators. Photoluminescence (PL) measurements were carried out in the present

samples at temperature ranging from 15 K to 300 K. Samples were kept in contact with the cold finger of a closed cycle liquid Helium cryostat (Janis Research Inc.). Here the temperature was maintained with an accuracy of $\pm$ 1 K, using a temperature controller (Lake Shore Model 321). The 532 nm line of frequency doubled Nd:YAG laser (20 mW, Melles Griot) was used to excite the sample (beam diameter ~ 1mm). Emission spectra were analyzed by employing spectrophotometer (Ocean optics USB2000), having a Si CCD array detector.

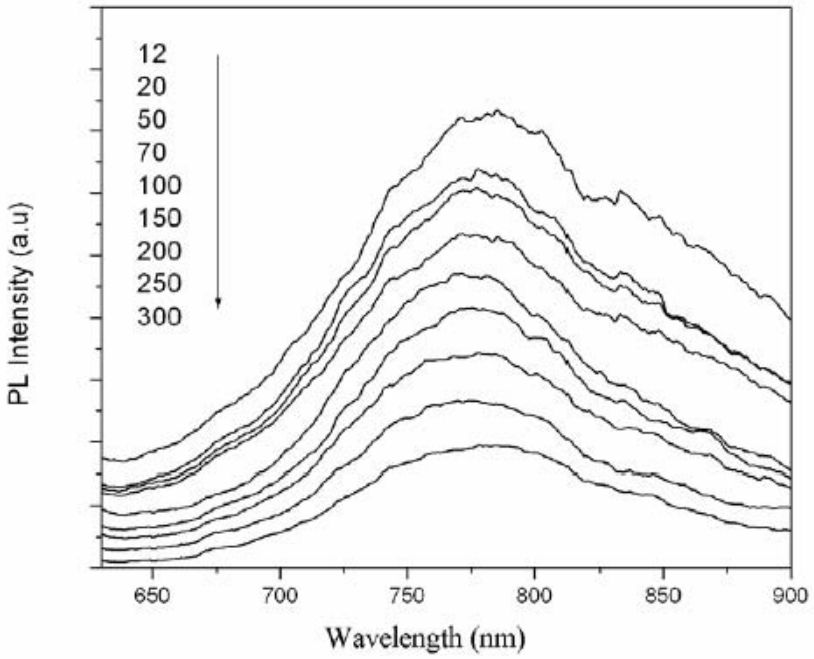

Fig. 3.10 Temperature dependence of PL spectra of sample IS:12Ag.

PL spectra of pristine and optimum doped sample, (IS:12Ag) where recorded in the temperature range 15 K to 300 K. Pristine sample showed no peak while IS:12Ag sample showed a strong emission at 768 nm (Fig.3.10). This emission was

relatively sharp with maximum intensity at 15 K and had an asymmetric Gaussian line shape corresponding to 1.61 eV. Even though the intensity decreased with increase in temperature, it was visible even at room temperature.

In order to calculate the PL quenching energy, the graph of Logarithmic value of integrated PL intensity vs. 1000/T was fitted using the relation [25],

$$I(T) = I(T=0)/ [1+ C \exp(-\Delta E/ k_B T)] \quad \ldots\ldots\ldots\ldots\ldots\ldots\ldots\ldots (3.8)$$

Where I (T) is the intensity at temperature T, C is a temperature independent constant describing the capture of carriers at a center and ΔE is the activation energy. Value of ΔE for the emission was obtained to be 49meV (Fig. 3.11), which was corresponding to the donor level formed by Indium interstitials [26].

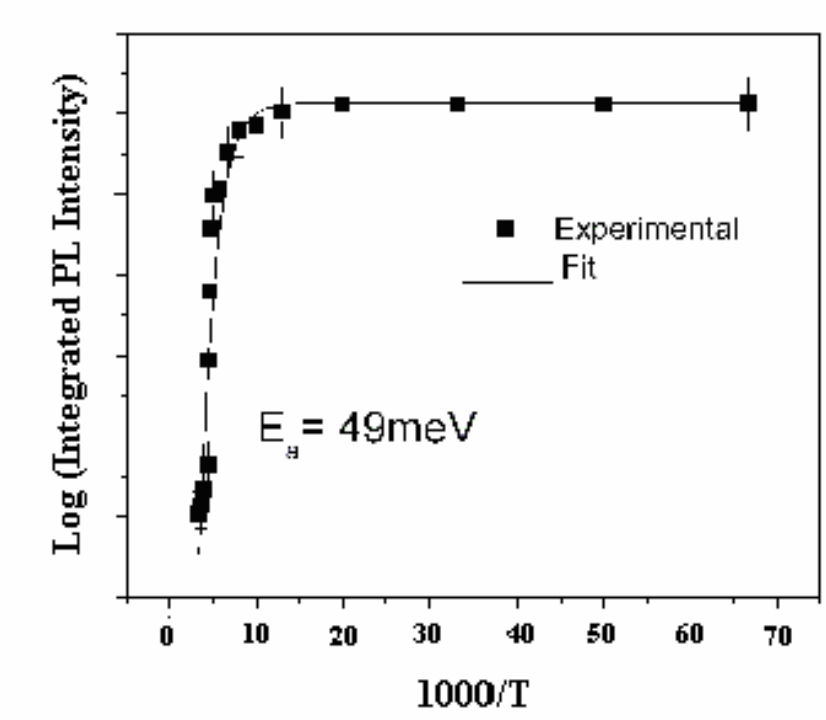

Fig. 3.11 Temperature dependence of integrated intensity of PL emission.

The emission energy of a Donor-Acceptor Pair (DAP) at a distance R is given by the relation [27],

$$h\nu = E_g-(E_a+E_d) + e^2/ \varepsilon R \quad \ldots\ldots\ldots\ldots\ldots\ldots\ldots\ldots(3.9)$$

Where hν is the photon energy, E_g is the band gap energy (2.24 eV), E_a and E_d (50 meV) are the acceptor and donor binding energies, R is the distance between the pairs and ε is the static dielectric constant. The fourth term in the RHS of Eq. (3.9) is a correction factor for the coulomb interaction between the pairs, which may be effective only at short distances. So the binding energy for the acceptor can be estimated from the minimum peak energy at low excitation power, assuming the Coulomb term in Eq. (2) to be negligible [28]. Acceptor level to which the transition takes place was calculated from the relation and found to be 580meV which corresponds well with the level obtained by TSC.

3.3.3. Electrical studies

Conductivity type of a semiconductor material can be determined by hot or thermoelectric probe method. This technique employs the 'Seebeck effect' to determine the type of conductivity. The sign of the thermal emf or Seebeck voltage generated by the temperature gradient tells whether the material has n-type or p-type conductivity. In this method two probes are kept in contact with the sample surface with one hot and the other cold. Thermal gradients produce currents in a semiconductor, the majority carrier currents for n and p-type materials are given by,

$$J_n = -qn\mu_n P_n \frac{dT}{dx} \quad \ldots\ldots\ldots\ldots\ldots\ldots\ldots\ldots\ldots (3.10)$$

$$J_p = -qp\mu_p P_p \frac{dT}{dx} \quad \ldots\ldots\ldots\ldots\ldots\ldots\ldots\ldots\ldots (3.11)$$

Where q is the charge, n and p are the number of electrons and holes; μ represents the mobility of the charge carriers, $\frac{dT}{dx}$ gives the temperature gradient, $P_n < 0$ and $P_n > 0$ shows the differential thermoelectric power. The electron current in an n-type sample flows from left to right. The thermoelectric power can be thought of as a current generator. As part of the current flows through the voltmeter, the hot probe develops positive potential with respect to the cold probe. Electrons diffuse from the hot to the cold region setting up an electric field that opposes diffusion. Analogous reasoning explains the opposite potential for p-type samples. Hot probe measurements proved all films (both pristine and doped) to be n-type.

For thin films, we can express the electrical resistance of the film as sheet resistance, given by

$$R_s = \frac{\rho}{t} = \frac{Rb}{l} \quad \text{..... (3.12)}$$

Where 'b' is the length of the electrode and 'l' the distance between the electrodes. In the present study for measuring the sheet resistance two electrodes were drawn 0.5 cm apart using silver paste with a length of 0.5 cm. Two probes from source measuring unit (digital multimeter) were connected to the silver electrodes using magnanin wires as pressure contacts. Voltage in the range 0-5 V was applied and corresponding current was measured with the help of a computer interfaced with the source measuring unit (SMU-123X, KEITHLY).

Resistivity of the samples reduced considerably due to Ag doping, [from 1.2×10^3 Ωcm to .06 Ωcm] as depicted in figure. 3.12. However among the doped samples, there was a slight increase in resistivity for samples IS:10Ag and IS:12Ag. But on increasing the doping concentration further, resistivity showed an abrupt decrease. Defect studies were done to analyze this behavior.

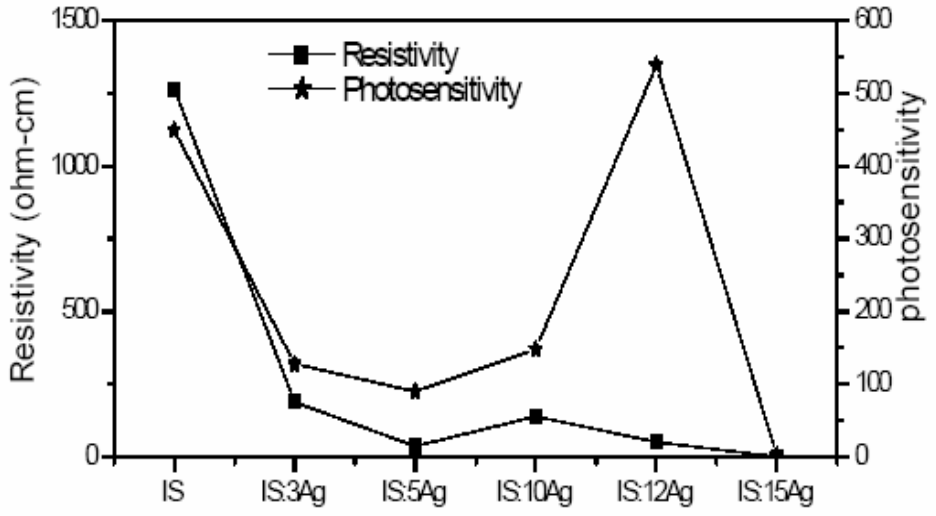

Fig 3.12 Variation of photosensitivity and resistivity with doping.

3.3.3.1. TSC (Thermally Stimulated Current) measurements

Measurement of "thermally stimulated current" has been used extensively as a defect characterization technique. It is one among the several photo-electronic techniques used to analyze and characterize crystalline, polycrystalline and amorphous materials. This technique also helps to identify the traps or defects present in the material and determine trap parameters [like activation energy and capture cross section]. A TSC spectrum usually consists of a number of [more or less resolved] peaks in current *versus* temperature graph called "glow curve". Each peak, in most cases, is related to a species of traps. Measured curve is then analyzed to obtain such characteristics as the location of the peak on the temperature scale, its width etc. These data are then utilized to compute trapping parameters by applying appropriate theoretical models.

In the present case TSC measurements were carried out employing Lab Equip IMS-2000 (with liquid nitrogen cooling system). LN2 pumping type cryostats with optical windows were used as sample holder for measurements. Contacts were made using spring loaded contacts. The tips and mounting area were gold plated to ensure low resistance contacts. This measurement was done in the temperature range 100 K to 450 K using Pt-100 resistance thermometer as the temperature sensor (with 0.025 degree temperature resolution). Sample was cooled to 100 K and was illuminated for 5 min, using white light source capable of giving 25 mW/cm^2 on the sample surface. Further it was heated to 450 K at a rate of 1.5 K/min. Current through the sample was measured by giving a biasing voltage of 2 V.

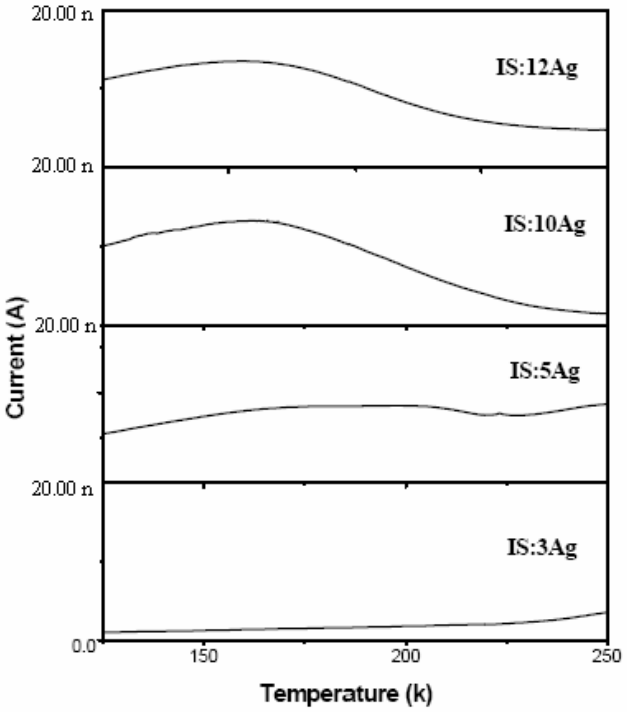

Fig. 3.13 TSC Spectra (100 K to 250 K)

Thermally stimulated conductivity studies were done for defect characterization of the samples. Activation energy of the traps was obtained using the formula 3.13[29],

$$E = 2kT_m^2/(T_2-T_1) \quad \ldots\ldots\ldots\ldots\ldots\ldots\ldots\ldots\ldots\ldots\ldots\ldots\ldots\ldots\ldots\ldots\ldots\ldots(3.13)$$

Where T_m is the temperature at the peak maximum and (T_2-T_1) is the width of half-maximum of the peak. Here Gaussian fitting was done for resolving the peaks. Though TSC was performed on pristine sample, no peaks could be obtained. This might be indicating lack of detectable levels in these samples. However TSC curve of doped samples exhibited two distinct peaks at 150 K and 415 K, revealing the existence of two traps in the material (Figs. 3.13, 3.14).

The defect level at 150 K, corresponding to activation energy of 50 meV, could be assigned to indium interstitial [26]. Intensity of TSC peak corresponding to this level increased with doping (Fig. 3.13), indicating increase in the density of states. We observed from EDAX and XPS measurements a simultaneous decrease in sulfur concentration with doping. W. Rehwald et al.[3] reported that low concentration of sulfur favored surplus of indium in the compound making concentration of quasi-interstitial indium atoms to be larger. Hence it was concluded that with Ag doping, the number of indium interstitials increased. Indium interstitials act as donors initiating the observed decrease in resistivity.

Another trap level was identified in doped samples at higher temperature, (412 K) which appeared to be a deep level with activation energy of ~ 1.2 eV (Fig. 3.14). When silver atoms get introduced into the crystalline matrix of β-In_2S_3 containing four cation vacancies per unit cell, ordered along the four-fold screw axis parallel to c axis, they could easily intercalate in the vacant tetrahedral cationic sites (similar results have been reported for Na incorporation [30]). So this deep level could be assumed to be the contribution of silver atoms occupying the vacant cationic site,

as proved by the increase in intensity of this level with silver concentration. However IS:10Ag showed a transition nature in the case of this defect.

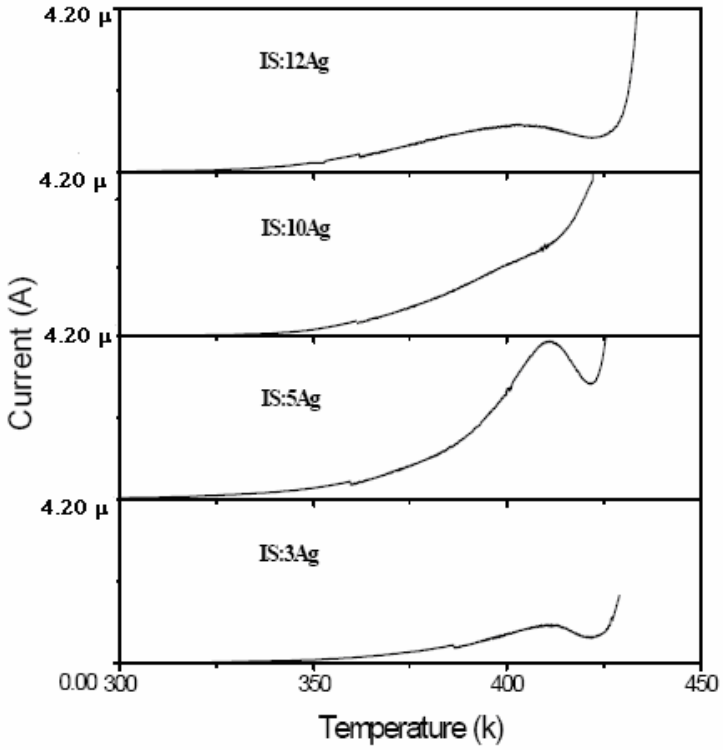

Fig. 3.14 TSC Spectra (300 K to 450 K)

For the sample IS:12Ag, the peak broadened and shifted to a lower temperature of 402 K and the activation energy of this trap was ~ 0.578 eV. PL of this sample also showed an emission at 1.61 eV. Transition causing the PL emission was to an acceptor level which was 0.58 eV above the valance band. The activation energy (0.578 eV) obtained from TSC studies of the sample also revealed the same. As the doping concentration increased, silver atoms might be replacing some of the

tetrahedral indium atoms [30], and naturally silver in indium site would act as an acceptor.

In general, we conclude that the drastic decrease in resistivity obtained by doping could be the contribution due to increased indium interstitials, which acted as donors thus increasing the conductivity [2,3]. TSC studies also proved that number of indium interstitials increased with doping. Moreover doping with Ag resulted in considerable increase in grain size (Table. 3.1), leading to reduction in grain boundary scattering. All these factors might have favored the increase in conductivity. Though the resistivity of the doped samples were much lower than the pristine one, among the doped samples a slight increase in resistivity was observed towards the optimum value of doping (Fig. 3.12). The presence of acceptor level might have reduced the majority carrier density slightly thereby increasing the resistivity. Based on these arguments we suggest the energy levels of the defects in IS:12Ag as depicted in figure.3.15.

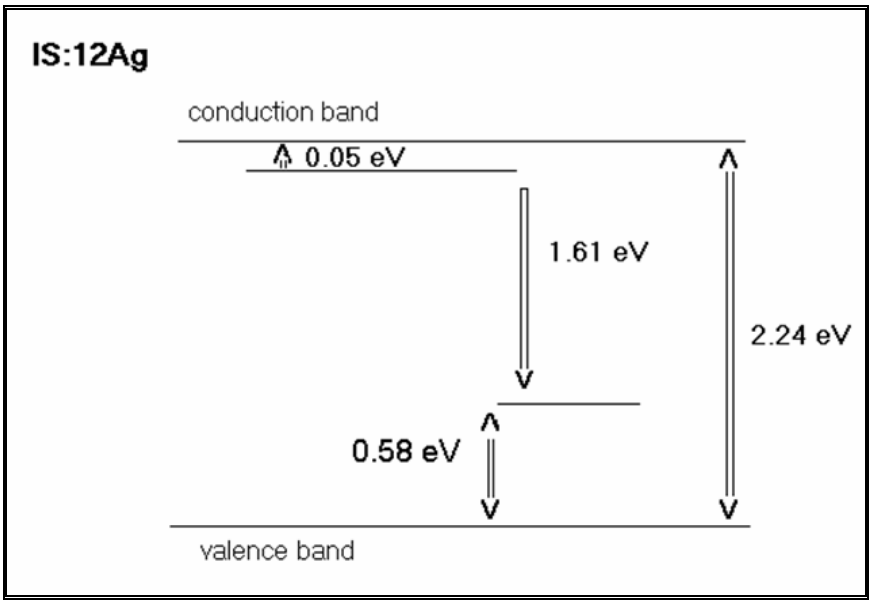

Fig. 3.15 Band diagram for IS:12Ag.

Further increase in silver concentration from IS:12Ag to IS:15Ag lead to a sharp decrease in resistivity to 0.06 Ωcm. The enhancement in conductivity might be due to the excess silver atoms occupying the interstitial positions. XPS of the samples showed an increase in the concentration of oxygen. Electrical properties of polycrystalline films are limited by their potential barriers created by grain boundaries. Introduction of oxygen in the thin films could modify the grain boundaries to induce an increase in electrical conductivity [24]. Bessergenev et al [31] has reported that substitution of sulfur by oxygen in the β-In_2S_3 crystalline matrix also decreased resistivity.

3.3.3.2. Photosensitivity measurements

Photosensitivity of a semiconductor material is defined as the measure of the minority carriers generated in the material under illumination, and is expressed as the ratio of difference between the dark current (I_d) and photocurrent (I_l) to the dark current. Photosensitivity is given by (I_L-I_D/I_D). Photosensitivity measurements were done using the Keithley 236 Source Measure Unit. Samples were illuminated using a tungsten halogen lamp of intensity 100 mW/ cm^2 for 60 s prior to photoconductivity measurement. An IR filter and a water column were used between sample and lamp to avoid heating of the sample. Silver electrodes were used for measurement. Distance between the electrodes and length of the electrodes were kept as 5 mm.

Photosensitivity of the samples is depicted in Table 3.4. Introduction of silver induced a drastic increase in photocurrent. Maximum photosensitivity (538) was obtained for sample IS:12Ag having optimum doping. This was obtained at a resistivity of only 50 Ωcm. Here it should be noted that pristine sample (IS) could obtain a photosensitivity of only 450, that too at a higher resistivity of 1266 Ωcm. Usually a decrease in photoconductivity was observed with the decrease in resistivity. But here, in contrary IS:12Ag showed an increased photosensitivity in spite of its low

resistivity. Hence it could be concluded that enhanced photosensitivity of this sample was due to the contribution of the acceptor level created. The holes generated by the acceptors might have reduced the majority carrier density slightly (resulting in considerable reduction of minority carrier loss due to recombination). This might have enhanced the photosensitivity even though the sample had low resistivity, making the sample extremely suitable for photovoltaic application as evident from our own work [11].

3.4 Effect of Annealing

Post annealing treatment was done to understand the impact of annealing on silver diffused samples as the diffusivity of silver could be increased with thermal assistance.

3.4.1 Experimental Details

The In_2S_3 thin films were deposited on soda lime glass substrate using CSP technique as mentioned in section 3.2. To understand the effect of thermal assistance on diffusion, the doped films were annealed at 100^0 C and 200^0C for one hour in vacuum (~$2x10^{-5}$ m bar). Different masses of silver (3, 5, 10, 12 and 15 mg) were evaporated for doping different sets of In_2S_3 films. These doped samples were named as IS: *(mass of silver evaporated)*Ag*(annealing temperature).*

3.4.2. Results and Discussion

3.4.2.1 Structure and morphology

XRD patterns of the annealed (post annealed after silver diffusion) samples also indicated a clear improvement in crystallinity as the silver doped samples. Crystallinity increased up to an optimum amount of doping and further a retracing phenomenon was observed. However it was seen that the quantity of silver needed for optimum performance decreased with thermal assistance (Table 3.5). In silver

diffused films with no post annealing, the crystallinity increased up to sample IS:12Ag and started decreasing from IS:15Ag. For the samples which underwent annealing at 100^0C for one hour, the optimum value of silver [up to which the crystallinity improved] decreased to 10 mg. i.e. for IS:10Ag(100) (Fig. 3.16) and for the samples which have undergone annealing at 200^0C for one hour the optimum value decreased to 5 mg i.e. IS:5Ag(200) (Fig. 3.17). The thermal assistance might be enhancing the silver diffusion, there by decreasing required quantity for optimum performance.

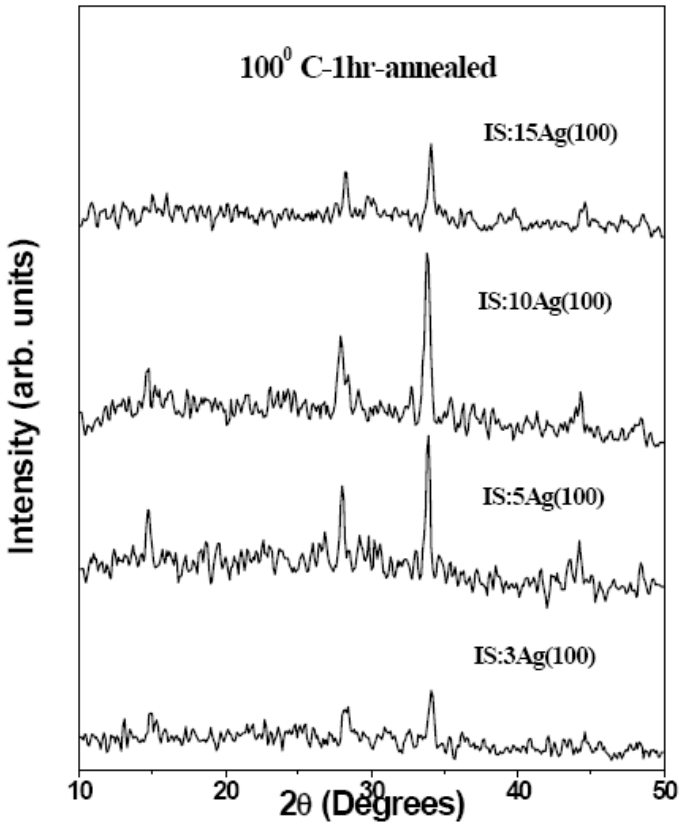

Fig. 3.16. Variation of XRD of doped samples post annealed at 100^0C for 1hour

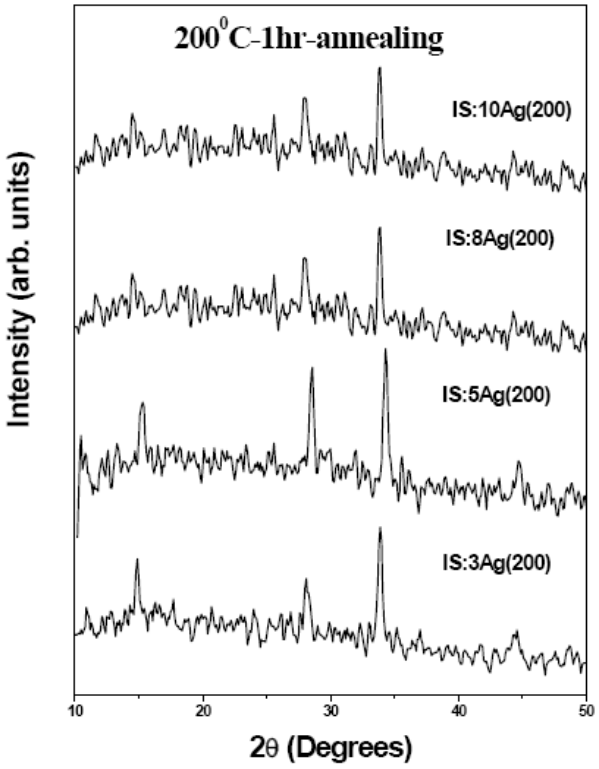

Fig. 3.17. XRD of doped samples, annealed at 200^0C after Ag deposition.

The *d* values coincided with that of β -In_2S_3 in standard JCPDS data card (25-390). Of note, new phase did not develop. This indicated that post annealing treatments of silver doped indium sulfide thin films did not change the structure of In_2S_3 nor did they result in the formation of new compounds. As in the case of silver doped samples the peak positions slightly shifted to lower values of 2θ on annealing. Correspondingly, value of lattice spacing (*d*) increased. This proved that lattice parameters increased with silver deposition. But with annealing, this occurred at relatively lower amount of silver. The *c/a* ratio was nearly constant for all samples. Grain size calculated using Debye Scherrer formula also showed a marginal increase

with post annealing treatments. The grain size of optimum doped samples at different annealing temperatures is tabulated in Table 3.5.

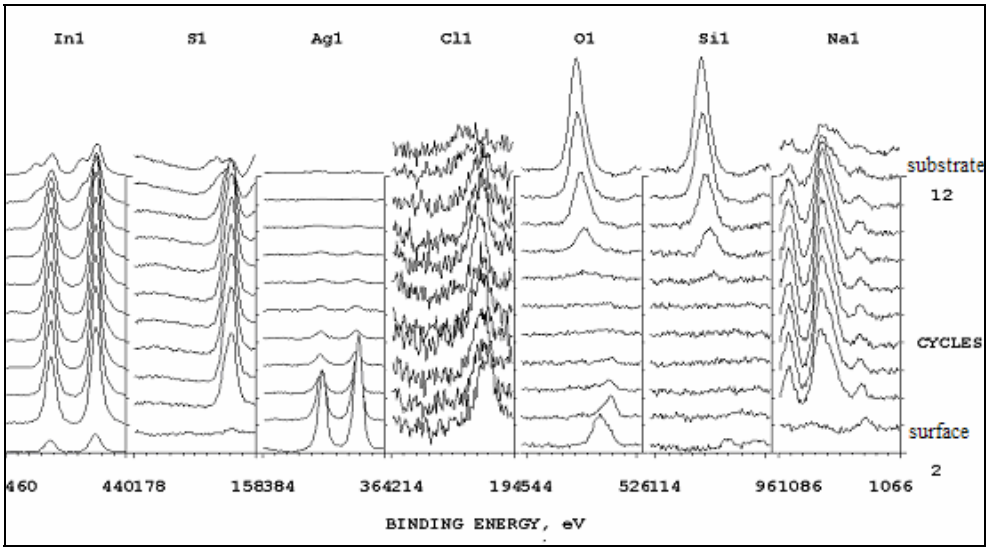

Fig.3.18 XPS depth profile of sample IS:12Ag (200^0 annealed)

XPS depth profile of the annealed samples proved that diffusivity was enhanced by the thermal process. Interestingly, it was observed that on achieving optimum value at lower doping levels, annealing sourced the excess silver to retrace to the surface of the films (Fig. 3.18). Comparison of figure 3.7 (XPS of optimum doped sample without post annealing (IS:12Ag)) with figure 3.18 (depth profiled XPS analysis of the same sample with post annealing at 200^0C for 1hr) gives a clear picture of retracing of excess silver to the film surface with annealing. From XRD analysis the optimum quantity of silver at 200^0C post annealing was found to be 5 mg i.e IS:5Ag(200), and excess silver could have retraced to surface layers. In this case, quantity of silver accommodated at vacant cationic and interstitial sites would have reached optimum level at a relatively lower amount of silver on increasing the

diffusion by thermal assistance. Binding energies of indium and sulfur indicated the formation of indium sulfide (162.5 eV for S2p, 444.9 eV and 452.9 eV for $In3d_{5/2}$ and $In3d_{3/2}$ respectively) and were in agreement with the reported values [20].

Oxygen was again present as a surface contaminant (532.5 eV). Towards the interior of the film, intensity of the peak corresponding to oxygen decreased and there was a shift in peak position, indicating the presence of metal oxide (530.5 eV for O 1s in In_2O_3 [21]. The Oxygen concentration increased on post annealing. Correspondingly there was a decrease in the peak height of sulfur at the surface of the doped samples indicating a decrease in atomic percentage. Chlorine was also present throughout the depth of the sample. Presence of sodium could be the result of diffusion from glass substrate during spraying, as it was done at 573 K.

3.4.2.2. Optical studies

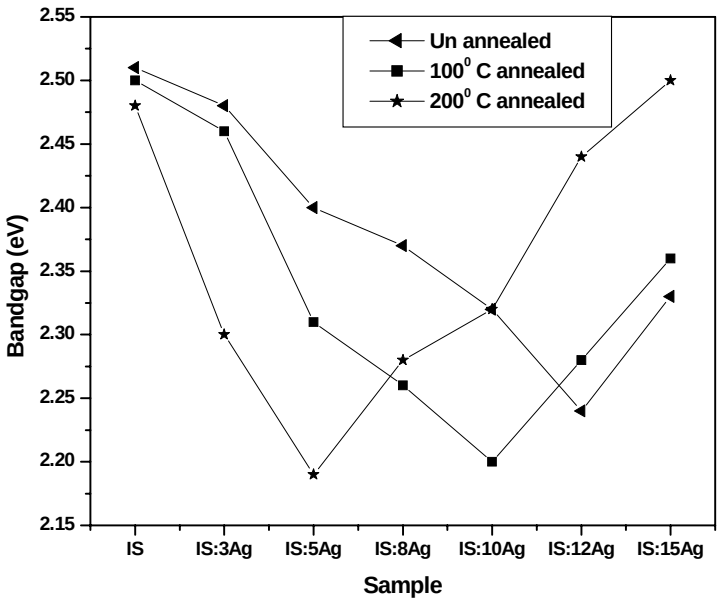

Fig. 3.19 Variation of bandgap on annealing

Optical absorption spectra, was recorded in the wavelength region 190 -1200 nm. The optical band gap was determined from $(\alpha h\nu)^2$ vs. hν graph . Band gap of pristine sample decreased from 2.51 eV to 2.48 eV with annealing. This could be due to the improvement in crystallinity observed during annealing. The doped sample preserved the same optical behavior on annealing. The bandgap decreased up to optimum doping and after that the retracing behavior was observed (Fig. 3.19). Lowest bandgap was 2.19 eV for IS:5Ag(200).

3.4.2.3. Electrical studies

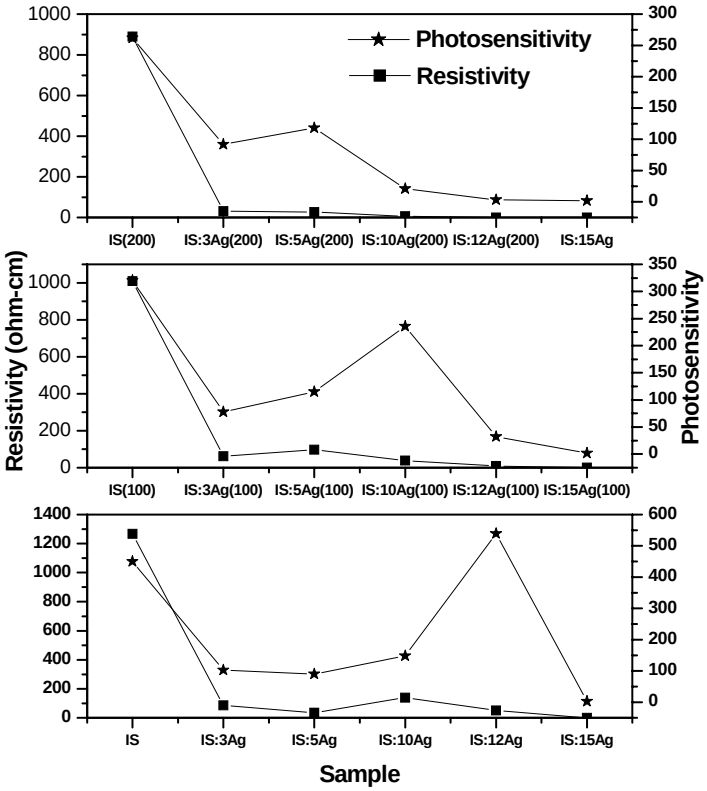

Fig. 3.20 Variation of electrical properties with annealing

Doped samples preserved the same electrical behavior even on annealing as revealed in figure 3.20. The resistivity of the samples decreased with doping but a small rise in resistivity was observed towards optimum value. In general the resistivities of annealed samples were lower than the unannealed one. Resistivity of the pristine sample also decreased on annealing. It was seen during XRD analysis that the overall crystallinity of the samples increased with annealing. Thus the decrease in resistivity on annealing could be explained as the contribution of increased crystallinity. Photosensitivity was found to be more for unannealed samples. The photosensitivity is in accordance with dark conductance value which corresponded to resistivity of the sample. For annealed samples resistivity decreased increasing the dark current of the samples hence diminishing the photosensitivity. Among doped samples photosensitivity was high for optimum doped samples. The values are tabulated (Table 3.5).

Table 3.5. Properties of optimum sample with annealing

	Un annealed	100^0C annealed	200^0C annealed
Optimum Quantity	12 mg	8 mg	5 mg
Grain size (nm)	36.87	37.76	39.48
Band gap (eV)	2.24	2.2	2.19
Resistivity (Ω cm)	50.5	38.82	26.24
Photosensitivity	538.88	235.84	118.25

3.5 Conclusion

Doping β-In_2S_3 thin films, (prepared using CSP), with Ag resulted in samples with enhanced crystallinity and grain size. From XPS depth profile of the sample, it

could be seen that silver diffused throughout the depth even without annealing. It was observed that there was an optimum amount of Ag, required for doping and further increase in doping concentration showed retracing effects. Electrical resistivity of the films decreased drastically from $1.2x10^3$ Ωcm to 0.06 Ωcm on doping. Defect studies showed an increase in indium interstitials with doping which could be the major reason for low resistivity of the samples. It was observed that at low doping concentration, silver atoms were positioned in the ordered vacancy sites (activation energy ~ 1.2 eV). At higher doping concentrations silver atoms were setting into indium sites creating an acceptor level (activation energy ~ 0.6 eV). On further increase in doping concentration, silver atoms are supposed to be at interstitial positions resulting in drastic decrease in resistivity. The most striking and interesting observation was that, photosensitivity of optimum doped β-In_2S_3 film was greater than the pristine sample, even when its resistivity was much less than the pristine sample. Presence of the acceptor level could have contributed to this anomalous increase in photosensitivity of the film. Thus doping β-In_2S_3 film with optimum amount of silver modified the structural and electrical properties of the films favorably to enhance the efficiency of buffer layer. Post annealing treatments on doped films could bring down the quantity of silver deposited for optimum performance.

References

[1] K. Kambas, J. Spyridelis and M. Balkanski, Phys. Status Solidi B **105** (1981)291.

[2] R. S. Becker, T. Zheng, J. Elton and M. Saeki, Solar Energy Mater. **13**(1986)97.

[3] M. Rehwald and G. Harbeke , J. Phys. Chem. Solids **26** (1965)1309.

[4] S. Yu, L. Shu, Y. Qian, Y. Xie, J. Yang, and L. Yang, Mater. Res. Bull. **33(5)** (1998) 717.

[5] E. Dalas and L. Kobotiatis, J. Mater. Sci. **28** (1993) 6595.

[6] K. Hara, K. Sayama and H. Arakawa, Sol. Energy Mater. Sol. Cells **62** (2000) 441.

[7] W. T. Kim, W. S. Lee, C. S. Chung and C. D. Kim, J. Appl. Phys. **63(11)** (1988) 5472.

[8] N. Kamoun, S. Belgacem, M. Amlouk, R. Bennaceur, J. Bonnet, F. Touhari, M. Nouaoura and L. Lassabatere, J. Appl. Phys. **89(5)** (2001) 2766.

[9] Roland Diehl and Rudolf Nitsche, J. Cryst. Growth **20** (1973) 38.

[10] N. Barreau, J. C. Bernede, C. Deudon, L. Brohan, S. Marsillac, J. Cryst. Growth **241** (2002) 4.

[11] Teny Theresa John, Meril Mathew, C. Sudha Kartha, K. P. Vijayakumar, T. Abe, Y. Kashiwaba, Sol. Energy Mater. Sol. Cells **89(1)** (2005) 27.

[12] R.R. Chamberlin, J.S. Skarman, J. Electrochem. Soc. **113** (1966) 86.

[13] C.M. Lampkin, Prog. Cryst. Growth Charact. **1** (1979) 406.

[14] M. Ortega – Lopez and A. Morales- Acevedo, Thin Solid Films **330** (1998) 96.

[15] N. Bouguila, H. Bouzouita, E. Lacaze, A. B. Amara, H. Bouchriha and A. Dhouib, J. de Physique III **7** (1997) 1647.

[16] Teny Theresa John, S. Bini, Y. Kashiwaba, T. Abe, Y. Yasuhiro, C. Sudha Kartha, K. P. Vijayakumar, Semicond. Sci. and Techol. **18** (2003) 491.

[17] Hand Book of Analytical Methods for Materials, Materials Evaluation and Engineering, INC (2000).

[18] Rosenberg and Tu Treatise on Materials Science and Technology, Academic Press **27 (**1988) 65.

[19] S. H. Yu, L. Shu, Y. S. Wu, J. Yang, Y. Xie and Y. T. Qian, J. Am. Ceram. Soc**. 82 (2)** (1999) 457.

[20] Shu-Hong Yu, Lei Shu, Yong-Sheng Wu, Jian Yang, Yi Xie and Yi-Tai Qian, J. Am. Ceram. Soc. **82 (2)** (1999) 457.

[21] L. Bhira, H. Essaidi, S. Belgacem, G. Couturier, J. Salardenne, N. Barreaux and J. C. Bernede, Phys. Status Solidi A. **181** (2000) 427.

[22] J. I. Pankov Optical Processes in Semiconductors, Dover publications, New York (1971) 34.

[23] J. George, K. S. Joseph, B. Pradeep and T. I. Palson, Phys. Status Solidi A. **106** (1988) 123.

[24] N. Barreau, S. Marsillac, D. Albertini, J. C. Bernede, Thin Solid Films **403-404** (2002) 331.

[25] J. P. Dean, Phys. Rev. **157** (1967) 655.

[26] R. Jayakrishnan, Teny Theresa John, C. Sudha Kartha, K. P. Vijayakumar, T. Abe, Y. Kashiwaba, Semicond. Sci. and Technol. **20** (2005) 1162.

[27] W. Z. Shen, S. C. Shen, Y. Chang, W. G. Tang, L. S. Yip, W. W. Lam and I. Shih, Infrared Phys.Technol. **37** (1996) 509.

[28] S. Zott, K. Leo, M. Ruckh and H. W. Schock, Appl.Phys.Lett. **68** (1996) 1144.

[29] Rupa R Pai, Teny Theresa John, Y. Kashiwaba, T. Abe, K. P.Vijayakumar, C. Sudha Kartha, J. Mater. Sci. **40** (2005) 741.

[30] N. Barreau, J. C. Bernede, S. Marsillac, J. Cryst. Growth **241** (2002) 51.

[31] V. G. Bessergenev, Inorg. Mater. **32(6)** (1996) 592.

Chapter 4
Tin Doped Indium Sulfide Thin Films

4.1 Introduction

Indium sulfide is a promising candidate for optoelectronic and photovoltaic applications [1-4] and is an important material for many technological applications due to its stability, wide band gap and photoconductivity [5]. This material can be used as an effective nontoxic substitute for cadmium sulfide (CdS) in Copper Indium Gallium Sulfide (CIGS) based solar cells. The motivation for using In_2S_3 as a buffer layer in CIGS solar cells is not only to eliminate toxic cadmium, but also to improve light transmission in the blue wavelength region, by using a material having band gap wider than that of CdS.

Optical band gap of indium sulfide is estimated to be 2.0 eV [6, 7]. It could be increased in thin films by several, physical or chemical processes. [8–18]. The optical band gap value reported for indium sulfide thin films varies from 2.0 [16] to 2.4 eV [17] depending on the deposition process. These values are too small for application as buffer layer in solar cells. However, several authors had found values higher than 2.4 eV. They explain this blue shift of the optical transmission threshold in different ways. Kim et al. [18] have interpreted the broadening of band gap in their indium sulfide thin films to be due to the presence of excess sulfur in the bulk, while some authors explained it by assuming quantum size effect [19, 20]. Blue shift can be induced by very small grain sizes [23]. But as discussed by Yoshida et al. [21], for this effect to be significant, the β-In_2S_3 grain size should be 8nm or less.

Other possibilities can nevertheless be imagined; for, one possibility to increase the optical band gap is to partially substitute indium by another element like Al [24] or by optimum diffusion of Na [25]. Another possibility is to substitute some sulfur with oxygen in order to synthesize a homogeneous $In2S_{3-3x}O_{3x}$ which could

induce anomalous broadening of the optical band gap [38-42]. The optical performance obtained with $In_x(OH,S)_y$ deposited by chemical bath deposition also exhibit bandgap widening [21,22]. In Solar cell Fabrication this broadening of bandgap was found to be quite beneficial enhancing the solar cell efficiency [22, 25 38]. In the present work, we report results to support the assertion that the incorporation of Sn [using $SnCl_4.5H_2O$] in In_2S_3 could increase the band gap to wider ranges.

The prime objective of this work was to decrease the resistance of In_2S_3 layer by doping it with Sn. This would reduce the series resistance of the cell resulting in an increase of the short circuit current. β-In_2S_3 belongs to $A_2^{III}B_3^{II}$ compounds which represent solids with a large concentration of vacancies with completely satisfied chemical bonds [26]. Due to large number of cationic vacancies, indium sulfide acts as a "sink" for many guest atoms. So β-In_2S_3 films prepared using CSP technique could be easily doped with Sn to reduce the resistivity as it is a +4 vacant compound and can act as a donor in interstitial as well as substitutional position. Becker et al. reported that doping of In_2S_3 films with Sn resulted in samples with low resistance [28]. Till now, no such efforts have been done on indium sulfide films prepared by CSP method. Moreover, a precise study on the properties of doped film is essential to control the doping parameters, which is indispensable for its applications.

This chapter describes the effects of both in-situ and ex-situ doping. Ex-situ doping was done through thermal diffusion, which was realized by annealing Sn/In_2S_3 bilayer films. In-situ doping was done by introducing Sn into the spray solution, by using $SnCl_4.5H_2O$. Interestingly, it was noted that different methods of doping yielded samples with very different properties. Through the 'ex-situ doping' conductivity of the sample enhanced by five orders without affecting the physical properties such as crystallinity or band gap while the 'in- situ doping' resulted in widening of optical bandgap through oxygen incorporation; also it gave highly photosensitive films.

4.2 Ex-Situ Doping

4.2.1 Experimental Details

In_2S_3 thin films were deposited on soda lime glass substrate using CSP technique [2] as mentioned in section 3.2. Spraying solution consisted of indium chloride ($InCl_3$) and thio-urea ($CS(NH_2)_2$) in the required molarities. Th spray rate was 30 ml/min. Thickness of the films was 0.25μm. Indium to sulfur ratio of the precursor solution was 1.2/8. This ratio was selected as it showed the maximum photosensitivity [2] and yielded nearly stoichiometric films. Ex-situ doping was achieved by diffusing the metal layer deposited over the In_2S_3 thin films (Process-I or PI). For this, thin layer of tin was deposited using vacuum evaporation technique (pressure during evaporation was ~$2x10^{-5}$ Torr). Sn/In_2S_3 bilayer system was annealed at 373 K, for one hour for the diffusion of the metal. Doping concentration was changed by varying the mass of the tin evaporated. Tin doped samples were named as PI:2Sn, PI:4Sn, PI:6Sn and PI:8Sn corresponding to 2 mg, 4 mg, 6 mg and 8 mg of tin evaporated.

Both pristine and doped samples were characterized with different experimental techniques for elucidating the electrical, optical and structural properties. Structural characterization was done using X-ray diffraction spectrometer (Rigaku D. Max C) employing CuK_α line (λ=1.5404 Å). Atomic concentration was studied with the help of Energy Dispersive X-ray Spectroscopy (EDAX), (Oxford Model 7060). X-ray Photoelectron Spectroscopy (XPS), (ULVAC- PHI unit, Model: ESCA 5600 CIM). Argon ion sputtering was used to obtain the depth profile and atomic ratio of the films. Optical absorbance of the samples at normal incidence was studied employing UV-VIS-NIR spectrophotometer (JASCO V-570 model). Resistivity and photosensitivity measurements were done with the help of Keithley 236 Source Measure Unit. Electrical contacts were applied using silver paint, in the form of two end contacts, having a distance of 5 mm between them. For photosensitivity measurements, sample was illuminated with tungsten halogen lamp (100 mW/cm^2).

Thermally Stimulated Current (TSC) measurement was carried out (Lab Equip IMS-2000) with liquid nitrogen cooling system. For TSC measurements, the sample was cooled to 100 K and was then illuminated for 5 min, using white light source capable of giving 25 mW/cm^2 on the sample surface. Then the sample was heated to 450 K at a rate of 1.5 K/min.

4.2.2 Results and Discussion

4.2.2.1 Structure and Composition

Figure 4.1 shows X-ray diffraction (XRD) pattern of pristine and PI samples with different tin concentrations. The'd' values corresponding to all peaks coincided with that of β-In_2S_3 in standard JCPDS data card (25-390). No new phase was observed even for PI:8Sn, indicating that the incorporation of tin neither changed the structure of In_2S_3 nor resulted in the formation of any new compounds. The PI samples had no change in crystallinity with doping up to PI:6Sn. But for higher doping concentrations (PI:8Sn) reduction in crystallinity was observed. The amorphous nature in XRD at $20^0 \sim 25^0$ exhibited by both pristine and doped samples could be the contribution of glass as it disappeared for thicker films.

In the case of PI samples one can naturally assume that Sn atoms might be occupying the vacant cationic sites present even in a completely satisfied structure of In_2S_3 due to its 'defect spinel structure' [26]. Since ionic radius of tin (71 pm for +4e) is compatible with that of Indium (81 pm for +3e,) Sn doping did not produce any shift in the peak position (lattice constants) as observed in the case of other dopants like silver [28] or sodium [29].Grain size (calculated using Debye Scherrer formula) showed a marginal increase when compared with the pristine sample (Table 4.1). But an increase in grain size of the pristine sample was observed on annealing at 100^0C for 1hr. So the marginal increase in grain size could be the effect of annealing given for diffusion.

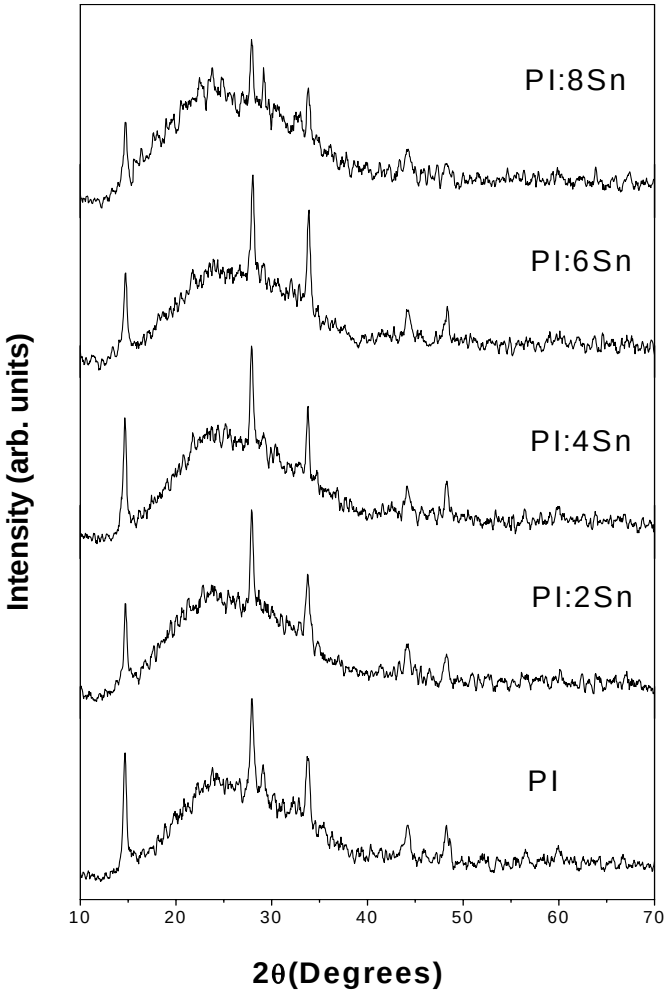

Fig. 4.1 Variation of XRD in Process I

XPS depth profile of PI samples showed the presence of In and S throughout the depth of the sample. Binding energies of indium and sulfur indicated the formation of indium sulfide (162.5 eV for S2p, 444.9 eV and 452.9 eV for $In3d_{5/2}$ and $In3d_{3/2}$ respectively) and were in agreement with the reported values [30]. However there was a decrease in the peak height of sulfur in doped samples, indicating a decrease in

atomic percentage. In PI samples this was a surface effect, which could be explained by considering the substitution of sulfur by oxygen. Binding energy of oxygen at the surface (532.5 eV) corresponded to that of surface contaminant (sulfate or sulfite) [5].

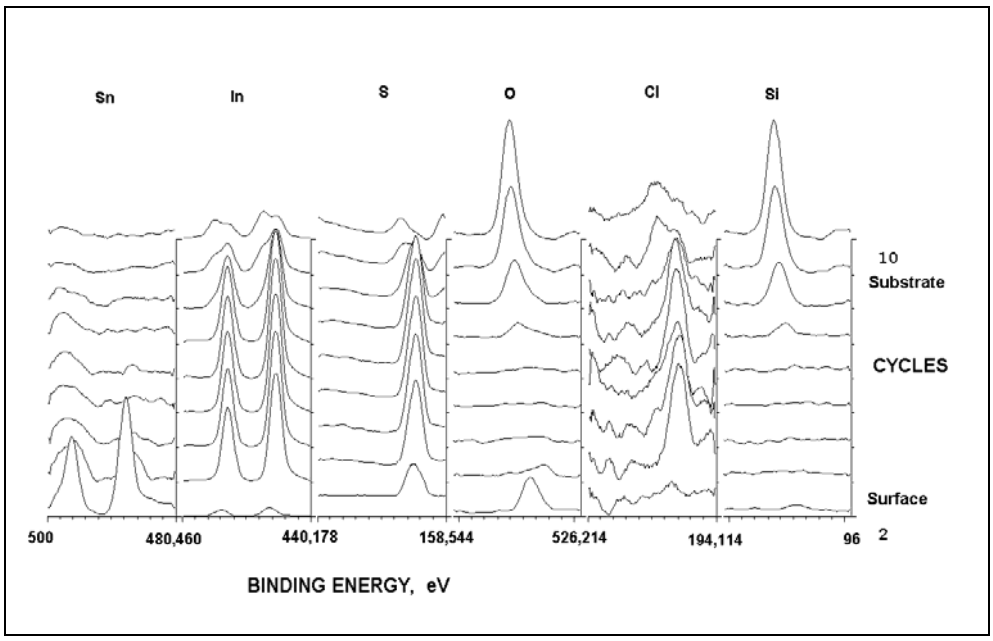

Fig. 4.2 XPS depth profile of sample PI:2Sn

Depth profile of the ex-situ doped samples proved the diffusion of tin (Fig.4.2). Binding energy corresponded to a mixed state ($Sn3d_{5/2}$ in Sn and $Sn3d_{5/2}$ in SnO). A shift in the binding energy was observed at the surface layer. In ex-situ doped samples, diffusion of Sn could be restricted to the surface layers and there was a gradient in Sn concentration (decreases) along depth (Fig. 4.2).So in PI films we have pure In_2S_3 layer near the substrate and tin diffused layer towards the surface; electrical properties proved this structure to be quite advantageous for photovoltaic applications. Chlorine was also present throughout the depth of the sample. Presence of sodium was caused by diffusion from glass substrate during spraying, as it was done at 573 K.

4.2.2.2 Optical Studies

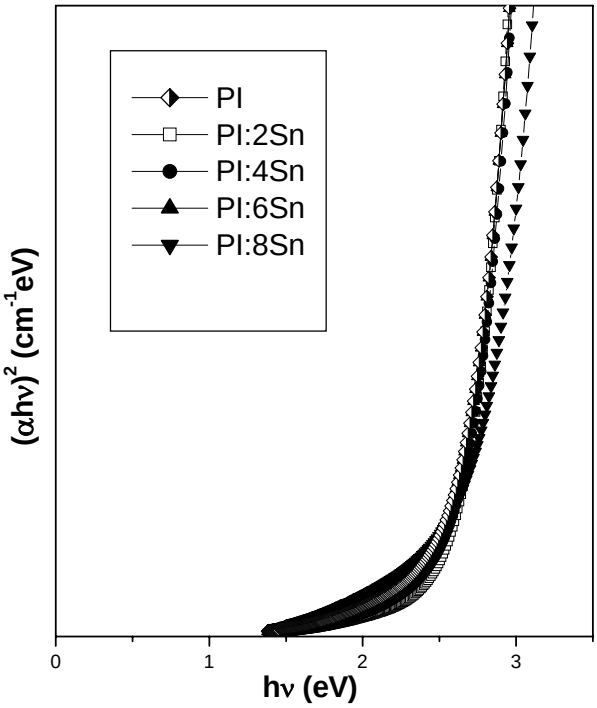

Fig. 4.3 Variation of band gap with doping (process I)

Optical absorption spectra were recorded in the wavelength region 350 -900 nm. In order to determine the optical band gap, $(\alpha h\nu)^2$ against hν graph was plotted (Fig. 4.3). In the case of PI samples, band gap was 2.57 eV which was same as that of the pristine sample. The value remained the same for PI:2Sn, PI:4Sn, PI:6Sn (Fig. 4.3). However this increased slightly with further increase in doping concentration and became 2.67eV for PI:8Sn. It was also noted that the absorption edge was not sharp for doped samples and there was absorption in long wavelength region also. This might be due to the introduction of shallow donor levels due to the doping.

4.2.2.3 Electrical Studies

Electrical resistivity was found to decrease with tin doping [31]. Variation of conductivity with tin concentration is tabulated in table. 4.1. Conductivity of the pristine sample was 9 X 10^{-4} S/cm whereas that of PI:8Sn was 33.3 S/cm. The increase in conductivity might be naturally due to the donor action of tin. On doping, tin atoms may be occupying the vacant cationic sites or indium might have progressively been replaced by the tin atom [27]. Since tin belonged to group IV, either in the interstitial position or in the substitutional position, it would act as a donor, contributing electron for enhancing conductivity. In addition, the indium interstitials formed by substitution might also act as donors [31], again promoting conductivity.

Table 4.1 Variation of grain size, bandgap, conductivity and photosensitivity with Doping

Sample	Grain size (nm)	Bandgap (eV)	conductivity (Siemens/cm)	Photosensitivity
PI	19.42	2.57	9 X 10^{-4}	452
PI:2Sn	20.29	2.57	2.7 X 10^{-1}	42
PI:4Sn	21.23	2.57	3.2	6
PI:6Sn	22.65	2.57	20	1
PI:8Sn	17.54	2.67	33.3	-ve

Photosensitivity $(I_L-I_D)/I_D$ (I_L is illuminated current and I_D is the dark current) measurements were taken using two-probe method. For the photocurrent measurement, the sample was illuminated using a tungsten halogen lamp (100 mW/cm^2). A potential difference of 1-2 volts was applied across the two silver

electrodes and the current was measured. Maximum photosensitivity was obtained for the pristine sample and this decreased with increase in tin concentration. This might be due to the creation of enormous number of majority carriers on doping with tin, leading to huge dark current (I_D). In fact, PI:8Sn sample showed a slight negative photosensitivity. Kul'bachinskii et al has reported negative persistent photoconductivity in GaAs structures with tin δ-doped vicinal faces [32]. Photosensitivity of the samples is tabulated in table 4.1.

In PI samples, the diffusion could be limited to the surface layers (Fig.4.2), and hence during junction fabrication for photovoltaic applications, it was possible to have a low resistive n-type layer near the electrode and highly photosensitive and resistive layer (pristine) towards the junction. Carrier generation and collection could be promoted by such a structure, which might be very useful for photovoltaic applications.

4.2.2.4. Defect Studies

Temperature dependence of conductivity (from 100 K) of the samples was measured using computerized setup (IMS 2000, Lab Equip). Conductivity increased with temperature, which very well proved the absence of any pure metallic layer on the surface of ex-situ doped samples. Values of activation energy could be evaluated from the Arrhenius plot of conductivity (100 K to 350K). The pristine sample showed the presence of a single level at 50 meV which could be attributed to indium interstitial [28, 33]. Due to the high resistance of the pristine sample, the conductivity measurements could not be carried out at temperatures below 180 K.

When In_2S_3 was doped with Sn (PI) we obtained two activation energies (110 meV and 25 meV) in addition to the level at 50 meV (Fig.4.4). These shallow levels might be contributing towards the high conductivity of the samples.

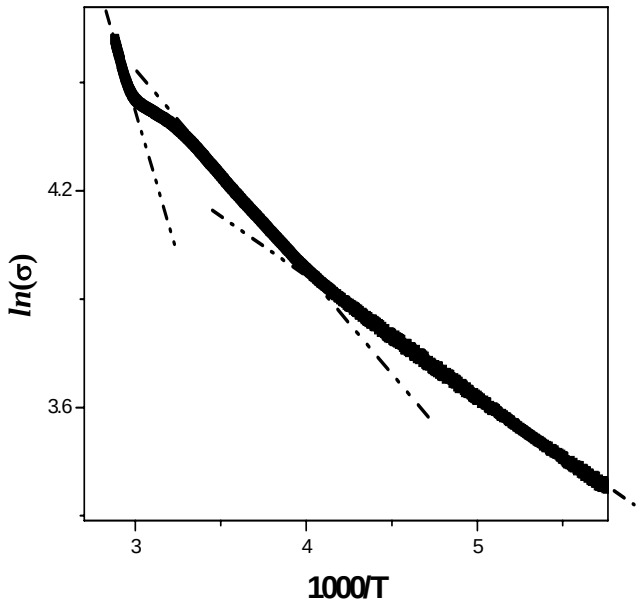

Fig. 4.4 ln (σ) vs 1000/T graph

Though TSC was performed on pristine sample, no peaks were obtained. TSC curve of doped samples exhibited two distinct peaks around 230 K and 310 K, revealing the existence of two traps in the material (Fig. 4.5). Fitting was done to resolve out the peaks (fitting is given in blue for Figs. 4.5, 4.6)

The defect level at 230 K corresponds to activation energy of 100 meV. Temperature dependent conductivity also yielded this level. The defect level at 310 K corresponded to activation energy of 230 meV. Defect at 230 meV was not seen during dark conductivity measurements Defect studies proved that three additional shallow defect levels were formed by Sn doping. These shallow levels were contributing towards the enhancement in conductivity.

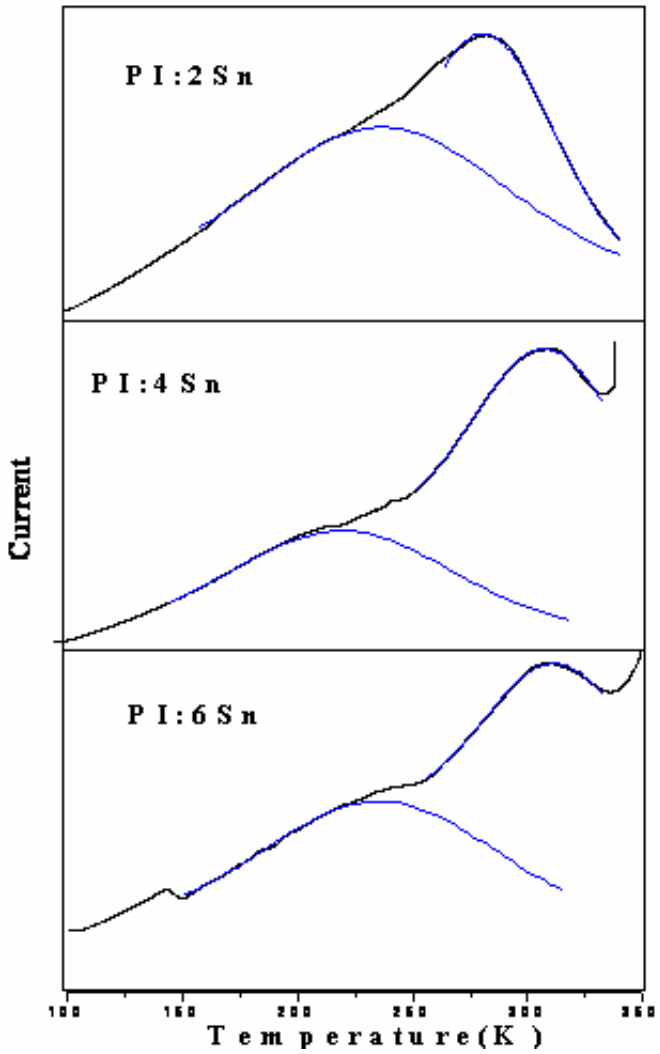

Fig. 4.5 TSC Spectra of sample PI:2 Sn, PI:4 Sn and PI:6 Sn

The three levels might be the result of Sn occupying different positions (substitutional and interstitial) [8]. At substitutional position, Sn act as an amphoteric dopant due to the different oxidation states it posses and this could induce different

defect levels. The temperature dependence of carrier concentration studies in tin doped GaSe have shown that tin can act as both acceptor and donor impurity [34].

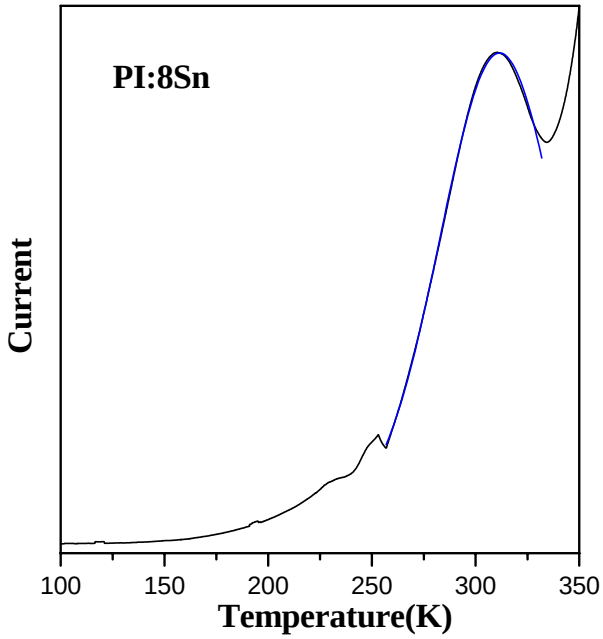

Fig. 4.6 TSC Spectra of sample PI:8 Sn

The formal oxidation number (sn^{2+} and Sn^{4+}) is an indicator of local situation occurring for Sn in the class of compounds. Sn^{2+} represents a distorted environment, while Sn^{4+} reflect amore isotropic environment [35]. The level at 230 meV, which is more prominent at higher doping concentrations (Fig 4.6), is suspected to be an acceptor level (Sn^{2+} substitution for Indium). This might be the reason for negative photosensitivity of highly doped sample, PI:8Sn. Though this level was present in other samples also, its effect might have been concealed by the occurrence of other prominent donor levels.

4.3 In-situ doping

In-situ doping achieved by the incorporation of Sn using [$SnCl_4.5H_2O$] in the precursor solution. Here we present the significant results obtained by these studies. Core work and optimization studies have been carried out to select these ratios. The doping was carried out from very small doping percentages of .01% of the Indium concentration in solution. this resulted in amorphous films with no improvement in properties. Incorporation of Sn to higher levels could increase the bandgap to wider ranges with acceptable electrical properties.

4.3.1. Experimental Details

In the second case of doping, i.e. the in-situ doping, tin was included in the spray solution by adding required volume of aqueous solution of $SnCl_4.5H_2O$ (Process-II or PII). This is yet another advantage of CSP that doping and mixing could be easily performed. The solution was sprayed on a substrate kept at a temp of 300 ± 5^oC, administered at a spray rate of 30 ml/min. The total volume of the solution sprayed was 200 ml and the thickness was 0.25μm with indium to sulfur ratio in the solution at 1.2/8. This ratio was selected as it showed the maximum photosensitivity [2] in our measurements. Doping percentage of Sn was varied as 0.1%, 0.25%, 0.5%, 0.75% and 1.0% of indium concentration in the precursor solution and these samples were referred as PII:0.1%Sn, PII:0.25%Sn, PII:0.5%Sn, PII:0.75%Sn and PII:1.0%Sn respectively.

4.3.2. Results and Discussions

4.3.2.1 Structure and Composition Studies

XRD analysis revealed that samples became amorphous (Fig. 4.7) with in-situ doping (adding Sn to the precursor solution in the CSP process). This phenomena remained the same irrespective of the Sn:In ratio in the solution.

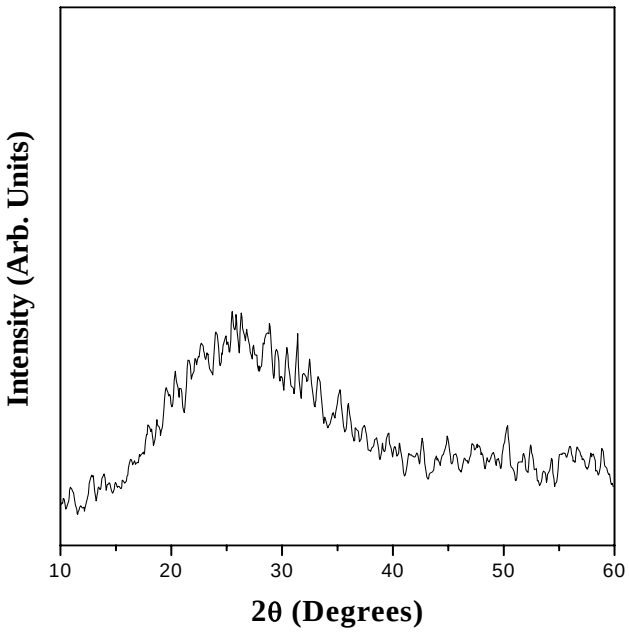

Fig. 4.7.XRD of process II samples

XPS depth profile of In_2S_3 thin films of varying doping concentrations showed uniform distribution of tin within the film. Binding energy measurements indicated a mixed state ($Sn3d_{5/2}$ in Sn and $Sn3d_{5/2}$ in SnO/SnO_2) [Fig. 4.8]. Binding energy oxygen at the bulk also confirmed the formation of a metal oxide.

Indium and sulfur were uniformly distributed throughout the depth of the sample. Binding energies of indium and sulfur proved the formation of indium sulfide (162.5 eV for S2p, 444.9 eV and 452.9 eV for $In3d_{5/2}$ and $In3d_{3/2}$ respectively) and were in agreement with the reported values. In the pristine sample oxygen was present only as surface contaminant (532.5 eV). Increase in doping concentration of Sn produced a corresponding increase in atomic concentration of oxygen. This was probably due to the higher chance of oxygen incorporation during spray pyrolysis. In addition XPS measurements showed a decrease in atomic percentage of sulfur. This

could be explained by considering the substitution of sulfur with oxygen during the thin film formation. Similar behavior was observed in In_2S_3 films containing sodium by others [36]. However in Sn mixed samples, the binding energy of oxygen exhibited a shift in peak position, indicating the presence of metal oxide (530.5 eV for O 1s).

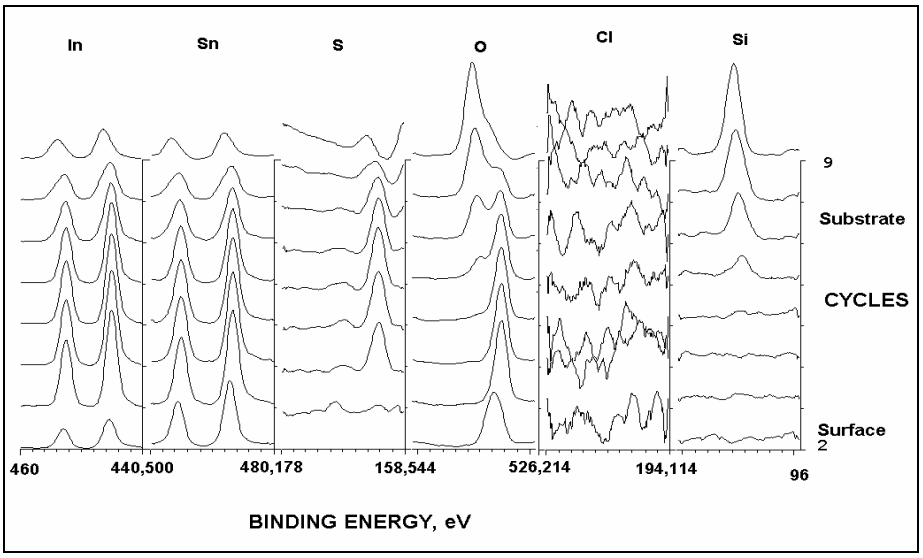

Fig. 4.8. XPS depth profile of various elements with depth in sample PII: 0.5%Sn

In pristine sample, chlorine was present at a significant level throughout the depth of the sample. Interestingly Chlorine was absent in in-situ doped samples even though $SnCl_4$ was used for mixing. Chemical reactions pointed out that in aqueous solution of tin chloride there was a higher chance of hydroxide formation, allowing chlorine to escape from the thin film. These results were obvious in the studies conducted on ageing of the precursor solution which allowed more oxygen incorporation. Presence of sodium was caused by diffusion from the glass substrate

during spraying, as it was done at 573 K. EDAX measurements also proved decrease in sulfur concentration with increase in Sn/In ratio.

4.3.2.2. Optical Studies

Optical absorption spectra were recorded in the wavelength region 350 -900 nm [Fig. 4.9]. In order to determine the optical band gap, $(\alpha h\nu)^2$ against $h\nu$ graph was plotted. By tin mixing, the band gap could be varied over wider ranges (2.51 eV to 3.78 eV). This was even higher than indium oxy-sulfides. In_2S_3/Sn samples showed high atomic concentration of oxygen. The increase in band gap could be attributed to the contribution of oxygen and formation of metal oxides. Amorphous nature of the sample could be also responsible for the widening of optical bandgap

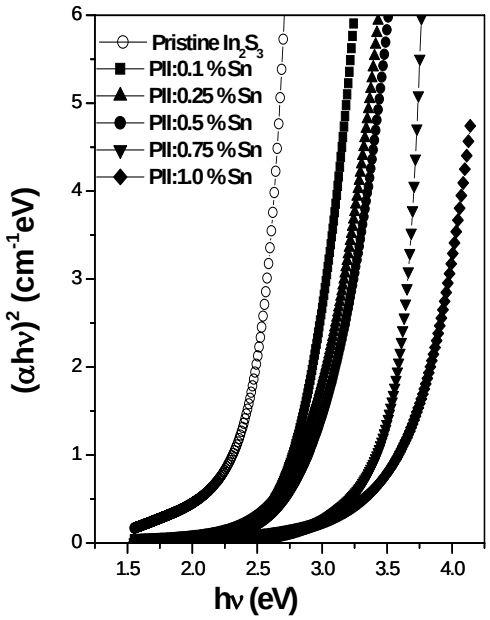

Fig. 4.9. Variation of bandgap with different tin concentrations in In_2S_3 thin film samples

. N. Barreau et al has investigated the evolution of the conduction and valence band levels with the increase in optical band gap [38]. The results obtained were discussed in terms of β-$In_2S_{3-3x}O_{3x}$ intrinsic property as well as in terms of its application as buffer layer in Cu(InGa)Se_2-based solar cell. The valance band discontinuity measurements suggested that the substitution of sulfur atoms by oxygen atoms in the crystalline matrix of β-In_2S_3 has only a small influence on the position of the valence band level of the material.

Robles *et al*.[39] had shown that the sulfur orbitals participated in both conduction and valence bands of β-In_2S_3 . On the another hand, Matar *et al*.[40] reported that the oxygen orbitals also contributed to both conduction and valence bands of β-In_2O_3 . Thus, in the event of an increase of optical band gap due to an electronic effect, both valence and conduction bands should shift, contrary to what was usually observed [38]. Robles *et al*. also reported that the compression of the β-In_2S_3 lattice induced the increase in its optical band gap. In the case of the indium sulfide thin films with oxygen, we have observed that the introduction of oxygen, substituted for sulfur in the crystalline matrix of β -In_2S_3, induced a decrease of its lattice parameters.[41] From these results, it seems that the increase of the optical band gap of these films with oxygen concentration is not due to the presence of oxygen orbitals, but instead is simply due to the decrease of the lattice parameter induced by its introduction.

Robles *et al*.[39] has presented a systematic study of the electronic structure of In_2X_3 (X=O ,Se, S, Te) semiconductors using the ab-initio tight- binding linear muffin-tin orbital (TB-LMTO) method. Taking in to account the experimental structure of each compound they have determined the lattice compression. The evolution of density of states (DOS) and energy gap under lattice compression has been determined by the site and orbital character of the states located around the Fermi level. For In_2S_3 the occupied part of DOS shows two main structures. The first one centered about 12 eV below the Fermi level (E_F) and has a band width of 3.4 eV

formed mainly by s character of S. The second one, of p-S and some of S-In and p-In character, is centered at 3.4 eV below E_F has a band width of 7 eV. The unoccupied region of DOS starts at about 1 eV above E_F with a narrow structure (1.5 eV band width) of p-S and s-In character followed by higher unoccupied p-S and P-In states. The experimental results prove that when the system undergoes compression the second structure of unoccupied part of the DOS preserves its center of gravity and bandwidth, but the first structure is pushed to higher energies thus increasing energy gap. Roles et al in his recent publication [42] has corroborated these findings. The consideration of β-$In_2S_{3-3x}O_{3x}$ as an alloy of two semiconductors as described by Hill [43] of In_2S_3 and In_2O_3 yields out a smaller band gap value than the real one and could not explain for the anomalous broadening of the optical band gap. The substitution of sulfur by oxygen in the crystalline matrix of β-In_2S_3 matrix induces a reduction of the lattice volume of the spinel. This substitution correlates with the increase of optical band gap of the films as a function of oxygen content. Therefore the evolution of the volume of the crystalline lattice and evolution of optical band gap can also be correlated. Here also the widening of band gap could be explained by the substitution of sulfur by oxygen as indicated by XPS studies.

4.3.2.3. Electrical Studies

Electrical resistivity measurement was done on both doped and pristine samples and was found to be decreasing with lower values of tin mixing. Conductivity of the pristine sample was 9×10^{-4} S/cm.

Samples showed better conductivity for lower mixing percentages of Sn (PII:0.1%Sn and PII:0.25%). The increase in conductivity of these thin film samples could be due to the donor action of tin. During the doping process, tin atoms might be occupying the vacant cationic sites or indium might get progressively replaced by tin atom. Since tin belongs to group IV of the periodic table, it would act as a donor either in the interstitial position or in the substitutional position contributing electrons which

would enhance the electrical conductivity. Indium interstitials formed due to the substitution of In by Sn might also act as donors, again promoting conductivity.

As shown in table 4.2, our measurements indicate that with increasing Sn concentration, the sheet resistance of the samples increased. The PII:0.5%Sn sample showed the sharpest decrease in conductivity. The increase in resistivity could be arising from the replacement of sulfur by oxygen. Greater electro negativity of the oxygen compared to sulfur might be contributing to this phenomenon as well. XPS analysis also proved the presence of larger incorporation of oxygen in In_2S_3/Sn samples.

Table. 4.2. Sheet resistance and photosensitivity of tin mixed samples

Sn/In ratio	Sheet Resistance	Photosensitivity
PII:0.1%Sn	64MΩ	40
PII:0.25%Sn	420 MΩ	296
PII:0.5%Sn	10 GΩ	10060
PII:0.75%Sn	14 GΩ	2518
PII:1.0%Sn	15 GΩ	156

Photosensitivity was measured from the illuminated current and the dark current. As shown in figure 4.10 the highest photosensitivity was obtained for sample PII:0.5%Sn, of the order of 10^4. A very high photosensitivity was observed when the sample was having a wide band gap of 3.1 eV.

High value of 'photo to current conversion efficiency' was reported on sulfurization of wide – band gap metal oxides [44] The photo response of wide band semiconductors (oxides) is extended towards visible region by the introduction of low band gaps (sulfides). The high photocurrent is explained by the phenomena [44] that,

photo-induced electrons in the conduction band of sulfide move towards sulfide/oxide interface with a high velocity due to energy gradient in the space charge layer. These electrons are transferred to the conduction band of metal oxide by jumping over the small discontinuity of both conduction bands. The energy difference at the interface prevents the reverse flow of electrons. The maximum energy difference is defined as that between the conduction bands. The efficient charge separation at interface results in high photocurrent.

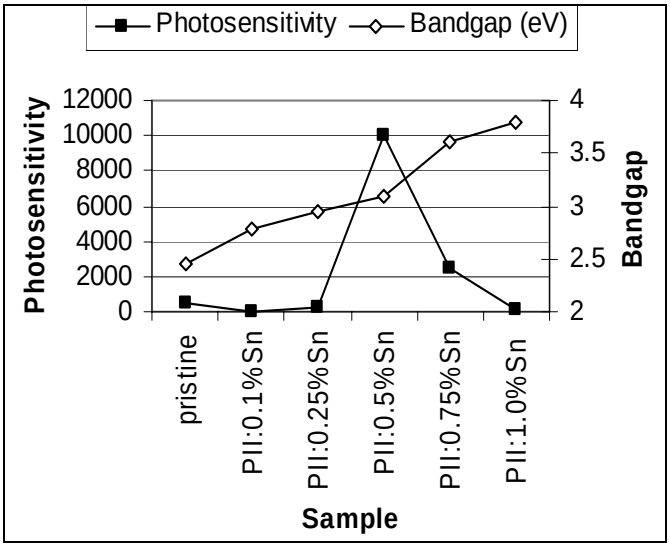

Fig. 4.10. Variation of bandgap and phot0sensitivity with different tin concentrations in In_2S_3 thin film samples

4.3.2.4. Defect Studies

TSC curve of doped samples exhibited two distinct peaks around 230 K and 310 K (Fig. 4.11), revealing the existence of two traps in the material. The defect level at 230 K was estimated to have activation energy of 100 meV. The defect level at 310 K corresponded to an activation energy of 230 meV. The defect levels of in-situ doped samples reveled during TSC measurements corresponded to that of ex-situ doped

samples. Our defect studies proved that two additional shallow defect levels were formed by Sn doping. The different defect levels might be the result of Sn occupying different positions (substitutional and interstitial) as well as due to the different oxidation states. At a substitutional position, Sn can also act as an amphoteric dopant due the multiple oxidation state it posses.

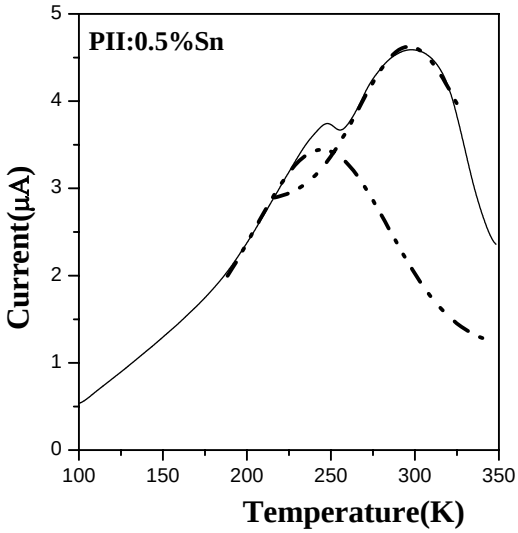

Fig. 4.11. Thermally Stimulated Conductivity (TSC) measurements on PII:0.5%Sn

4.4 Conclusion

In this study, we could illustrate wider band gap as well as better conductivity in In_2S_3 by Sn doping. These properties are highly useful for buffer layer applications in solar cells. Effect of both ex-situ and in-situ doping was analyzed, viz by diffusion (PI) and incorporation during spray (PII). Conductivity of the films enhanced by five orders with ex-situ doping, without changing the physical properties such as crystallinity or band gap. In this case we could limit the diffusion to surface layers, so that during junction fabrication for photovoltaic applications we can have a low resistive n-type layer near the electrode and highly photosensitive and resistive layer

(pristine) towards the junction. Carrier generation and collection can be promoted in photovoltaic application by such a structure. However it was also noted that a considerable increase in doping concentration resulted in samples with low crystallinity, negative photosensitivity and marginal increase in bandgap.

In-situ doping by incorporation of Sn using [$SnCl_4.5H_2O$] could increase the bandgap to wider ranges. Depth profile of various constituent elements using x-ray photoelectron spectroscopy (XPS) showed that incorporation of Sn increased the concentration of oxygen in samples. Sn doped In_2S_3 films showed an increase in band gap with Sn concentration. Depending on the Sn/In ratio, bandgap of In_2S_3/Sn could be varied from 2.72 eV to 3.78 eV. At lower mixing levels of Sn, wide band gap low resistive In_2S_3/Sn films could be obtained which are highly useful for buffer layer applications. Low resistive buffer layer will decrease the series resistance of the cell and wider band gap will improve light transmission in the blue wavelength, two important factors that will assist in increasing the short circuit current of the photovoltaic cell. Samples having higher Sn/In ratios showed wider band gap up to 3.78 eV. Even though the In_2S_3/Sn samples had very high bandgap and high resistivity, these samples were highly photosensitive. These results proved that tin incorporation modified the band gap and electrical properties of the Sn doped In_2S_3 films favorably over wider ranges making it highly suitable for optoelectronic applications.

References

[1] Teny Theresa John, Meril Mathew, C. Sudha Kartha, K. P. Vijayakumar, T. Abe, Y. Kashiwaba, Sol. Energy. Mat. Sol. Cells, 89**(1)** (2005)27.

[2] Teny Theresa John, S. Bini, Y. Kashiwaba, T. Abe, Y. Yasuhiro, C. Sudha Kartha, K. P. Vijayakumar, Semicond. Sci. and Tech, **18**,(2003) 491.

[3] Paul O' Brien, David J. Octway and John R. Walsh, Thin Solid Films, **315** (1998) 57-61.

[4] Amlouk M et al, Jpn. J. Appl. Phys., **38** (1999) 26-30.

[5] Bhira L. et al, Phys. Stat. Sol. (a), **181** (2000) 427.

[6] W.Rehwald, G.Harbeke, J.Phys.Chem. Solids **26** (1965) 1309.

[7] G.F.J. Garlick, M. Sprigford, H. Chesinska, Proc. Phys. Soc. **82** (1963) 16.

[8] A.G. Fitzgerald, P. Drapacz, A.O. Tooke, S.M. Potrous, Inst. Phys. Conf. Ser. **147 (10)** (1995) 409.

[9] A.A. El Shazly, D. Abd. Elhady, H.S. Metwally, M.A.M. Seyam, J.Phys. Condens. Matter **10** (1998) 5943.

[10] A.Goswami, G.D. Talele, S.B. Badachhape, Indian J. Pure Appl.Phys.**14** (1976) 716

[11] V.G. Bessergenev, A.V. Bessergenev, E.N. Ivanova, Yu.A. Kovalevskaya, J.Solid State Chem. **137** (1998) 6.

[12] G Shang, K. Kunze, M.J. Hampden-Smith, E.N. Duesler, Chem. Vap.Deposition **9** (1996) 242.

[13] W.T. Kim, C.D. Kim, J. Appl. Phys. **60 (7)** (1986) 2631.

[14] T. Asikainen, M. Ritala, M.Leskela,¨ Appl.Surf. Sci. **82y83** (1994) 122.

[15] T.Y oshida, K.Y amaguchi, H. Toyoda, K. Akao, T.Sugiura, H. Minoura, Y.Nosaka, Electrochem. Soc.Pr oc.**97 (20)** (1997) 37.

[16] J.George, K.S.Joseph, B. Pradeep, T.I. Palson, Phys. Stat. Sol. A **106** (1988) 123.

[17] G.Kitaiev, V. Dvoinine, A.Oustiantseva, M. Bieliaˉıeva, L. Skorniakov, Neorg.Mater . **12** (1976) 1760.

[18] W.T. Kim, C.D. Kim, J. Appl. Phys. **60 (7)** (1986) 2631.

[19] T. Yoshida, K. Yamaguchi, H. Toyoda, K. Akao, T. Sugiwra, H. Minoura, Y. Nosaka, Electrochem. Soc. Proc. **97** (1997) 37.

[20] Y.Yasaki, N.Sonoyama, T.Sakata, J. Electroanal. Chem. **469** (1999) 116.

[21] D. Brauger, D. Hariskos, T. Walter, H.W. Shock, Solar Energy Mater. Solar Cells **40** (1996) 97.

[22] D. Hariskos, M. Ruckh, U. Ruˉ hle, T. Walter, H.W. Shock, J. Hedstroˉm, L. Stolt, Solar Energy Mater. Solar Cells **41/42** (1996) 345.

[23] L. Brus, J. Phys. Chem. **90** (1986) 255.

[24] N. Barreauˈ , J. C. Bernède, H.El Maliki, S. Marsillac, X. Castel, J. Pinel, Solid State Communications **122** (2002) 445-450.

[25] N. Barreau, S. Marsillac, D. Albertini, J. C. Bernede, Thin Solid Films **403-404** (2002) 331.

[26] K. Kambas, J. Spyridelis and M. Balkanski, Phys. Status Solidi B. **105** (1981) 291.

[27] R. S. Becker, T. Zheng, J. Elton and M. Saeki, Solar Energy Mater. **13** (1986) 97.

[28] Meril Mathew, R.Jayakrishnan, P.M.Ratheesh Kumar, C.Sudha Kartha, Y.Kashiwaba, T.Abe and K.P.Vijayakumar; J. Appl. Phys. **100** (2006) 033504

[29] N. Barreau, J. C. Bernede, C. Deudon, L. Brohan, S. Marsillac, J. Cryst. Growth. **241** (2002) 4.

[30] Shu-Hong Yu, Lei Shu, Yong-Sheng Wu, Jian Yang, Yi Xie and Yi-Tai Qian, J. Am. Ceram. Soc. **82 (2)** (1999) 457.

[31] D. Braunger, D. Hariskos, T. Waltre and H. W. Schock, Sol. Energy Mater. Sol. Cells. **40** (1996) 97.

[32] V.A. Kul'bachinskii, V.G. Kytin, R. A. Lunin, A. V. Golikov, A. V. Demin, A. S. Bugaev, A. P. Senichkin, A. De Visser and R. T. F. Van Schaijk, Journal of experimental and theoretical physics **89 (6)** (1999) 1154.

[33] R. Jayakrishnan, Teny Theresa John, C. Sudha Kartha, K. P. Vijayakumar, T. Abe, Y. Kashiwaba, Semicond. Sci. and Technol. **20** (2005) 1162.

[34] I Lefebvre, M. Lannoo, J. Olivier-Fourcade, and J. C Jumas, Physical Review B **44 (3)** (1991)1004.

[35] J. F. Sanchez-Royo, D. Errandonea, A Segura, L. Roa and A, Chevy, Journal of Applied physics **83 (9)** (1998) 4750.

[36] N. Barreau, J. C. Bernede, C. Deudon, L. Brohan, S. Marsillac, J. Cryst. Growth **241**(2002) 4.

[37] M. A. Contreras, B. Egaas, K. Ramanathan, J. Hiltner, A. Swartzlander, F. Hason, and R. Noufi, Progr. Photov. Res. Appl. **7** (1999) 311.

[38] N. Barreau, S. Marsillac, J. C. Berne`de, and L. Assmann, Journal of Applied Physics **93(9)** (2003) 5456-5459.

[39] R. Robles, A. Vega, and A. Mokrani, Opt. Mater. **17** (2001) 497.

[40] S. F. Matar, A. Villesuzanne, G. Campet, J. Portier, and Y. Saikali, C.R. Acad. Sci., Ser. IIc: Chim **4** (2001)367.

[41] N. Barreau, J. C. Berne`de, S. Marsillac, and A. Mokrani, J. Cryst. Growth **235**, 439 (2002)

[42] T. Minemoto, Y. Hashimoto, W. Shams-Kolahi, T. Satoh, T. Negami, H. Takakura, and Y. Hamakawa, Sol. Energy Mater. Sol. Cells **75** (2003) 121.

[43] R. Hill, J. Phys. C: Solid State Phys. **7** (1974) 521.

[44] P.M. Sirimanne and T. Sakate, Materials chemistry and Physica **82** (2003) 466-470

Chapter 5

Thermal Diffusion of Copper: A Different Approach for the Preparation of $CuInS_2$ / In_2S_3 Junction

5.1 Introduction

Cu-In based compounds are emerging as promising absorber materials for solar cells [1-3]. Conversion efficiencies exceeding 19.5% has been achieved for CIGS based solar cells using CdS as buffer layer [4]. Copper indium sulfide ($CuInS_2$) has theoretically the highest conversion efficiency among the chalcopyrite CIS based solar cells [5] due to its direct band gap of 1.55 eV and high absorption coefficient (10^5 cm^{-1}). However, so far, practically, only 13.1% total area conversion efficiency could be achieved for the $CuInS_2$ based solar cells [6]. In order to use its potential fully one has to optimise the material/preparation techniques. However, it is well known that the controlled growth of high quality single crystals having a large area is very difficult, especially for ternary compounds [7]. Hence it is better to follow less complicated and easier thin film preparation techniques for fabrication of the solar cells and optimization of the same for a better performance.

Different methods are reported for the preparation of $CuInS_2$ thin films, such as sputtering [8], chemical spray pyrolysis (CSP) [9], chemical bath deposition (CBD) [10], electrodeposition [11], etc. Films prepared using many of these techniques exhibit diffusion of copper during junction fabrication with indium sulfide [12-16] altering the expected properties. In the present work, a different technique is used for the preparation of $CuInS_2$ thin films by exploiting the phenomenon of copper diffusion in indium sulfide thin films.

Diffusion coefficient of Cu is rather high [17]. Studies of copper diffusion in semiconductors, particularly in $CuInSe_2$ have proved high diffusivity of Cu [18].

Grain boundary diffusion coefficients are generally much higher than that of lattice diffusion and they serve as very efficient diffusion paths for copper [19]. Indium sulfide films prepared through spray pyrolysis facilitate grain boundary diffusion as this technique results in films with small grains and hence large density of grain boundaries. However, films prepared using other techniques like physical vapor deposition do not exhibit this property.

There are many reports on copper diffusion in CdS, facilitating the fabrication of homojunction. Kashiwaba et al. [20] reported the p-type characteristics of copper doped CdS thin films prepared using vacuum evaporation. Sunny Mathew et al. [21] reported the p-type characteristics of cadmium sulfide thin film prepared using spray pyrolysis technique by doping with copper. Sebastian [22] reported the formation of p-type CdS thin film prepared using chemical bath deposition. Another group from Japan also reported the preparation of p-type CdS thin film in which laser ablation was applied to a mixed target of CdS and copper [23]. Solar cell having an efficiency of 3%, fabricated by copper diffusion into CdS film, was reported by Varkey et al [24]. K. C. Wilson et al also reported the preparation of copper indium sulfide thin films on In_2S_3 thin films [25].But in this work, copper indium sulfide thin films were prepared by copper diffusion into argon ion irradiated In_2S_3 thin films, proving that copper diffusion in implanted samples was an easier method to prepare $In_2S_3/CuInS_2$ solar cell.

In this chapter, we report a novel, simple and cost-effective way of achieving a junction. On ITO (indium tin oxide) coated glass, In_2S_3 layer was coated using CSP technique. This acted as the window layer. Now the absorber layer was achieved by thermal diffusion of Cu into the In_2S_3 layer, in order to convert the top layer into $CuInS_2$ (*p* type), through solid state reaction between copper and indium sulfide. This would result in a $CuInS_2/ In_2S_3$ bilayer *p-n* junction. This is a simple process quite similar to the one adapted in silicon technology.

5.2. Experimental details

The diffusion work was initially carried out on In_2S_3 thin films deposited on soda lime glass substrate using CSP technique. Spray rate was kept as 20 ml/min. Total volume of the solution sprayed was varied from 200 ml to 400 ml in order to vary the thickness of the films from 0.5 μm to 1μm. Indium to sulfur ratio was 1.2/8 in precursor solution. This ratio was selected as it showed the maximum photosensitivity and rendered nearly stoichiometric films, prepared by spray pyrolysis technique [26]. Thin layer of copper was deposited using vacuum evaporation technique (pressure during evaporation was ~$2x10^{-5}$ Torr). subsequent annealing was given at 300˚C in vacuum for one hour to give thermal assistance for the diffusion of the metal. The post annealing temperature was selected after optimisation. Diffusion depth was changed by varying the mass of the metal used. Diffused samples were named as IS:5Cu, IS:10Cu, IS:15Cu, IS:20Cu and IS:25Cu corresponding to 5 mg, 10 mg, 15 mg, 20 mg and 25 mg of Cu evaporated.

5.3 Results and Discussion

In_2S_3 samples prepared using CSP technique revealed the formation of $CuInS_2$ on copper diffusion at optimized conditions.

5.3.1. Structure and Morphology

5.3.1.1. X-Ray Diffraction (XRD)

The 'd' values of pristine In_2S_3 film having a thickness of 0.5 μm coincided with that of β-In_2S_3 in standard JCPDS data card (25-390). Pristine In_2S_3 existed in tetragonal structure. Characteristic peaks of In_2S_3 appeared at 2θ values 14.31°, 27.59°, 33.48°, 43.95°, and 48.08°.Copper diffused In_2S_3 samples revealed the presence of $CuInS_2$ phase along with the In_2S_3 phase. Figure 5.1 depicts the variation in XRD with diffusion concentration.

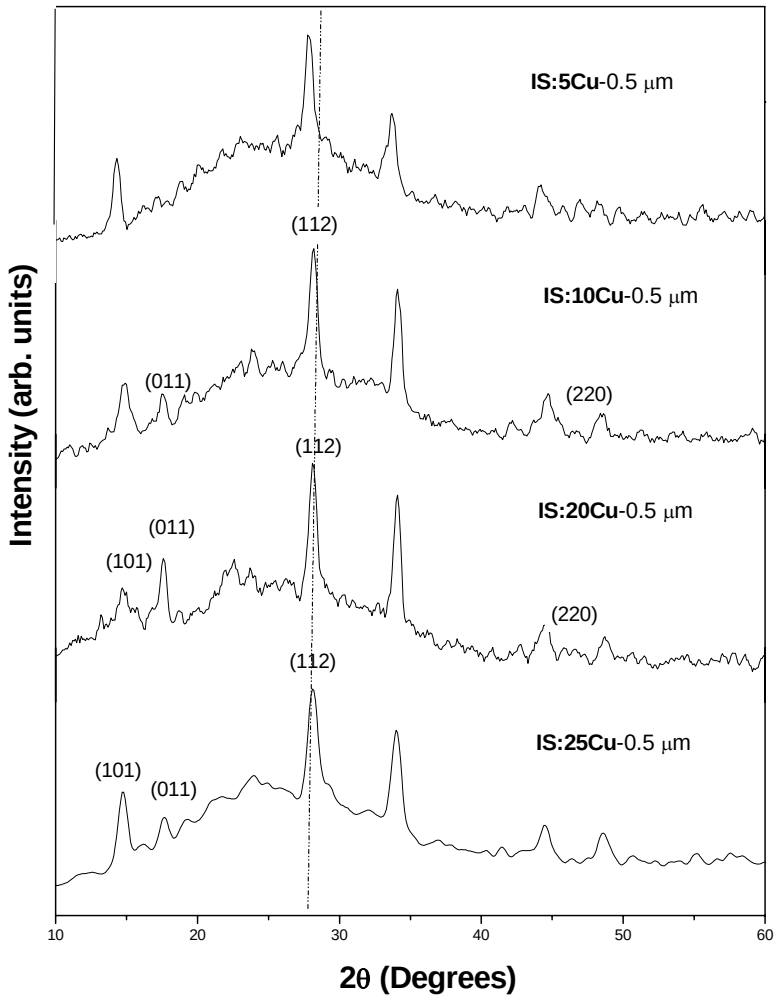

Fig. 5.1. Variation in XRD pattern with Cu diffusion in to In_2S_3 film thickness 0.5 μm

Here the In_2S_3 samples, on which the Cu diffusion is done, have thickness of 0.5μm as mentioned in section 5.2. In samples IS:10Cu-0.5μm, IS:15Cu-0.5μm and IS:20Cu-0.5μm, peaks corresponding to planes of tetrahedral $CuInS_2$ could be observed. Most of the peaks assigned to $CuInS_2$ were weak and overlapped with those of In_2S_3. For copper diffused sample, the peak at $2\theta = 27.59^0$ corresponding to (109)

plane of In_2S_3 shifted to $2\theta = 28.10^0$ peak, corresponding to (112) plane of $CuInS_2$. This peak exhibited broadening, due to the presence of (109) plane of In_2S_3 as a shoulder peak. The peaks corresponding to (101) of $CuInS_2$ and (109) of In_2S_3 merged and resulted in a broad peak at 14^0. However the peak at $2\theta \approx 17^0$ [which is the characteristic peak of $CuInS_2$] does not overlap with other compounds [27]. A fingerprint of chalcopyrite XRD is the presence of a weak peak at $2\theta \approx 17^0$-18^0 [28]. Thus the XRD result suggests the formation of $CuInS_2$.

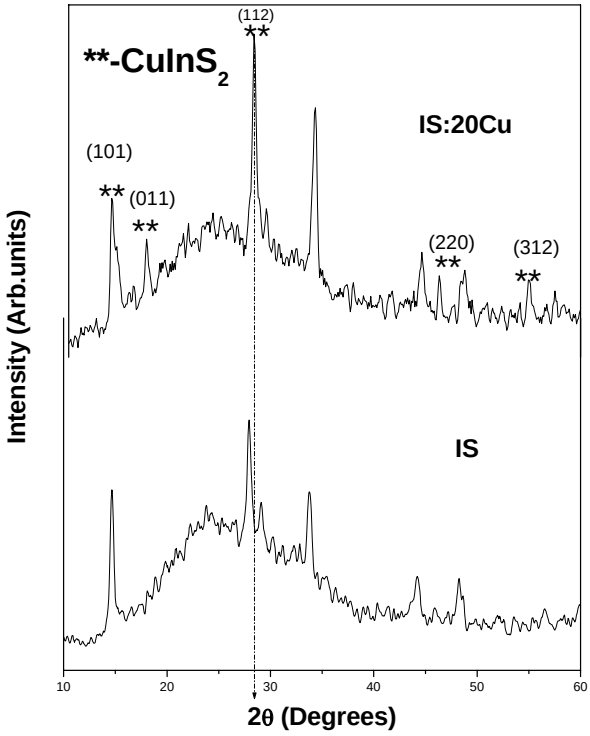

Fig. 5.2. XRD of pristine and Cu diffused sample IS:20Cu

The thickness of the In_2S_3 films increased from 0.5 μm to 1 μm on the outlook of application of this finding (formation of $CuInS_2$ by diffusion) for junction (solar

cell) fabrication . Further studies were carried out at this increased thickness. Figure 5.2 gives the XRD pattern of pristine and diffused sample having this higher thickness. On increasing the thickness to 1 μm, only sample IS:20Cu revealed the formation of $CuInS_2$ and further studies were carried out at this condition. Diffused samples having lower or higher diffusion concentration on comparison to IS:20Cu and pristine sample showed transition behavior. IS:20Cu sample clearly exhibited $CuInS_2$ peaks at 2θ values of 28.10°, 32.64°, 46.42°, and 55.06°, with (112) plane (at 2θ=28.10°) as a preferential orientation plane. (109), (220) and (2212) planes of In_2S_3 could also be observed along with $CuInS_2$.

5.3.1.2. XPS Analysis

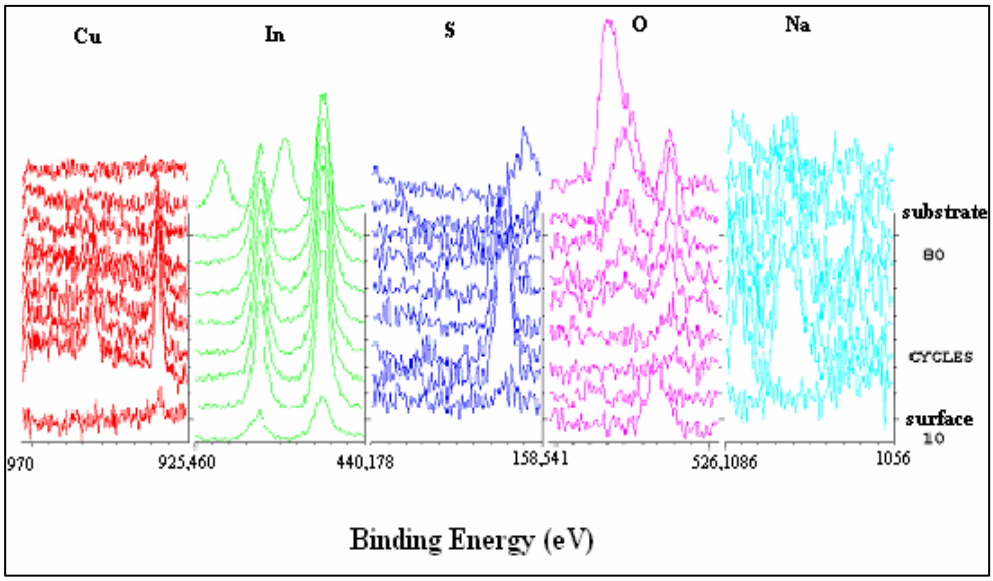

Fig. 5.3. XPS depth profiling of sample IS:20Cu

XPS Depth profiling revealed the diffusion of copper in to the surface layers. Binding energy of Cu indicated the formation of $CuInS_2$ indicating absence of any

binary phase formation in the sample. There was a gradient of Cu from surface layer towards the bottom layer of the In_2S_3 film. Another observation was that diffusion of copper created sulfur deficiency at the surface, probably due to the formation of CIS layer. The binding energy of sulfur was 162 eV while that of Indium shifted to lower values at the surface, due to the formation of $CuInS_2$. Surface contamination due to oxygen was also observed. However there was no oxygen in the bulk of the sample. Table 5.3 gives the binding energy value of Cu, In and S as observed from XPS Analysis

Table 5.3 BE value of Cu, In and S as observed from XPS Analysis

Element	Binding Energy (eV) (surface)
$Cu2p_{3/2}$	932.5
$Cu2p_{1/2}$	952.5
$In3d_{5/2}$	444.7
$In3d_{3/2}$	452.7 (surface),453
S2p	162.0

5.3.2 Optical Studies

Optical absorption spectrum of β-In_2S_3 shows absorption in the region of 475nm and does not show any absorption peak in the long wavelength range. But optical absorption spectra of IS:20Cu showed a shift of the absorption edge towards long wavelength, presenting another hump around 850 nm, which could be due to absorption of $CuInS_2$. In order to determine the optical band gap, $(\alpha h\nu)^2$ against $h\nu$ graph was plotted [Fig. 5.4]. Optical band gap could be obtained from this plot by the

linear fit in the straight portion of the graph. Band gap of pristine sample was 2.57 eV. A decrease in bandgap was observed for doped samples. For sample IS:20Cu two edges could be seen in the regions of 1.42 eV and 2.48 eV, corresponding to the band gaps of $CuInS_2$ and In_2S_3 respectively. This indicated coexistence of both the phases.

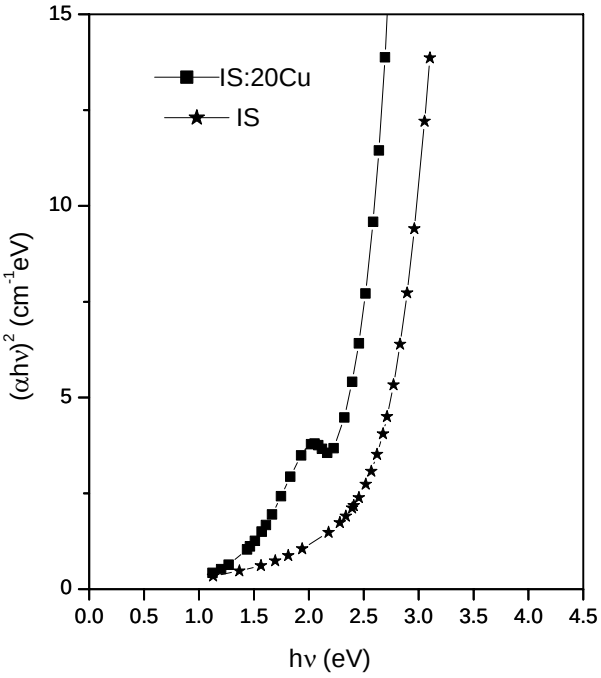

Fig. 5.4 Variation of band gap with Cu diffusion

5.3.3 Electrical resistivity measurements

Resistivity of the In_2S_3 thin films decreased with Cu diffusion. For sample IS:20Cu resistivity decreased to 1.02×10^{-3} ΩCm. Photosensitivity also decreased to 0.6. Decrease in resistivity might be due to the presence of high metal concentration at the surface. Hot probe measurements proved the films to be p-type at the surface.

5.4 Device Fabrication

This section describes fabrication and characterization $CuInS_2$ based solar cell by a novel method with Cd-free β-In_2S_3 buffer layer. Copper was diffused into In_2S_3 (*n*-type) by annealing bi layer films having structure Cu/In_2S_3. Through solid state reaction between copper and indium sulfide the top layer could be converted into $CuInS_2$ (*p* type), so as to make a $CuInS_2$/ In_2S_3 bilayer *p-n* junction.

For device fabrication $Al/CuInS_2/In_2S_3$//ITO configuration was selected. The configuration was having the 'superstrate' structure of a solar cell and the illumination was given through ITO.

5.4.1 Back Contact (ITO)

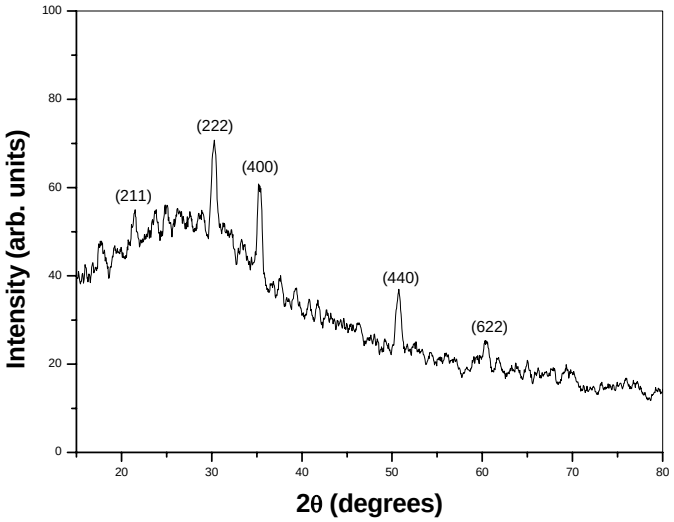

Fig. 5.5. XRD pattern of ITO

Several types of transparent conducting oxides (TCOs) are commercially produced to be used as front/back contact of solar cells. In the present work, we used commercially available ITO (indium tin oxide) films [Thickness – 1500 A; optical

transmission ~ 82% ; electrical resistivity 2.25×10^{-4} Ω-cm] as the bottom electrode for fabricating the cell.(Fig.5.6 shows transmission spectrum of the ITO films while Fig 5.5 depicts the XRD pattern)

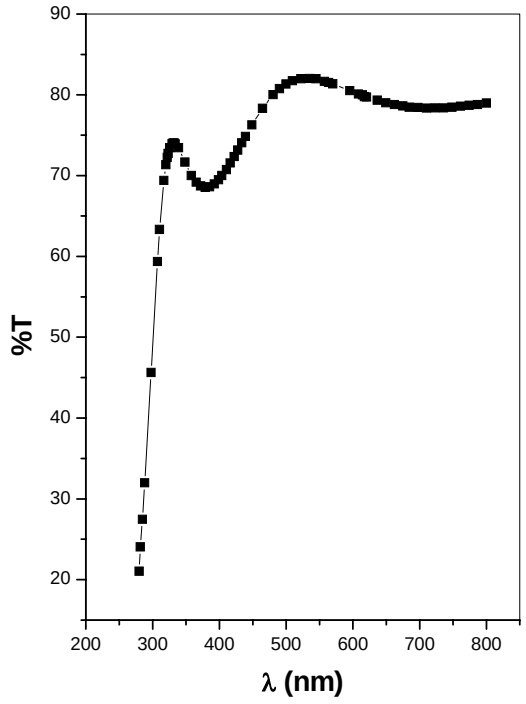

Fig.5.6. Transmission spectrum of ITO

5.4.2 In_2S_3 buffer layer

Over ITO, In_2S_3 layers were deposited using CSP technique. Aqueous solution of indium chloride ($InCl_3$) and thiourea was used to deposit In_2S_3 films. For the fabrication of the junction, we used In/S ratio in the precursor solution as 1.2/8. For this the molarity of $InCl_3$ was kept at 0.015 M and that of thiourea at 0.1 M. The solution was sprayed on the substrate, kept at a temp of 300 ± 5^{o}C, keeping the spray

rate at 20 ml/min. The total volume of the solution sprayed was 400 ml and the thickness was 1µm Band gap was found to be 2.65 eV, wider than that of sample coated on glass.

5.4.3 $CuInS_2$ absorber layer

Here copper was diffused into In_2S_3 (*n*-type) thin films in order to convert the top layer into $CuInS_2$ (*p* type). Copper was diffused into In_2S_3 by annealing bi layer films having structure Cu/In_2S_3. Through solid state reaction between copper and indium sulfide the top layer could be converted into $CuInS_2$ (*p* type) which act as the absorber layer.

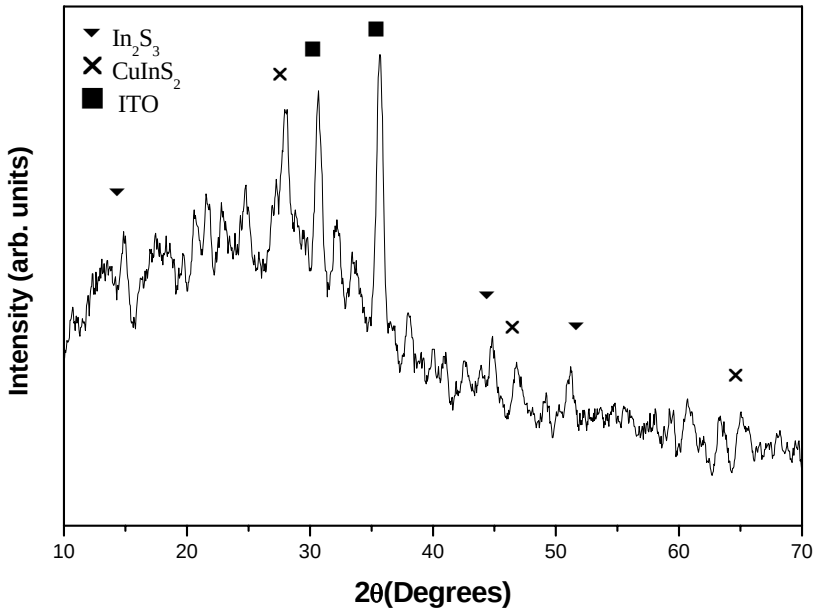

Fig 5.7 XRD pattern of Cu diffused indium sulfide film on ITO.

Figure 5.7 gives the XRD pattern of the device fabricated over the ITO layer. Both $CuInS_2$ and In_2S_3 phases were observed in the XRD results of the cell. The Peaks

corresponding to ITO could be identified from table 5.1 Absorption spectrum of the device depicted clear absorption edges for $CuInS_2$ layer (~1.46 eV) and indium sulfide layer (~2.53 eV) (Fig. 5.8).

Table 5.1 XRD analysis of ITO film

2θ (degrees)	d (Å) (observed)	d(Å) (standard)	hkl
21.45	4.1400	4.1770	211
30.20	2.9570	2.9470	222
35.30	2.5406	2.5371	400
50.75	1.7975	1.7880	440
60.42	1.5310	1.5250	622

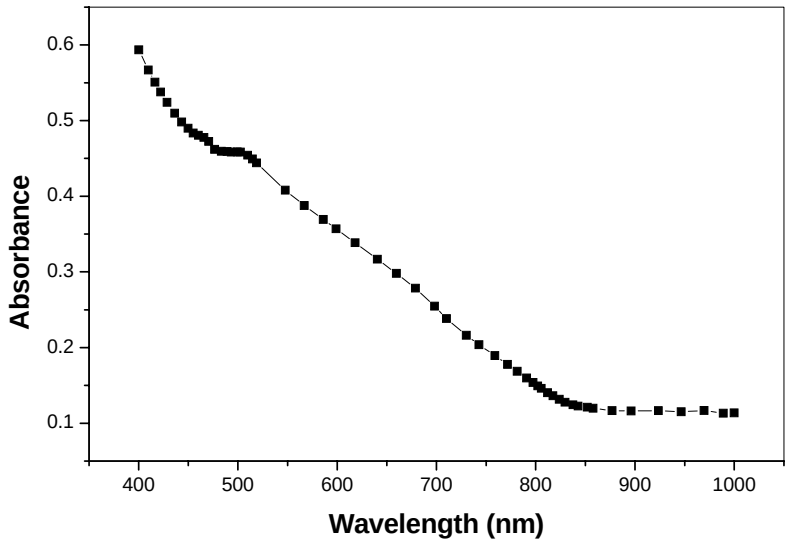

Fig. 5.8. Absorption spectrum of device fabricated

5.4.4 Electrode Deposition

We deposited Aluminium as the top electrode using Physical Vapour Deposition (PVD). As the grain size of the samples were small (grain size of In_2S_3 is ~ 16 nm), the grid or comb structure of the electrodes may result in the loss of photo generated carriers collected at the electrode. Hence we have given the electrode as a square block, having area 0.1 cm^2 and thickness 50 nm.

5.4.5 J-V characteristics of the cell

Dark and illuminated J-V characteristics of the cell were recorded using Keithley Source Measure Unit (SMU, K 236) and Metric's Interactive Characterisation Software (ICS). The cell was illuminated using a tungsten halogen lamp having intensity 100 mW/cm^2 on the sample surface. An infrared filter and a water jacket were used to remove heat content from the incident light to ensure that there was no heating of the cell during measurement. Input power was measured using a "suryamapi" (A-136 model of CEL). Distance between the cell and the source was 8 cm.

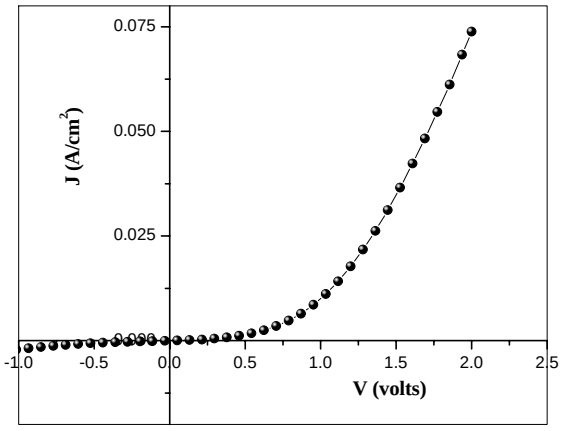

Fig. 5.9 Dark characteristics of the cell

Dark I-V characteristic of the device (ITO/ In_2S_3/ CIS/electrode) was proving the action of p-n junction, as given in figure 5.9. Diode quality factor was calculated to be 4.12 from dark characteristics of the cell [slope (λ) of the ln J versus V graph [29]. λ=q/AkT; A is diode quality factor, kT/q is thermal voltage, I_{ph} is the light generated current density, T = 300K and kT/q = 0.025]. Diode quality factor >2 indicates domination of interface recombination [30], leading to reduced short circuit current density, J_{sc}. For the cells prepared by this technique, interface is not sharp and this might be the reason for the low value of short circuit current density in the present work.

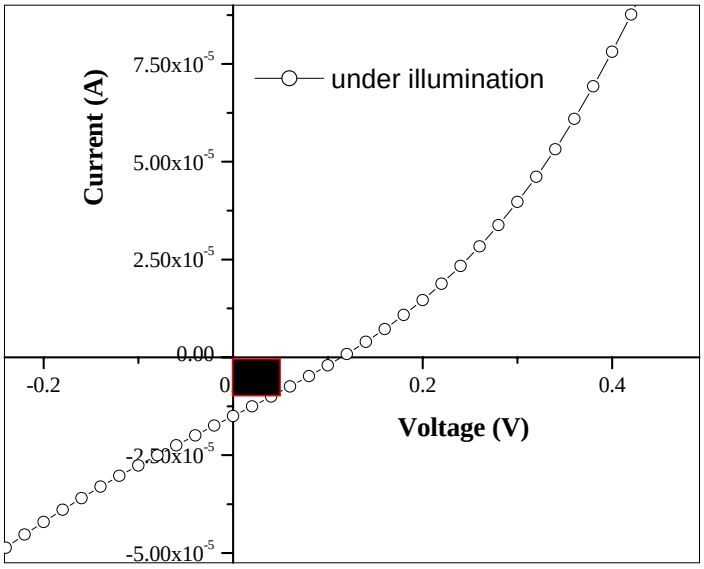

Fig. 5.10 I-V characteristics of the device under illumination

In the present case since the cell was having a superstrate structure, junction was illuminated through the substrate side. On illumination, the device exhibited photovoltaic action (Fig. 5.10). I-V characteristics of the device shifted towards the

fourth quadrant, indicating that this junction behaved as a solar cell giving open circuit voltage (*V*oc) of 103 mV and short circuit current density (*J*sc) of 1.55 mA/cm^2. Other cell parameters, [viz., fill factor (FF) and efficiency (η) of the cell], were calculated using the relation FF=*JmVm*/*J*sc*V*oc and η=*JmVm*/*P*inX100, where *P*in is the input power, *Jm* and *Vm* are the current density for maximum power and the voltage for maximum power, respectively, and *J*sc and *V*oc are the short circuit current density and open circuit voltage, respectively. By substituting the values of *Jm*, *Vm*, *J*sc, and *V*oc the fill factor and efficiency of the cell were found to be 27.2% and 0.043%, respectively. Though the values obtained for cell are quite small, this opens up a new path to achieve a photoactive junction. Low values of current density and voltage might be due to the absence of perfect junction. Controlling the thickness of the indium sulfide, thickness of metallic film, annealing temperate and annealing time, one can get a better junction yielding better efficiency.

5.5 Conclusion

In_2S_3 film could be conveniently converted into $CuInS_2$ by diffusing copper into it. Cationic vacancies of the stoichiometric In_2S_3 films, grain boundaries and dangling bonds made the diffusion of copper much easier. Junction could be fabricated by adjusting depth of the copper diffusion by controlling the annealing temperature and thickness of the Cu and / or that of indium sulfide layer. This junction was found to be photoactive and can act as a solar cell. The most important step required for the improvement is the optimization of parameters of device fabrication to passivate the interface defects. However the possibility of establishment of photoactive heterojunction using this novel and simple technique is an encouraging result.

References

[1] J A M Abushama, S Johnston, T Moriarty, G,Teeter K Ramanathan, R.Noufi, Prog.Photovolt: Res.Appl. **12 (**2004) 39-45.

[2] Powalla M, Dimmler B. Thin Solid Films. **361-362** (2000) 540-546.

[3] Watanabe T, Matsui M., Jpn. J. Appi. Phys, **38** (1999) L1379-L1381

[4] K Ramanathan, M A Contreras, C L Perkins, S Asher, F S Hasoon, J Keane, D Young, M Romero, W Metzger, R Noufi, J Ward, A Duda, Prog.Photovolt: Res. Appl. **11** (2003) 225-230

[5] S. Siebentritt, Thin Solid Films **403/404** (2002) 1.

[6] H. Goto, Y. Hashimoto, and K. Ito, Thin Solid Films **451/452** (2004) 552.

[7] H. Metzner, Th. Hahn, J. H. Bremer, and J. Conrad, Appl. Phys. Lett. **69** (1996) 1900.

[8] P Steven. Grindle, Charles W. Smith, and Steven D. Mittleman, Appl. Phys. Lett. **35** (1979) 24.

[9] Teny Theresa John, K. C. Wilson, P. M. Ratheeshkumar, C. Sudha Kartha K. P. Vijayakumar, Y. Kashiwaba, T. Abe, and Y. Yasuhiro, Phys. Status Solidi A **202** (2005) 79.

[10] N. A. Zeenath, P. K. V. Pillai, K. Bindu, M. Lakshmi, and K. P. Vijayakumar,J. Mater. Sci. **35** (2000) 2619.

[11] J. Herrero and J. Ortega, Sol. Energy Mater. **20** (1990) 53.

[12] N. Naghavi, S. Spiering, M. Powalla, B. Cavana3and D. Lincot Prog. Photovolt: Res. Appl.; **11** (2003) 437–443.

[13] N.Naghavi, S.Spiering, M.Powalla, D.Lincot, , Proc. of 3rd World Conference on Photovoltaic Energy Conversion. 2003., **1** (2003) 340 – 343.

[14] A.Lafond, C. Guillot-Deudon, S. Harel, A. Mokrani, N. Barreau, S. Gall and J. Kessler, Thin Solid Films , **515(15, 31)** (2007) 6020-6023.

[15] S. Spiering, A. Eicke, D. Hariskos, M. Powalla, N. Naghavi and D. Lincot, Thin Solid Films**, 451-452** (2004) 562-566.

[16] S. Spiering, D. Hariskos, M. Powalla, N. Naghavi and D. Lincot, Thin Solid Films**, 431-432** (2003) 359-363.

[17] Teny.T John, Meril Mathew, C. Sudha Kartha, K. P.Vijayakumar, T. Abe, Y. Kashiwaba, Sol.Energy.Mat.Sol.Cells **89(1)** (2005) 27-36.

[18] L. Chernyak, D. Cahen, S. Zhao and D. Maneman, Appl. Phys. Lett. **65** (1994) 427.

[19] K. Djessas, S. Yapi, G. Massé, M. Ibannain and J. L. Gauffier, J. Appl. Phys. **95(8)** (2004) 4111.

[20] Y Kashiwaba, I Kanno, T.Ikeda, Jpn J Appl Phys **31** (1992) 1170.

[21] Mathew Sunny, PS Mukerjee, KP.Vijayakumar, Jpn J Appl Phys **34** (1995) 4940.

[22] P Sebastian, J. Appl Phys Lett **62(23)** (1993) 2956.

[23] S Keitoku, H Ezumi, H Osono, M. Ohta Jpn J Appl Phys **34** (1995) L138.

[24] K. P. Varkey, K. P. Vijayakumar, T. Yoshida, and Y. Kashiwaba, Renewable Energy **18** (1999) 465.

[25] K. C. Wilson, Tina Sebastian, Teny Theresa John, C. Sudha Kartha, K. P. Vijayakumar, P. Magudapathi and K. G. M. Nair, Appl. Phys. Lett. **89**, (2006) 013510.

[26] Teny Theresa John, S. Bini, Y. Kashiwaba, T. Abe, Y. Yasuhiro, C. Sudha Kartha, and K. P. Vijayakumar, Semicond. Sci. Technol. **18** (2003) 491.

[27] Noriyuki Sonoyama, Satoshi Shiosaki, Prasad Manjusri Sirimanne and Tadayoshi Sakata, Electochem.and solid state letters, **3(4)** (2000) 189.

[28] Gary Hodes, Chemical solution deposition of semiconductor films, CRC press (2003) 295.

[29] Harold J. Hovel Semiconductors and Semimetals; Vol. II, Solar Cells, Academic Press, New York (1975).

[30] M. Saad and A. Kassis, Sol. Energy Mater. Sol. Cells **77** (2003) 415.

Chapter 6

Role of Involuntary Dopant, Chlorine in Chemical Spray Pyrolysed In_2S_3 thin films

6.1 Introduction

In recent years, there has been a significant increase in research on III-VI materials they application in the electronic industry for optoelectronic and photovoltaic applications [1, 2]. Indium sulfide is a III-VI compound which can be prepared using different chemical methods. It is of note that most of the chemical deposition techniques for coating In_2S_3 compounds use chloride based precursor solutions [3-11]. In atomic layer epitaxy, In_2S_3 films are deposited using $InCl_3$ and H_2S as precursors [5]. In all the reports dealing with deposition of indium sulfide using spray pyrolysis, indium chloride and thiourea are used as the precursor solutions. [6,7,8,9]. Indium sulfate $In_2(SO_4)_3$, 80% hydrazine hydrate, thioacetamide, triethanolamine and ammonium chloride are used for the deposition of indium sulfide using chemical bath [4]. On using chloride based precursor solutions, the incorporation of Cl in the indium sulfide films is observed [12, 13].

Generally the thin films of compounds, grown under lower vacuum conditions or by chemical reactions, have a better chance of introducing unintentional dopants to the films which are contributed by the precursors, the grounding environment, the process sequence etc. Many of these unintentional dopants [like oxygen, sodium etc] were found to be beneficial in the case of indium sulfide thin films. The oxygen present in the CBD and PVD films has been found to be the origin of the special optical properties, which made them a good substitute for CdS as buffer layer in thin film solar cells [14, 15].

Presence of sodium was detected in indium sulfide samples deposited on soda lime glass. Sodium diffused from glass substrate into the samples [16]. Detailed

analysis and purposeful doping of indium sulfide thin films with Na proved that it was beneficial for the films and optimum doping could enhance the band gap (2.95 eV in comparison to 2.1 eV of pure In_2S_3 films) and electrical conductivity [17]. The sodium incorporated In_2S_3 films were named as BINS films and has proved to be an ideal candidate for CIGS based solar cells. Mo/ CIGS/BINS structures have reached a conversion efficiency of 8.2% [18].

Also compositional analysis reported on In_2S_3 films prepared using CBD technique contain a mixture of oxide and hydroxyl compounds of indium (difficult to attribute clearly to either contribution) along with indium sulfide [19]. This in fact converted the material into a buffer layer having good electronic and structural properties and matching to the absorber material. Comparing the device performance of solar cells using a standard CBD-CdS buffer layer with the cadmium free CBD-$In_x(OH,S)_y$ it was found that the Voc greatly improved and the FF values were comparable. There is a significant gain in spectral quantum efficiency below 540 nm, which is the absorption edge of CdS, due to the higher band gap of $In_x(OH,S)_y$ [20].

In the previous chapters we described intentional diffusion/doping in In_2S_3 films with transition metals and their influence on its properties. This chapter explores the effect of chlorine, the involuntary dweller in In_2S_3 films which are prepared by chemical methods using chloride based precursor solutions, on the properties of indium sulfide thin films.

Preparation and properties of indium sulfide films by spray pyrolysis using indium chloride [13] and indium nitrate [21] has been presented by Teny et al. It was noted that the properties of the films depend greatly on the precursor solution used for deposition. The results proved that precursor influenced the structural and electrical properties of the films. Our motivation behind this work was to find the role of chlorine in In_2S_3 films, as the films prepared using chloride based precursor solution yielded better performance than nitrate based ones, presenting a possibility of chlorine traces altering the properties of the films. In this work, we studied the impact of

chlorine on the properties of In_2S_3 films by intentionally introducing chlorine to In_2S_3 films prepared using indium nitrate precursor solutions. Indium nitrate will eliminate the likelihood of inclusion of chlorine in the pristine film making the comparison more appropriate. The doping studies were carried out on $InCl_3$ based In_2S_3 films to have a comparative look on Cl doping.

6.2 Experimental Details

β-In_2S_3 thin films were prepared using CSP technique with indium nitrate ($In(NO_3)_3$) and thiourea ($CS(NH_2)_2$) as precursor solutions. Indium nitrate was prepared by dissolving high purity (99.99%) indium in concentrated HNO_3. Micro glass slides, having dimensions of 37×12×1.4 mm^3 were used as substrates. Chlorine was doped purposefully in the sample by adding ammonium chloride to the precursor spray solution. The doping concentration was varied by changing the molar concentrations of ammonium chloride in the spray solution. In these samples, the molarity of indium nitrate was kept at 0.025 M and that of thiourea was changed to vary the In:S ratio. Doping studies were carried out in different ratios to clarify the role of Cl with respect to the indium and sulfur concentration in the films. The total volume of the solution sprayed was 200 ml and the rate of spray was 20 ml/min in all cases keeping the substrate at 300°C. Air was used as the carrier gas. These films were yellowish in color. Samples having an In/S ratio of 2/3, 2/5 and 2/8 in the precursor solution were studied at different doping concentrations. The doped samples were named by specifying the doping concentration along with In:S ratio as (N (In/S ratio in solution): % of doping in the total solution Cl).

Samples were also prepared using chloride based precursor solutions and doping studies were done on these films to make out the changes that could be achieved on increasing the chlorine concentration. The doping studies were carried out on films prepared using the two different In/S ratios (2/5 and 1.2/8 in the solution)

known to yield the best crystallinity and highest photosensitivity among chloride based samples [13]. The chloride based samples were named as (C (In/S ratio in solution): % of doping in the total solution Cl). In nomenclature, chloride based samples are prefixed with C and Nitrate based samples with N. The chloride based films responded to very small percentage of doping in comparison with nitrate based samples.

6.3 Results and Discussion

6.3.1 Structural Analysis

Structural analysis was done using XRD. In_2S_3 thin films prepared from indium nitrate showed diverse property in the XRD analysis. The trial was carried out with different In:S ratio in the precursor solution (2:2, 2:3, 2:4, 2:5, 2:8, 1.2:8,1.5:3, 1.75:3, 2.25:3, 2.5: 3). All the samples were amorphous in nature irrespective of indium to sulfur ratio. Even though earlier report presented the single ratio 2:3 to be crystalline [23], repeated analysis never yielded such a result making the entire samples prepared using indium nitrate to be amorphous. Thickness of the sample increased from 0.5 μm to 1 μm by increasing the volume of spray from 200 ml to 400 ml. Thickness of the film was measured using stylus profiler. Amorphous nature of the samples persisted even at increased thickness.

On doping with chlorine the films became crystalline. The *d* values of doped samples coincided with that of β-In_2S_3 in standard JCPDS data card (25-390). On increasing doping concentration (in precursor solution), the Bragg peaks in XRD pattern became more intense indicating a clear improvement in crystallinity. All samples (different series having different In:S ratio) showed similar behavior on Cl doping. (Figs. 6.1 - 6.3)

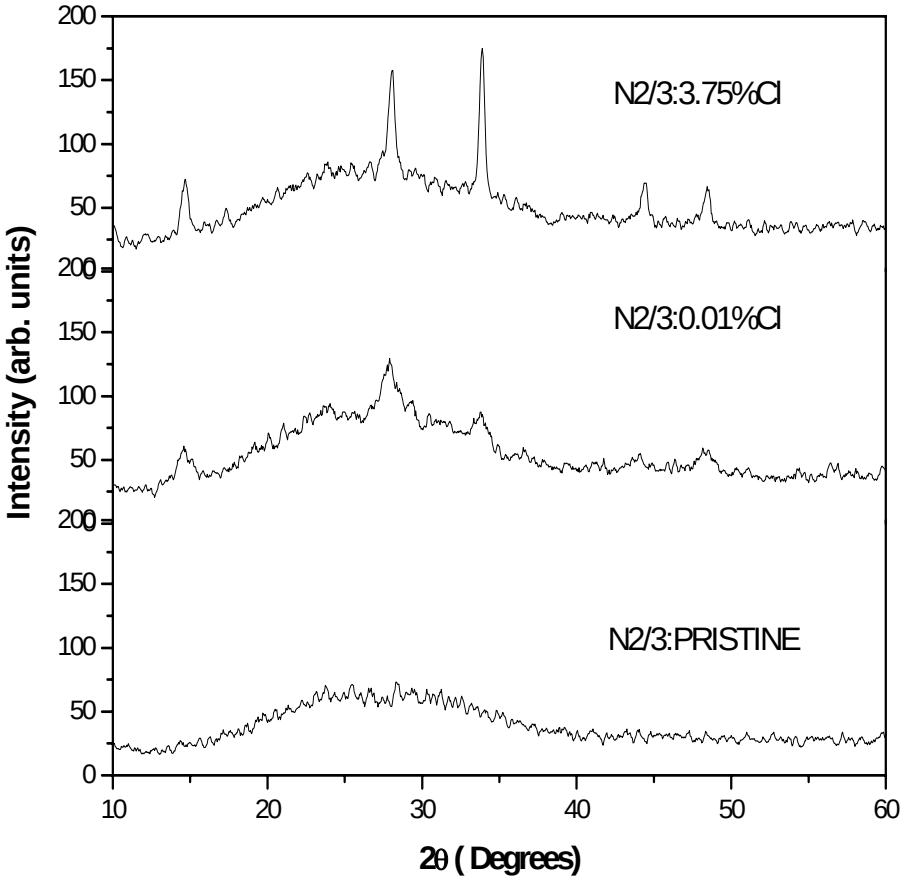

Fig.6.1 XRD pattern of N2/3 series with doping

The grain size was calculated using the Debye-Scherrer formula D = 0.9λ/βCosθ, where *D* is the diameter of the crystallites forming the film, λ is the wavelength of CuK_α line, β is FWHM in radians and θ is the Bragg angle. The grain size of the films also indicated a significant increase along with Crystallinity. The values are tabulated in table 6.1. For N2/5: 5%Cl the grain size became 26.4 nm on doping with Cl while the pristine films were amorphous.

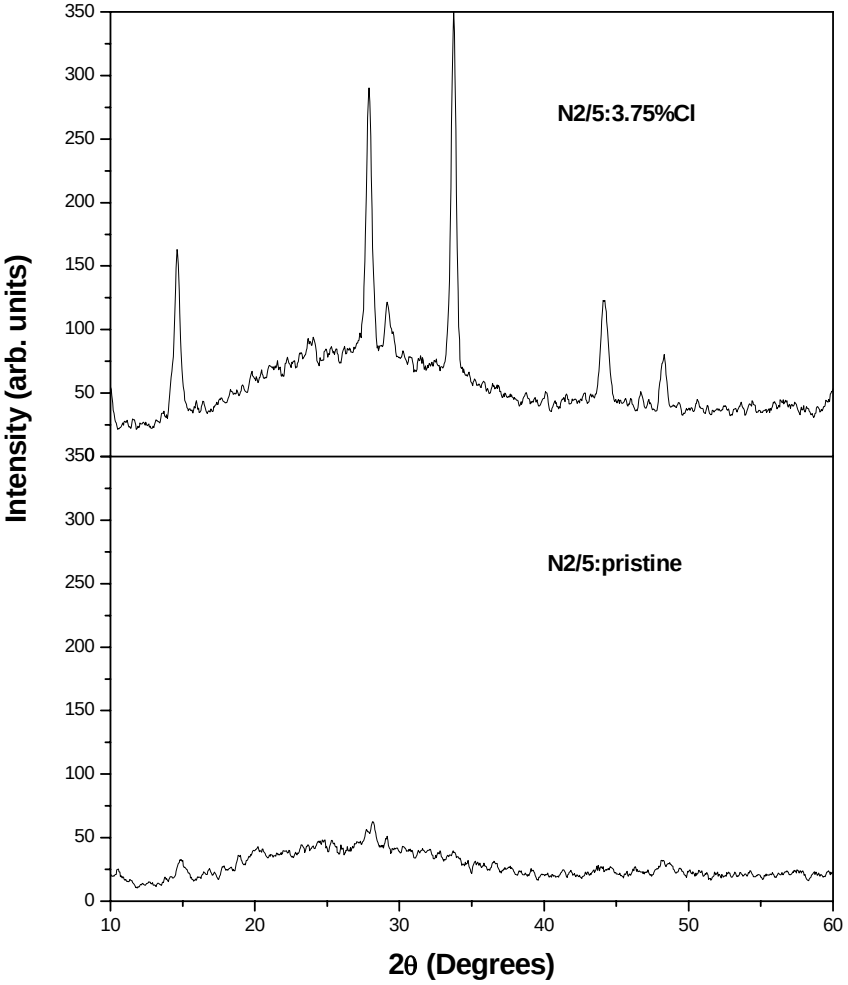

Fig.6.2 XRD graph of N2/5: pristine and N2/5: 3.75%Cl

Lattice constants '*a*' and '*c*' for the samples were calculated from the results of x-ray diffraction patterns using the (103) and (109) planes. For doped samples of N2/3 series, the values were found to be a = b = 7.58 Å, c = 32.08 Å. As the In/S ratio decreased, the lattice constants increased slightly (for the ratio 2/8 series and 2/5

series) a = b = 7.6 Å, c = 32.4 Å [7]. These values are comparable with those for β-In_2S_3 shown in JCPDS card (25-390).

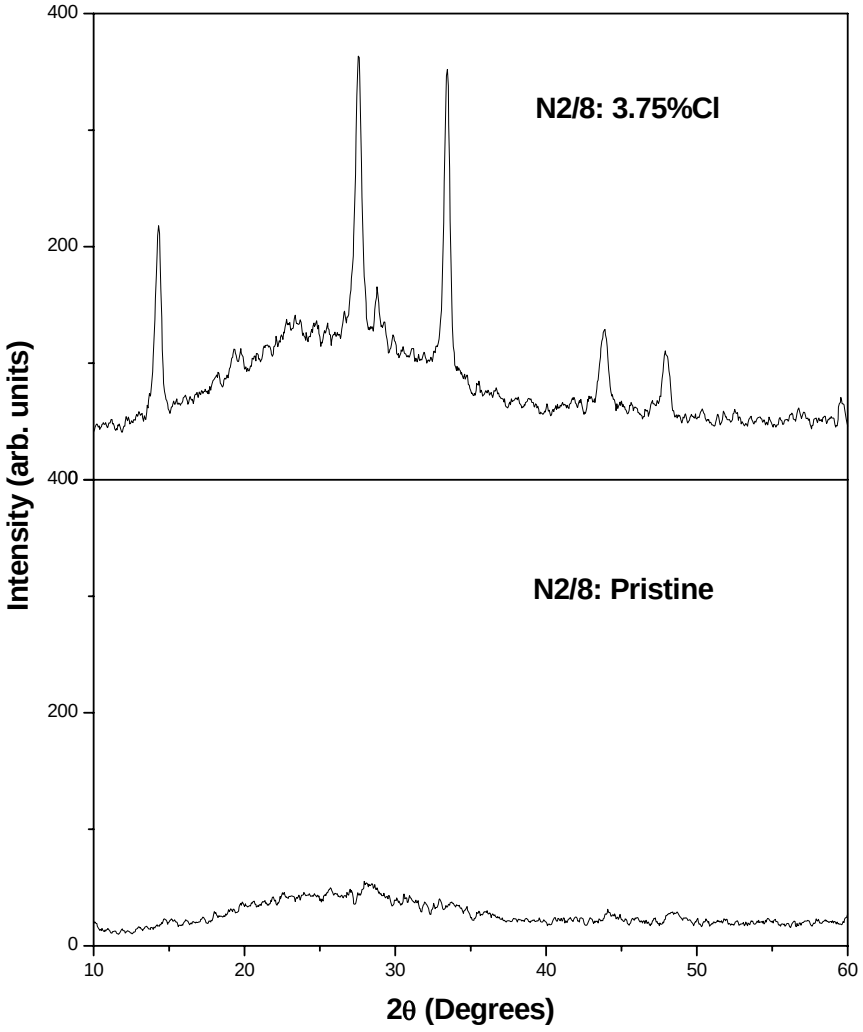

Fig.6.3 XRD graph of N2/8: pristine and N2/8: 3.75%Cl

Table 6.1 Variation in grain size with doping for different ratios

2:3 Ratio		2:5Ratio		2:8 Ratio	
Sample	Grain size	Sample	Grain size	Sample	Grain size
N2/3-Pristine	amorphous	N2/5-Pristine	amorphous	N2/8-Pristine	amorphous
N2/3-0.1%Cl	12 nm	N2/5-0.1%Cl	18.8 nm	N2/8-0.1%Cl	17.7 nm
N2/3-1%Cl	16.3 nm	N2/5-1%Cl	19.4 nm	N2/8-1%Cl	18.9 nm
N2/3-2.5%Cl	18.9 nm	N2/5-2.5%Cl	21.8 nm	N2/8-2.5%Cl	21.3 nm
N2/3-3.75%Cl	20.6 nm	N2/5-3.75%Cl	23.2 nm	N2/83.75%Cl	22.8 nm
N2/3-5%Cl	22.1 nm	N2/5-5%Cl	26.4 nm	N2/8-5%Cl	25.7 nm

Samples prepared using indium chloride also showed β-In_2S_3 phase with preferential orientation along the (220) plane. The intensity of the peak corresponding to this plane increased along with the increase in doping concentration (Fig. 6.4) indicating an improvement in crystallinity. There was no change in preferential orientation. The amorphous nature which was observed in pristine sample C 1.2/8 series also disappeared with doping. Grain size of the sample also increased with doping. It became 33 nm for the sample C1.2/8:1% Cl while it was 16.28 nm for C1.2/8: pristine.

The change in crystallization observed with Cl doping was quite similar to the results reported by Teny et al on increasing the ratio of indium in the solution [13]. In that study, the ratio of indium was increased by increasing the ratio of $InCl_3$ in the solution. $InCl_3$ can yield three Cl^- ions along with single In^{3+} ion. So the increase in crystallinity with $InCl_3$ could also be suspected to be the role of Cl ions as the same

results could be obtained by introducing Cl by adding ammonium chloride where ammonium forms gaseous residual.

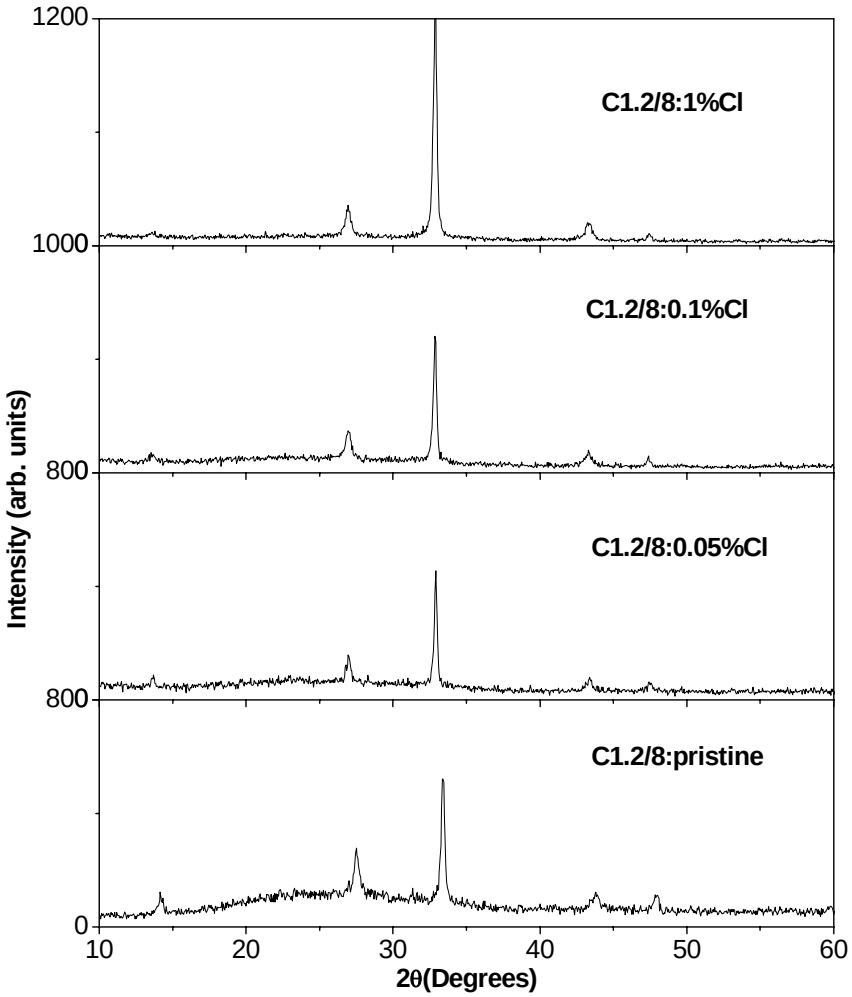

Fig.6.4 Variation in XRD for C1.2/8 series with doping

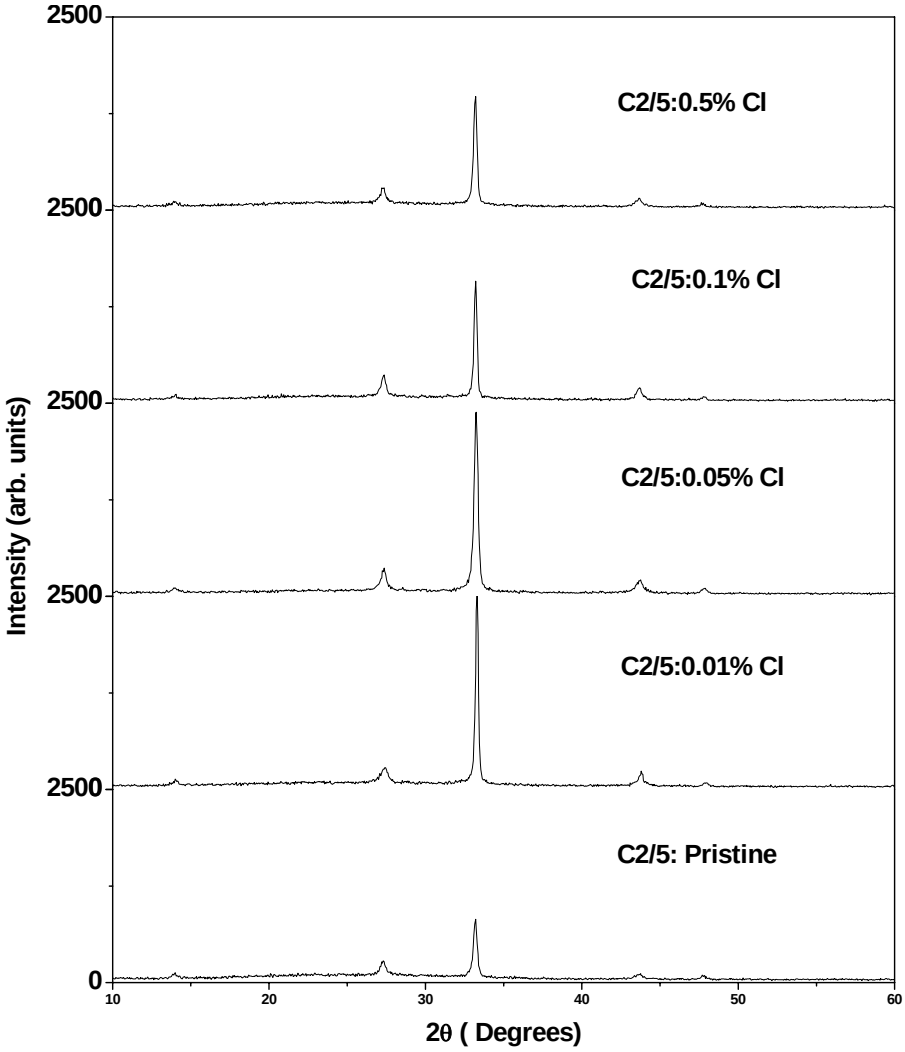

Fig.6.5 Variation in XRD for C2/5 series with doping

On increasing the chlorine concentration in 2/5 series, the intensity of the peak corresponding to this plane increased till C2/5:0.05%Cl. Further increase of chlorine concentration (C2/5:1%Cl) resulted in the decrease of the peak intensity (Fig. 6.5). However there was no change in preferential orientation.

6.3.2 Surface Morphology

6.3.2.1 SEM

Surface morphology was examined employing Scanning Electron Microscopy (SEM). Pure nitrate based samples revealed a dense structure with no cracks or voids. From figure 6.6 it could be clearly seen that granularity was lost on these samples compared to the samples prepared using chloride based solutions (Chapter 3).

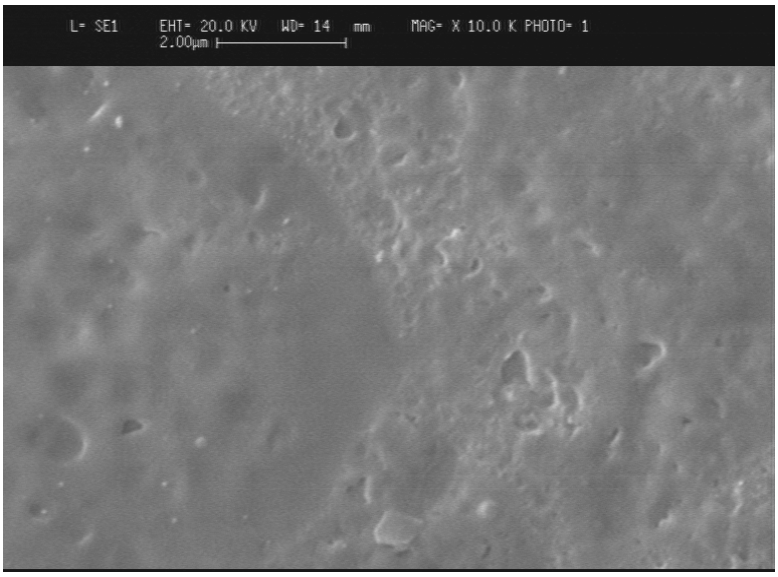

Fig.6.6 SEM micrographs of N2/5:pristine

Samples regained its granular structure with chlorine doping. The SEM micrograph gave an illustration of the crystallinity improvement observed in doped films. The grain formation was seen in clusters or islands at small doping concentration and yielded uniform grain formation at higher doping concentration for N2/5 and N2/8 series as shown on figures.6.7 to 6.9.

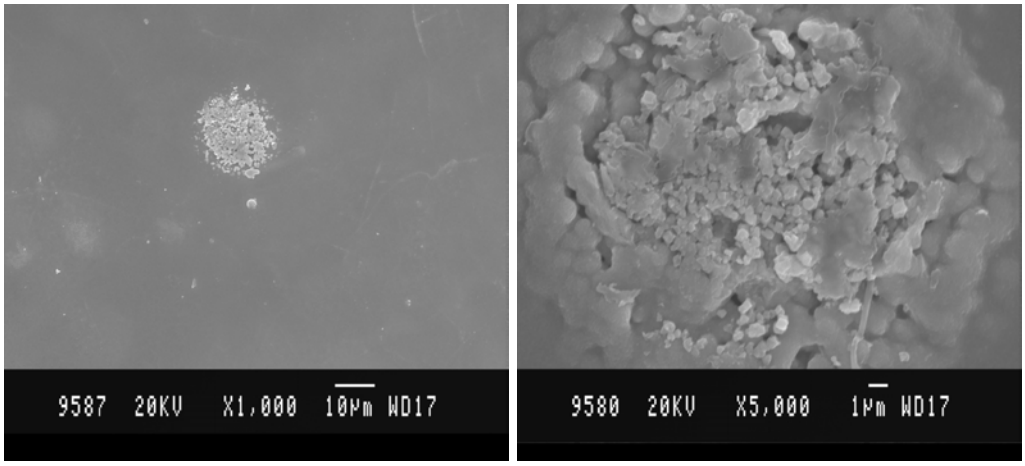

Fig.6.7 SEM micrographs of N2/5:0.1%Cl

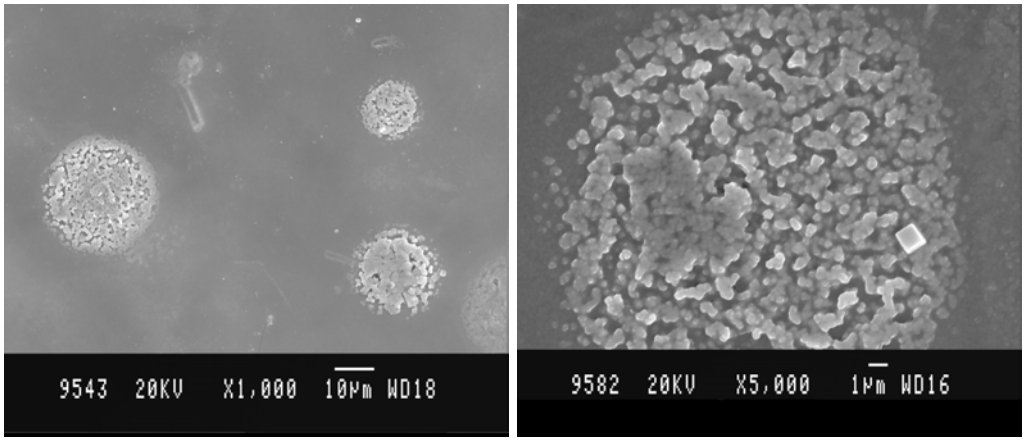

Fig.6.8 SEM micrographs of N2/5: 1%Cl

The grain formation was observed in clusters (Fig. 6.7). From EDAX measurements it could be seen that the chlorine concentration was quite high at these clusters. Number of clusters increased on increasing doping concentration (Fig 6.8). Also the grains became discrete at higher doping concentration.

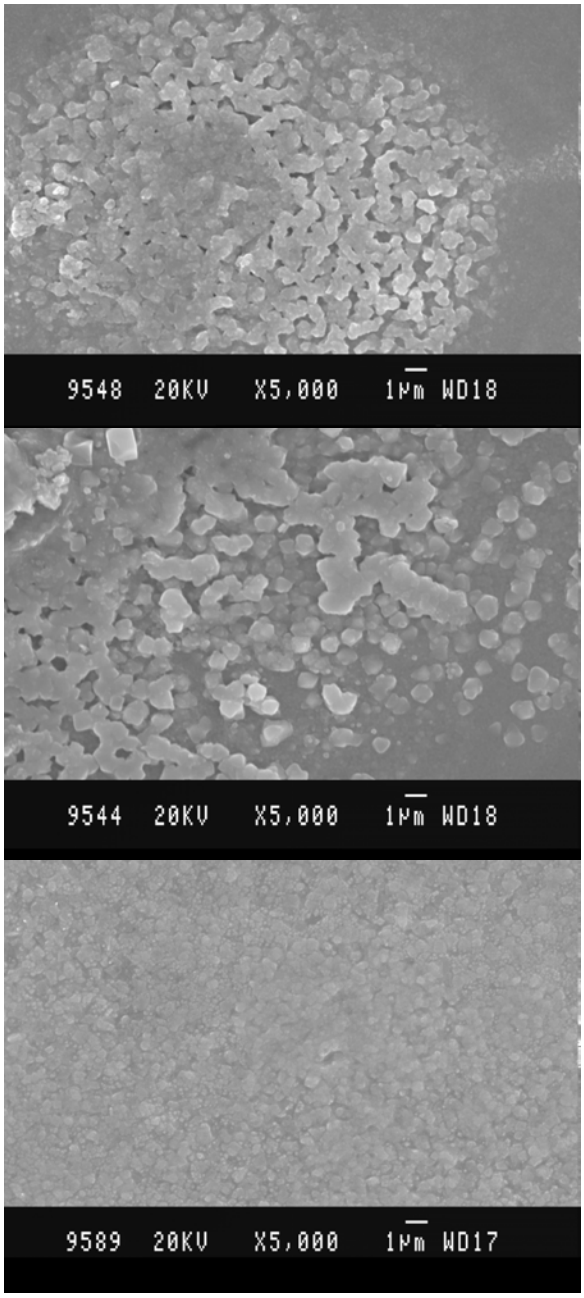

N2/5:2.5%

N2/5:3.75%

N2/5:5%Cl

Fig.6.9 SEM micrographs of N2/8 series

Figure 6.9 gives a clear illustration of clusters spreading out into uniform granular films with increased doping concentration of chlorine. The 2/8 series also yielded similar micrographs.

The SEM micrographs of 2/3 series presented some interesting observations. At low doping concentrations of Cl, we could achieve micro/ nano structures. For doping concentration of 0.001 % of chlorine (such a low concentration was tried on observing the peculiarity), the SEM micro graphs demonstrated flowery constructions. The grain size calculated from XRD yielded 7 nm at this doping concentration (Fig. 6.10). At higher magnification it was seen that the flowery constructions were of net like formations.

Increasing the doping concentration to 0.005 % resulted in 'rod-like' structures (Fig 6.12). These structures were distributed uniformly throughout the film and were observed in the samples having doping concentration from 0.005% to 0.1%. Number of rods increased with doping concentration in this range. However these structures were obtained only for 2/3 ratio, in which the atomic concentration of In (metal) is high. The atomic concentration of chlorine was quite high in these rods [16%] compared to that [6%] in the film.

For other ratios there was no significant effect on doping at lower doping percentages less than 1%. Usually nano crystallinity is reported for materials having 1:1 or greater stoichiometric ratio of metal atoms to atoms of chalcogenide in the unit cell [22, 23 24, 25]. EDAX measurements of N2/3 series showed In : S ratio to be 1:1. This could be the reason why nano structures were observed only for this series. But the pristine film on satisfying this criterion also yielded dense amorphous films (Fig. 6.12). So it has to be assumed that at the concentration (N2/3), by controlling the crystalline formation by small doping concentrations of Cl we could achieve micro/ nano structures.

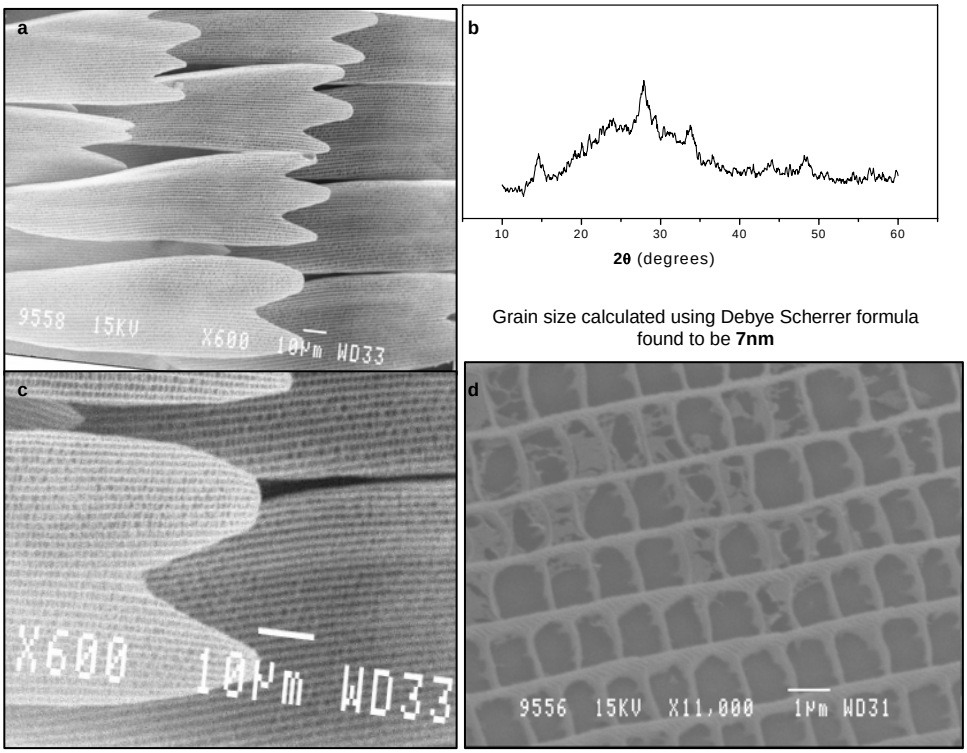

Fig.6.10 Net like structures forming flowery appearance in SEM micrograph of N2/3:0.001%Cl

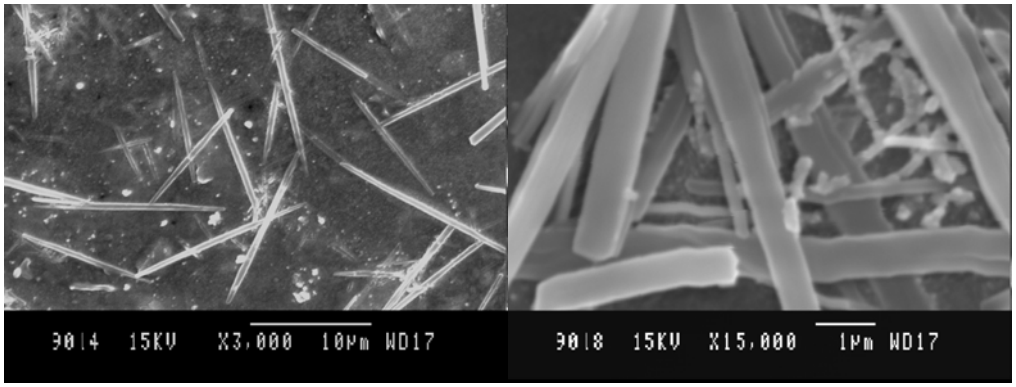

Fig. 6.11. SEM micrographs displaying Rod Structures

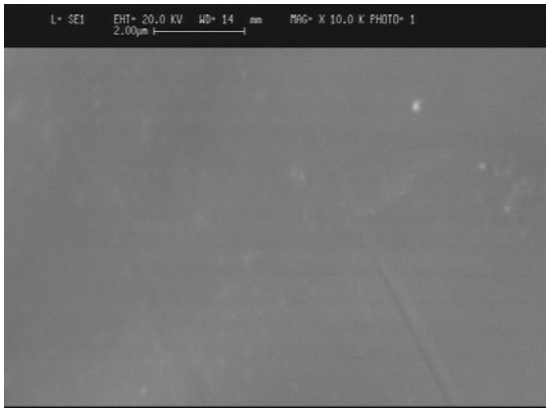

Fig.6.12 SEM micrographs of N2/3:pristine

At higher doping percentages, 2/3 series also exhibited cluster formations (Fig 6.13) as in the case of 2/5 and 2/8 series. But N2/5 and N2/8 series showed clear granularity representing better crystallinity. The EDAX measurements on these clusters showed high chlorine content compared to the rest of the films. This nature was observed in samples of all series.

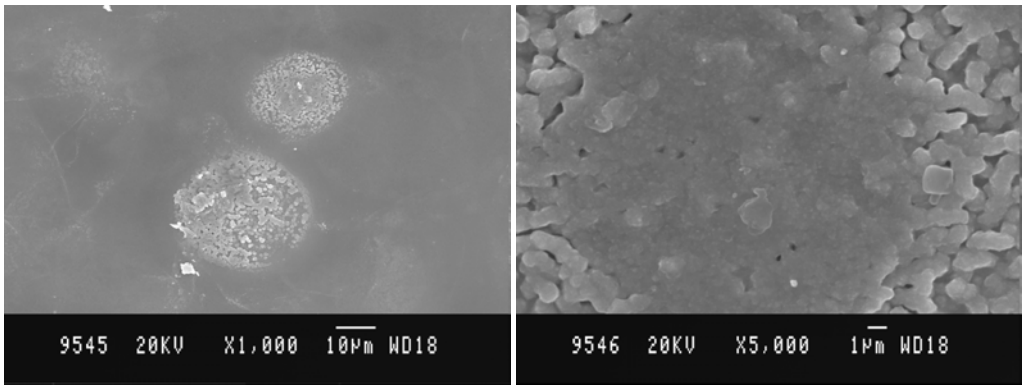

Fig.6.13 SEM micrographs of N2/3:2.5%Cl

6.3.2.2 AFM

AFM is a form of Scanning Probe Microscopy (SPM) where a small probe is scanned across the sample to obtain information about the sample's surface. The information gathered from the probe's interaction with the surface can be as simple as physical topography or as diverse as measurements of the material's physical, magnetic or chemical properties. These data are collected as the probe is scanned in a raster pattern across the sample to form a map of the measured property relative to the X-Y position.

The AFM probe has a very sharp tip, [often less than 100 Å in diameter], and is kept at the end of a small cantilever beam. The probe is attached to a piezoelectric scanner tube, which moves the probe across a selected area of the sample surface. Inter atomic forces between the probe tip and the sample surface cause the cantilever to deflect as the sample's surface topography (or other properties) changes. A laser light reflected from the back of the cantilever measures the deflection of the cantilever. This information is fed back to a computer, which generates a map of the topography and/or other properties of interest. Areas as large as 100 μm square to less than 100 nm square can be imaged.

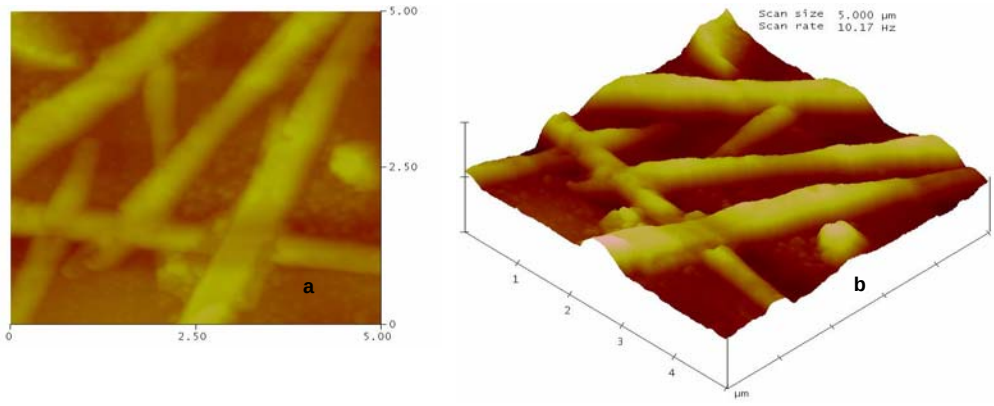

Fig. 6.14 AFM image of sample N2/3:0.1%Cl (a) 2D and (b) 3D

Figure 6.14 (a) and (b) depicts the AFM image (2D and 3D) of 5 micrometer square area of the sample N2/3:0.1%Cl. As seen in SEM measurements the sample revealed micro/nano rod structures.

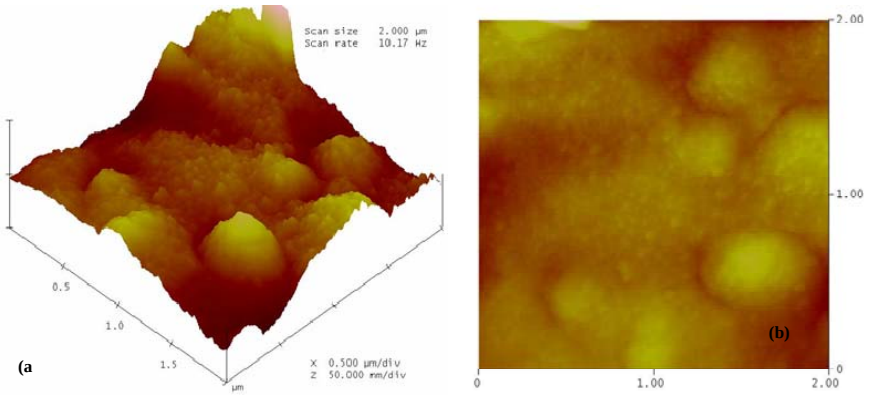

Fig. 6.15 AFM image of sample N2/3:2.5%Cl (a) 2D and (b) 3D

AFM image (2D and 3D) of 2 micrometer square area of the sample N2/3:2.5%Cl revealed that the rod structure disappears at higher doping concentrations and dense films are formed. The results were quite similar to the results obtained by SEM analysis.

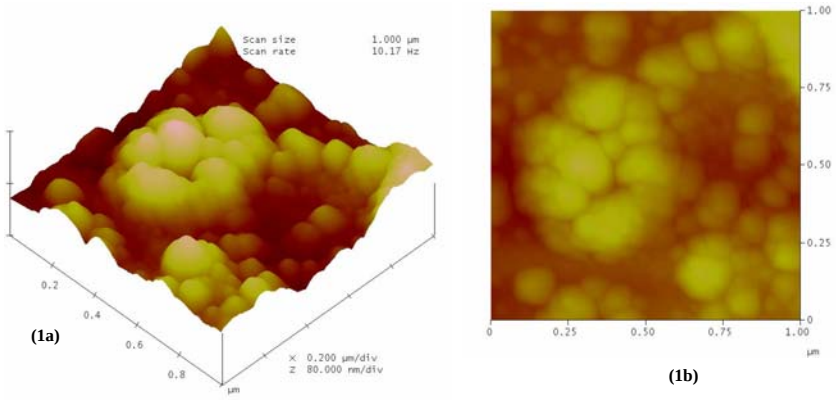

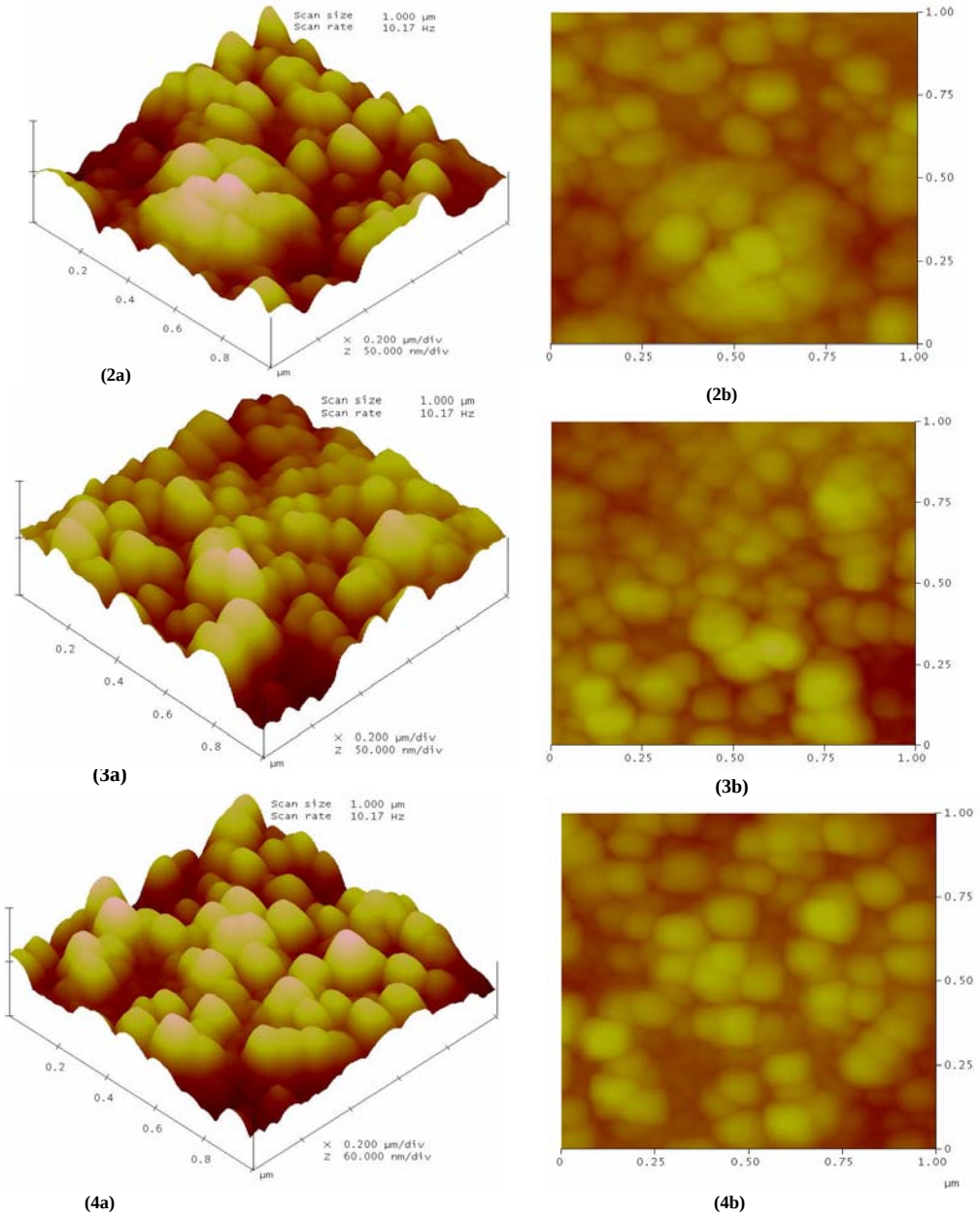

Fig. 6.16 AFM images of samples (a) 2D and (b) 3D

{**1-**N2/8:1%Cl, **2-** N2/8:2.5%Cl, **3-** N2/8:3.75%Cl , **4-** N2/8: 5%Cl }

AFM images of N2/5 and N2/8 series revealed the formation of grains at clusters quite similar to the observations from SEM analysis (Fig 6.16). At higher doping concentrations, uniform grain formation could be observed. Figure 6.16 depicts grain formation in N2/8 series.

6.3.3 Compositional Analysis

Atomic **c**oncentration of sulfur in the sample never reached 60% when indium chloride was used to prepare the samples. Stochiometric films were obtained only when indium chloride was replaced by indium nitrate. N2/5: pristine yielded stochiometric film. Atomic concentration of sulfur was found to be low for samples N2/3: pristine (~50%) giving indium rich films and N2/8: pristine yielded sulfur rich films where the concentration of sulfur exceeded 60%.

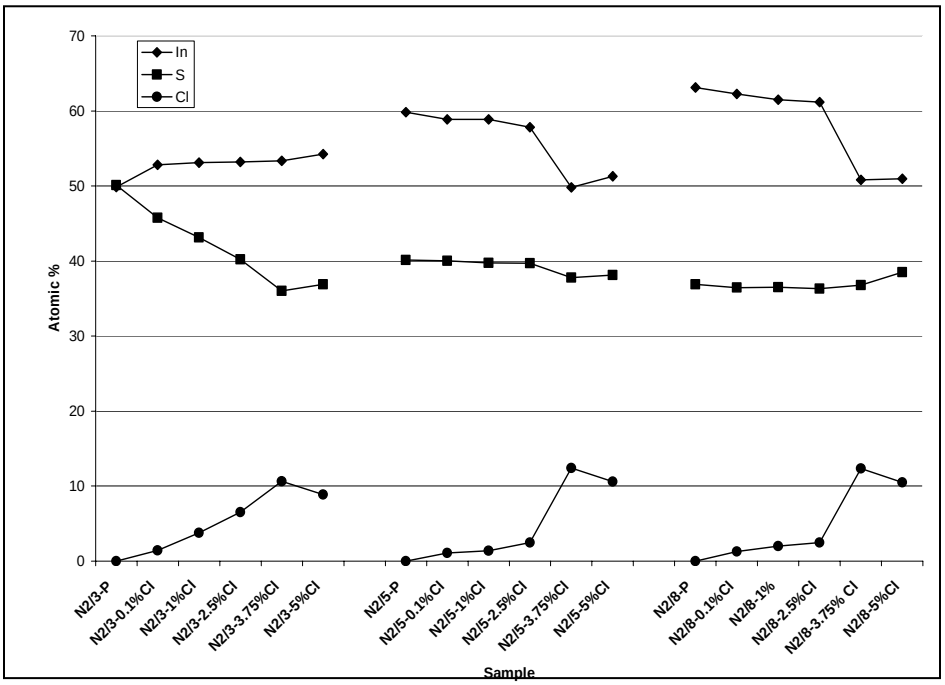

Fig.6.17 Variation of atomic concentration with doping

Variation of atomic concentration of In, S and Cl with doping is given in figure 6.17. For N2/3 series, it is seen that the indium concentration decreased with doping, presenting a slight increase in the sulfur concentration whereas in the other two series (N2/5 and N2/8) the sulfur concentration decreased with chlorine incorporation.

Table 6.2 Variation of atomic concentration with doping in chloride based samples

Sample	Atomic concentration (%)		
	S	In	Cl
C2/5-p	48.7	39.14	12.16
C2/5-0.01%Cl	42.12	39.6	18.28
C2/5-0.1%Cl	49.39	36.92	13.69
C2/5-1%Cl	49.57	38.37	12.06
C2/5-10%Cl	49.96	38.48	11.56
C1.2/8-p	56.01	37.91	6.08
C1.2/8-0.01%Cl	53.58	37.2	9.22
C1.2/8-0.05%Cl	52.15	35.62	12.23
C1.2/8-1%Cl	52.76	37.68	9.56

In all the three series (N2/3, N2/5, N2/8) chlorine incorporation increased till doping level reached 3.75% and Further showed a retracing phenomenon. In XRD analysis, it was observed that crystallinity increased linearly till 5%Cl doping where the atomic concentration of Cl was lower for 5%Cl than 3.75% Cl. Thus the crystallinity of the doped samples did not correspond to the chlorine incorporation rather it increased with doping concentration in the precursor solution.

In chloride based samples the atomic concentration of sulfur was below 60%. Atomic concentration of chlorine increased for low doping concentration and then decreased as given in table 6.2.

6.3.4 Optical Studies

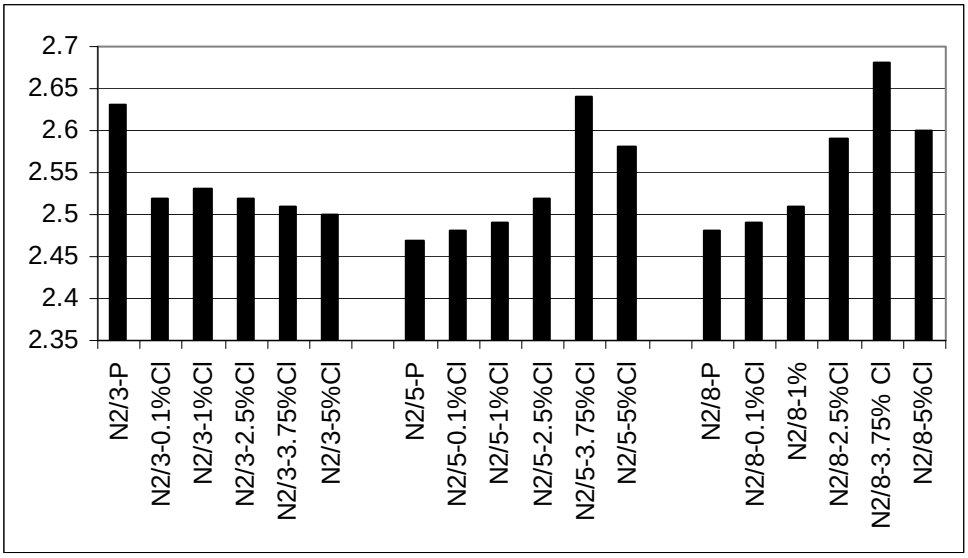

Fig.6.18 Bandgap variation in samples with doping for different In/S ratio

Optical absorption spectra were recorded in the fundamental absorption edge of pristine and doped samples, having different In/S ratio in order to investigate their optical absorption properties. Direct band gap of the samples were calculated from the plot of $(\alpha h\nu)^2$ vs $h\nu$ where $h\nu$ is the incident photon energy and α is the optical absorption coefficient calculated from the optical absorption spectra measured near the fundamental absorption edge. The value of $h\nu$ at $(\alpha h\nu)^2 = 0$ obtained by extrapolation is the optical energy bandgap. Figure 6.18 depicts the band gap variation with chlorine doping for different In/S ratios. Comparing these values we could observe that bandgap varied on Cl incorporation. Nature of variation differed

depending on In/S ratio. For N2/3 series the bandgap decreased with doping, whereas in N2/8 and N2/5 series the bandgap increased with doping. This change in behavior of bandgap could neither be explained in terms of Cl incorporation nor in terms of crystallinity. But the behavior showed correlation to the sulfur concentration in films.

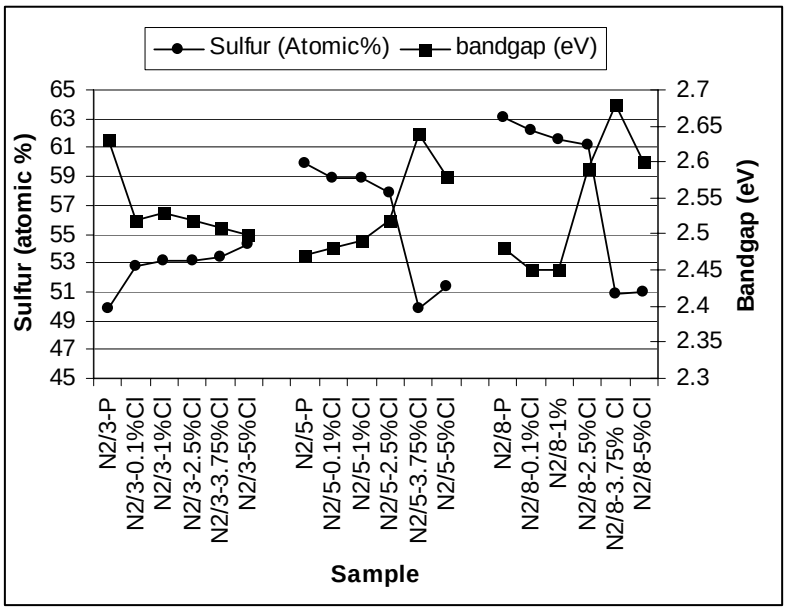

Fig. 6.19Variation of sulfur concentration and bandgap with doping

Figure 6.19 gives the correlation between sulfur concentration and bandgap. The band gap decreased with increase in sulfur concentration. For N2/3: pristine the sulfur concentration was quite low providing a wide bandgap to the material (2.64 eV). The bandgap decreased with Cl doping in N2/3 series, as the sulfur concentration increased with the same. But for the other two series, band gap increased with doping as the sulfur concentration decreased. There are also reports on decrease in band gap with increase in sulfur concentration [13, 26].

The impurity absorption spectra in the wavelength region 800 nm to 2000 nm of the doped samples were measured using pristine sample (nitrate based) as the reference, in order to understand the change in optical absorption due to Cl impurity. The absorption spectra of the doped samples at long wavelength region indicated that the introduction of Cl to the films initiated defect level absorption at the long wavelength region. Such a defect level was observed in the case of chloride based indium sulfide samples as an inherent property. Impurity absorption is observed in the case of cobalt doped indium sulfide samples [26-29].

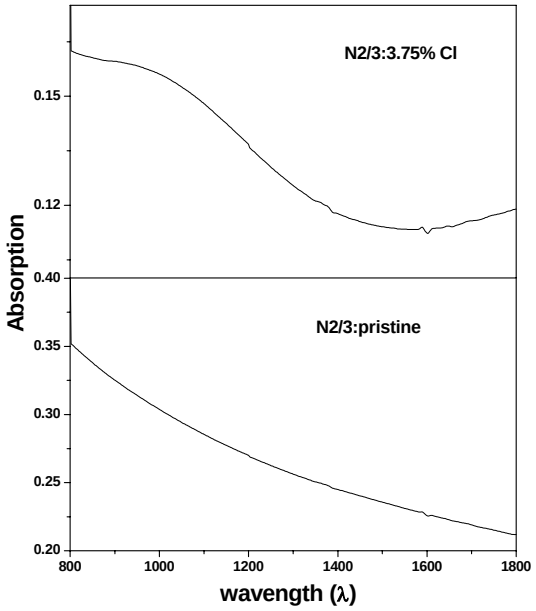

Fig. 6.20 Defect level absorption for N2/3 series

The defect level absorption was observed at around 933 nm, [corresponding to 1.33 eV], for N2/3 series (fig.6.20). It was observed that the defect level absorption was dependent on chlorine incorporation as the absorption was high for N2/3: 3.75% Cl in N2/3 series which, from EDAX measurements, proved to have highest atomic concentration of chlorine in N2/3 series.

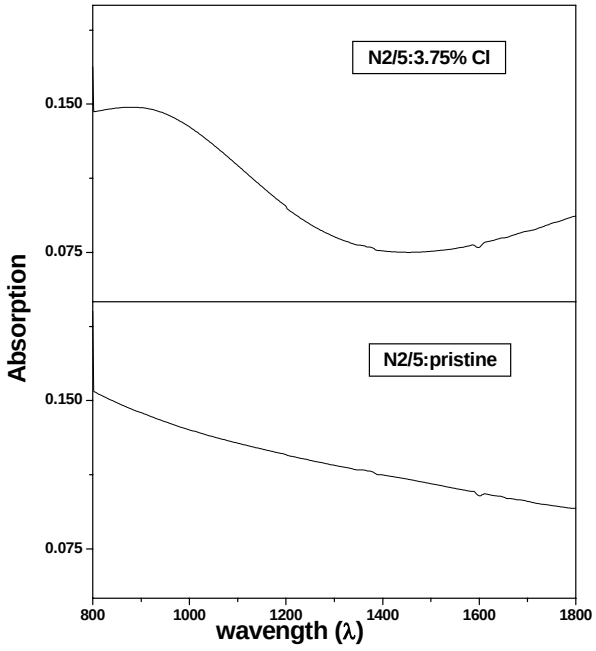

Fig. 6.21 Defect level absorption for N2/5 series

For N2/5 series, (Fig.6.21) the defect level absorption due to Cl doping was initiated around a shorter wavelength of 863 nm (corresponding to1.44 eV). Here also the absorption peak corresponded to Cl incorporation, giving the maximum peak height for N2/5:3.75% Cl, sample having highest atomic concentration of Cl in N2/5 series.

From figure 6.22 it could be seen that there were two defect levels in N2/8 series due to Cl doping, peaks corresponding to 820 nm (1.64 eV) and 1460 nm (.84 eV). Here the maximum peak height was for N2/8: 3.75%Cl, the sample having the highest atomic concentration of Cl in the N2/8 series.

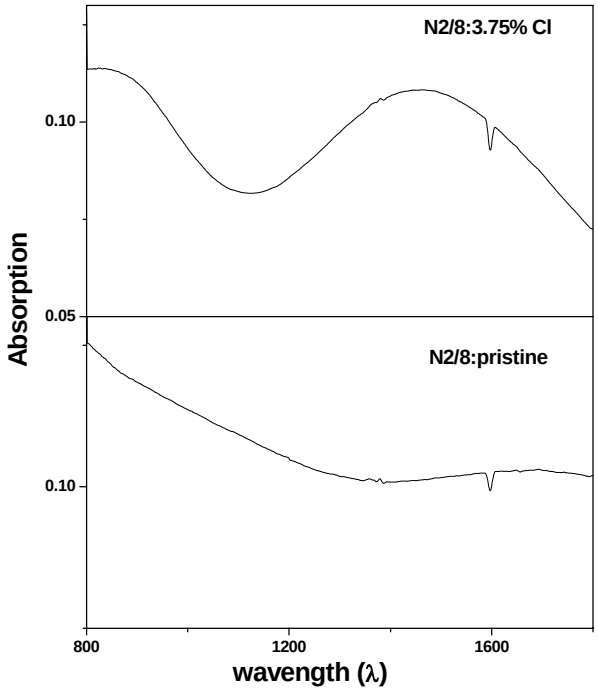

Fig. 6.22 Defect level absorption for N2/8 series

Though there was variation in the impurity absorption peak position; the difference between the band gap (Eg) and defect level absorption disclosed the presence of a defect level at ≈ 1.18 eV (Table 6.3).

Table 6.3. Band gap and impurity level absorption for different In/S ratios

Sample	N2/3-3.75% Cl	N2/5-3.75% Cl	N2/8-3.75% Cl
Bandgap (Eg) eV	2.51	2.63	2.68
Impurity absorption (Ia) eV	1.33	1.44	1.5
(Eg-Ia) eV	1.18	1.19	1.18

6.3.5 Resistivity and Photosensitivity

On comparing the resistivity of pristine samples, N2/3: pristine was found to have 86 Ω-cm, which was very low when compared with samples having higher sulfur concentration, N2/8: pristine and N2/5:pristine. For N2/3 series the resistivity of the samples increased with Cl concentration as seen in the graph.

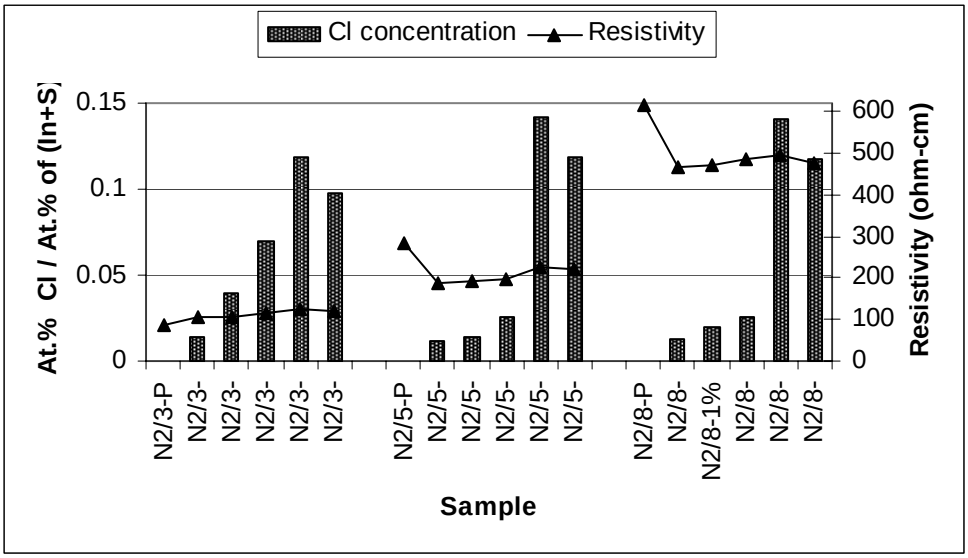

Fig. 6.23 Variation of resistivity chlorine with Cl doping.

But for N2/8 and N2/5 series, having high sulfur concentration, the resistance of the pristine sample was quite high which decreased on doping. This could be due to the development of crystallinity. But even when the resistivity values of the doped films were quite lower than the pristine films, among the doped samples, a slight increase in resistivity could be observed corresponding to Cl incorporation. Nature remained the same for N2/5 and N2/8 series. Figure 6.23 depicts the variation of resistivity with Cl doping along with ratio of chlorine to In and S in the film. For

chloride based samples, the resistivity increased with chlorine incorporation for both series as seen in figure 6.25.

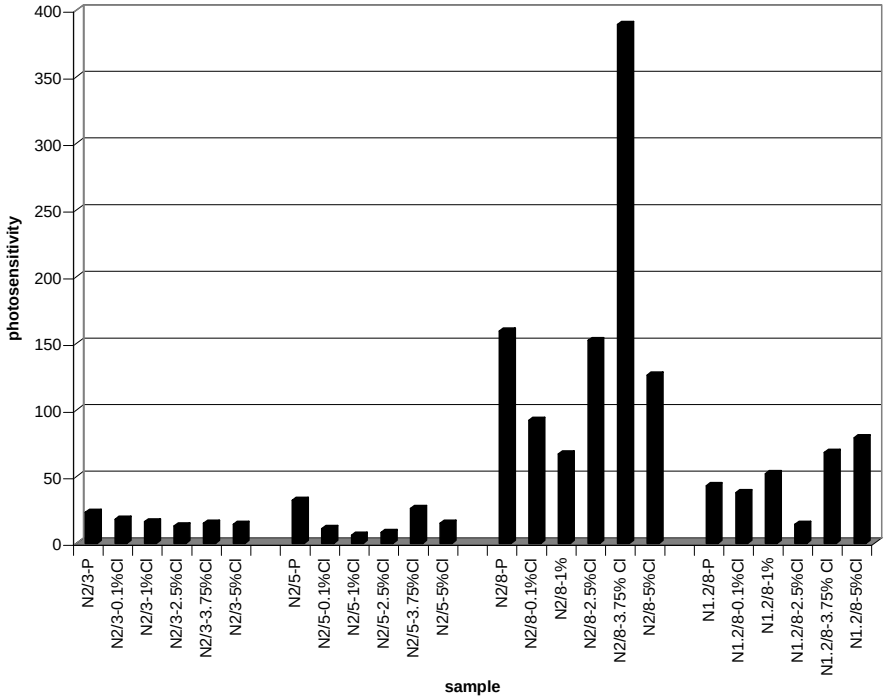

Fig. 6.24 Variation in photosensitivity with Cl doping for various In/S ratio

The photosensitivity of the nitrate based samples did not show a steady state behavior with doping. But for N2/8 Series the photosensitivity of the sample N2/8:3.75%Cl showed a high value, compared to that of N2/8:pristine. Photosensitivity studies were done on N1.2/8 ratio because, in chloride based samples, C1.2/8 gave maximum photosensitivity [13]. But in nitrate based samples, N2/8 series exhibited a better photosensitivity compared to other series. More over, in chloride based samples, the photosensitivity could be increased by chlorine incorporation as given in figure.6.25.

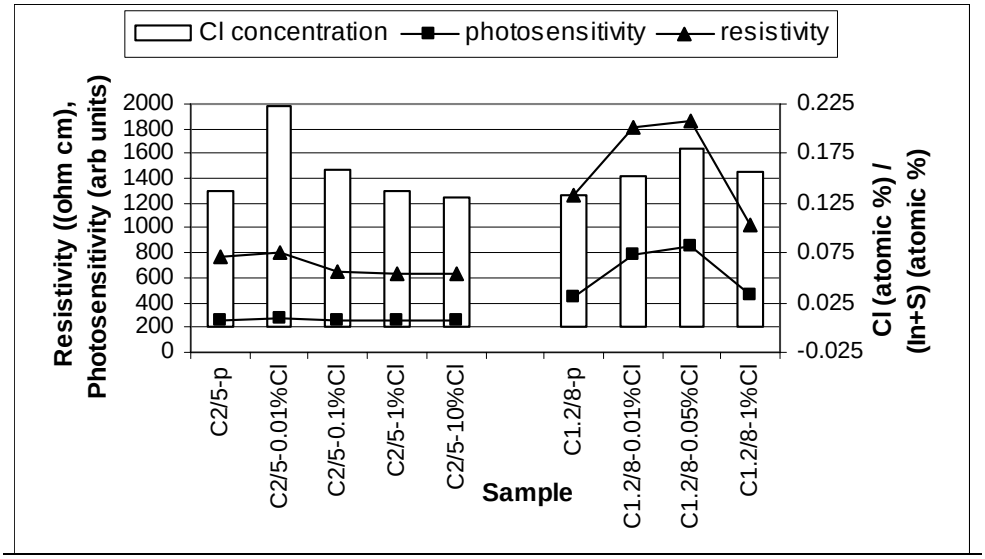

Fig. 6.25 Variation of resistivity and photosensitivity with chlorine concentration for different In/S ratios in chloride based samples

Time dependent photoconductivity measurements were carried out using a white light source. This was done on the observation that chloride based samples were having persistence in photocurrent decay. The transient photoconductivity curves for the doped and un-doped films are shown in figure 6.26. Here the important observation was that the persistence of photoconductivity was introduced with chlorine doping.

Correlating atomic concentration of chlorine from EDAX measurements and figure 6.26 we conclude that the persistence of photoconductivity increased with chlorine incorporation in the films.

The Sample which was un-doped did not have the decay tail. Sample N2/8:3.75%Cl, which contained maximum Cl, failed to return to its dark current value, even after 1200s since cutting the illumination. This conclusively proved that Cl impurity was responsible for the decay tail. Chlorine needs only one electron to

complete the octet structure and can act as a strong acceptor; hence it can create a *trap* which could lead to persistence in the decay of photocurrent.

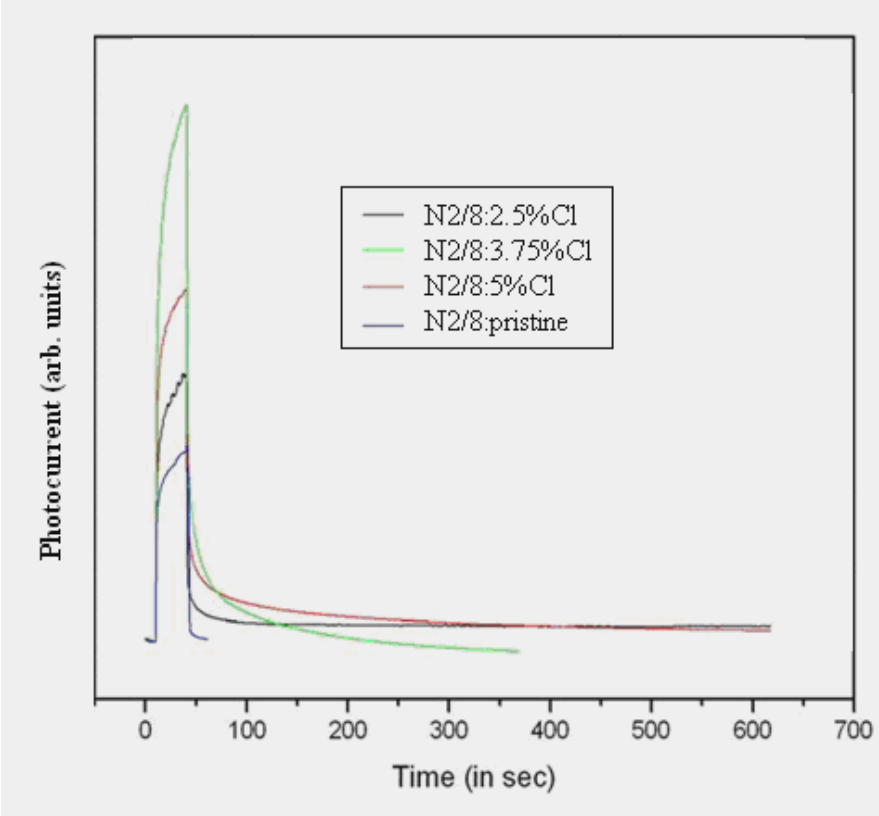

Fig. 6.26 Photoconductivity spectra for pristine and doped films

Variation of photosensitivity with temperature was studied to identify the trap level .Figure 6.27 shows the plots for photoconductivity at 13 K and 300 K. Similarly the plots at various temperatures were obtained. Keeping the excitation energy at 2.33 eV (532 nm), fixing the excitation intensity at 20 mW and maintaining a constant pulse width of (0.3 s) the temperature dependence of photosensitivity in thin films was studied from 13 K to 300 K.

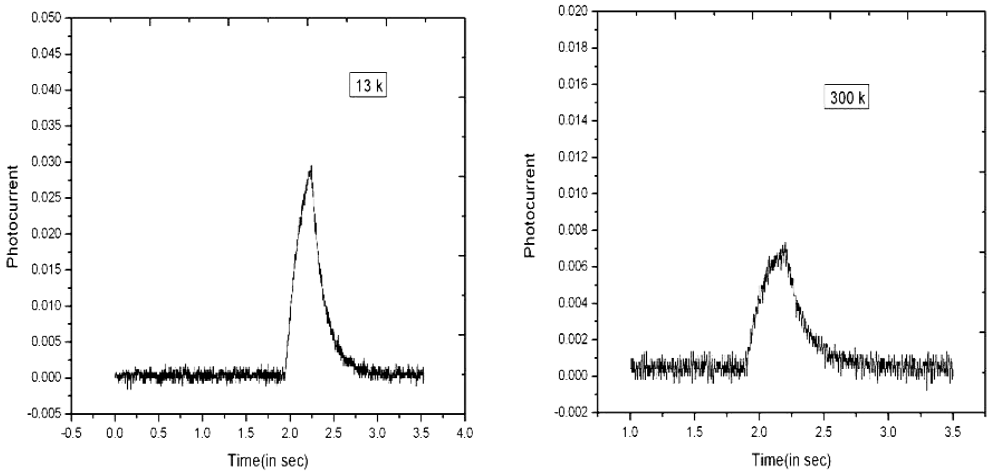

Fig. 6.27 Photoconductivity spectra at 13 K and 300 K for N.2/8:3.75%Cl thin film under excitation of 2.33 eV.

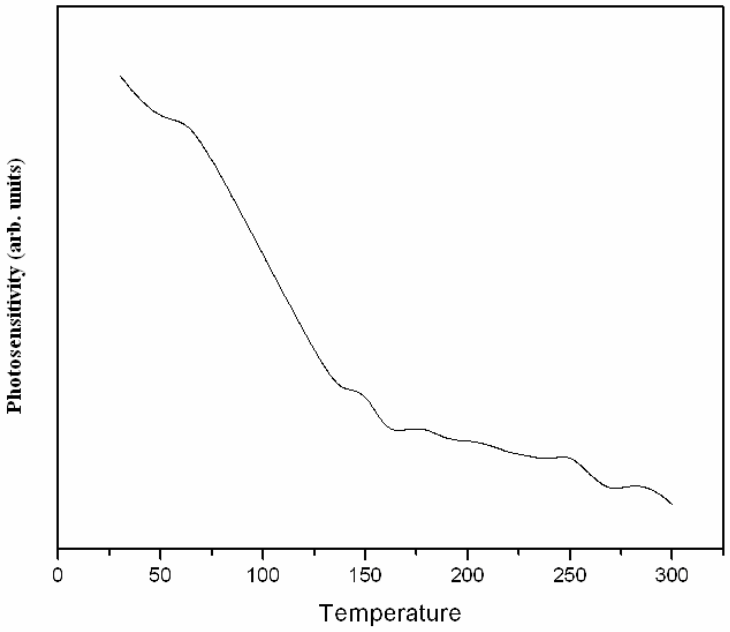

.

Fig. 6.28. Temperature dependence of Photosensitivity

Figure 6.28 represents the plot of photosensitivity versus temperature for the Cl doped sample, N2/5:3.75%Cl. As shown in the figure it was observed that the photosensitivity of the material was high at low temperatures and decreased with increase in temperature.

The temperature dependence of photocurrent can be used to calculate activation energies of shallow traps from Arrhenius plot as shown in figure 6.28.The temperature dependence of photocurrent was fitted using the relation

$$I_{ph}(T) = I_0/(1+c \exp(-E_a/KT)) \quad (6.1)$$

Where $I_{ph}(T)$ is the photocurrent at a temperature T, I_0 is the photocurrent at temperature at 0 K, c is a constant related to the capture cross section of traps/defect levels and E_a is the activation energy of the respective traps/defect level.

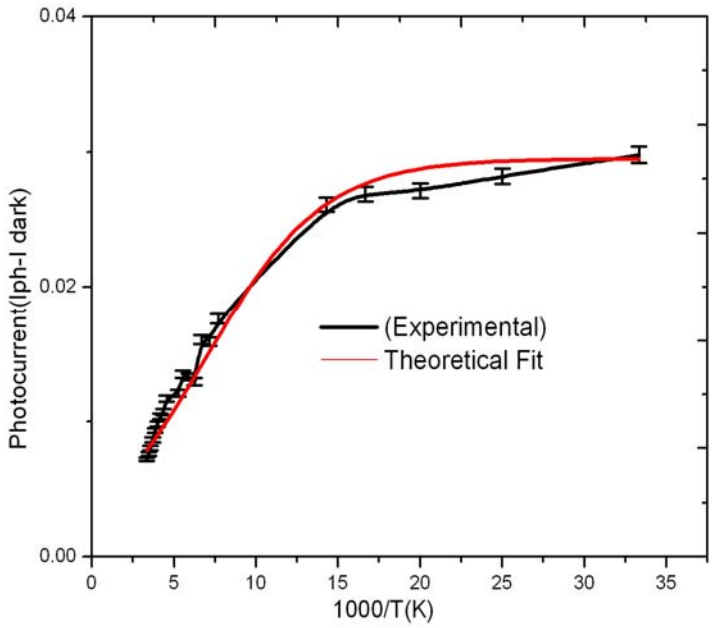

Fig. 6.29: Arrhenius plot of Photocurrent versus 1000/ T for the film under excitation of 2.33 eV.

Activation energy of the order of 24 meV was obtained based on the fitting of the experimentally obtained results using the relation 6.1. Thus temperature dependence of photoconductivity proved the presence of a shallow level at 24 meV which could be easily thermalized at room temperature.

6. 4 Conclusions

β-In_2S_3 thin films, prepared using CSP technique with indium nitrate as precursor solution instead of indium chloride, were found to be amorphous irrespective of indium to sulfur ratio or thickness. On Cl doping, the films became crystalline and crystallinity increased with doping concentration in the precursor solution. SEM and AFM showed that grain formation was initiated in clusters where the atomic concentration of Cl was found to be high. On increasing the doping concentration, the cluster concentration increased in films providing uniform grain formation at high doping concentrations. EDAX measurements showed that the Cl incorporation did not directly correspond to doping concentration in solution. But there is a maximum value up to which the atomic concentration of Cl in the In_2S_3films increased linearly and after that, a decrease in incorporation was observed.

Optical absorption studies proved the onset of defect level absorption with Cl doping. The bandgap corresponded to Sulfur concentration which varied with Cl incorporation. Interestingly samples exhibited persistence in photocurrent decay with Cl incorporation. Existence of a defect level at 24 meV was detected using temperature dependent photoconductivity studies. Photosensitivity and resistivity of chloride based samples showed a direct correlation to the atomic concentration of chlorine. For nitrate based samples, no such correspondence could be seen. But for N2/8 series photosensitivity could be increased by increasing chlorine incorporation. Thus some aspects of the role of chlorine in controlling properties of indium sulfide films prepared by spray pyrolysis could be understood.

References

[1] A. R. Barron, Adv. Mater. Opt. Electro. **5** (1995) 245.

[2] M. Amlouk, M. A. Ben Said, N. Kamoun, S. Belgacem, N. Brunet and D. Barjon, Jpn. J. Appl. Phys. **38** (1999) 26.

[3] R. Nomura, K. Konishi and H. Matsuda, Thin Solid Films **198** (1990) 339.

[4] C. D. Lokhande, A. Ennaoui, P. S. Patil, M. Giersig, K. Diesner, M. Muller and H. Tributcsh, Thin Solid Films **340** (1999) 18.

[5] T. Asikainen, M. Ritala and M. Leskelä, Appl. Surf. Sci. **82/83** (1994) 122.

[6] N. Kamoun, S. Belgacem, M. Amlouk, R. Bennaceur, J. Bonnet, F. Touhari, M. Nouaoura and L. Lassabatere, J. Appl. Phys. **89(5)** (2001) 2766.

[7] W. T. Kim and C. D. Kim, J. Appl. Phys. **60(7)** (1986) 2631.

[8] L. Bhira, H. Essaidi, S. Belgacem, G. Couturier, J. Salardenne, N. Barreaux and J. C. Bernède, Phys. Stat. Sol. (a) **181** (2000) 427.

[9] M. Amlouk, M. A. Ben Said, N. Kamoun, S. Belgacem, N. Brunet and D. Barjon, Jpn. J. Appl. Phys. **38** (1999) 26.

[10] R. Bayón , C. Maffiotte and J. Herrero, Thin Solid Films **353** (1999) 100.

[11] R. Bayón and J. Herrero, Applied Surface Science, **158** (2000) 49.

[12] K. Ernits, D. Brémaud, S. Buecheler, C.J. Hibberd, M. Kaelin, G.Khrypunov, U. Müller, E. Mellikov and A.N. Tiwari, Thin Solid Films**, 515 (15)** (2007) 6051.

[13] Teny Theresa John, S.Bini, Y.Kashiwaba, T.Abe, Y.Yasuhiro, C.Sudha Kartha and K.P.Vijayakumar, Semiconductor Science and Technology, **18** (2003) 491.

[14] N. Barreau, J. C. Bernède, H. El Maliki, S. Marsillac, X. Castel and J. Pinel, Solid State Communications, **122(7-8)** (2002) 445-450.

[15] N. Barreau , J. C. Bernède, S. Marsillac and A. Mokrani, Journal of Crystal Growth, **235(1-4)** (2002) 439-449.

[16] N. Barreau, J. C. Bernède, C. Deudon, L. Brohan and S. Marsillac, Journal of Crystal Growth 241(1-2) (2002) 4-14.

[17] N. Barreau' , J. C. Bernède and S. Marsillac, Journal of Crystal Growth,volume **241(1-2)** (2002) 51-56.

[18] S. Gall' , N. Barreau, S. Harel, J.C. Bernède and J. Kessler**,** Thin Solid Films **480-481**(2005) 138-141.

[19] N. Barreau' , J. C. Bernède, H.El Maliki, S. Marsillac, X. Castel, J. Pinel, Solid State Communications **122** (2002) 445-450.

[20] Dimitri Hariskos, Martin Ruckh, Ulfert Riihle, Thomas Walter, Hans Werner Schock, Jonas Hedstrom, Lars Stolt, Solar Energy Materials and Solar Cells **41/42** (1996)345-353.

[21] Teny Theresa John, C.Sudha Kartha, K.P.Vijayakumar, T.Abe and Y.Kashiwaba, Applied Surface Science, **252** (2005) 1360.

[22] A. P Alivisatos, J. Phys. Chem. **100** (1996) 13226-13239.

[23] Weller, H. Philos, Trans. R. Soc. London A, **354** (1996) 757-766.

[24] Brus, L. E.; Trautman, J. K. Philos, Trans. R. Soc. London A, **353** (1995) 313-321.

[25] M. G.Bawendi, Solid State Commun. **107** (1998) 709.

[26] W. T. Kim, C. S. Yun, H. M. Jong and C. D. Kim, J. Appl. Phys. **60(7)** (1986) 2357.

[27] S. H. Choe, T. H. Bang, N. O. Kim, H. G. Kim, C. I. Lee, M. S. Jim, S. K. Oh and W. T. Kim, Semicond. Sci. Technol. **16** (2001) 98.

[28] C. D. Kim, H. Lim, H. L. Park, H. Y. Park, J. E. Kim, H. G. Kim, Y. G. Kim and W. T. Kim, Thin Solid Films , **224 (1)** (1993) 69.

[29] W. T. Kim, W. S. Lee, C. S. Chung and C. D. Kim, J. Appl. Phys. **63** (11) (1988) 5472.

Chapter 7
Summary and Conclusions

The structural, optical and electrical properties of indium sulfide, an important material for optoelectronic and photovoltaic applications, are tuned by specific and controlled doping. This binary compound semiconductor is a promising candidate for many technological applications due to its stability, comparatively wider band gap and photoconductive behavior. It can be used as an effective nontoxic substitute for cadmium sulfide (CdS) in Cu(In,Ga)Se_2 based solar cells. Even though CdS is capable of forming efficient heterojunction, there is great interest in replacing CdS by a cadmium-free buffer, due to environmental reasons. Also performance gain is expected for wider band gap materials like indium sulfide due to lower light absorption. Thus indium sulfide buffer layers are to be optimized for an improved performance than CdS.

The present work is on engineering the properties of indium sulfide by doping so as to make it an ideal buffer layer for thin film solar cells. Silver, tin, copper and chlorine were used as the dopants. Interestingly, Cl is an unnoticed [but involuntary] dopant in most of the indium sulfide films prepared by chemical methods, where indium chloride is used.

In_2S_3 thin films were deposited on soda lime glass substrates using chemical spray pyrolysis (CSP) technique. Doping was achieved either by diffusion or by incorporating the dopant in the spray solution itself. For doping by diffusion, a two-stage process was adapted. As the first stage a thin layer of the metal was deposited over the In_2S_3 layer, using vacuum evaporation technique (pressure during evaporation was ~$2x10^{-5}$ m bar). Silver diffusion occurred even at this stage. Second stage provided thermal assistance to diffusion by annealing the bilayer structure at a higher temperature. The latter technique was applied for doping Sn and Cu. In situ

doping of Sn and Cl was achieved by incorporating the dopant in the spray solution itself. Doping concentration was varied to achieve optimum performance.

Doping β-In_2S_3 thin films with Ag resulted in samples with enhanced crystallinity and grain size. From XPS depth profile of the sample, it could be seen that silver diffused throughout the depth even without annealing. It was also observed that there was an optimum amount of Ag, required for doping and further increase in doping concentration showed retracing effects. Electrical resistivity of the films decreased drastically from $1.2x10^3$ Ωcm to 0.06 Ωcm due to doping. Defect studies showed an increase in indium interstitials with doping which could be the major reason for low resistivity of the samples. It was observed that at low doping concentration, silver atoms were positioned in the ordered vacancy sites (activation energy ~ 1.2 eV). At still higher doping concentration, silver atoms were setting into indium sites creating an acceptor level (activation energy ~ 0.6 eV). On further increase in doping concentration, silver atoms got into interstitial positions commencing drastic decrease in resistivity. The most striking and interesting observation was that, photosensitivity of optimum doped β-In_2S_3 film was greater than the pristine sample, even when its resistivity was much lesser. Presence of the acceptor level might have helped the increase of photosensitivity of the film. Thus doping β-In_2S_3 film with optimum amount of silver modified the structural and electrical properties of the films favorably so that the Ag electrodes given to the ITO/$CuInS_2$/In_2S_3 cell structure itself acted as a doping agent for the In_2S_3 layer enhancing the cell efficiency.

Sn doping considerably enhanced the conductivity of the In_2S_3 samples. Effect of both ex-situ (by diffusion) and in-situ (incorporating in spray) doping was analyzed. Conductivity of the films enhanced by five orders on ex-situ doping, There was no impact on the physical properties like crystallinity or band gap. By ex-situ doping, we could limit the diffusion to surface layer so that during junction fabrication

for photovoltaic applications, we can have a low resistive n-type layer near the electrode while the highly resistive and photosensitive layer (pristine) remains near the junction. Carrier generation and collection can be promoted by such a structure, which is very useful for photovoltaic applications. However, it was also noted that high doping concentration resulted in samples with low crystallinity, negative photosensitivity and slight increase in band gap. Through in-situ doping of Sn, we could achieve a wider band gap and lower resistivity, which is very useful for buffer layer applications in solar cells. Low resistive buffer layer will decrease the series resistance of the cell and wider band gap will improve light transmission in the blue wavelength. Both factors facilitate in increasing the short circuit current of the photovoltaic cell. This was specifically observed for low percentage of doping. Higher band gap could be attributed to oxygen incorporation in the samples and lower resistance might be due to the donor action of tin. Samples having higher doping concentration of Sn exhibit wider band gap (up to3.78 eV). Though the samples had very high band gap and resistivity, anomalously they exhibited very high photosensitivity [$> 10^4$]. Studies proved that the change in band structure with higher oxidation of the samples was responsible for this phenomenon. The results also proved that tin incorporation modified the band gap and electrical properties of the In_2S_3 films favorably over wider ranges, making it suitable for different optoelectronic applications.

Copper was diffused into In_2S_3 (*n*-type) by annealing bi layer films having structure Cu/In_2S_3. Through solid state reaction between copper and indium sulfide, the top layer could be converted into $CuInS_2$ (*p* type), so as to make a $CuInS_2/ In_2S_3$ bilayer *p-n* junction. XRD analysis revealed formation of $CuInS_2$ in addition to tetragonal β-In_2S_3 phase. Optical absorption edge of these films showed a shift towards longer wavelength proving the presence of $CuInS_2$. Sheet resistance of the sample also reduced considerably. Hot probe measurements proved that Cu diffused samples resulted in p-type nature. Cationic vacancies of the stoichiometric In_2S_3 films,

grain boundaries and dangling bonds might have made the diffusion of copper much easier. Junction could be fabricated by controlling the diffusion of copper by adjusting the thickness of Cu and In_2S_3 layers at optimized temperature. This junction was found to be photoactive and hence could be used as a simple technique for the fabrication of solar cell.

Chlorine is an involuntary dopant in most of indium sulfide films prepared by chemical methods that use chloride based precursor solutions. However none of the earlier studies have revealed the role of Cl on the properties of the films. Hence, In_2S_3 films were purposefully doped to find the part played by chlorine as a dopant. Chlorine was found to be helpful in improving the crystallinity of the films. SEM and AFM proved that grain formation was initiated in clusters where the atomic concentration of Cl was high. Cluster concentration increased with doping concentration providing uniform grain formation at higher doping concentrations. Controlling the Cl doping concentration in metal rich indium sulfide films yielded micro/nano structures. Optical absorption studies proved the onset of defect level absorption with Cl doping. Interestingly samples exhibited persistence in photocurrent decay with Cl incorporation. In these samples, a defect level at 24 meV was detected by temperature dependent photoconductivity studies. Photosensitivity and resistivity of chloride based samples showed a direct correlation to the atomic concentration of chlorine.

Many of the results obtained over here could be explained from the perspective of “impurity photovoltaic effect (IPV)”, which is believed to be the future generation of photovoltaics that can take the efficiencies beyond the theoretical limits. Indeed through doping of In_2S_3, we could create levels in the band gap resulting in IPV. Defect analysis proved the formation of such intermediate levels by doping which contributed on molding the doped indium sulfide as an ideal buffer layer.

Future Scopes

Natural progression of present research would be its application in solar cell fabrication. Combining the goodness of different dopants by co- doping can be the direction of future research. Silver doping towards the junction and surface doping with tin could give better performance. The wide bandgap photosensitive material developed can be optimized for its potential application in see-through PV modules. Junction fabrication by Cu diffusion is a very simple cost effective way to achieve junction. The simplicity of the process is quite admirable and the junction fabrication by diffusion is quite similar to process adapted in silicon technology, renowned for its simplicity among the solar cell fabrication processes. This has opened up a new avenue of cell fabrication that has to be further optimized for optimal performance. Fine adjustments in the thickness of both layers and annealing temperatures may result in better efficiency of the cell. Chlorine doping using acid based compound has to be carried out to have a better understanding of electrical properties of nitrate based samples.